OXAMATO-BASED DICOPPER(II) METALLACYCLOPHANES AS PROTOTYPES OF MAGNETIC DEVICES FOR MOLECULAR SPINTRONICS

A Joint Experimental and Computational Study

Memoria de Tesis Doctoral presentada por
María Castellano Sanz

Dirigida por
Catedrático Francesc Lloret Pastor y Doctor Joan Cano Boquera

Para optar al Grado de Doctor en Nanociencia y Nanotecnología

València 2013

INDEX

SUMMARY

The work presented in this thesis constitutes a successful extension of our group's research on the chemistry of dinuclear copper(II) metallacyclic complexes with dinucleating aromatic dioxamato ligands containing potential redox- and photoactive, π-conjugated aromatic spacers. In doing this, we have followed a joint experimental and theoretical approach based on ligand design that profits from the use of several physical (spectroscopic, magnetic, electrochemical, and photochemical) and computational (DF and TDDF) characterization techniques.

This novel class of oxamato-based dicopper(II) metallacyclophanes provides excellent synthetic and theoretical models for the *fundamental study* on long distance electron exchange and electron- or photo-triggered electron exchange phenomena, which are two central topics in the emerging area of molecular spintronics. Indeed, these simple molecules appear as very promising candidates to get multifunctional molecule-based magnetic devices facilitating the spin communication ('molecular magnetic wires', MMWs) or exhibiting spin charge storage ('molecular magnetic capacitors', MMCs) and bistable spin behavior ('molecular magnetic switches', MMSs) for *potential applications* in information processing and storage.

This work is placed at the intercrossing area of several molecular and supramolecular disciplines including coordination chemistry, spectro- and magnetochemistry, and electro- and photochemistry. The design and synthesis of metallacyclic molecules that contain multiple electro- and photoactive, either metal- or ligand-based, spin carriers and the study of their spectroscopic and magnetic properties as well as their redox and photochemical activity are of large interest in the multidisciplinary field of *molecular magnetism*. The variety of single-molecule magnetic behaviors reported in each chapter of this thesis illustrates the potential of electro- and photoactive, oxamato-based dicopper(II) metallacyclophanes as prototypes of molecular magnetic devices in the emerging field of *molecular spintronics*.

Chapter 1

In this preliminary chapter, we present an introduction on electron exchange (EE) and electron transfer (ET) phenomena, which are intimately related processes that rely on the transmission of spin- and charge-based electronic effects respectively, outlining strategies to achieve long-distance intramolecular magnetic and electronic coupling in dinuclear copper(II) complexes. A brief overview is given on the present state of the art in molecular spintronic circuitry based on organometallic and metal complexes to introduce the challenges for research in this thesis. In fact, besides their use as models for the fundamental research on EE and ET between metal centers through extended π-conjugated aromatic ligands, oxamato-based dicopper(II) metallacyclophanes containing electro- and photoactive, ligand- and/or metal-based, spin containing electro- and chromophores emerge as potential electronic and magnetic devices in the emerging field of molecular spintronics.

Chapter 2

In this second chapter, we report on two novel dinuclear copper(II) metallacyclophanes with *para*-substituted diphenylethyne- and di(phenylethynyl)phenylenedioxamato ligands which show a moderate to weak intramolecular antiferromagnetic coupling ($-J$ values from 1 up to 4 cm^{-1}) between two Cu^{II} ions separated from 15 up to 22 Å. To our knowledge, these are the largest intermetallic distances for which a non-negligible intramolecular exchange interaction has been observed experimentally. It deserves to be noted that in most of the dinuclear copper(II) complexes with extended π-conjugated organic bridges reported so far, the intramolecular exchange interaction is very small ($J < 1.0$ cm^{-1}) for such very long intermetallic distances. Further developments may be then envisaged for this new class of *oxamato-based dicopper(II) oligo-p-phenylethynophanes* as *molecular antiferromagnetic wires*, which are the basic component of a spin-based molecular electronic circuit.

Chapter 3

In this third chapter, we report on two novel dinuclear copper(II) metallacyclophanes with *para*-substituted 9,10-anthraquinonedioxamato ligands which exhibit a unique metal- and ligand-based multielectron redox behavior involving the transfer of up to 6

e^- upon one-electron oxidation of the two antiferromagnetically coupled Cu^{II} ions and two-electron reduction of the two anthraquinone spacers in *anti* conformation. To our knowledge, these are the first examples of anthraquinone-based dinuclear copper(II) metallacyclophanes, referred to as dicopper(II) anthraquinophanes, incorporating both redox-active metal-based spin carriers and noninnocent quinoid-type bridging ligands. Hence, this new class of *oxamato-based dicopper(II) anthraquinophanes* illustrates the potential of multifunctional (electroactive and magnetic) metallacyclic complexes with multiple chemically accessible oxidation levels at the metal and/or the ligand components (electrophores and spin carriers) as *magnetic molecular capacitors*.

Chapter 4

In this fourth chapter, we report on three novel dinuclear copper(II) metallacyclophanes with polymethyl-substituted *p*-phenylenedioxamato ligands which exhibit a unique magnetic electroswitching (ON/OFF) behavior upon reversible one-electron oxidation of one of the two permethylated phenylene spacers. The corresponding fully delocalized, dicopper(II) π-radical monooxidized species constitutes a metallacyclic analogue of the purely organic Wurster blue cyclophanes. This new class of *oxamato-based permethylated dicopper(II) paracyclophanes* represents an attractive design concept for *molecular magnetic electroswitches* incorporating two metal-based spin carriers and a redox-active ('non-innocent') bridging ligand. Another examples of this class reported recently by our group are linear oxamato-based tricopper(II) metallacyclophanes of the mesocate-type featuring a redox-active metal ion.

Chapter 5

In this fifth chapter, we report on two novel dinuclear copper(II) metallacyclophanes with α,α'-naphthalene- and β,β'-anthracenedioxamato ligands exhibiting a reversible antiferromagnetically coupled to magnetically uncoupled (ON/OFF) switching behavior upon light irradiation and heating. To our knowledge, they are the first prototypes of magnetic switches with two metal-based spin carriers and photoactive oligoacene spacers, the other few examples reported so far being organic diradicals or metal-organic radicals with photoactive diarylethene spacers reported by Irie. Although their efficiency and reversibility are still limited, the reported photomagnetic bistability

illustrates the potential of *oxamato-based dicopper(II) oligoacenophanes* as *molecular magnetic photoswitches* in the emerging field of molecular spintronics.

Chapter 6

In this last but not least chapter, we summarize our major achievements on the control of the long-distance magnetic coupling through extended π-conjugated, electro- and photoactive organic spacers in oxamato-based dicopper(II) metallacyclophanes by ligand design. Using simple dinuclear metallacyclic complexes as dynamic chemical systems to perform specific and selective tasks under the control of an external stimulus that switches "ON" and "OFF" their electronic (optical, redox, and/or magnetic) properties may have an enormous impact in several domains of molecular nanosciences. Finally, we show how to use this new class of electro- and photoactive, oxamato-based dicopper(II) metallacyclophanes as building blocks in the development of a new class of multifunctional molecular materials, such as *switchable single-molecule nanomagnets* and *molecule-based dynamic porous magnets*, which are brand-new targets in the emerging field of molecular spintronics.

RESUMEN

El trabajo presentado en esta tesis constituye una exitosa extensión de la investigación de nuestro grupo sobre la química de los complejos metalacíclicos de cobre(II) con ligandos dinucleantes de tipo bis-oxamato con espaciadores aromáticos extendidos π-conjugados. Durante este proceso, hemos seguido una aproximación conjunta, teórica y experimental, basada en el diseño de ligandos y que implica el uso de diversas técnicas físicas (espectroscópicas, magnéticas, electroquímicas y fotoquímicas) y computacionales (DF y TDDF) de caracterización.

Las novedosas clases de metalaciclofanos de cobre(II) con ligandos bis-oxamato desarrolladas en esta tesis proveen excelentes modelos teóricos y sintéticos para el estudio fundamental del canje electrónico a larga distancia y los fenómenos de canje electrónico activados foto- o electroquímicamente, los cuales constituyen dos temas fundamentales de estudio en las áreas relacionadas del magnetismo molecular y la espintrónica molecular. Además, estas moléculas sencillas constituyen candidatos muy prometedores para la obtención de dispositivos magnéticos multifuncionales que faciliten la comunicación entre los espines (cables magnéticos moleculares o "molecular magnetic wires", MMWs), que exhiban capacidad de almacenamiento de carga eléctrica y de espín (condensadores magnéticos moleculares o "molecular magnetic capacitors", MMCs), o que tengan comportamiento biestable (interruptores magnéticos moleculares o "molecular magnetic switches", MMSs). Cada uno de estos dispositivos moleculares poseen aplicaciones potenciales en el procesamiento y almacenamiento de la información.

Este trabajo se sitúa en la frontera entre diferentes disciplinas moleculares y supramoleculares, entre las que se incluyen la Química de Coordinación, la Espectroquímica, la Magnetoquímica, la Electroquímica y la Fotoquímica. El diseño y síntesis de moléculas metalacíclicas que contengan múltiples portadores de espín, tanto electro- como fotoactivos (basados en el metal o en el ligando), y el estudio de sus propiedades magnéticas y espectroscópicas, así como de su actividad fotoquímica y rédox, son de un gran interés en el campo multidisciplinar del magnetismo molecular. La variedad de comportamientos magnéticos moleculares anotados en cada uno de los capítulos de esta tesis ilustra el potencial de los complejos metalaciclofanos de cobre(II)

con ligandos puente bis-oxamato foto- o electroactivos como prototipos de dispositivos magnéticos moleculares en el campo emergente de la espintrónica molecular.

Capítulo I

En este capítulo preliminar, presentamos una introducción a los fenómenos de canje y transferencia electrónica, que son procesos íntimamente relacionados que se basan en la transmisión de los efectos electrónicos de espín y de carga eléctrica, respectivamente, subrayando las diferentes estrategias posibles para conseguir acoplamiento magnético a larga distancia en complejos dinucleares de cobre(II). Además, se proporciona una visión general sobre el estado actual del diseño de circuitos electrónicos y magnéticos basados en complejos metálicos y organometálicos, con el objetivo de introducir los retos perseguidos en esta tesis en el área de la espintrónica molecular. De hecho, aparte de su uso como modelos en la investigación fundamental sobre canje electrónico a través de ligandos aromáticos extendidos π-conjugados, los complejos metalaciclofanos de cobre(II) con ligandos puente bis-oxamato que contengan electróforos y cromóforos que presenten espín (ya se basen éstos en el ligando o en el metal) se presentan como potenciales dispositivos electrónicos y/o magnéticos en el campo emergente de la espintrónica molecular.

Capítulo II

En el segundo capítulo, presentamos dos nuevos complejos dinucleares de cobre(II) de tipo metalaciclofano con ligandos difeniletino- y di(feniletinil)fenilenobis(oxamato) *para*-sustituidos, los cuales muestran un acoplamiento antiferromagnético intramolecular entre moderado y débil (valores de $-J$ de 1 a 4 cm^{-1}) entre los dos iones Cu^{II} separados por distancias largas (valores de r de 15 a 22 Å). Éstas son las mayores distancias intermetálicas que conocemos para las cuales se ha observado experimentalmente una interacción de intercambio intramolecular no despreciable. Es interesante subrayar que en la mayoría de los complejos dinucleares de cobre(II) con puentes aromáticos π-conjugados extendidos, la interacción de canje intramolecular es muy pequeña ($J < 1$ cm^{-1}) para distancias intermetálicas muy grandes. Estos resultados pueden otorgar a estos complejos oligo-*p*-fenilenoetinofanos de cobre(II) de tipo oxamato la categoría de *cables magnéticos moleculares*, los cuales son componentes básicos de los circuitos electrónicos basados en el espín.

Capítulo III

En el tercer capítulo, presentamos dos nuevos complejos dinucleares de cobre(II) de tipo metalaciclofano con el ligando puente 9,10-antraquinonabis(oxamato) 1,4-sustituido, los cuales exhiben un comportamiento rédox multielectrónico único (basado tanto en los centros metálicos como en el ligando) que conlleva la transferencia de entre 1 y 6 electrones, desde la oxidación monoelectrónica de los dos iones Cu^{II} acoplados antiferromagnéticamente hasta la reducción bielectrónica de los dos espaciadores antraquinona en conformación *anti*. Éstos son los primeros ejemplos conocidos de complejos dinucleares metalaciclofanos de cobre(II) basados en ligandos antraquinona que incorporan, al mismo tiempo, transportadores de espín rédox-activos tanto en los centros metálicos como en los ligandos puente no inocentes de tipo quinona. Esta nueva clase de antraquinofanos de cobre(II) de tipo oxamato ilustra el potencial de los complejos metalacíclicos multifuncionales (magnéticos y electroactivos) que poseen niveles de oxidación múltiples y accesibles químicamente como *condensadores magnéticos moleculares*.

Capítulo IV

En el cuarto capítulo, presentamos tres nuevos complejos dinucleares de cobre(II) de tipo metalaciclofano con ligandos *p*-fenilenobis(oxamato) polimetilsustituidos que exhiben un comportamiento único de interruptor electroquímico basado en oxidaciones monoelectrónicas reversibles de uno de los dos espaciadores fenileno permetilados. Las correspondientes especies de cobre(II) monooxidadas π-radicalarias constituyen un análogo metalacíclico de los ciclofanos puramente orgánicos de tipo azul de Wurster. Esta nueva clase de paraciclofanos permetilados de cobre(II) de tipo oxamato representa un concepto de diseño atractivo para preparar *interruptores electroquímicos magnéticos moleculares*, incorporando dos transportadores de espín y un ligando puente no inocente (rédox-activo). Otro ejemplo de esta clase de complejos obtenido recientemente por nuestro grupo de investigación son los los complejos trinucleares metalaciclofanos de cobre(II) de tipo mesocato, que incluyen un ión metálico central rédox-activo.

Capítulo V

En el quinto capítulo, presentamos dos complejos dinucleares de cobre(II) de tipo metalaciclofano con ligandos naftaleno- y antracenobis(oxamato) α,α'- y β,β'-

sustituidos que exhiben un comportamiento de interruptor reversible, pasando de un estado antiferromagnéticamente acoplado (ON) a otro magnéticamente desacoplado (OFF) tras la irradiación con luz y el calentamiento. Estos compuestos son los primeros prototipos conocidos de interruptores fotoquímicos con dos transportadores de espín sobre los centros metálicos y con espaciadores oligoaceno fotoactivos. Los otros ejemplos conocidos son diradicales orgánicos o radicales metaloorgánicos con espaciadores fotoactivos diarileteno. Aunque su eficiencia y reversibilidad son todavía limitadas, la biestabilidad magnética observada ilustra el potencial de los oligoacenofanos de cobre(II) de tipo oxamato como *interruptores fotoquímicos magnéticos moleculares* en el campo emergente de la espintrónica molecular.

Capítulo VI

En este último pero no menos importante capítulo, se resumen nuestros logros más significativos en el control del acoplamiento magnético a larga distancia a través de espaciadores orgánicos extendidos π-conjugados, electro- y fotoactivos, mediante el diseño racional de ligandos. El uso de complejos metalaciclofanos de cobre(II) como sistemas magnéticos multifuncionales dinámicos para llevar a cabo tareas selectivas y específicas bajo el control de estímulos externos que permiten activar y desactivar sus propiedades electrónicas (ópticas, rédox y/o magnéticas) podría tener un enorme impacto en muchos dominios de la nanociencia molecular. Así mismo, mostramos cómo pueden utilizarse estas nuevas clases de complejos dinucleares metalaciclofanos de cobre(II) de tipo oxamato como precursores electro- y fotoactivos para el desarrollo de un nuevo tipo de materiales moleculares multifuncionales, tales como moléculas imán conmutables e imanes porosos dinámicos moleculares, los cuales son objetivos novedosos y de gran interés en el campo emergente de la espintrónica molecular.

A Rafa

AGRADECIMIENTOS

En estas líneas, me gustaría dar las gracias a todas las personas que, en mayor o menor proporción, han contribuido a la realización de esta Tesis Doctoral.

En primer lugar, querría agradecer a mis directores de Tesis Francisco Lloret y Joan Cano el haberme dado la oportunidad de trabajar en el grupo de Química de Coordinación para desarrollar mi tesis, poniendo todas las oportunidades a mi alcance. Especialmente, quería darte las gracias, Joan por el tiempo (que no te sobra, precisamente) que invertiste en enseñarme a hacer cálculos teóricos, y la paciencia que demostraste en incontables ocasiones, no sólo en lo que a dichos cálculos se refiere.

Rafa, cualquier cosa que escriba se quedará corta para expresar lo que tu ayuda ha supuesto para mí. Durante los cuatro años que ha durado mi tesis has estado en todo momento a mi lado, ayudándome con el trabajo experimental y explicándome y enseñándome una parte muy importante de lo que he aprendido, y en los últimos meses has sufrido mi presencia en tu despacho y dirigido con todo el interés, cariño y paciencia del mundo la redacción de mi tesis, que no habría llegado a buen puerto sin ti. Colaboradores como tú son muy difíciles (si no imposibles) de encontrar. De todo corazón, mil gracias.

Emilio, si bien no he sido estudiante tuya, has estado siempre ahí en los momentos de la tesis que no han resultado tan sencillos o agradables como hubiese sido deseable. Sin tu apoyo, no habría pasado todo con la misma facilidad. Gracias mil por tu comprensión, por tus consejos, que me temo que no siempre he sabido seguir, pero que intentaré tener en la cabeza siempre; y por los paseos en el parque. En este último punto incluyo también a Ángela, que sin comerlo ni beberlo ha tenido que soportarme bastante también…

Miguel, gracias por tu optimismo, tu sonrisa, tus ánimos, y por hacer posible que en el grupo todos tengamos todas las oportunidades y contactos que se puedan querer gracias al esfuerzo, la tolerancia, las horas de trabajo interminables y a la buena colaboración con todo el mundo, tanto de tu parte como de la de Paco Lloret.

Salah, gracias por el apoyo y el interés en mi trabajo que has mostrado siempre, en particular en las reacciones fotoquímicas y la síntesis orgánica, de la cual es una parte importantísima Abdeslem Bentama, sin el cual mis ligandos no serían lo que son (a este respecto debo dar las gracias también a Fran por su colaboración). Por el tiempo que me dedicasteis y por las enseñanzas acerca de las reacciones orgánicas, y todo siempre con la mejor de las sonrisas, muchas gracias.

Especialmente, han supuesto un apoyo y una ayuda muy importantes a lo largo de la tesis mis compañeros de laboratorio. Jesús, gracias por haberme enseñado y asesorado todo cuanto pudiste desde el principio de los tiempos (cuando yo hacía el proyecto de fin de carrera y tú estabas empezando la tesis, qué tiempos…) y a lo largo de todos estos años, por todos los buenos ratos que hemos pasado juntos en congresos, cenas, fiestas, o ejecutando estrambóticas coreografías en el laboratorio… y por el cariño, la paciencia y los cuidados cuando las cosas no han ido bien; en definitiva, por haber sido como un hermano mayor para mí. Lumi, aunque sólo hemos convivido durante un año en el laboratorio, has sido alguien esencial para mí, me has aconsejado y apoyado como una hermana cuando más falta me hacía, y recordaré siempre las incontables tazas de café compartidas al sol y las clases de body combat que descubrí gracias a ti. Tía Xelo, millones de gracias por tu buen humor, por tus consejos, por tu cariño, por hacerme

saber siempre que estás ahí a un mensaje de facebook de distancia, por las cenas y las risas que hemos compartido, y más importante, por ponerme los pies en el suelo cuando me disperso demasiado. Thais, desde el momento de tu llegada al laboratorio me has abierto tu corazón, me has demostrado tu simpatía y tu apoyo incondicional en todas las circunstancias en un momento en que eran realmente necesarios, y me has aportado alegría y optimismo, portándote como una verdadera amiga, te lo agradezco infinitamente y no olvidaré allá donde vaya las cerbatanas, el canto y los dragones. Jérémy, gracias por tu amistad, por tu cariño, por tu hospitalidad en Lyon, por estar a mi lado en los momentos buenos y en los no tan buenos, en España o en Francia, por las fiestas y por todo lo que nos hemos divertido juntos. Jose Lillo, muchas gracias por todos tus buenos consejos, por compartir conmigo tu experiencia y conocimientos sobre el mundo de la investigación y los diferentes grupos de laboratorio, además de por las historias del Colegio de España en París. María Vanda, tu amistad y tu dulzura hicieron que la convivencia en el laboratorio durante el año que pasaste aquí fueran más fáciles, gracias por todo… y aunque ahora estés ya de vuelta en Brasil, recuerda que siempre nos quedará París. Tatiana, tu simpatía y tu carácter alegre me han dado muchos ánimos durante el año de redacción de la tesis, gracias por haber estado a mi lado y haber aguantado mi estrés y mis improperios. Álvaro, gracias por tu sonrisa y tu apoyo incondicional, suerte con la expansión de mis dímeros en el rational design de los MOFs, me alegra ver que mis "hijos" crecen. Y a Paco Camallonga, le expreso mi más sincera gratitud por su carácter paciente frente a mis ocasionales estallidos de cólera, que se ha visto obligado a sufrir, por su asesoramiento informático siempre que ha sido necesario, y por el tiempo que invirtió y las imaginativas historias que se inventó para conseguir que yo llegara a dominar el VIM que tanta falta me hacía para los cálculos teóricos.

Fuera del grupo de Química de Coordinación, quiero mostrar también mi más sincero agradecimiento a toda la gente que ha sido parte de mi tesis y mi vida en estos últimos cuatro años. En primer lugar, querría dar las gracias a Yves Journaux y al Laboratoire de Matériaux Magnetiques Moléculaires et Absorption X de París, por la amable acogida que me dispensó en mis estancias, y por el aprendizaje de las medidas del voltametría cíclica que me han sido de gran utilidad en mi trabajo. En especial, quería agradecerle a Rodrigue Lescouëzec su apoyo en todo lo que he necesitado, por facilitarme la vida en el laboratorio y por ayudarme en la búsqueda de mi postdoc. A Ruxi y a Abhi, muchas gracias por su amistad y por los buenos ratos que pasamos juntos durante mis estancias en París, o durante las visitas a Valencia. Y a Yanling Li, a quien debo el ajuste de una proporción importante de los espectros EPR de mi tesis, le agradezco mucho el tiempo que les dedicó, así como que me enseñara a hacer los ajustes yo misma.

Una parte fundamental del trabajo de la tesis son las estructuras de los compuestos. A ese respecto, agradezco profundamente a Catalina Ruiz Pérez, Jorge Pasán y Laura Cañadillas, del Laboratorio de Rayos X y Materiales Moleculares de la Universidad de La Laguna; así como a Giovanni de Munno y Donatella Armentano, del Departamento de Química de la Universidad de Calabria, el esfuerzo, la minuciosidad y el interés que han prestado siempre a la resolución de mis estructuras, obteniendo excelentes resultados que aportan una gran calidad al trabajo realizado.

En cuanto a las medidas EPR de mis compuestos, he de darles mil gracias a Chema y a Gloria, del Instituto de Ciencia Molecular, por la realización de las mismas, por su gran disponibilidad para ello y por sus esfuerzos y organización para que se obtuvieran los mejores resultados posibles, y todo ello siempre con una sonrisa en la cara. Muchas gracias a los dos por todo.

Dentro del grupo de Reactividad Fotoquímica, tengo que agradecerle muy sinceramente a Julia Pérez y a Raquel Galián el haberme permitido usar su fotorreactor durante los primeros años de mi tesis. Sin esta colaboración, mis compuestos fotomagnéticos no podrían haberse caracterizado tan cómodamente. En especial, gracias a Jordi, Carlos y Salva, siempre recordaré los interminables turnos para utilizar el equipo, así como el natural bronceado que todos lucíamos en pleno invierno gracias a él.

A todos los miembros del equipo de Química Supramolecular, quiero daros millones de gracias por vuestra amistad y vuestro apoyo incondicionales a lo largo de los cuatro años que ha durado esta tesis, por la acogida y la "adopción" infinitamente amables que me habéis dispensado, y por todos los inolvidables buenos ratos que he pasado a vuestro lado: cafés, cenas, fiestas, congresos, paellas, terapias, ratos de black stories (en sentido literal y figurado)… Fany, Raki, Javi, Jorge, Mario, Salva, Elena, Cristina, Teresa, Mari Paz, Esther, Bego… Sois unos amigos estupendos, gracias por haber estado ahí, sin vosotros lo hubiera tenido mucho más difícil.

A Noemí, con quien he conectado siempre de forma especial desde que nos conocimos en el QIES de Cartagena en 2010, por su simpatía, su buen humor, su paciencia para escuchar mis historias, y por estar siempre pendiente y preocupándose por mí desde el Departamento de Química Analítica, mil gracias.

A Tania, por su ayuda y su sinceridad cuando más necesarias han sido, y por sus ánimos, gracias de todo corazón.

A Mari Carmen, que desde el principio de la tesis ha estado a mi lado, animándome con sus bromas, participando en todas nuestras juergas y ha sido un apoyo moral constante durante estos cuatro años, muchísimas gracias. Un abrazo para la "loca del mocho", que allá donde vaya no creo que encuentre otra igual.

Fuera del ámbito científico, he de agradecer muy especialmente a mis padres y a mi hermano, y a toda mi familia en general, el cariño y el apoyo que me han dado siempre en cada situación, y todas las oportunidades que me han brindado en la vida, que hacen que a día de hoy esté donde estoy y que han permitido que la tesis saliera adelante.

A todos mis amigos, muchas gracias por estar siempre ahí, por los buenos ratos que siempre hemos pasado y pasaremos juntos, y por el apoyo moral que habéis supuesto desde siempre y especialmente durante el doctorado, sin vosotros no lo habría conseguido.

Al Ministerio de Ciencia e Innovación español, gracias por la financiación de la beca que me ha permitido realizar el master, la tesis y las estancias en el extranjero. Ha sido una etapa inolvidable donde he aprendido infinidad de cosas, a todos los niveles, que me serán muy útiles en el futuro.

Y por último, pero no menos importante, gracias, muchas gracias, a Julien. Desde que te conocí al final de mi primera estancia en París en primavera de 2011 has sido incondicional de mí, me has apoyado en los buenos y en los malos momentos, me has aportado un sinfín de consejos valiosísimos y has contribuido de manera muy importante a la búsqueda de mi postdoc, de la continuación de mi carrera investigadora y de mi integración en Francia a tu lado. Me has dado tu amor, tu risa y tu optimismo cuando más falta me hacían. Siempre, GRACIAS.

CHAPTER I

Introduction:
From Molecular Magnetism to Molecular Spintronics

Molecular spintronics is considered as one promising way for miniaturization of electronic circuits leading to highly integrated electronic and magnetic systems.[1] In order to build up a molecular spintronic circuit based on metal complexes,[2] it is necessary to generate and combine many molecular magnetic components such as wires, switches, or transistors.

As a result of extensive studies, various types of molecular electronic wires have been developed. In particular, organometallic wires consisting of a π-conjugated system bridging the redox active metal centers such as in (oligoalquinyl dinuclear ruthenium complexes, M–(C≡C)$_n$–M (Figure I.1), turn out to be highly efficient.[3-5]

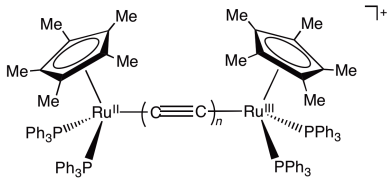

Figure I.1 General chemical structure of the dinuclear mixed valence pentamethylcyclopentadienylbis(triphenylphosphine)ruthenium(II,III) complexes with oligoethinyl bridging ligands.

Although molecular switching systems have also been studied,[6] examples of switching of the conducting and non-conducting states of molecular wires by external stimuli are still rare. For instance, a photoswitchable molecular electronic wire containing the photochromic dithienylethene (DTE) unit as linker has been recently reported,[7] the communication between the redox active iron centres being switched on and off by UV/visible light irradiation (Figure I.2).

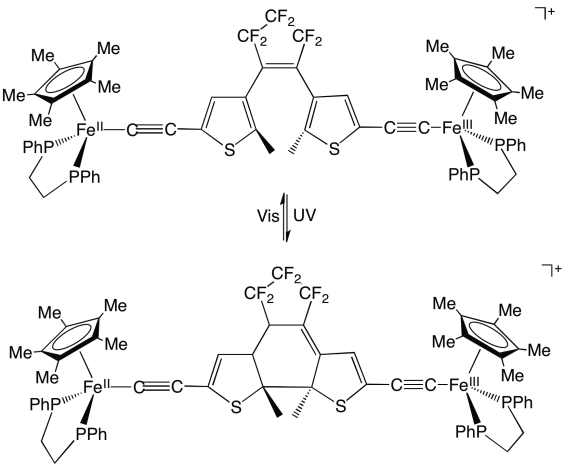

Figure I.2 General chemical structure of the dinuclear mixed valence pentamethylcyclopentadienyl-bis(1,2-diphenylphosphineethane)iron(II,III) complex with a photochromic diethinyl-dithyenylethene bridging ligand illustrating the open and closed isomers responsible for the photoswitchable electronic behavior.

The design and synthesis of novel bridging ligands which can transmit both **electronic** and **spin coupling** effects over long distances in a switchable manner are a major goal in the field of molecular spintronics, which requires both a skillful organic synthesis and a deep understanding of the electron exchange mechanism. With the advent of calculations based on the density functional theory (DFT) combined with the broken-symmetry (BS) approach, it has been possible not only to reproduce but also to predict the electronic and magnetic properties of polynuclear metal complexes.[8]

In the present thesis, we report the preparation of dinuclear copper(II) complexes with a new family of extended π-conjugated aromatic bridging ligands. We studied our ligands ability of acting as molecular wires in the transmission of the magnetic coupling between metal centers separated by relatively long intermetallic distances. Moreover, we demonstrated that non-innocent ligands are able to work as molecular switches because of the two different spin states ("ON-OFF" mechanism) that can be reversibly afforded by simple electro- or photochemical processes. Let us briefly develop this point in the following two sections by including a recall of our previous results in this area, together with a proposal of the main objectives of this thesis.

I.1 Long-Range Magnetic Coupling through Extended π-Conjugated Aromatic Bridges: Background and Foundations

Polymetallic complexes with strong intramolecular electronic interactions have been a topic of large interest in molecular magnetism and molecular electronics.[9] Besides their interest as models for the fundamental research on electron exchange and electron transfer phenomena between distant metal centers through extended bridges, homo- and heterovalent polynuclear complexes are also of great importance in the ''bottom-up" approach to molecular spintronic devices.[10,11]

From a fundamental point of view, electron exchange and electron transfer are intimately related processes that rely on the transmission of spin- and charge-based electronic effects, respectively.[12] Since the pioneering work of Creutz and Taube,[12a] long-distance intervalence electron transfer through extended π-conjugated aromatic bridges has been achieved in dinuclear mixed valence pentaammineruthenium complexes with either *meta*- or *para*-substituted oligophenylenedipyridine bridging ligands that allow the variation of the intermetallic distances between 8 and 20 Å (Figure I.3).[13] However, similar examples of long-range magnetic coupling in dinuclear exchange coupled complexes are still scarce.[14]

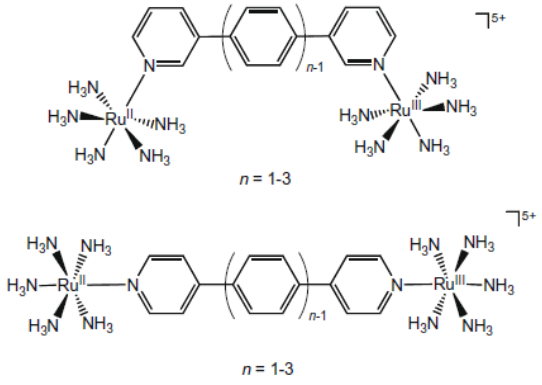

Figure I.3 General chemical structure of the dinuclear mixed valence pentaammineruthenium(II,III) complexes with oligophenylenedipyridine bridging ligands illustrating the two octahedral metal redox sites separated by a *meta*- or *para*-substituted oligophenylene spacer made up of several benzene rings as repeat units connected by carbon–carbon single bonds.

Dinuclear copper(II) complexes with one unpaired electron by metal center constitute the simplest systems to investigate electron exchange interactions through extended organic bridges from both experimental and theoretical points of view (see Panels A and B).[15–22]

Panel A: ***Spin hamiltonian formalism of the electron exchange interaction in dinuclear copper(II) complexes***

The exchange interaction which takes place between the two metal ions in a dinuclear complex is described by the spin Hamiltonian:

$$\mathbf{H} = -J\,\mathbf{S}_A \cdot \mathbf{S}_B$$

being S_A and S_B the individual spin values referred to the metal centers A and B, and J the magnetic coupling constant between them ($J = J_{AB}$). A total spin value of the system (S) can be defined, with values from the substraction to the addition of the individual spin values of the two separated metal centers (S_A and S_B):

$$S = |S_A + S_B| \ \ldots \ |S_A - S_B|$$

Dinuclear copper(II) complexes constitute the simplest situation ($S_A = S_B = 1/2$) (Scheme I.1). In this case, only values $S = 0$ and $S = 1$ are available. These values define the energy levels generated in the system by the magnetic coupling, just two in this case, singlet ($2S + 1 = 1$) and triplet ($2S + 1 = 3$). The gap of energy between these two states is given by the magnetic coupling constant J:

$$J = E(S = 0) - E(S = 1)$$

For the distribution of energetic states, there are thus two possibilities:

- $E(S = 0) < E(S = 1)$: the system lies on a singlet fundamental state preferently. Attending to the previously defined hamiltonian, negative values are found for the magnetic coupling constant J, so the system presents an antiferromagnetic interaction, with a preferent antiparallel disposition of local spins (Scheme I.1a).

- $E(S = 1) < E(S = 0)$: the system lies on a triplet fundamental state preferently. Attending to the previously defined hamiltonian, positive values are found for the magnetic coupling constant J, so the system shows an antiferromagnetic interaction, with a preferent antiparallel disposition of local spins (Scheme I.1b).

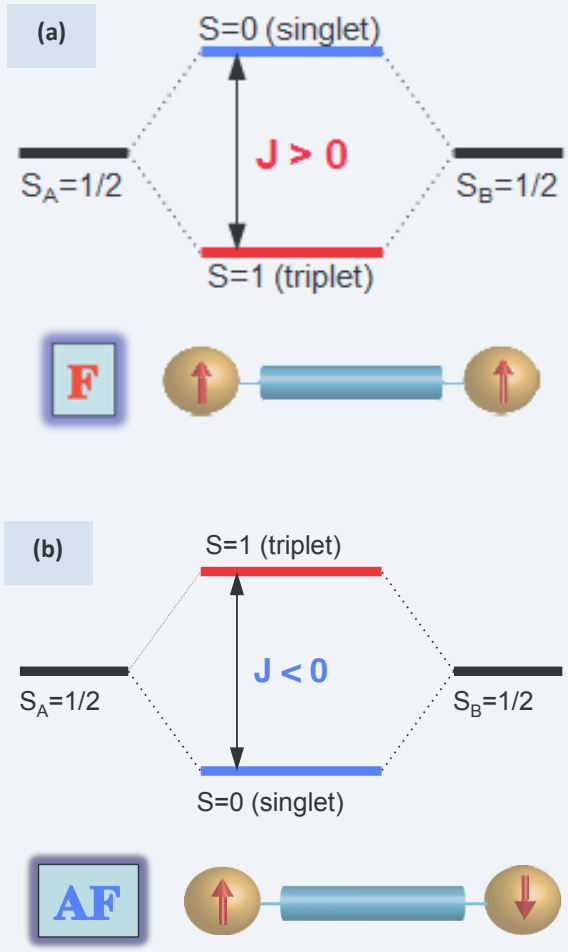

Scheme I.1 Energy level diagram for (a) ferro- and (b) anfiterromagnetically coupled dinuclear copper(II) complexes.

Panel B: ***Mechanism of the magnetic interaction in dinuclear copper(II) complexes: molecular orbital vs. valence bond models***

The mechanism of the magnetic interaction, called electron exchange (or super-exchange), in a dinuclear copper(II) complex can be easily described by considering the molecular orbital model developed by Hoffman *et al*.[15a] In this model, the singlet-triplet energetic separation ($\Delta E_{ST} = -J$) has both ferromagnetic (J_F) and antiferromagnetic (J_{AF}) contributions, as expressed in eq I.1.

$$-J = J_F + J_{AF} = -2K_{ab} + (\varepsilon_1 - \varepsilon_2)^2 / (J_{aa} - J_{ab}) \qquad \text{(I.1)}$$

The ferromagnetic contribution is described by the bielectronic exchange integral (K_{ab}) between the unpaired electrons over each metalllic center. On the other hand, the antiferromagnetic contribution is ruled by the energetic gap ($\delta = \varepsilon_1 - \varepsilon_2$) between the two singly occupied molecular orbitals (SOMOs) resulting from the interaction of the metallic fragments and the bridging ligands orbitals, as shown in Scheme I.2.

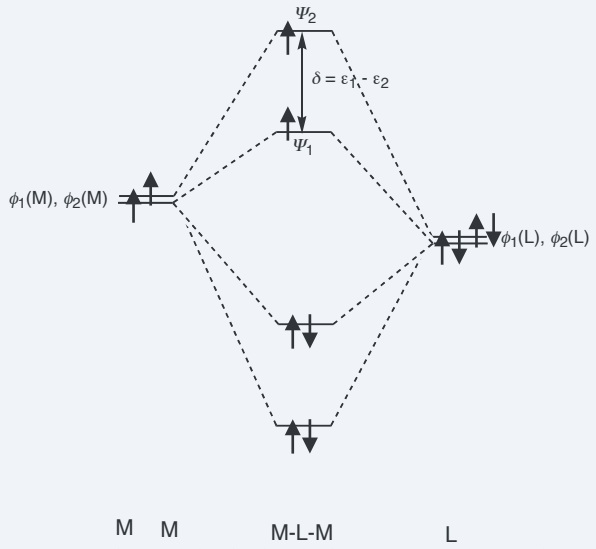

Scheme I.2 Singly occupied molecular orbitals (SOMOs) resulting from the interaction of the orbitals of the metallic centers and the bridging ligand in the Hoffman mechanism.

The ψ_1 and ψ_2 SOMOs coming from the symmetric and antisymmetric antibonding combinations of the metals and ligands orbitals (eq I.2 and I.3, being a, c >> b, d) respectively, have a basically metallic character. In most of cases, a negligible ferromagnetic contribution is found, so that the energetic gap between SOMOs **($\delta = \varepsilon_1 - \varepsilon_2$)** is directly related to the value of the magnetic coupling constant ($-J$).

$$\psi_1 = a\phi_1(M) - b\phi_1(L) \qquad \text{(I.2)}$$

$$\psi_2 = c\phi_2(M) - d\phi_2(L) \qquad \text{(I.3)}$$

There exists, however, an alternative valence bond model of the magnetic interaction in a dinuclear copper(II) complex, known as the Anderson generalized mechanism.[12e] In this model, the electrons jump from one site to the other through the ligand orbitals, with the intermediacy of several neutral, metal-to-ligand or ligand-to-metal charge transfer configurations, as shown in Scheme I.3.

The magnetic coupling between the unpaired electrons occupying the *a* and *b* magnetic orbitals of the two metal centers through the bridging ligand is also governed by two main factors, as expressed in eq I.4.

$$-J = J_F + J_{AF} = -2K - 4\,t^2 / U \qquad \text{(I.4)}$$

The first contribution is the direct exchange integral, $K = \langle a(1)b(2)|r_{12}^{-1}|b(1)a(2)\rangle$, which is always positive and hence favors a ferromagnetic coupling, but which is expected to decrease rapidly with the intermetallic distance. The second contribution is the kinetic exchange, which is always negative and hence favors an antiferromagnetic coupling, provided that the hopping integral *t* between *a* and *b* is non-zero. The on-site repulsion *U* is the energy difference between the neutral and the ionic configurations. This contribution is brought by the delocalization of the electrons between the two magnetic orbitals.

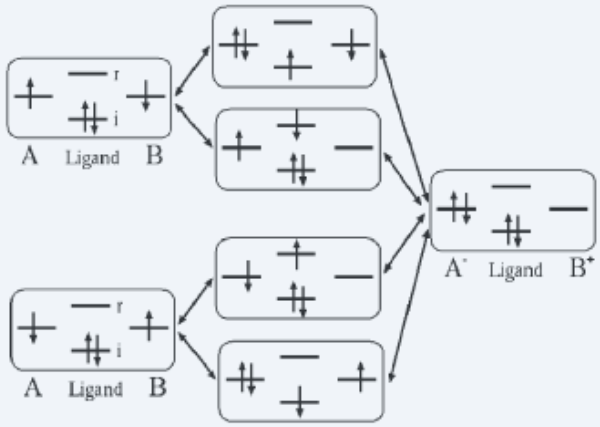

Scheme I.3 Configurations involved in the Anderson generalized mechanism. Only one of the two ionic forms is represented. The matrix elements (not indicated) are hopping integrals between the magnetic centers and the ligands (taken from ref. 12e)
.

Besides this spin delocalization mechanism, there is a spin polarization mechanism which goes through excited configurations involving a triplet state on the bridge and a triplet state in the magnetic orbitals, as shown in Scheme I.4.

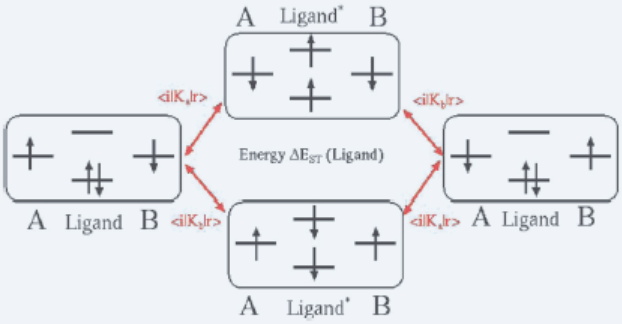

Scheme I.4 Configurations involved in the mechanism of the double spin polarization. (Ligand)* means that the ligand is in an excited state, namely a triplet. The matrix elements between the determinants are indicated by the arrows (taken from ref. 12e) .

Since this mechanism never involves any ionic configuration, its effect on the magnetic coupling results in a modification of the exchange integral K, such that the one showed in eq I.5:

$$K^{\text{eff}} = K + 2\sum_{i,r}\frac{\langle i|K_a|r\rangle\langle r|K_b|i\rangle}{\varepsilon_r - \varepsilon_i} \qquad \text{(I.5)}$$

where i and r are respectively, occupied and vacant MOs of the ligand, ε_r - ε_i is their energy difference, and K_a and K_b are the exhange integrals $\langle i|K_a|r\rangle = \langle i(1)a(2)|r_{12}^{-1}|r(2)a(1)\rangle$ and $\langle i|K_b|r\rangle = \langle i(1)b(2)|r_{12}^{-1}|r(2)b(1)\rangle$, respectively. One should notice that while K is always positive, K_{eff} can be either positive or negative.

The spin polarization mechanism is a real physical phenomenon. It is for instance responsible for the appearance of local spin densities which are opposite to the dominant ones in radicals. Considering a dinuclear copper(II) complex, the occurrence of a spin polarization mechanism for the exchange interaction between the two distant unpaired electrons, as an alternative pathway to the usually dominant spin delocalization mechanism, has come up. Specifically, the prevalence of the spin polarization mechanism was proposed on the basis of the appearance of non-negligible spin density on the bridge.

Thus, it would mainly be taken in consideration for long polarizable organic bridging ligands, in which relative contributions of spin polarization and kinetic exchange to the resulting magnetic coupling would be found. On the contrary, for short organic bridging ligands, the magnetic exchange would be only controlled by usual direct exchange. In fact, varying percentage of the relative contributions of the Anderson and spin polarization mechanisms as a function of the bridge length are expected. While magnetic couplings are dominated by the kinetic exchange for short-length bridges, the relative contribution of spin polarization increases with the length of the bridge. One may therefore expect that long, highly spin polarizable ligands would induce a better magneto-communication than shorter ones.

In their seminal work,[21a,b] Felthouse and Hendrickson reported a series of dicopper(II) complexes with *p*-phenylene- (ppda) and *p*-biphenylenediamine (bpda) bridges that possess strong to moderate intramolecular antiferromagnetic couplings, respectively. Although they pointed out that the exchange interaction between the CuII ions through the *para*-substituted phenylene and biphenylene spacers mainly involved σ-type orbital pathways, the alternative π-type orbital pathways cannot be totally neglected in the light of our recent results.[21c] In fact, we have reported on the structure and magnetic properties of the related pair of *meta*- and *para*-phenylenediamine-bridged dicopper(II) complexes with the tetradentate tris(2-aminoethyl)amine tripodal ligand (Figure I.4).

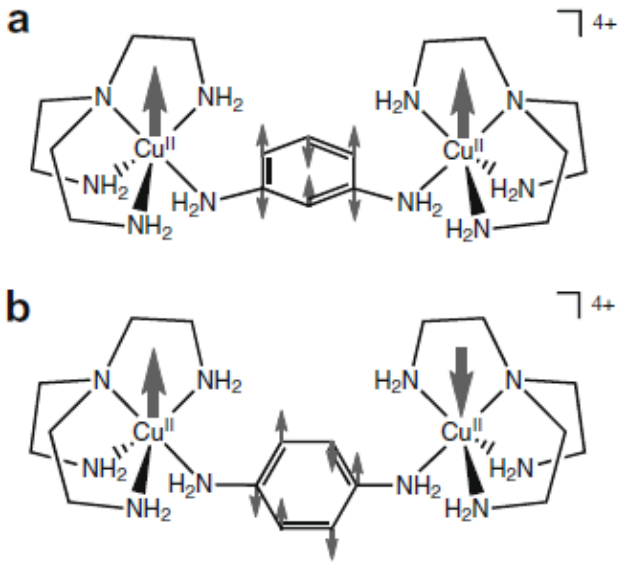

Figure I.4 Chemical structure of the dinuclear tris(2-aminoethyl)aminecopper(II) complexes with (a) *meta*- and (b) *para*-substituted phenylenediamine bridging ligands showing the different spin alignment resulting from the alternance of the spin densities on the phenylene spacer. This fact is extracted from McConnell mechanism.

The overall orthogonal conformation of the resulting dicopper(II) complexes has allowed for an evaluation of the efficiency of the π- versus σ-pathway for the propagation of the exchange interaction between the two unpaired electrons occupying the d_{z^2} type orbital (so-called "magnetic orbitals") of each trigonal bipyramidal Cu^{II} ion across the extended aromatic bridge (Figure I.5). In fact, coordination bonds in these systems involve the p_z-type orbitals of the nitrogen atoms that are orientated parallel to the p_z-type orbitals of the carbon atoms. Because of the orthogonal disposition of the trigonal axis of each Cu^{II} ion with respect to the mean plane of the benzene rings, a delocalized spin density is expected from d_{z^2} copper orbital through p_z nitrogen orbital and along the π system of the spacer.

Hence, in spite of the relatively large intermetallic separations, moderate ferro- to strong antiferromagnetic coupling have been observed for these two dicopper(II) complexes with *meta*- and *para*-phenylenediamine bridges, respectively. Both effects result from the spin polarization of the extended π-conjugated bond system of the phenylene spacer with *meta*- and *para*-substitution patterns, as confirmed by DFT calculations.[21c]

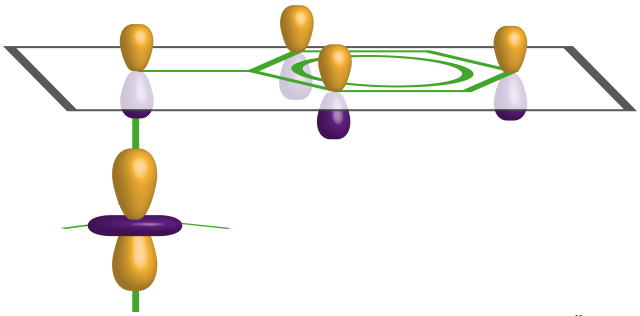

Figure I.5 Illustration of the magnetic orbital of the trigonal bipyramidal Cu^{II} ion in phenylendiamine-bridged dinuclear tris(2-aminoethyl)aminecopper(II) complexes.

A spin polarization mechanism is able to explain the ferromagnetic interaction for *meta*- substitution pattern, and, on the contrary, the antiferromagnetic exchange for *para*- substitution pattern in these aromatic diamine-bridged dicopper(II) complexes (Figures I.4a and I.4b, respectively). In this situation, this spin density would be equal to the one showed by the carbene radical group in a phenylenedicarbene. So, as it happens with phenyldicarbenes, the magnetic interaction is ruled by the exchange mechanism called spin polarization, which is related to McConnell mechanism (see Panel C).

In a subsequent work,[21d] we have shown both experimentally and theoretically that linear π-conjugated oligophenylenediamines with either one, two, or three *para*-substituted phenylene units, $-(C_6H_4)_n-$ (n = 1–3), are really effective to transmit electron exchange interactions between two Cu^{II} ions separated by relatively large intermetallic distances (Figure I.6).

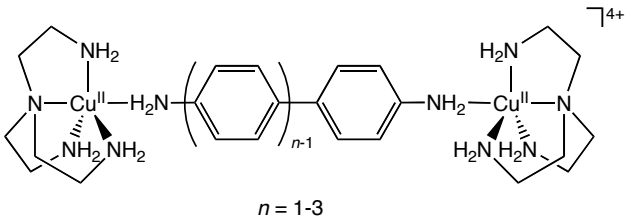

Figure I.6 General chemical structure of the dinuclear copper(II) complexes with *para*-substituted oligophenylenediamines as bridging ligands.

Together with an almost linear increase in the estimated intermetallic distance (r), a rather slow exponential decay of the antiferromagnetic coupling ($-J$) with the number of phenylene repeat units (n = 1–3) is experimentally observed in the corresponding oligo-*p*-phenylenediamide-bridged dinuclear copper(II) complexes.

The antiferromagnetic nature of the electron exchange interaction results from a **spin polarization mechanism** through the extended π-conjugated bond system of the oligophenylene spacers with *para*-substitution pattern, as confirmed by theoretical calculations. This unique series of dinuclear copper(II) complexes with oligo-*para*-phenylenediamine bridging ligands, which can be viewed as the simplest analogues of the well-known Creutz-Taube complexes with oligophenylenedipyridine bridging ligands (see Figure I.3), constitutes thus a rare example of long-distance magnetic coupling in transition metal complexes.

Panel C: ***Spin polarization mechanism of the electron exchange interaction in phenylenedicarbenes***

The spin polarization mechanism in π-polyradicals relates the magnetic properties to the number of atoms that conform the exchange pathway between the metallic centers (*n*). As a matter of fact, a ferromagnetic behavior is found for even values of *n*. On the contrary, for odd values of *n*, the system presents an antiferromagnetic coupling, as it is shown in Scheme I.5 for the simplest phenylenedicarbene diradicals.

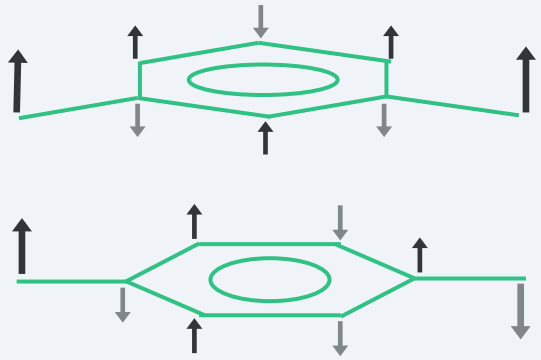

Scheme I.5 Spin polarization mechanism of magnetic exchange coupling in (a) *meta*- and (b) *para*-substituted phenyldicarbenes.

The magnetic properties in phenylenedicarbene diradicals are ruled by the McConell mechanism, whereby the magnetic interaction does not consider individual spins localized over the paramagnetic centers A and B:

$$\mathbf{H} = -J_{AB}\, S_A \cdot \mathbf{S}_B$$

but it considers a delocalized spin density over all the atoms in the π system, so there is an effective interaction of the spin densities of adjacent atoms i and j, according to:

$$\mathbf{H} = -J_{ij}\, \mathbf{S}_i \cdot \mathbf{S}_j$$

Considering a chemical bond between atoms i and j, spin densities corresponding to that atoms are opposite due to the spin polarization phenomena. As a consequence, there is a ferromagnetic interaction for an exchange containing an odd number of atoms (Scheme I.5a). On the contrary, when the two metal centers are separated by an even number of atoms, an antiferromagnetic exchange is found (Scheme I.5b).

From a molecular orbital theory point of view, it is found that most of organic compounds present all their electrons contained in deep and very stable orbitals in their fundamental state. On the contrary, in π-n-radical systems, unpaired electrons are placed in degenerated non-bonding molecular orbitals (SOMOs), which leads to the presence of different states that are very close from an energetic point of view.

In the particular case of biradicals, two specific conditions for the triplet state being more stable than the singlet are necessary. First of all, the overlap integral including the two orbitals containing the unpaired electrons must be close to zero. On the other hand, the exchange integral between the two orbitals must be large. This way, the antiferromagnetic contribution will be null, while the ferromagnetic one will be sizeable, so that ferromagnetic behavior will prevail. For a *meta*-substitution pattern, SOMOs orbitals of the two carbene radicals are degenerated. Thus, the overlap integral between them and consequently the antiferromagnetic contribution are null, and a global ferromagnetic exchange is found.

For a *para*-substitution pattern, the molecular orbitals containing the unpaired electrons of the two carbene radicals (SOMOs) are partially constituted by orbitals of the phenylene spacer presenting different bonding and anti-bonding contributions with different energies. So that, each SOMO presents a different energy. For this reason, singlet state becomes less energetic than the triplet and an important antiferromagnetic contribution is found.

More recently, we have theoretically shown that linear π-conjugated oligoacenediamines consisting of linearly fused benzenoid units, $-(C_{2+4n}H_{2+2n})-$ (n = 1–10), with either *meta*- or *para*-substitution pattern at the carbon atoms of the terminal benzene rings, are much more effective than oligo-*p*-phenylenediamines to transmit electron exchange interactions between two Cu^{II} ions separated by similar intermetallic distances (Figure I.7).[21e]

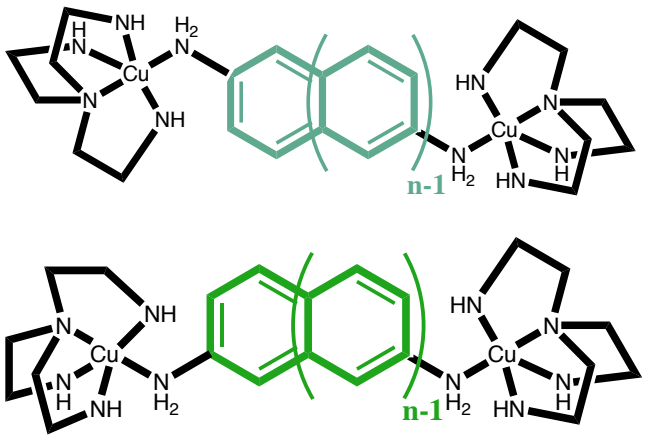

Figure I.7 General chemical structure of the dinuclear copper(II) complexes with (a) *meta*- and (b) *para*-substituted oligoacenediamines as bridging ligands.

The ferromagnetic or antiferromagnetic nature of the electron exchange interaction (for *meta*- and *para*- substitution patterns, respectively) results from a **spin polarization mechanism** through the extended π-conjugated bond system of the oligoacene spacers, as confirmed by theoretical calculations. This unique series of dinuclear copper(II) complexes with oligoacene bridging ligands, becomes a further step in long-distance magnetic coupling in transition metal complexes.

Together with an almost linear increase in the estimated intermetallic distance (r), a rather slow exponential decay of the antiferromagnetic coupling ($-J$) with the number of benzenoid repeat units (n = 1–4) is theoretically observed in the corresponding dinuclear copper(II) complexes for low n values.

However, for higher values of n (n > 4), long polyradical spacers are found, whose nature provides a stronger magnetic coupling than the shorter ones. So that, the magnetic exchange does not remain constant from n = 4, but it is increased for longer spacers. Thus, we get a wire-like magnetic behavior, which was not found for the previous series with oligo-*para*-phenylenediamine.

I.2. Electro- and Photoswitchable Molecular Magnetic Wires: Aims and Scope

Dinuclear copper(II) metallacyclophanes have recently emerged as ideal model systems for the study of the electron exchange mechanism between paramagnetic metal centers containing one unpaired electron ($S_A = S_B = 1/2$) through extended π-conjugated aromatic bridges in a discrete metallacyclic entity, but however they have received limited attention.[23–25] The variation of the ligand spacer may control both the overall structure and the magnetic behavior of the metallacyclophane complex, and the influence of different factors such as the topology and conformation of the bridging ligand can then be investigated in a systematic way.

In particular, the research on long distance magnetic coupling between two Cu^{II} ions have been addressed by several groups through the use of coordinating group substituted aromatic diamines[23] and related diimine[24] and diamide[25] derivatives as bridging ligands which self-assemble to give the corresponding double-stranded metallacyclic complexes, with more or less satisfactory results (Table 1 and Figure I.8).

Hence, with one notable exception,[24d] weak antiferromagnetic couplings ($-J$ values smaller than 2.2 cm^{-1}) have been observed for the dicopper(II) metallacyclophanes with amine- and imine-based aromatic bridges possessing rather long intermetal distances (r values larger than 7.0 Å) (Table 1, entries 1–8).[23,24b,c,e] On the contrary, Inoue *et al.* have reported moderate to strong antiferromagnetic couplings in the related dicopper(II) metallacyclophanes with amide-based aromatic bridges ($-J$ values up to 105 cm^{-1}) (Table 1, entries 9–11).[25d] It appears that the exchange interaction between the Cu^{II} ions involves predominantly π-type orbital pathways in the amide series, whereas it is mainly transmitted through the σ-electron system of the aromatic bridge in the amine and imine series, with little or no contribution from the π-electron system.

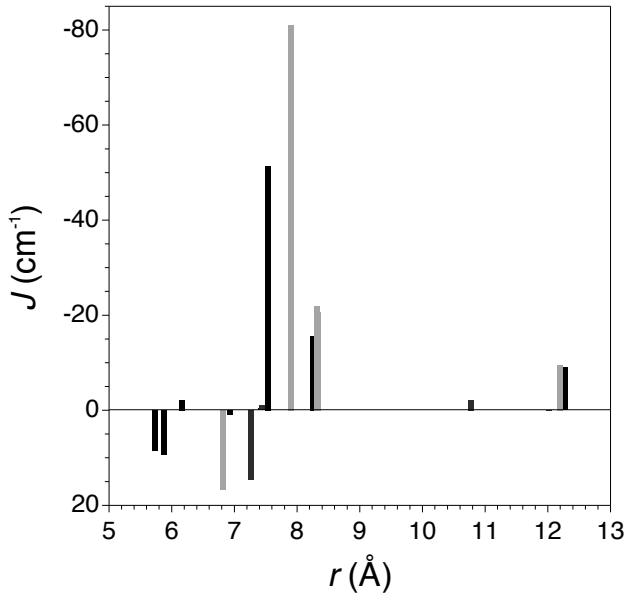

Figure I.8 Variation of the magnetic coupling constant with the intermetallic distance in dinuclear copper(II) metallacyclophanes with different coordinating group-substituted aromatic diamines as bridging ligands: amine (white bars), imine (grey bars), and amide (black bars) series (data from Table 1).

Table I.1 Selected experimental magneto-structural data for dinuclear copper(II) metallacyclophanes

Complex[a]	Bridge	*r* (Å)[b]	*J* (cm^{-1})[c]	Ref
	Amine series			
$Na_4[Cu_2(m\text{-pdta})_2] \cdot 18H_2O$	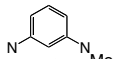	6.93	< 1.0	23a
$Na_4[Cu_2(2,4\text{-tdta})_2] \cdot 20H_2O$	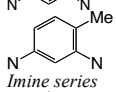	n.a.	< 1.0	23b
	Imine series			
$[Cu_2(m\text{-salphen})_2] \cdot 2CHCl_3$	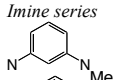	7.44	–1.0	24a, 24b
$[Cu_2(2,4\text{-saltoen})_2]$	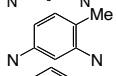	n.a.	–0.9	24c
$[Cu_2(2,6\text{-saltoen})_2]$	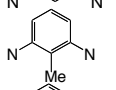	n.a.	–1.1	24c
$[Cu_2(m\text{-acacphen})_2]$	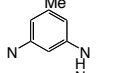	7.27	+14.6	24d
$[Cu_2(hbca)_2] \cdot 2CHCl_3 \cdot 2H_2O$	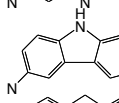	10.78	–2.2	24e
$[Cu_2L_2] \cdot 2MeCN$	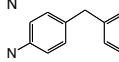	12.02	–0.025[d]	24f
	Amide series			
$[Cu_2(bis\text{-}edtapdn)]^{4-}$	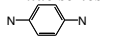	n.a.	–70 to 105[e]	25d
$(NH_4)_4[Cu_2(bis\text{-}edtanap)] \cdot 18.5H_2O \cdot (CH_3)_2CHOH$	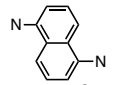	8.32	–22[e]	25b, 25d
$[Cu_2(bis\text{-}edtabpe)]^{4-}$	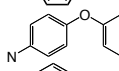	n.a.	≤ 0[e]	25d
$Na_4[Cu_2(mpba)_2] \cdot 8H_2O$	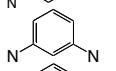	6.82	+16.8	26a
$(Bu_4N)_4[Cu_2(Mempba)_2] \cdot 4H_2O$	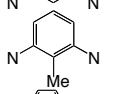	7.20	+16.4	26d
$Li_4[Cu_2(ppba)_2] \cdot 10H_2O$	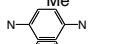	n.a.	–95	26b
$Na_4[Cu_2(ppba)_2] \cdot 11H_2O$	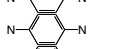	7.91	–81	26b
$(Ph_4P)_4[Cu_2(ppba)_2] \cdot 8H_2O$		n.a.	–94	26b
$Li_4[Cu_2(bpba)_2] \cdot 12H_2O$	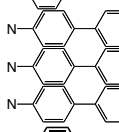	n.a.	–11.5	26b
$Na_4[Cu_2(bpba)_2] \cdot 12H_2O$		12.19	–9.5	26b
$(Bu_4N)_4[Cu_2(bpba)_2] \cdot 10H_2O$		n.a.	–8.7	26b
$Li_4[Cu_2(naba)_2] \cdot 12H_2O$	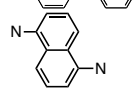	n.a.	–20.5	26c
$(Ph_4P)_4[Cu_2(naba)_2] \cdot 8H_2O$	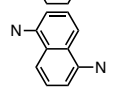	8.33	–20.7	26c
$Li_4[Cu_2(anba)_2] \cdot 12H_2O$	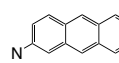	n.a.	–21.2	26c
$(Ph_4P)_4[Cu_2(anba)_2] \cdot 4H_2O$	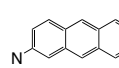	n.a.	–23.0	26c

[a] Ligand abbreviations: H_4-*m*-pdta = 1,3-phenylenediamine-*N,N,N',N'*-tetraacetic acid; H_4-2,4-tdta = 2,4-toluenediamine-*NN,N',N'*-tetraacetic acid; H_2-*m*-salphen = *N,N'*-1,3-phenylenebis(salicylideneimine); H_2-2,4-saltoen = *N,N'*-2,4-toluenebis(salicylideneimine); H_2-*m*-acacphen = *N,N'*-1,3-phenylenebis(acetylaceteneimine); H_2hbca = *N,N'*-3,6-9*H*-carbazolebis(salicylideneimine); H_2L = *N,N'*-4,4'-methylenebiphenylenebis(2-tosylaminobenzaldimine); H_8bis-edtapdn = 2,9,18,25-tetraoxo-4,7,20,23-tetrakis(carboxymethyl)-1,4,7,10,17,20,23,26-octaaza[10.10]paracyclophane; H_8bis-edtanap = 2,9,22,29-tetraoxo-4,7,24,27-tetrakis(carboxymethyl)-1,4,7,10,21,24,27,30-octaaza[10.10](1,5)naphthalenophane; H_8bis-edtabpe = 2,9,25,32-tetraoxo-4,7,27,30-tetrakis(carboxymethyl)-1,4,7,10,24,27,30,33-octaaza[10.1.10.1]paracyclophane; H_4mpba = *N,N'*-1,3-phenylenebis(oxamic acid); H_4Mempba = *N,N'*-2-methyl-1,3-phenylenebis(oxamic acid); H_4ppba = *N,N'*-1,4-phenylenebis(oxamic acid); H_4bpba = *N,N'*-4,4'-biphenylenebis(oxamic acid); H_4naba = *N,N'*-1,5-naphthalenebis(oxamic acid); H_4anba = *N,N'*-2,6-anthracenebis(oxamic acid). [b] *r* is the intermetallic distance. [c] *J* is the exchange coupling constant in the spin Hamiltonian $H = -J\ S_A \cdot S_B$ ($S_A = S_B = 1/2$). [d] Intermolecular magnetic coupling. [e] Magnetic data evaluated from the temperature dependence of the EPR solution spectra in 60% MeOH (pH ca. 10).

Our strategy in this field is based on the use of bridging ligands possessing two oxamato donor groups separated by extended π-conjugated aromatic spacers that are able to self-assemble spontaneously with Cu^{II} ions to form exchange-coupled double-stranded dicopper(II) metallacyclophanes (Figure I.9).[26]

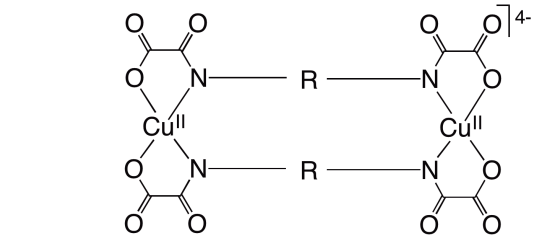

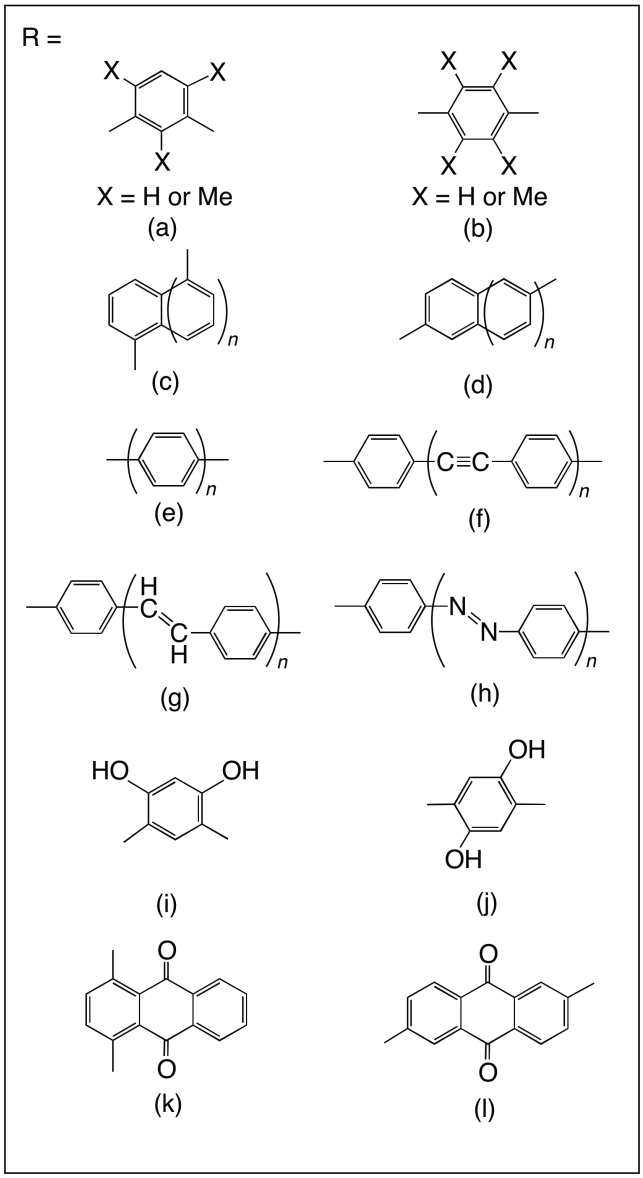

Figure I.9 Chemical structure of the oxamato-based dicopper(II) metallacyclophanes with electro- and photoswitchable aromatic spacers as prototypes of molecular magnetic devices for molecular spintronics.

Panel D: ***Magnetic wire behavior***

"Molecular magnetic wires" (MMWs) are a major and basic goal in the emerging field of molecular spintronics. In contrast to conventional charge transport-based molecular electronic wires, MMWs may offer a new design concept for the transfer of information over long distances based on purely electron exchange interactions and without current flow.

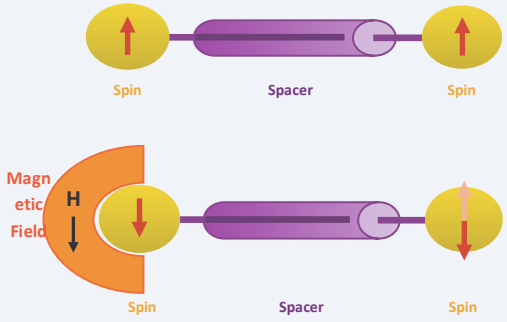

Scheme I.6 Illustration of the transfer of information through a molecular magnetic wire.

The target in this field is the obtention of a long-distance magnetic coupling between two metal centers bonded by a bridging ligand that leads to a **wire-like magnetic behavior** (Scheme I.6). So that, a perturbation induced at the beginning of the wire generates a change at the end of it. A transmission of information takes place in this process through either of these situations:

- Along the σ-pathway of the spacer: very efficient at short distances but nearly negligible for long spacers.

- Along the π-pathway of the spacer: more efficient that the previous one and being possible for long spacers.

In these systems, two different cases can be distinguished: polyradical or non-polyradical spacers (Scheme I.7).

A weak but non-negligible interaction between metal centers would be observed for a system in which the electronic density of the metals is just partially delocalized over the ligands (non-polyradical spacer). In this case, the π-pathway of the spacer does not allow for the long distance transmission of information (Scheme I.7a). This is a consequence of the drastic decay of the magnetic coupling with the distance.

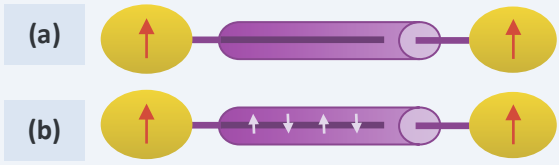

Scheme I.7 Illustration of the weak and strong magnetic coupling in a non-polyradical (a) and a polyradical spacer (b).

A different situation is found for long polyradical spacers with a low gap HOMO-LUMO that allow transmission along their π-pathway (Scheme I.7b). In this case, the unpaired electrons are found in determined regions of the ligand skeleton. This radical zones act as intermediates in magnetic exchange, providing thus two strongly correlated metal centers. Each metal presents a strong coupling with the closest radical in the spacer, at the same time connected to the next unpaired electron of the ligand. This connecting chain is followed until the second metal center is reached.

This way, the magnetic exchange does not take place between the unpaired electrons over the two distant metal centers but through the ligand electrons, reminding an electric field behavior over a wire, in which electrons move slowly one after other, making the impression of a high speed current.

So, it is much stronger than the one found for the previous systems with non-polyradical spacers. The two metal centers are further in distance but magnetically closer.

Panel E: ***Magnetic charge storage behavior***

"Molecular magnetic capacitors" (MMCs) are electroactive (oxidizable and reducible) molecules with several chemically accessible oxidation levels at the exchange-coupled spin carriers that can store and deliver an electric charge. As a result of this behavior, a parallel separation of the spin carriers occurs in their corresponding oxidized and reduced states, so that a transistor-like behavior on the molecular scale can be achieved (Scheme I.8).

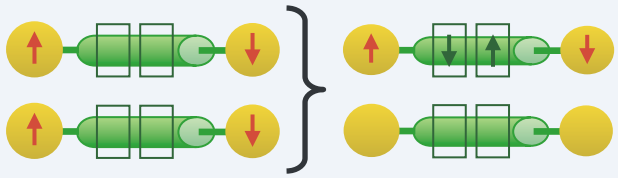

Scheme I.8 Illustration of the charge storage process in a molecular magnetic capacitor.

An alternative molecular-scale transistor design, and one particularly well suited to construction from metal centers, is that based on the Quantum-dot Cellular Automata (QCA) paradigm. In this context, the term "dot" refers to a unit charge, and can therefore be represented by a redox center, which essentially treats binary information as one of two electronic or magnetic states of a single molecule or nanoscale island.[27]

For example, a majority logic gate can be constructed from three QCA cells, as shown in Scheme I.9. Therefore, the state of the central cell depends on the state of the adjacent input cells.[28] Given the robust, chemically reversible redox processes associated with a vast array of simple metal–ligand combinations, there is obviously great potential for polymetallic complexes to find application in the construction of such QCA-based molecular logic systems.

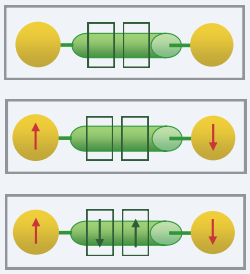

Scheme I.9 Illustration of the three possible redox states for a QCA cell to be used in the construction of a logic gate.

Panel F: ***Magnetic switching behavior***

"Molecular magnetic switches" (MMSs) are molecules presenting two metastable states ('ON/OFF') having totally different magnetic properties which can be reached in a reversible manner through the operation of an external stimuli. The spins of the magnetic centers are ferro- or antiferromagnetically coupled in one of the states ('ON'), whereas they are magnetically uncoupled in the other one ('OFF') (Scheme I.10).

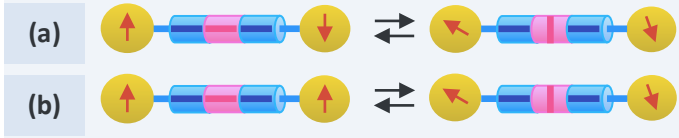

Scheme I.10 Illustration of the switching behavior in a molecular magnetic switch, being the magnetic exchange either antiferromagnetic (a) or ferromagnetic (b).

These external stimuli can be electronic or photonic. For example, there are molecules formed by two localized spins whose magnetic interaction can be switched ON and OFF by means of a redox-active bridging unit (electroswitching magnetic behavior).

Another possibility is to have systems in which the magnetic connection between the spins depends on the wavelength of the irradiation light. These photo stimuli are able to modify the molecule, permitting or forbidding the magnetic exchange through the photo-active bridging unit (photoswitching magnetic behavior).

Apart from the previous ones, there is a huge variety of factors that can have influence over these magnetically coupled/isolated systems in a reversible way, such as pH, pressure, temperature, etc. Thus, a vast amount of non-exploded molecular switches are available to be explored and become essential components of electronic circuits in the field of molecular nanospintronics.

In general terms, extension of the control of current flow or localization of charge through a molecular assembly in response to one or many input signals leads to the concept of developing molecule-based logic circuits.[29] The ability of the metal centers to respond to changes in photoexcitation or electrochemical potential together with the geometrical features which allow the precise positioning in space of substituent groups makes such systems particularly attractive for the construction of highly integrated molecular circuits.[30]

First, we demonstrated that the appropriate choice of the topology of the bridging ligand allows to control the nature and magnitude of the magnetic coupling between the metal centers in the corresponding dicopper(II) meta- and paracyclophanes (Figures I.9a and I.9b).[26a,b,d] In these systems, the ferromagnetic or antiferromagnetic nature of the electron exchange interaction results from a **spin polarization mechanism** through the extended π-conjugated bond system of the phenylene spacers with *meta* and *para* substitution pattern, as shown earlier for the aforementioned dinuclear copper(II) complexes with *meta*- and *para*-substituted phenylenediamine bridges (see Figure I.4). Furthermore, we showed that *para*-substituted oligophenylene and α,α'- and β,β'-substituted oligoacene spacers are really effective to transmit exchange interactions between paramagnetic metal centers separated by relatively long intermetallic distances in the corresponding dicopper(II) oligophenylenophanes[26b] and oligoacenophanes[26c] (Figures I.9c-e).

These promising results have directed our current research efforts toward other dicopper(II) metallacyclophanes with extended π-conjugated aromatic spacers like linear oligophenyleneethynylenes (OPEs), oligophenylvinylidenes (OPVs), and oligoazobenzenes (OABs) (Figures I.9f-h). So, the linear rod-like OPE spacers are potential candidates to get a **magnetic wire behavior** (see Panel D). In Chapter II, we describe the synthesis and structural characterization, spectroscopic and magnetic properties, and theoretical calculations of a novel series of dicopper(II) metallacyclophanes with 4,4'-diphenylethyne and 1,4-di(4-phenylethynyl)phenylene spacers as prototypes of "molecular magnetic wires" (MMWs).

In our ligand design approach to molecular magnetic devices based on exchange-coupled dinuclear copper(II) metallacyclophanes, we also pursuit to get a **magnetic charge storage behavior** (see Panel E). Hence, by using redox-active ("non-innocent") aromatic spacers that are able to experience reversible redox processes, we plan the obtention of dicopper(II) metallacyclophanes that can behave as molecular magnetic capacitors (MMCs). A good example of this kind would be the oligoacenequinones (OAQs) like benzoquinones and anthraquinones (Figure I.9i-l). In Chapter III, we describe the synthesis and structural characterization, redox and magnetic properties, and theoretical calculations of a novel series of dicopper(II) metallacyclophanes with 1,4-disubstituted 9,10-anthraquinone spacers as prototypes of MMCs.

The next step in our ligand design approach to molecular magnetic devices will be the incorporation of electro- or photo-active aromatic spacers in the dicopper(II) metallacyclophanes to get a **magnetic switching behavior** (see Panel F). At this respect, oligoacenes (OAs) are appealing candidates as electro- and photoswichable wires in "molecular magnetic switches" (MMSs) because of their unique redox and photochromic properties. In Chapter IV, we describe the synthesis, redox and magnetic properties, and theoretical calculations of a novel series of dicopper(II) metallacyclophanes with polymethyl-substituted 1,4-phenylene spacers as prototypes of redox-triggered MMSs. On the other hand, in Chapter V, we describe the synthesis and structural characterization, magnetic properties and photochemistry of a novel series of dicopper(II) metallacyclophanes with 1,5-naphthalene and 2,6-anthracene spacers as prototypes of photo-triggered MMSs.

References

[1] a) J. Jortner, M. Ratner, *Molecular Electronics*, Blackwell Science, Oxford, **1997**. b) *Molecular Nanoelectronics*, eds. M. A. Reed and T. Lee, *American Scientific Publishers*, Stevenson Ranch, CA, **2003**.

[2] a) A. Aviram, M. Ratner, *Ann. NY Acad. Sci*. **1998**, 852. b) M. Ratner, *Nature* **2000**, *404*, 137. c) J. M. Tour, *Acc. Chem. Res*. **2000**, *33*, 791. d) K. W. Hipps, *Science* **2001**, *284*, 536. e) D. Cahen, G. Hodes, *Adv. Mater*. **2002**, *14*, 789. f) R. L. Caroll, C. B. Gorman, *Angew. Chem. Int. Ed.* **2002**, *41*, 4378. g) N. Robertson, G. A. McGowan, *Chem. Soc. Rev*. **2003**, *32*, 96. h) A. H. Flood, J. F. Stoddart, D. W. Steuerman, J. R. Heath, *Science* **2004**, *306*, 2055. i) A.C.Benniston, *Chem.Soc.Rev*. **2004**, *33*, 573. j) K. Nørgaard, T. Bjørnholm, *Chem. Commun*. **2005**, 1812. k) P. J. Low, *DaltonTrans*. **2005**, 2821. l) J. M. Clemente-Juan, E. Coronado, A. Gaita-Ariño, *Chem.Soc.Rev*. **2012**, *41*, 7464.

[3] Special Issue on "Molecular Spintronics and Quantum Computing" (Guest Editors: E. Coronado, A. J. Epstein): a) J. Camarero, E. Coronado, *J. Mater. Chem.* **2009**, *19*, 1678. b) M. Mas-Torrent, N. Crivillers, V. Mugnaini, I. Ratera, C. Rovira, J. Veciana, *J. Mater. Chem.* **2009**, *19*, 1691. c) F. Wang, Z. V. Vardeny, *J. Mater. Chem.* **2009**, *19*, 1685. d) T. Sugawara, M. M. Matsushita, *J. Mater. Chem*. **2009**, *19*, 1738.

[4] a) P. F. H. Schwab, M. D. Levin, J. Michl, *Chem. Rev*. **1999**, *99*, 1863. b) P. F. H. Schwab, J. R. Smith, J. Michl, *Chem. Rev*. **2005**, *105*, 1197. c) M. I. Bruce, P. J. Low, *Adv. Organomet. Chem*. **2004**, *50*, 231. d) Q. L. Zheng, J. A. Gladysz, *J. Am. Chem. Soc*. **2005**, *127*, 10508. e) D. Touchard, P. H. Dixneuf, *Coord. Chem. Rev*. **1998**, *178–180*, 409. f) F. Paul, C. Lapinte, *Coord. Chem. Rev*. **1998**, *178*, 431.

[5] M. Akita, Y. Tanaka, C. Naitoh, T. Ozawa, N. Hayashi, M. Takeshita, A. Inagaki, M.-C. Chung, *Organometallics,* **2006**, *25*, 5261.

[6] a) S. Fraysse, C. Coudret, J.P. Launay, *Eur. J. Inorg. Chem*. **2000**, 1581. b) E. H. van Dijk, D. J. T. Myles, M. H. van der Veen, J. C. Hummelen, *Org. Lett*. **2006**, *8*, 2333. c) A. Fernandez-Acebes, J.M. Lehn, *Chem. Eur. J*. **1999**, 3285. d) *Molecular Switches*, ed. B. L. Feringa, Wiley-VCH, Weinheim, **2001**.

[7] a) M. Irie, *Chem. Rev*. **2000**, *100*, 1685. b) M. Irie, K. Uchida, *Bull. Chem. Soc. Jpn*. **1998**, *71*, 985. c) G. H. Brown, *Photochromism,* Wiley-Interscience, New York, **1971**. d) H. Bouas-Laurent, H. Dürr, *Pure Appl. Chem*. **2001**, *73*, 639. e) P. Bamfield, *Chromic Phenomena, Technological Applications of Color Chemistry,* RSC, Cambridge, **2001**. f) H. Dürr, H. Bouas-Laurent, *Photochromism: Molecules and Systems*, Elsevier, Amsterdam, **2003**.

[8] a) A. Bencini, D. Gatteschi, F. Totti, D. Nieto-Sanz, J.A. McCleverty, M.D.J. Ward, *Phys. Chem.* **1998**, *102*, 10545. b) E. Ruiz, A. Rodríguez-Fortea, S. Alvarez, *Inorg. Chem.* **2003**, *42*, 4881. c) F. Nunzi, E. Ruiz, J. Cano, S. Alvarez, *J. Phys. Chem.* **2007**, *111*, 618. d) W. Li, F. Yang, Z. Wang, J. Hu, J. Ma, *J. Phys. Chem.* **2009**, *113*, 3375. e) R.G. Hadt, V.N. Nemykin, *Inorg. Chem.* **2009**, *48,* 3982.

[9] O. Kahn, Molecular Magnetism, VCH Publishers, New York, **1993**.

[10] a) R.R. Caroll, C.B. Gorman, *Angew. Chem. Int. Ed.* **2002**, *41*, 4379. b) N. Robertson, C.A. McGowan, *Chem. Soc. Rev.* **2003**, *32*, 96. c) A. Dei, D. Gatteschi, C. Sangregorio, L. Sorace, *Acc. Chem. Res.* **2004**, *37*, 827.

[11] a) M.P. Shores, J.R. Long, *J. Am. Chem. Soc.* **2002**, *124*, 3512. b) W. Liang, M.P. Shores, M. Bockrath, J.R. Long, H. Park, *Nature* **2002**, *417*, 725. c) M. Fabre, J. Bonvoisin, *J. Am. Chem. Soc.* **2007**, *129*, 1434. d) P. Hamon, F. Justaud, O. Cador, P. Hapiot, S. Rigaut, L. Toupet, L. Ouahab, H. Stueger, J.-R. Hamon, C. Lapinte, *J. Am. Chem. Soc.* **2008**, *130*, 17372.

[12] a) C. Creutz, *Prog. Inorg. Chem.* **1983**, *30*, 1. b) G. Blondin, J.J. Girerd, *Chem. Rev.* **1990**, *90*, 1359. c) R.J. Crutchley, *Adv. Inorg. Chem.* **1994**, *41*, 273. d) B.S. Brunschwig, N. Sutin, *Coord. Chem. Rev.* **1999**, *187*, 233. e) T. Terencio, R. Bastardis, N. Suaud, D. Maynau, J. Bonvoisin, J.P. Malrieu, C. J. Calzado, N. Guihery, *Phys. Chem. Chem. Phys.* **2011**, *13*, 12314.

[13] a) C. Creutz, H. Taube, *J. Am. Chem. Soc.* **1973**, *95*, 1086. b) G.M. Tom, C. Creutz, H. Taube, *J. Am. Chem. Soc.* **1984**, *96*, 7827. c) J.E. Sutton, P.M. Sutton, H. Taube, *Inorg. Chem.* **1979**, *18*, 1017. d) Y. Kim, C.M. Lieber, *Inorg. Chem*. **1989**, *28,* 3990.

[14] a) J.A. McCleverty, M.D. Ward, *Acc. Chem. Res.* **1998**, *36*, 3447. b) J.P. Launay, *Chem. Soc. Rev.* **2001**, *30*, 386. c) W. Kaim, G.K. Lahiri, *Angew. Chem., Int. Ed.* **2007**, *46*, 1778.

[15] a) J.P. Hay, J.C. Thibeault, R. Hoffmann, *J. Am. Chem. Soc.* **1975**, *97*, 4884. b) R.E. Coffman, G.R. Buettner, *J. Phys. Chem.* **1979**, *83*, 2387. c) O. Kahn, *Angew. Chem. Int. Ed. Engl.* **1985**, *24*, 834.

[16] a) E.F. Hasty, T.J. Colburn, D.N. Hendrickson, *Inorg. Chem.* **1973**, *12*, 2414. b) C.G. Pierpont, L.C. Francesconi, D.N. Hendrickson, *Inorg. Chem.* **1977**, *16*, 2367. c) C.G. Pierpont, L.C. Francesconi, D.N. Hendrickson, *Inorg. Chem.* **1978**, *17*, 3470. d) M. Hadded, D.N. Hendrickson, J.P. Cannady, R.S. Drago, D.S. Bieksza, *J. Am. Chem. Soc.* **1979**, *101*, 898. e) J.T. Reinprecht, J.G. Miller, G.C. Vogel, M.S. Haddad, D.N. Hendrickson, *Inorg. Chem.* **1980**, *19*, 927.

[17] a) M. Verdaguer, J. Gouteron, S. Jeannin, Y. Jeannin, O. Kahn, J.M. Savariault, *Inorg. Chem.* **1984**, *23*, 4291. b) F. Tinti, M. Verdaguer, O. Kahn, J.M. Savariault, *Inorg. Chem.* **1987**, *26*, 2380.

[18] a) M. Julve, M. Verdaguer, J. Faus, F. Tinti, J. Moratal, A. Monge, E. Gutiérrez-Puebla, *Inorg. Chem.* **1987**, *26*, 3520. b) X. Solans, M. Aguiló, A. Gleizes, J. Faus, M. Julve, M. Verdaguer, *Inorg. Chem.* **1990**, *29*, 775. c) I. Castro, J. Sletten, J. Faus, M. Julve, Y. Journaux, F. Lloret, S. Alvarez, *Inorg. Chem.* **1992**, *31*, 1889. d) J. Cano, G. De Munno, J.L. Sanz, R. Ruiz, J. Faus, F. Lloret, M. Julve, A. Caneschi, *J. Chem. Soc. Dalton Trans.* **1997**, 1915. e) J. Cano, G. De Munno, J.L. Sanz, R. Ruiz, F. Lloret, J. Faus, M. Julve, *Anales de Química Int. Ed.* **1997**, *93*, 174. f) I. Castro, M.L. Calatayud, J. Sletten, F. Lloret, M. Julve, *Inorg. Chim. Acta* **1999**, *287*, 173.

[19] a) E.G. Bakalbassis, C.A. Tsipis, J. Mrozinski, *Inorg. Chem.* **1985**, *24*, 4231. b) E.G. Bakalbassis, J. Mrozinski, C.A. Tsipis, *Inorg. Chem.* **1985**, *25,* 3684. c) S.K. Hakhatreh, E.G. Bakalbassis, I. Brüdgam, H. Hartl, J. Mrozinski, C.A.Tsipis, *Inorg. Chem.* **1991**, *30*, 2801. d) S.K. Hakhatreh, E.G. Bakalbassis, I. Brüdgam, H. Hartl, J. Mrozinski, C.A. Tsipis, *Inorg. Chim. Acta* **1991**, *186*, 113.

[20] a) P. Chaudhuri, K. Oder, K. Wieghardt, S. Gehring, W. Haase, B. Nuber, J. Weiss, *J. Am. Chem. Soc.* **1988**, *110*, 3657. b) K.S. Bürger, P. Chaudhuri, K. Wieghardt, B. Nuber, *Chem. Eur. J.* **1995**, *1*, 583.

[21] a) T.R. Felthouse, E.N. Duesler, D.N. Hendrickson, *J. Am. Chem. Soc.* **1978**, *100*, 618. b) T.R. Felthouse, D.N. Hendrickson, *Inorg. Chem.* **1978**, *17*, 2636. c) C. Yuste, J. Ferrando-Soria, D. Cangussu, O. Fabelo, C. Ruiz-Pérez, N. Marino, G. De Munno, S.-E. Stiriba, R. Ruiz-García, J. Cano, F. Lloret, M. Julve, *Inorg. Chim. Acta* **2010**, *363*, 1984. d) J. Ferrando-Soria, M. Castellano, C. Yuste, F. Lloret, M. Julve, O. Fabelo, C. Ruiz-Pérez, S.-E. Stiriba, R. Ruiz-García, J. Cano, *Inorg. Chim. Acta* **2010**, *363*, 1666. e) M. Castellano, J. Cano, unpublished work.

[22] a) S. Schindler, D. Szalda, C. Creutz, *Inorg. Chem.* **1992**, *31*, 2255. b) T. Buchen, A. Hazell, L. Jessen, C.J. McKenzie, L.P. Nielsen, J.Z. Pedersen, D. Schollmeyer, *J. Chem. Soc. Dalton Trans.* **1997**, 2697. c) S.P. Foxon, G.R. Torres, O. Walter, J.Z. Pedersen, H. Toftlund, M. Hüber, K. Falk, W. Haase, J. Cano, F. Lloret, M. Julve, S. Schindler, *Eur. J. Inorg. Chem.* **2004**, 335. d) S.P. Foxon, O. Walter, R. Koch, H. Rupp, P. Müller, S. Schindler, *Eur. J. Inorg. Chem.* **2004**, 344. e) S. Turba, O. Walter, S. Schindler, L.P. Nielsen, A. Hazell, C.J. McKenzie, F.Lloret, J. Cano, M. Julve, *Inorg. Chem.* **2008**, *47,* 9612.

[23] a) A. Mederos, P. Gili, S. Domínguez, A. Benítez, M. S. Palacios, M. Hernández-Padilla, P. Martín-Zarza, M. L. Rodríguez, C. Ruiz-Pérez, F. J. Lahoz, L. A. Oro, F. Brito, J. M. Arrieta, M. Vlassi, G. Germain, *J. Chem. Soc. Dalton Trans.* **1990**, 1477. b) S. Domínguez, A. Mederos, P. Gili, A. Rancel, A. E. Rivero, F. Brito, F. Lloret, X. Solans, C. Ruiz-Pérez, M. L. Rodríguez, I. Brito, *Inorg. Chim. Acta* **1997**, *255*, 367.

[24] a) C. A. Bear, J. M. Waters, T. N. Waters, *J. Chem. Soc.***1970**, *17*, 2494. b) D. Y. Jeter, W. E. Hatfield, *Inorg. Chim. Acta* **1972**, *6*, 440. c) R. Hernández-Molina, A. Mederos, P. Gili, S. Domínguez, F. Lloret, J. Cano, M. Julve, C. Ruiz-Pérez, X. Solans, *J. Chem. Soc. Dalton Trans.* **1997**, 4327. d) A. R. Paital, T. Mitra, D. Ray, W. T. Wong, J. Ribas-Ariño, J. J. Novoa, J. Ribas, G. Aromí, *Chem. Commun.* **2005**, 5172. e) A. R. Paital, A. Q. Wu, G. G. Guo, G. Aromí, J. Ribas-Ariño, D. Ray, *Inorg. Chem.* **2007**, *46*, 2947. f) M. Vázquez, A. Taglietti, D. Gatteschi, L. Sorace, C. Sangregorio, A. M. González, M. Maneiro, R. M. Pedrido, M. R. Bermejo, *Chem. Commun.* **2003**, 1840.

[25] a) M. B. Inoue, E. F. Velázquez, F. Medrano, K. L. Ochoa, J. C. Gálvez, M. Inoue, Q. Fernando, *Inorg. Chem.* **1998**, *37*, 4070. b) M. B. Inoue, I. C. Muñoz, L. Machi, M. Inoue, Q. Fernando, *Inorg. Chim. Acta* **2000**, *311*, 50. c) M. B. Inoue, M. Inoue, R. Sugich-Miranda, L. Machi, E. F. Velázquez, Q. Fernando, *Inorg. Chim. Acta* **2001**, *317*, 181. d) L. V. Mosina, A. V. Raitsimring, M. B. Inoue, Q. Fernando, M. Inoue, *Appl. Magn. Reson.* **2001**, *20*, 249.

[26] a) I. Fernández, R. Ruiz, J. Faus, M. Julve, F. Lloret, J. Cano, X. Ottenwaelder, Y. Journaux, M.C. Muñoz, *Angew. Chem. Int. Ed.* **2001**, *40*, 3039. b) E. Pardo, J. Faus, M. Julve, F. Lloret, M.C. Muñoz, J. Cano, X. Ottenwaelder, Y. Journaux, R. Carrasco, G. Blay, I. Fernández, R. Ruiz-García, *J. Am. Chem. Soc.* **2003**, *125*, 10770. c) E. Pardo, R. Carrasco, R. Ruiz-García, M. Julve, F. Lloret, M.C. Muñoz, Y. Journaux, E. Ruiz, J. Cano, *J. Am. Chem. Soc.* **2008**, *130*, 576. d) E. Pardo, J. Ferrando-Soria, M. C. Dul, R. Lezcouëzec, Y. Journaux, R. Ruiz-García, J. Cano, M. Julve, F. Lloret, L. Cañadillas-Delgado, J. Pasán, C. Ruiz-Pérez, *Chem. Eur. J.* **2010**, *16*, 12838.

[27] a) C. S. Lent, *Science* **2000**, *288*, 1597. b) N. Hush, *Nat. Mater.* **2003**, *2*, 134. c) R. P. Cowburn, M. E. Welland, *Science* **2000**, *287*, 1466.

[28] C. S. Lent, B. Isaksen, M. Lieberman, *J. Am. Chem. Soc.* **2003**, *125*, 1056.

[29] a) F. M. Raymo, *Adv. Mater.* **2002**, *14*, 401. b) V. Balzani, A. Credi, M. Venturi, *Chem. Phys. Chem.* **2003**, *4*, 49. c) A. P. de Silva, N. D. McClenaghan, *Chem. Eur. J.* **2004**, *10*, 574. d) A. P. de Silva, *Nat. Mater.* **2005**, *4*, 15.

[30] J. C. Ellenbogan, J. C. Love, *IEEE* **2000**, *88*, 386.

CHAPTER II

Dicopper(II) Diphenylethynecyclophanes as Molecular Magnetic Wires

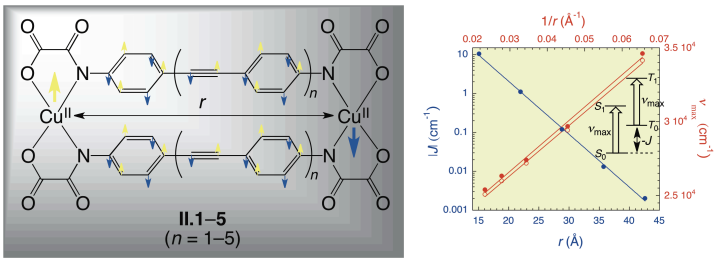

On the road to molecular wires: the very long-distance antiferromagnetic coupling between the two Cu^{2+} ions found in a new class of oxamato-based di-copper(II) metallacyclophanes with rigid rod-like oligo-*p*-phenylethyne spacers serve as ground test for molecular magnetic wires, which are the basic component of a spin-based molecular electronic circuit.

II.1 Introductory Aspects

Polymetallic complexes with strong intramolecular electronic interactions between distant metal centers across extended bridges are a common topic in molecular magnetism and molecular electronics.[1] Besides their interest as models for the fundamental research on through-ligand, long-distance electron exchange (EE) and electron transfer (ET) phenomena,[2,3] they are also of great importance in the "bottom-up" approach to nanometer-scale electronic devices such as molecular wires and switches.[4] Dinuclear complexes would then allow investigating the transmission of EE interactions through potential molecular magnetic wires,[5] by comparison with conventional molecular electronic wires which are based on ET interactions instead.[6] In fact, they may offer a new design concept for the transfer of information over long distances based on purely EE (Coulomb) interactions and without any current flow.[5b] However, the examples of long-range magnetic coupling in exchange-coupled dinuclear complexes are relatively scarce with regard to the more abundant examples of long-range electron transport in mixed-valent ones.[7] The design and synthesis of novel bridging ligands which can transmit spin coupling effects over long distances are then a major goal in the field, which requires both a skillful organic synthesis and a deep understanding of the EE mechanism.[2c] With the advent of ground and excited state calculations based on the density functional (DF) and time-dependent density functional (TD-DF) theory combined with the broken-symmetry (BS) approach, it has been possible not only to reproduce but also to predict very accurately the electronic and magnetic properties of simple dinuclear complexes.[8]

Along this line, dicopper(II) metallacyclophanes emerge as ideal model systems for the study of the EE mechanism between paramagnetic metal centers containing one unpaired electron ($\mathbf{H} = -J\,\mathbf{S_1}\cdot\mathbf{S_2}$ with $S_1 = S_2 = S_{Cu} = ½$) through extended π-conjugated aromatic spacers, both from experimental and theoretical viewpoints.[9] The variation of the ligand spacer in the metallacyclic entity may control both the overall structure and the magnetic properties and then, the influence of different factors such as the topology and conformation of the bridging ligand can be investigated in a systematic way.[10–13] So, the problem of long-range magnetic coupling in dicopper(II) metallacyclophanes have been addressed by several research teams through the use of diverse coordinating group substituted amine-,[10] imine-,[11] and amide-based[12] aromatic bridging ligands, with more or less satisfactory results.

Our strategy in this field involves a unique family of double-stranded dicopper(II) metallacyclophanes resulting from the side-by-side coordination of aromatic bis(oxamato) bridging ligands to square planar Cu^{II} ions (Figure II.1).[13] This type of more or less rigid, dinucleating ligands leads to discrete, self-assembled dicopper(II) metallacyclic entities with a π-stacked arrangement of the aromatic spacers connected by two N–Cu–N linkages. The almost perpendicular disposition among the two coplanar basal planes of the square planar metal ions and the two parallel planes of the

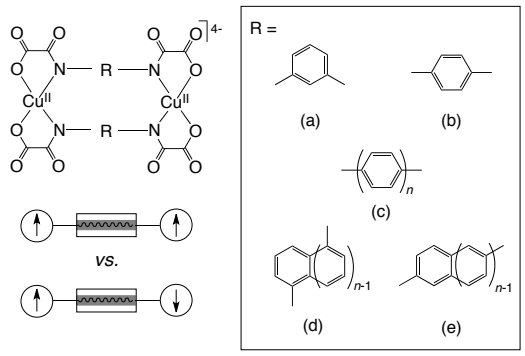

Figure II.1 Oxamato-based dicopper(II) metallacyclophanes with *m*- (a) or *p*-phenylene (b), *p*-oligophenylene (c), and *α,α'*- (d) or *β,β'*-oligoacene (e) spacers as molecular ferro- or antiferromagnetic wires

aromatic spacers ensures a unusual π-type orbital pathway for the EE interaction between the unpaired electrons of the Cu^{II} ions through the extended π-conjugated aromatic spacers.

Hence, a moderate ferromagnetic coupling has been reported for the oxamato-based dicopper(II) metallacyclophanes with 1,3-phenylene spacers (Figure II.1a), independently on the *syn* or *anti* arrangement of the two facing benzene rings (J = +16.8 and +16.4 cm^{-1}, respectively).[13a,d] On the contrary, the oxamato-based dicopper(II) metallacyclophanes with 1,4-phenylene spacers (Figure II.1b) exhibit a strong antiferromagnetic coupling ($-J$ = 81–94 cm^{-1}).[13b] This pair of dicopper(II) metallacyclophanes constitutes thus a unique example of the spin control in metal complexes by the topology of the bridging ligand, according to the well-known spin polarization mechanism. In each case, the ferro- or antiferromagnetic nature of the EE interaction results from the spin density alternation in the π-conjugated bond system of the phenylene spacers with *meta*- and *para*-substitution pattern respectively, as supported by DF calculations.[13a,b]

These results have oriented our research toward oxamato-based dicopper(II) metallacyclophanes with linear oligo-*p*-phenylene (OP) spacers (Figure II.1c).[13b] Indeed, the magnetic coupling decreases for the related oxamato-based dicopper(II) metallacyclophanes with 4,4'-diphenylene spacers (Figure II.1c with n = 2), which exhibit however a moderate antiferromagnetic coupling ($-J$ = 8.7–11.5 cm^{-1}) at a relatively large intermetallic distance (r = 12.2 Å).[13b] This effect has been supported by DF calculations which predict an exponential decay of the magnetic coupling with the intermetallic distance when increasing the number of benzene rings, $-(C_6H_4)_n-$, in the OP spacers (Figure II.1c with n = 1–5).[13b]

In a subsequent work, we have shown both experimentally and theoretically that oligoacene (OA) spacers consisting of linearly fused benzenoid units, $-(C_{6+4n}H_{4+2n})-$, differently substituted at the carbon atoms of the terminal benzene rings, either *α,α'*- or *β,β'*-substituted (Figures II.1d and II.1e, respectively), are really effective to transmit EE interactions between two Cu^{II} ions separated by relatively large intermetallic distances.[13c] So, the related

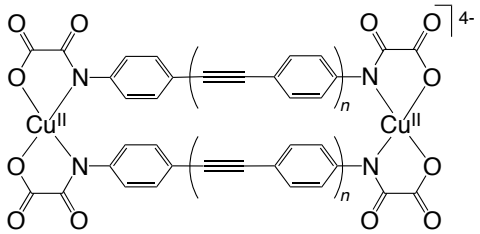

II.1–**5**
(*n* = 1–5)

Figure II.2 Structural formula of the oxamato-based dicopper(II) metallacyclophanes with oligo(*p*-phenylene-ethynylene) spacers

pair of oxamato-based dicopper(II) metallacyclophanes with 1,5-naphthalene and 2,6-anthracene spacers (Figures II.1d and II.1e with n = 2 and 3, respectively) show a similar moderate antiferromagnetic coupling ($-J$ = 20.5–20.7 cm^{-1} and 21.2–23.9 cm^{-1}, respectively) despite the largely different intermetallic distances (r = 8.3 and 12.5 Å, respectively).[13c,13f] DF calculations on these two series of oxamato-based dicopper(II) metallacyclophanes with OA spacers confirm the better efficiency of the β,β'- over α,α'-substitution pattern on long-range magnetic coupling.[13c] More importantly, they predict a unprecedented wire-like magnetic behavior for the longer members of the series with octacene through decacene spacers (Figures II.1d and II.1e with n = 8–10), which is accompanied by a change from antiferro- to ferromagnetic coupling (J values up to +3.0 cm^{-1} for r = 28.8 Å).[13c]

Oligo(*p*-phenylene-ethynylene) (OPE) spacers are also very appealing candidates as molecular wires.[14,15] In fact, the rigid rod-like OPE spacers have a potential extended π-conjugation that would allow a strong electronic as well as magnetic coupling between very distant metal centers in both organometallic and coordination compounds, as recently reported by us in a preliminary communication (see first communication in Appendices).[13e] In order to further extend this promising result, herein we report on the complete synthesis, general physical and/or structural characterization, spectroscopic and magnetic properties of two new examples of oxamato-based dicopper(II) metallacyclophanes of formula (nBu$_4$N)$_4$[Cu$_2$(dpeba)$_2$] · 4MeOH · 2Et$_2$O (**II.1**) and (nBu$_4$N)$_4$[Cu$_2$(tpeba)$_2$] · 12H$_2$O (**II.2**) [nBu$_4$N$^+$ = tetra-*n*-butylammonium, H$_4$dpeba = *N,N′*-4,4'-diphenylethynebis(oxamic acid), and H$_4$tpeba = *N,N′*-1,4-di(4-phenylethynyl)phenylenebis(oxamic acid)]. Complexes **II.1** and **II.2** can be considered as the first two members of a novel series of oxamato-based dicopper(II) metallacyclophanes with OPE spacers of different length, –C$_6$H$_4$(C≡CC$_6$H$_4$)$_n$– (n = 1–5), as potential candidates to molecular magnetic wires (**II.1**–**II.5**, Figure II.2). DF and TD-DF calculations on the electronic structure of the ground and excited states of the model complexes **II.1**–**II.5** with an overall orthogonal molecular geometry have been carried out in order to analyze the effect of the increase of the conjugation length with the number of phenylethyne units in the OPE spacer on the magnetic coupling and the electronic spectra of dinuclear copper(II) complexes with intermetallic distances varying in the range of 15–43 Å.

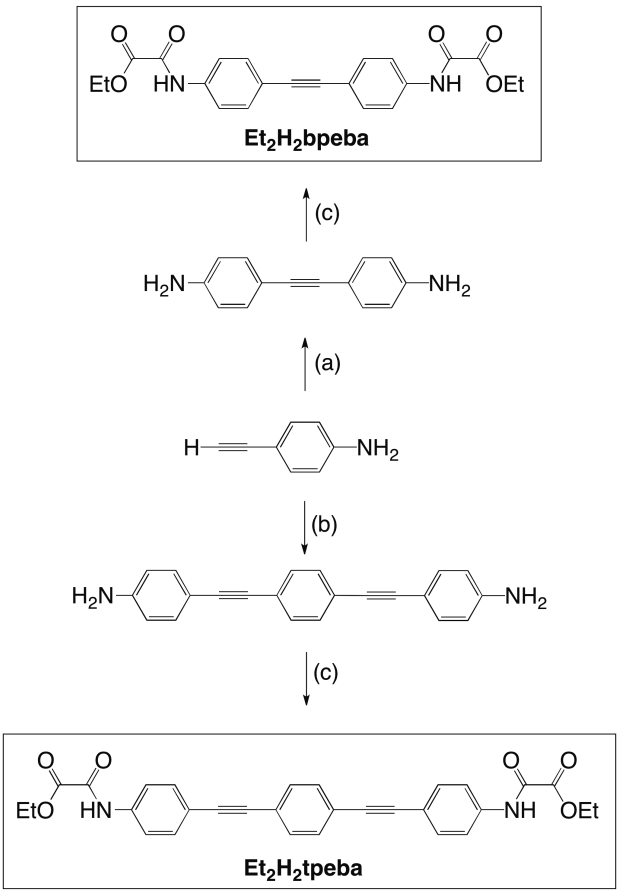

Figure II.3 Synthesis of the diethyl ester derivatives of the H$_4$dpeba and H$_4$tpeba ligands. Reaction conditions: (a) *p*-IC$_6$H$_4$NH$_2$, PdCl$_2$(PPh$_3$)$_2$/CuI, NEt$_3$; (b) *p*-C$_6$H$_4$I$_2$, PdCl$_2$(PPh$_3$)$_2$/CuI, NEt$_3$; (c) C$_2$O$_3$EtCl, NEt$_3$, THF.

II.2 Synthesis of Ligands and Complexes

The *N,N′*-4,4'-diphenylethynebis(oxamic acid) (H$_4$dpeba) and *N,N′*-1,4-di(4-phenylethynyl)phenylenebis(oxamic acid) (H$_4$tpeba) ligands were prepared in two consecutive steps from the Pd/Cu catalyzed, Sonogashira-type cross-coupling reaction of *p*-ethynylaniline and *p*-iodoaniline or *p*-diiodophenylene respectively,[15a] followed by the straightforward condensation of the resulting 4,4'-diphenylethyne- and 1,4-di(4-phenylethynyl)phenylenediamine precursors with ethyl oxalyl chloride ester (1:2 molar ratio) in the presence of triethylamine in THF (Figure II.3). They were isolated as the *N,N′*-4,4'-diphenylethynebis(oxamic acid ethyl ester) (Et$_2$H$_2$dpeba) and *N,N′*-1,4-di(4-phenylethynyl)phenylenebis(oxamic acid ethyl ester) (Et$_2$H$_2$tpeba) derivatives in good yields (*ca.* 80–85%, see Experimental Section).

Complexes **II.1** and **II.2** were then prepared by the reaction of the Et$_2$H$_2$dpeba and Et$_2$H$_2$tpeba proligands with Cu^{2+} perchlorate (1:1 molar ratio) using nBu$_4$NOH as base in methanol, and they were isolated as their tetra-*n*-butylammonium salts in good yields (*ca.* 65–70%, see Experimental Section). X-ray quality dark green

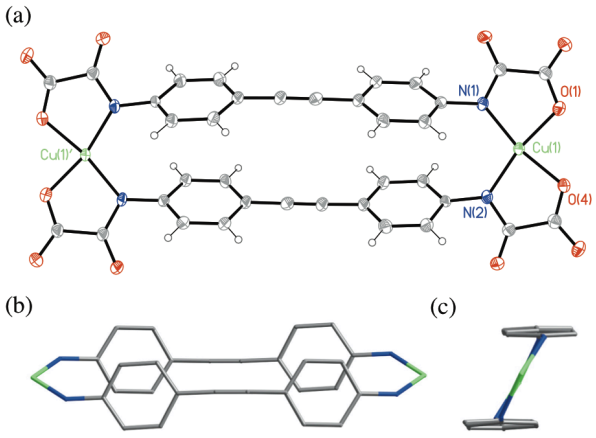

Figure II.4 (a) ORTEP drawing of the centrosymmetric anionic dicopper unit of **II.1** with the atom-numbering scheme of the metal environment [symmetry code: (a) = 2 – *x*, 1 – *y*, 2 – *z*]. The thermal ellipsoids are drawn at the 50% probability level. (b) Front and (c) top projection views of the metallacyclic core of **II.1**.

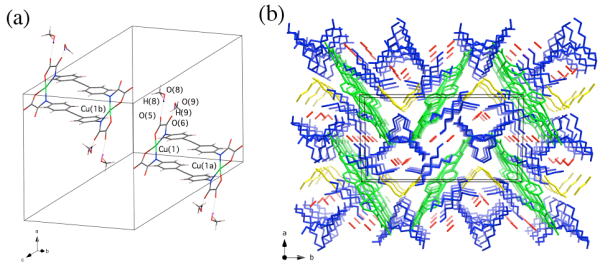

Figure II.5 (a) View of the unit cell of **1** showing the discrete anionic dicopper units [symmetry code: (a) = 2 – *x*, 1 – *y*, 2 – *z* ; (b) = 1 – *x*, 1 – *y*, 1 – *z*]. The hydrogen bonds with the crystallization methanol molecules are represented by dashed lines. (b) Perspective view of the crystal packing of **II.1** along the crystallographic *c* axis. The dicopper anions and the tetrabutylammonium cations are shown in green and blue colors respectively, while the methanol and diethyl ether molecules of crystallization are shown in red and yellow colors, respectively.

prims of **II.1** were obtained by diethyl ether layering on the methanol solution. Unfortunately, all our attempts to grow X-ray quality crystals of **II.2** were unsuccessful. The chemical identity of the ligand and complexes was established by elemental analyses and ^{1}H NMR and FT–IR spectroscopies (see Experimental Section and Appendices). The structure of **II.1** was further confirmed by single-crystal X-ray diffraction. A summary of the crystallographic data of **II.1** is given in Table II.1, while selected bond distances and interbond angles are listed in Table II.2.

II.3 Description of the Structure

The structure of **II.1** consists of centrosymmetric dicopper(II) complex anions, $[Cu^{II}_2(dpeba)_2]^{4-}$,and tetra-*n*-butylammonium cations, with methanol and diethyl ether as crystallization molecules (Figure II.4 and Figure II.5). In the crystal lattice, the discrete anionic dicopper(II) complexes establish weak hydrogen bonds with the methanol molecules through the carboxylate- and carbonyl-oxygen atoms from the oxamato groups [O(5)···O(8) = 2.760(4) Å and O(6)···O(9) = 2.804(4) Å] (Figure II.5a). Yet they are well separated from each other by the bulky tetra-*n*-butylammonium cations and the diethyl ether molecules (Figure II.5b). The intramolecular Cu(1)–Cu(1a) distance (*r*) across the double *para*-substituted diphenylethynediamidate bridge is 14.95(1) Å, while the shortest intermolecular Cu(1)–Cu(1b) separation is 8.09(1) Å.

Table II.1 Summary of crystallographic data for **II.1**.

Formula	$C_{112}H_{196}Cu_2N_8O_{18}$
M (g mol^{-1})	2069.85
Crystal system	monoclinic
Space group	$P2_1/c$
a (Å)	15.261(2)
b (Å)	25.691(4)
c (Å)	17.279(3)
β (°)	116.180(6)
V (Å^3)	6079.4(16)
Z	2
ρ_{calc} (g cm^{-3})	1.131
μ (mm^{-1})	0.412
T (K)	100(2)
Reflect. collcd.	10675
Reflect. obs. [$I > 2s(I)$]	9467
Data / restraints / parameters	10675 / 0 / 645
R_1[a] [$I > 2\sigma(I)$] (all)	0.0740 (0.0836)
wR_2[b] [$I > 2\sigma(I)$] (all)	0.2073 (0.2220)
S[c]	1.175

[a] $R_1 = \sum(|F_o| - |F_c|)/\sum|F_o|$. [b] $wR_2 = [\sum w(F_o^2 - F_c^2)^2/\sum w(F_o^2)^2]^{1/2}$. [c] $S = [\sum w(|F_o| - |F_c|)^2/(N_o - N_p)]^{1/2}$.

Table II.2 Selected bond distances (Å) and angles (°) for **II.1**.[a]

Cu(1)–N(1)	1.993(3)	Cu(1)–N(2)	1.994(3)
Cu(1)–O(1)	1.948(3)	Cu(1)–O(4)	1.973(3)
N(1)–Cu(1)–N(2)	108.43(13)	N(1)–Cu(1)–O(1)	83.92(12)
N(1)–Cu(1)–O(4)	167.80(12)	N(2)–Cu(1)–O(1)	165.63(12)
N(2)–Cu(1)–O(4)	83.24(12)	O(1)–Cu(1)–O(4)	85.01(11)

[a] The estimated standard deviations are given in parentheses.

The anionic dicopper(II) complex is a novel metallamacrocycle of the dicoppertetraaza[3.3]4,4'-diphenylethynophane-type, where the two 4,4'-diphenylethyne spacers of the bis(bidentate) dpeba bridging ligands are connected by two N–Cu–N linkages (Figure II.4a). The two centrosymmetrically-related Cu atoms adopt a essentially square planar geometry. The CuN_2O_2 coordination environment is defined by two amidate-nitrogen and two carboxylate-oxygen atoms from the oxamato donor groups [mean plane deviations of ±0.093(1) Å at N(1) and N(2), and of ±0.114(2) Å at O(1) and O(4)]. The value of the tetrahedral twist angle (τ) between the Cu(1)N(1)O(1) and Cu(1)N(2)O(4) mean planes is 9.4(1)°. The average value of the Cu–N bond distances [1.994(3) Å] is larger than the Cu–O ones [1.961(3) Å], while the value of the N–Cu–N interbond angle [108.43(13)°] is greater than that of the O–M–O one [85.01(11)°]. This situation obeys to the π–π repulsive interactions between the facing benzene rings of the two 4,4'-diphenylethyne spacers within the metallacyclic core, which cause both a lengthening of the Cu–N bond distances and a broadening of the N–M–N interbond angles.

Within the dinuclear metallacyclic core of **II.1**, $Cu^{II}_2(p\text{-}N_2C_{14}H_8)_2$, each of the two 4,4'-diphenylethyne spacers is almost planar reflecting thus potential extended π-conjugation for the

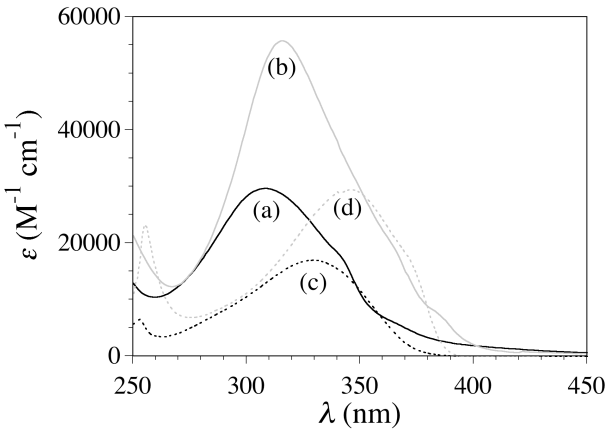

Figure II.6 UV–Vis spectra of **II.1** (a) and **II.2** (b) in acetonitrile solution compared with those of Et_2H_2dpeba (c) and Et_2H_2tpeba (d) in dimethylsulphoxide.

dpeba bridging ligands. The torsion angle (ψ) between the terminal benzene rings around the central carbon-carbon triple bond is 7.8(1)º. This situation contrasts with that found for the related dicopper(II) metallacyclophane with 4,4'-diphenylene spacers, whereby the phenylene rings are significantly tilted around the carbon-carbon single bond because of the repulsive interactions between the *ortho-ortho'* benzene hydrogen atoms (ψ = 19.7°).[13b] Indeed, the short C–C distance of 1.212(6) Å between the carbon atoms of the central ethyne group is typical of a C(*sp*)–C(*sp*) triple bond (1.20 Å), while the long C–C distance of 1.452(5) Å with the carbon atoms of the terminal benzene rings is characteristic of a C(*sp*)–C(sp^2) single bond (1.43 Å). The two 4.4'-diphenylethyne spacers show a noneclipsed disposition because of the parallel-displaced π-stacked arrangement of the two pairs of facing benzene rings (Figure II.4b). The average inter-ring C–C distance of 3.60(1) Å is somewhat longer than the van der Waals contact (3.40 Å). The angle between the centroid-centroid vector from the facing benzene rings and their normal (θ) is 23.9(1)°. Hence, the molecule has an approximate C_{2h} symmetry, whereby the copper mean basal planes are not exactly oriented perpendicular to the benzene planes [dihedral angles (ϕ) of 56.4(1) and 58.4(1)°] (Figure II.4c). Deviations from the ideal D_{2h} molecular symmetry (ψ = 0° and ϕ = 90°) may be originated from the favorable π-π interactions in the parallel-displaced configuration of the 4,4'-diphenylethyne spacers.

II.4 Spectroscopic Properties

The electronic absorption spectra of **II.1** and **II.2** in acetonitrile solution show a common pattern consisting of one broad and intense band in the near UV region, together with two distinct shoulders that extend into the visible zone, whose intensity vary almost proportionally with the number of phenylethyne groups in the OPE spacer (Figure II.6a and b). The main peak centered at 308 (**II.1**)/316 nm (**II.2**) and the two shoulders located around 340 (**II.1**)/365 nm (**II.2**) and 360 (**II.1**)/385 nm (**II.2**) are typical of intraligand (IL) π–π* transitions within the OPE spacers (Table II.3).[15c] In fact, they are also present in somewhat perturbed yet identifiable form with almost half intensity in the electronic absorption spectra of the Et_2H_2dpeba and Et_2H_2tpeba proligands in dimethylsulphoxide (Figure II.6c and d), which show a broad and intense band centered at 330 (Et_2H_2dpeba)/345 nm (Et_2H_2tpeba) with a distinct shoulder located around 355 (Et_2H_2dpeba)/370 nm (Et_2H_2tpeba) (Table II.3). Moreover, the relatively large bathochromic shift in the position of these IL bands for both the complexes ($\Delta\nu_1$ = 822 cm^{-1}, $\Delta\nu_2$ = 2015 cm^{-1}, and $\Delta\nu_3$ = 1804 cm^{-1}; Table II.3) and the proligands ($\Delta\nu_1$ = 1317 cm^{-1} and $\Delta\nu_2$ = 1142 cm^{-1}; Table II.3) is as expected for the increase in the effective π-conjugation length upon increasing the number of phenylethyne units (*n*) from **II.1** to **II.2** in the OPE spacer.

Table II.3 Selected UV–Vis spectroscopic data for **II.1** and **II.2** and the corresponding proligands.

Compound	λ_1[c] (nm)	λ_2[c] (nm)	λ_3[c] (nm)
II.1[a]	308 (29710) [32468]	340 (18850) [29412]	360 (7065) [27778]
II.2[a]	316 (55815) [31646]	365 (22375) [27397]	385 (7770) [25974]
Et_2H_2dpeba[b]	330 (17015) [30303]	355 (9180) [28169]	
Et_2H_2tpeba[b]	345 (29480) [28986]	370 (18140) [27027]	

[a] In acetonitrile solution at room temperature. [b] In dimethylsulphoxide solution at room temperature. [c] The values of the molar extinction coefficient (ε in M^{-1} cm^{-1} units) and the transition energy ($\nu_i = 1/\lambda_i$ in cm^{-1} units) are given in parentheses and brackets, respectively.

The X-band EPR spectra of frozen-matrix acetonitrile solutions of **II.1** and **II.2** at 4.0 K consist of a rhombic signal with a complex multiline splitting pattern which is typical of antiferromagnetically coupled dinuclear copper(II) complexes (Figure II.7). In fact, a seven-line splitting of the g_z signal due to the hyperfine coupling with the nuclear spins of the two Cu^{II} ions ($2nI_{Cu}$ + 1 = 7 with n = 2 and I_{Cu} = 3/2) is expected when the magnetic coupling parameter is much larger than the electron-nucleus hyperfine coupling constant ($|J| >> A_{Cu}$). In contrast, an EPR spectrum formally identical to that of a mononuclear one with a simple four-line splitting resulting from the hyperfine coupling with the nuclear spin of the magnetically isolated Cu^{II} ions ($2I_{Cu}$ + 1 = 4 with I_{Cu} = 3/2) must be observed for an uncoupled system.

These EPR spectral features of **II.1** and **II.2** were satisfactorily simulated by using the XSOPHE program.[16] The calculated values of the Zeeman factors associated with the *x*, *y*, and *z* components of the allowed $M_s = 0 \rightarrow M_s = \pm 1$ transitions for the excited triplet (S = 1) spin state are g_x = 2.044 (**II.1**)/2.045 (**II.2**), g_y = 2.070 (**II.1**)/2.065 (**II.2**), and g_z = 2.240 (**II.1**)/2.216 (**II.2**), while the hyperfine coupling constants are A_x = 20 (**II.1**)/10 G (**II.2**), A_y = 5 (**II.1**)/20 G (**II.2**), and A_z = 134 (**II.1**)/143 G (**II.2**) (Table II.4). The electron-nucleus hyperfine coupling constant of **II.1** and **II.2** can then be estimated from the calculated A_z values resulting from the simulation of the EPR spectra as $A_z = 1/2A_{Cu}$.[17] The calculated anisotropic A_{Cu} values of 268 (**II.1**) and 286 G (**II.2**) are similar, as expected for antiferromagnetically coupled dinuclear copper(II) complexes with the same type of ligands, and they give a minimum value for the magnetic coupling parameter of **II.1** and **II.2** [$|J| >> A_{Cu}$ = 0.0276 (**II.1**) and 0.0296 cm^{-1} (**II.2**)].

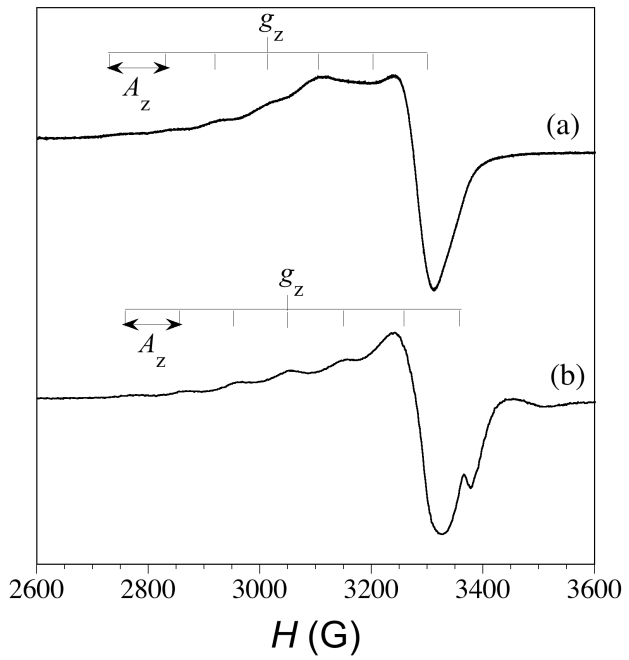

Figure II.7 X-band EPR spectra of frozen-matrix acetonitrile solutions of **II.1** (a) and **II.2** (b) at 4.0 K.

II.5 Magnetic Properties

The magnetic properties of **II.1** and **II.2** in the form of the χ_M and $\chi_M T$ *vs*. T plots (χ_M being the molar magnetic susceptibility per dinuclear unit and T the absolute temperature) and M *vs.* H plots (M being the molar magnetization per dinuclear unit and H the applied magnetic field) conform with moderate (**II.1**) to weak (**II.2**) antiferromagnetically coupled Cu^{II}_2 pairs both in the solid state and in solution (Figures II.8 and II.9).

At room temperature, $\chi_M T$ of powdered samples of **II.1** and **II.2** are equal to 0.84 $cm^3\ mol^{-1}$ K, a value which is close to that expected for two magnetically isolated Cu^{II} ions [$\chi_M T = 2 \times (N\beta^2 g_{Cu}^2/3k_B) S_{Cu}(S_{Cu} + 1) = 0.83\ cm^3\ mol^{-1}$ K with $S_{Cu} = ½$ and $g_{Cu} = 2.1$, where N is the Avogadro number, β is the Bohr magneton, and k_B is the Boltzmann constant]. Upon cooling, $\chi_M T$ of powdered samples and frozen-matrix methanol solutions of **II.1** remain constant until *ca.* 50 K and then it decreases abruptly to reach values of 0.22 and 0.18 $cm^3\ mol^{-1}$ K respectively, at 2.0 K (Figure II.8). By comparison, $\chi_M T$ of powdered samples and frozen-matrix methanol solutions of **II.2** remains constant until *ca.* 20 K and then it decreases slightly to reach values of 0.70 and 0.75 $cm^3\ mol^{-1}$ K respectively, at 2.0 K (Figure II.9). In addition, the powdered samples and frozen-matrix methanol solutions of **II.1** show a χ_M maximum at 3.3 and 3.5 K respectively (inset of Figure II.8), which unambiguously supports the occurrence of a ground singlet ($S = 0$) spin state resulting from the antiferromagnetic interaction between the two spin doublets ($S_{Cu} = 1/2$) of each Cu^{II} ion. Otherwise, the isothermal magnetization curves at 2.0 K of powdered samples and of frozen-matrix methanol solutions of **II.2** are slightly below than that of the Brillouin function for two doublet spin states of two magnetically isolated Cu^{II} ions ($S_{Cu} = 1/2$ with $g = 2.1$) (inset of Figure II.9). The similar magnetic behavior in the solid state and in solution for both **II.1** and **II.2** unambiguously demonstrates that the magnetic coupling is intramolecular in origin, the intermolecular interactions in the solid state, if any, being negligible.

Table II.4 Selected EPR spectroscopic data for **II.1** and **II.2**.[a]

Compound	g_x [b]	g_y [b]	g_z [b]
II.1	2.044 (20) [0.0019]	2.070 (5) [0.0005]	2.240 (134) [0.0138]
II.2	2.045 (10) [0.0010]	2.065 (20) [0.0019]	2.216 (143) [0.0148]

[a] In acetonitrile solution at 4.0 K. [b] The values of the Zeeman factors (g_i) and the hyperfine coupling constants (A_i) associated with the x, y, and z components of the allowed $M_s = 0 \rightarrow M_s = \pm 1$ transitions of the excited triplet ($S = 1$) spin state were calculated by using the XSOPHE program. The calculated A_i values in G and cm^{-1} units are given in parentheses and brackets, respectively.

The analysis of the magnetic susceptibility data of **II.1** and **II.2**, both in the solid state and in solution, was carried out through the spin Hamiltonian for a dinuclear copper(II) complex (eq II.1 with $S_1 = S_2 = S_{Cu} = 1/2$), where J is the magnetic coupling parameter and g is the Zeeman factor of the Cu^{II} ions ($g = g_1 = g_2 = g_{Cu}$). The least-squares fits of the experimental data through the well-known Bleaney-Bowers expression (eq II.2) gave $-J$ = 3.87(3) (**II.1**)/0.90(1) cm^{-1} (**II.2**) and g = 2.124(3) (**II.1**)/2.122(1) (**II.2**) with $R = 1.5 \times 10^{-5}$ (**II.1**)/1.0×10^{-5} (**II.2**) in the solid state, while they gave $-J$ = 4.05(3) (**II.1**)/0.48(1) cm^{-1} (**II.2**) and g = 2.105(3) (**II.1**)/2.105(1) (**II.2**) with $R = 1.8 \times 10^{-5}$ (**II.1**)/1.5×10^{-5} (**II.2**) in solution (Table II.5). The theoretical curves match very well the experimental ones for **II.1** and **II.2** (solid lines in Figures II.8 and II.9). Otherwise, the slight deviations between the $-J$ values in the solid state and in solution for **II.2** may indicate very small variations of the molecular geometry in each medium.

$$\mathbf{H} = -J\mathbf{S_1} \cdot \mathbf{S_2} + g\beta(\mathbf{S_1} + \mathbf{S_2})H \qquad \text{(II.1)}$$

$$\chi_M = (2N\beta^2 g^2/k_B T) / [3 + \exp(-J/k_B T)] \qquad \text{(II.2)}$$

The moderate antiferromagnetic coupling for **II.1** ($-J$ = 3.9–4.1 cm^{-1}) is quite remarkable given the large Cu–Cu separation across the two 4,4'-diphenylethynediamidate bridges ($r \approx 16.0$ Å), and the $-J$ values for **II.1** are only slightly weaker than those reported earlier for related oxamato-based dicopper(II) metallacyclophanes with 4,4'-diphenylene spacers ($-J$ = 8.7–11.5 cm^{-1}) having a rather shorter intermetallic distance (r = 12.2 Å).[13b] Even the antiferromagnetic coupling for **II.2** ($-J$ = 0.5–0.9 cm^{-1}) is weak, it is non-negligible given the very long intermetallic distance through the two 1,4-di(4-phenylethynyl)phenylenediamidate bridges ($r \approx 22.0$ Å). To our knowledge, **II.2** is the exchange-coupled dinuclear copper(II) complex with the largest intermetallic distance for which EE effects has been evidenced. This case shows thus that one nanometer was definitely not the upper limit for the observation of magnetic coupling in dinuclear copper(II)

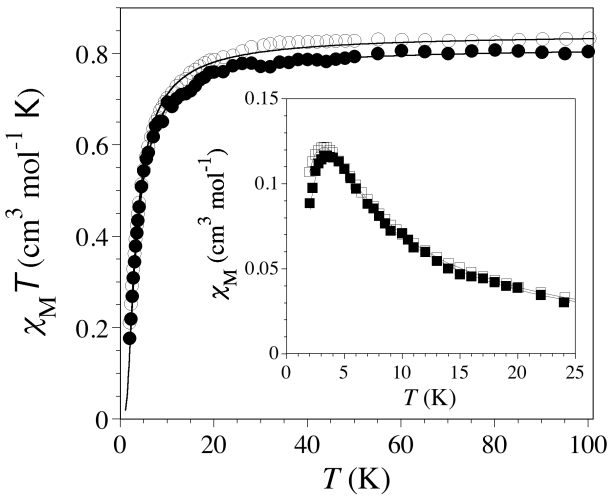

Figure II.8 Temperature dependence of $\chi_M T$ of powdered samples (○) and frozen-matrix methanol solutions (●) of **II.1** under applied magnetic fields of 100 G (T < 25 K) and 1.0 T ($T \geq 25$ K). The inset shows the temperature dependence of χ_M of powdered samples (□) and frozen-matrix methanol solutions (■) of **II.1**. The solid lines are the best-fit curves (see text).

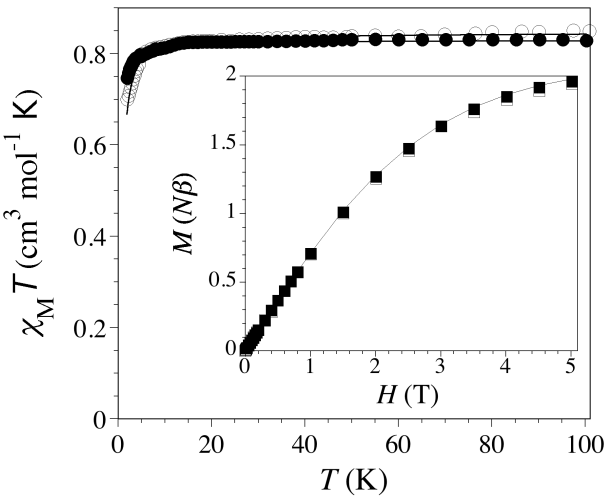

Figure II.9 Temperature dependence of $\chi_M T$ of powdered samples (○) and frozen-matrix methanol solutions (●) of **II.2** under applied magnetic fields of 100 G (T < 25 K) and 1.0 T ($T \geq 25$ K). The solid lines are the best-fit curves (see text). The inset shows the field dependence of M of powdered samples (□) and frozen-matrix methanol solutions (■) of **II.2** at 2.0 K. The solid line corresponds to the Brillouin curve for the sum of two doublet spin states (see text).

complexes.[2] At this respect, we have recently reported a quite rare *p*-triphenylenediamine-bridged dinuclear copper(II) complex possessing a similarly weak intramolecular antiferromagnetic coupling (J = –2.0 cm^{-1}) but with a rather shorter intermetallic distance ($r \approx 16.4$ Å).[8f]

The moderate to weak, long-range antiferromagnetic coupling in **II.1** and **II.2** indicates that strongly delocalized π-type orbital pathways through the *para*-substituted diphenylethyne (**II.1**) and di(phenylethynyl)phenylene (**II.2**) spacers are involved, as previously observed for the related oxamato-based dicopper(II) metallacyclophanes with *para*-substituted phenylene spacers which show a strong antiferromagnetic coupling (–J = 81-95 cm^{-1}).[13b] This situation clearly contrasts with that predicted by Coffman and Buettner (–J < 1.0 cm^{-1} at r > 9.0 Å),[2b] showing thus that OPE spacers can act as effective antiferromagnetic wires for the propagation of EE interactions between two Cu^{II} ions separated by intermetallic distances larger than one nanometer. As a matter of fact, a slow rate of decay of the magnetic coupling with the number of phenylethyne repeated units on the organic spacer, –$C_6H_4(C{\equiv}CC_6H_4)_n$– ($n$ = 0–2), is experimentally observed. So, the strong antiferromagnetic coupling across the *p*-phenylene spacers (n = 0) previously reported for the parent oxamato-based dicopper(II) paracyclophane (–J = 81–95 cm^{-1})[13b] is no more than 25- and 100-fold that those observed for **II.1** (–J = 3.9–4.1 cm^{-1}) and **II.2** (–J = 0.5–0.9 cm^{-1}) through the *p*-diphenylethyne (n = 1) and *p*-di(phenylethynyl)phenylene (n = 2) spacers, respectively.

II.6 Theoretical Calculations

Energy and molecular orbital calculations: distance dependence of the magnetic coupling. DF energy calculations were performed in acetonitrile solution on the BS singlet (S = 0) and triplet (S = 1) spin states of the model complexes **II.1**–**II.5** with an imposed coplanar conformation of the *para*-substituted benzene rings connected by carbon-carbon triple bonds (ψ = 0°) and a perpendicular orientation of the benzene rings with respect to the copper mean basal planes (ϕ= 90°) (see Computational Details). Selected calculated structural and energy data are listed in Table II.6.

Table II.5 Selected magnetic data for **II.1** and **II.2**.[a]

Compound	J[b] (cm^{-1})	g[c]	R[d] × 10^{-5}
II.1	–3.87(3)	2.124(3)	1.5
	[–4.05(3)]	[2.105(3)]	[1.8]
II.2	–0.90(1)	2.122(1)	1.0
	[–0.48(1)]	[2.105(1)]	[1.5]

[a] In the solid state. The magnetic data in methanol solution are given in brackets. [b] Magnetic coupling parameter (see eq II.1). The calculated errors are given in parentheses. [c] Zeeman factor of the Cu^{II} ions (see eq II.1). The calculated errors are given in parentheses. [d] Agreement factor defined as $R = \sum[(\chi_M T)_{exp} - (\chi_M T)_{calcd}]^2/\sum[(\chi_M T)_{exp}]^2$.

For all these orthogonal model molecules with an ideal D_{2h} symmetry (ψ = 0° and ϕ = 90°), the DF energy calculations showed a ground singlet spin state lying below the excited triplet spin state. The calculated value of the singlet-triplet energy gap for the orthogonal model complexes decreases when increasing the intermetallic distance. Nevertheless, two nanometers appears to be the upper limit for the observation of magnetic coupling (–J < 1.0 cm^{-1}) in the longer homologues including several C≡C bonds in the OPE spacers, –$C_6H_4(C{\equiv}CC_6H_4)_n$–. So, for instance, the DF energy calculations indicate an almost negligible singlet-triplet energy gap between the two Cu^{II} ions separated by up to 29.069 Å through the 4,4'-di(4-phenylethynyl)diphenylethyne spacers in **II.3** (ΔE_{ST} = –J = 0.119 cm^{-1}).

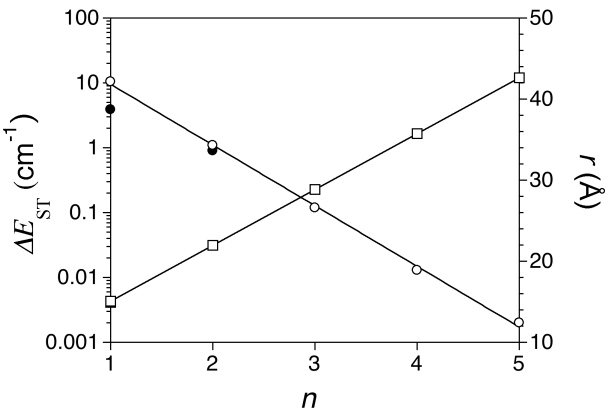

Figure II.10 Dependence of the calculated singlet-triplet energy gap (on a semilog scale) (○) and the intermetallic distance (□) for **II.1**–**II.5** (data from Table II.6) with the number of repeating units in the OPE spacers, $–C_6H_4(C{\equiv}CC_6H_4)_n–$ (n = 1–5). The experimental values of $–J$ (●) and r (■) for powdered samples of **II.1** and **II.2** are also shown for comparison (data from Table II.5). The solid lines correspond to the best-fit curves (see text).

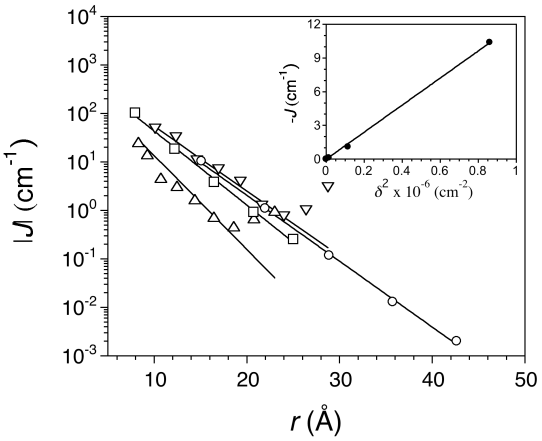

Figure II.11 Decay law of the calculated magnetic coupling (J) with the intermetallic distance (r) for **II.1**–**II.5** (○) (data from Table II.6) compared with those of related oxamato-based dicopper(II) metallacyclophanes with *p*-substituted oligophenylene (□) and *α,α'*- (△) or *β,β'*-substituted (▽) oligoacene spacers. The inset shows the linear dependence of the calculated values of $–J$ (●) with the square of the energy gap between the two SOMOs (δ) for **II.1**–**II.5** (data from Table II.6). The solid lines correspond to the best-fit curves (see text).

Table II.6 Selected calculated magnetostructural data for **II.1–II.5**.[a]

Compound	r[b] (Å)	ΔE_{ST}[c] (cm^{-1})	ν[d] (cm^{-1})
II.1	15.266	10.399	927.54
II.2	21.979	1.095	338.75
II.3	29.069	0.119	120.98
II.4	35.931	0.013	40.33
II.5	42.833	0.002	16.13

[a] DF calculations were performed on the BS singlet (S = 0) and triplet (S = 1) states of the D_{2h}-symmetric model complexes **II.1**–**II.5** (ϕ = 90° and ψ = 0°, see Computational Details). [b] Intermetallic distance. [c] Singlet-triplet energy gap ($\Delta E_{ST} = –J$). [d] Energy gap between the two singly occupied molecular orbitals (SOMOs) for the triplet state.

Concretly, the calculated singlet-triplet energy gap for the orthogonal model complexes **II.1** and **II.2** decreases when increasing the intermetallic distance [$\Delta E_{ST} = –J$ = 10.399 (**II.1**) and 1.095 cm^{-1} (**II.2**) for r = 15.095 (**II.1**) and 21.979 Å (**II.2**); Table II.6], as experimentally observed [$\Delta E_{ST} = –J$ = 10.399 (**II.1**) and 1.095 cm^{-1} (**II.2**) for r = 15.095 (**II.1**) and 21.979 Å (**II.2**); Table II.6], as experimentally observed. The deviations between the calculated and the experimental $–J$ values [$–J$ = 3.9–4.1 (**II.1**) and 0.5–0.9 cm^{-1} (**II.2**); Table II.5] are likely due to the loss of π-conjugation between the benzene rings by conformational rotation about the carbon-carbon triple bond ($\psi \neq 0°$) and/or the loss of orthogonality between the benzene and the copper mean basal planes ($\phi \neq 90°$), as shown earlier for the related oxamato-based dicopper(II) metallacyclophanes with 4,4'-biphenylene spacers.[13b] In fact, DF energy calculations on the actual structure of **II.1** possessing an overall parallel-displaced π-stacked conformation of the two not exactly planar 4,4'-diphenylethyne spacers [ψ = 7.8(1)°; ϕ = 56.4(1) and 58.4(1)°] gave a smaller singlet-triplet energy gap ($\Delta E_{ST} = –J$ = 6.1 cm^{-1}) which is closer to the experimental one in the solid state ($–J$ = 3.9 cm^{-1}).[13e]

The results of the DF calculations on the D_{2h}-symmetric model complexes **II.1**–**II.5** with extended π-conjugated OPE spacers, $–C_6H_4(C{\equiv}CC_6H_4)_n–$ (n = 1–5), are shown in Figure II.10 in terms of both structural and magnetic data. Together with a linear increase in the estimated intermetallic distance (r), the calculated singlet-triplet energy gap ($–J$) decreases in an exponential manner with the number of phenylene repeat units (n = 1–5) connected by C≡C bonds along this series (solid lines in Figure II.10). The fit of the calculated magnetostructural data for **II.1**–**II.5** provides a decay law of the exchange interaction with the intermetallic distance as $–J = 1.08 \times 10^3 \exp(–0.31r)$ (Figure II.11). The calculated value of 0.31 Å^{-1} for the exponential factor is lower than that found in the related series of oxamato-based dicopper(II) metallacyclophanes with *p*-substituted oligophenylene (OP) spacers (0.35 Å^{-1}) (solid lines in Figure II.11).[13b] This indicates a higher efficiency on long-range magnetic coupling for the OPE spacers compared to the OP ones, suggesting thus that the inclusion of additional C≡C bonds between the benzene rings occurs without any loss of π-conjugated aromatic character. In fact, the calculated γ value for **II.1**–**II.5** is identical to that found in the fully π-conjugated *β,β'*-substituted oligoacene (OA) spacers (γ = 0.31 Å^{-1}), being significantly lower than that found in *α,α'*-substituted ones (γ = 0.45 Å^{-1}) (solid lines in Figure II.11).[13c] However, no unique wire-like magnetic behavior was observed for **II.1**–**II.5**, as reported earlier for the longer members of the series of oxamato-based dicopper(II) metallacyclophanes with fully π-conjugated OA spacers (Figure II.11).[13c]

In contrast, the earlier relation obtained by Coffman and Buettner[2b] together with the more recent ones based on experimental magnetostructural data on simple dicopper(II) complexes[13b] announce a dramatically faster decay of the magnetic coupling with the intermetallic distance (γ = 1.5–1.8 Å^{-1}). A notable exception is the series of oligo-*p*-phenylenediamine-bridged dicopper(II) complexes recently reported by us showing a slow experimental decay rate of the magnetic coupling which is, how-

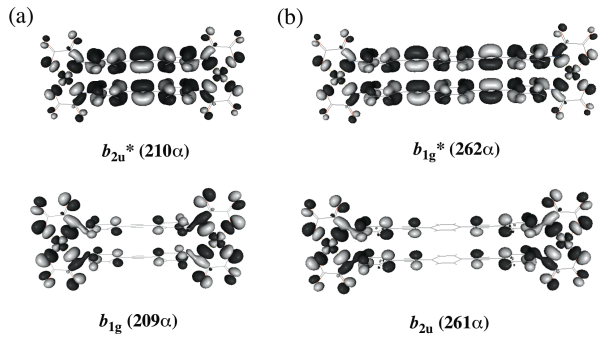

Figure II.12 Perspective views of the calculated magnetically active SOMOs for the triplet spin state of **II.1** (a) and **II.2** (b). The isodensity surface corresponds to a cutoff value of 0.04 e bohr^{-3}.

ever, somewhat higher than that predicted by the DF calculations (γ = 0.37 *vs*. 0.18 Å^{-1}).[8f] Fabre *et al.* have also reported the occurrence of strong exchange coupling interactions in Ru^{III}_2 complexes with oligophenyl-, oligophenylethene-, and oligophenylethynedicyanamido bridging ligands (γ = 0.10 Å^{-1}),[7k] as predicted theoretically by Ruiz *et al.* for related oligoacenedicyanamido-bridged M^{III}_2 complexes (M = Cr, Mn, and Fe).[8b] Once again, this reflects the large efficiency of π- *vs.* σ-type exchange pathways, as expected because of the larger spin delocalization and spin polarization contributions to the ground state electronic structure in the former case.

Molecular orbital (MO) calculations on the D_{2h}-symmetric model complexes **II.1**–**II.5** evidence that the exchange interaction between the two unpaired electrons occupying the π-type d_{xy} orbitals of the square planar Cu^{II} ions ('magnetic orbitals') and pointing toward the equatorial Cu–N and Cu–O bonds, is mainly transmitted through the π-bond system of the OPE spacers (see Figure II.2). This is nicely illustrated by the pair of singly occupied molecular orbitals (SOMOs) for the triplet spin state of **II.1** and **II.2**, which show a high metal-ligand covalency and strongly ligand delocalized character (Figure II.12). These two pairs of SOMOs, noted b_{1g} and b_{2u}* (**II.1**) or alternatively b_{2u} and b_{1g}* (**II.2**), are composed by the symmetric and antisymmetric combinations of the d_{xy}(Cu) orbitals mixed with the corresponding combinations of appropriate symmetry of the two π-type orbitals of the diphenylethyne (**II.1**) and di(phenylethynyl)phenylene (**II.2**) spacers, which are in turn made up of p_z(C) orbitals of the sp^2- and *sp*-type carbon atoms from the benzene rings and from the ethyne groups, respectively. As expected, the energy separation (δ) between the two SOMOs for the triplet spin state of **II.1**–**II.5** decreases continuously along this series (Table II.6), in such a way that the calculated $-J$ values vary fairly well with the square of δ as $-J = 12.0 \times 10^{-6}\ \delta^2$ (inset of Figure II.11), according to the

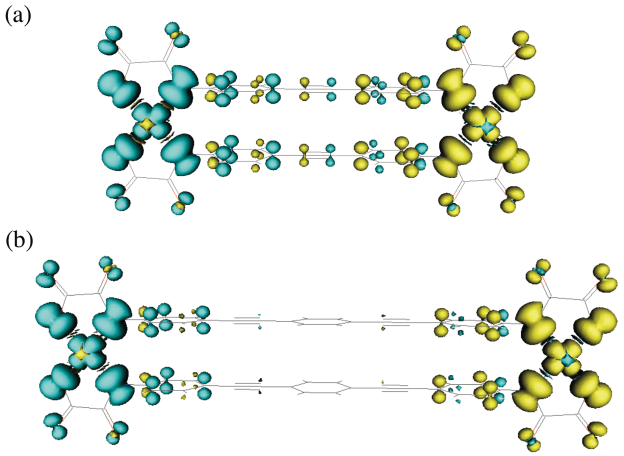

Figure II.13 Perspective views of the calculated spin density distribution for the BS singlet spin state of **II.1** (a) and **II.2** (b). Yellow and blue contours represent positive and negative spin densities, respectively. The isodensity surface corresponds to a cutoff value of 0.001 e bohr^{-3}.

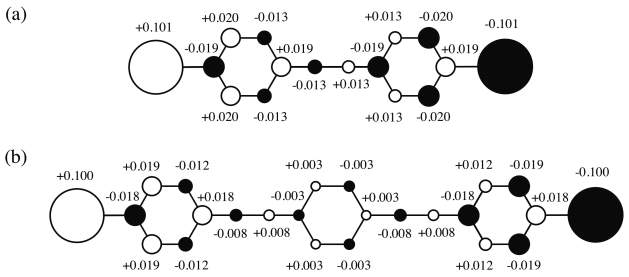

Figure II.14 Projection view of the spin density distribution on the oligo(*p*-phenylene-ethynylene)diamidate bridges for the BS singlet spin state of **II.1** (a) and **II.2** (b) with the calculated atomic spin density values (in e units). Empty and full circles represent positive and negative spin densities respectively, with scaled surface areas.

simplest orbital models of the electron exchange interaction.[2a] This situation reflects the similar decrease of the d_{xy}(Cu)/π(L) metal-ligand orbital mixing for **II.1**–**II.5** and the smaller delocalization of the unpaired electrons of the Cu^{II} ions onto the π-conjugated electron system of the OPE spacers with the increasing number of phenylethyne units (*n*) from 1 to 5 along this series.

Spin density analysis: spin delocalization *vs.* spin polarization mechanism. Spin densities obtained by natural bond orbital (NBO) analysis on the BS singlet state of **II.1** and **II.2** reflect the relative importance of spin delocalization and spin polarization effects for the propagation of the exchange interaction between the unpaired electrons of the two metal centers through the π-type orbital pathways of the *p*-diphenylethyne (**II.1**) and *p*-di(phenylethynyl)phenylenediamidate (**II.2**) bridges (Figure II.13).

The values of the spin density at the amidate-nitrogen atoms are important [±0.101 (**II.1**) and ±0.100 e (**II.2**)] and, moreover, they have the same sign as in the copper atoms to which they are coordinated [±0.564 (**II.1**) and ±0.565 e (**II.2**)] (Figure II.14). This fact indicates that the spin delocalization from the metal toward the amidato donor groups dominates over the spin polarization because of the strong covalency of the Cu–N bonds. In contrast, the sign alternation of the spin density at the carbon atoms of the *p*-diphenylethyne- (**II.1**) and *p*-di(phenylethynyl)phenylene (**II.2**) spacers agrees with a spin polarization by the amidate-nitrogen atoms, as reported earlier for the related dicopper(II) metallacyclophane with *p*-phenylenediamidate bridges.[13b] So, the values of the spin density of opposite sign on the adjacent sp^2-type carbon atoms of the two terminal benzene rings [from ±0.013 to ±0.020 e (**II.1**) and from ±0.012 to ±0.019 e (**II.2**)] are as important as those at the *sp*-type carbon atoms from the ethyne groups [±0.013 (**II.1**) and ±0.008 e

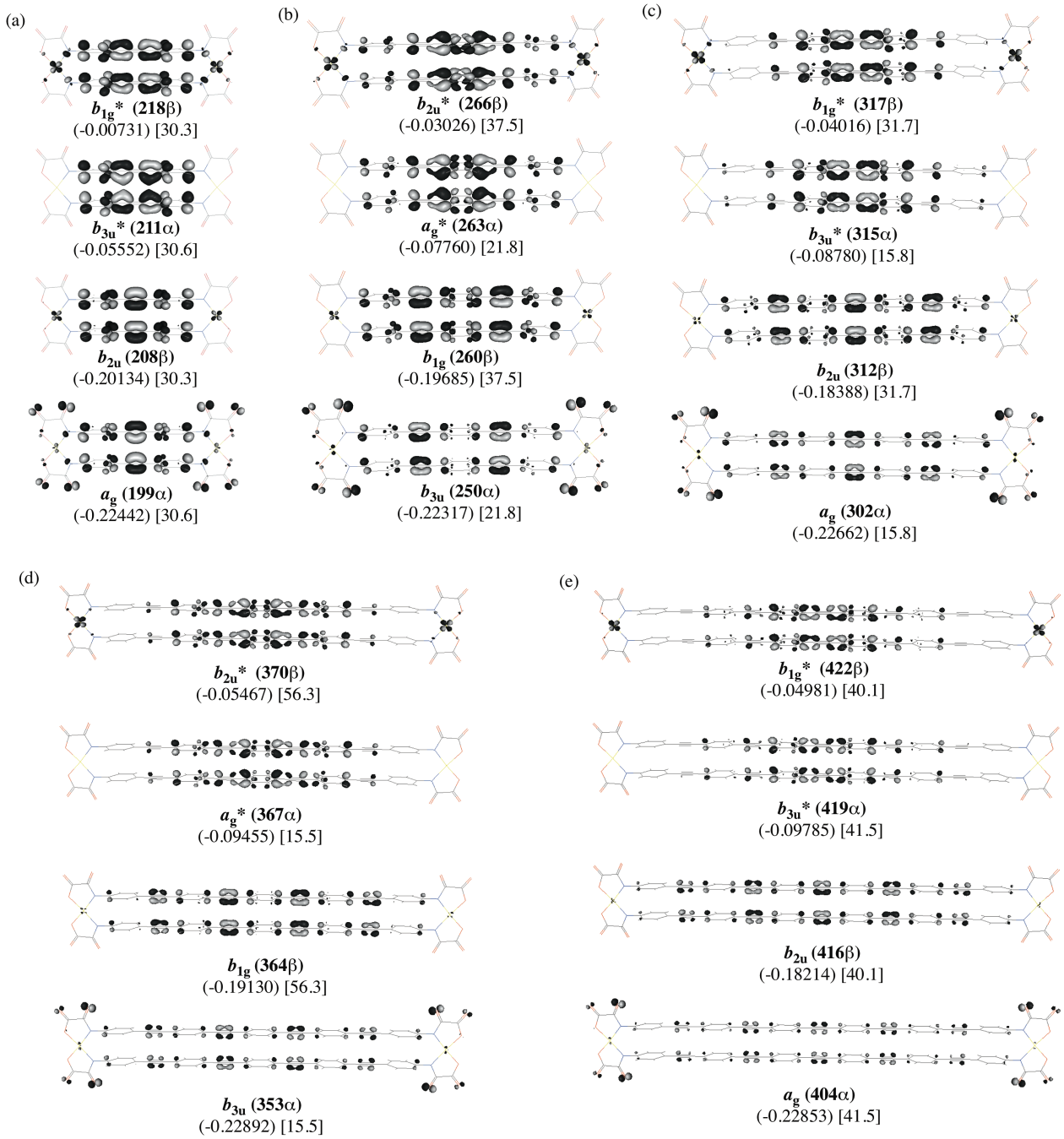

Figure II.15 Perspective views of the two calculated pairs of optically active LUMOs and HOMOs involved in the intraligand π–π* transitions for the triplet spin state of **II.1**–**II.5** (a)-(e). The orbital energies (in a.u.) and the transition contribution percentages are given in parentheses and brackets, respectively. The isodensity surface corresponds to a cutoff value of 0.04 e bohr^{-3}.

Table II.7 Selected calculated spectrostructural data for **II.1**–**II.5**.[a]

Compound	r^b (Å)	$\lambda_{max}{}^c$ (nm)	
		$S = 0$	$S = 1$
II.1	15.266	293 (1.24) [34130]	289 (1.08) [34602]
II.2	21.979	340 (2.60) [29412]	337 (1.94) [29674]
II.3	29.069	368 (3.14) [27174]	365 (1.73) [27397]
II.4	35.931	385 (3.69) [25974]	380 (2.88) [26316]
II.5	42.833	399 (2.38) [25063]	394 (1.65) [25381]

[a] TD-DF calculations were performed on the BS singlet ($S = 0$) and triplet ($S = 1$) states of the D_{2h}-symmetric model complexes **II.1**–**II.5** ($\theta = 90°$ and $\varphi = 0°$, see Computational Details). [b] Intermetallic distance. [c] Intraligand transition wavenumber. The values of the oscillator strength (f) and the transition energy (cm^{-1}) are given in parentheses and brackets, respectively.

(**II.2**)] (Figure II.14). This situation evidences the partial preservation of the π-conjugation with the incorporation of additional C≡C bonds connecting the phenylene groups into the OPE spacers for **II.1** and **II.2**. Indeed, the values of the spin density at the sp^2-type carbon atoms of the central benzene ring in **II.2** are smaller but nonnegligible [±0.003 e] (Figure II.14), as expected because of the appreciable attenuation of the spin delocalization with the incorporation of an additional phenylene group into the OPE spacers. Hence, a net decrease of the antiferromagnetic exchange interaction results with the successive incorporation of additional phenylethyne units into the OPE spacers, as experimentally observed for **II.1** and **II.2** and theoretically predicted for **II.1**–**II.5**.

Transition energy and molecular orbital calculations: distance dependence of intraligand optical transitions. TD-DF calculations were performed in acetonitrile solution on the BS singlet ($S = 0$) and triplet ($S = 1$) spin states of the D_{2h}-symmetric model complexes **II.1**–**II.5** (see Computational Details). Selected calculated structural and transition energy data are listed in Table II.7.

The most remarkable feature of the calculated electronic spectra for both the BS singlet and triplet states of the orthogonal model complexes **II.1**–**II.5** is the presence of an intense UV band of IL nature, whose energy decreases when increasing the intermetallic distance along this series. Hence, the calculated values of the transition energy for both the BS singlet and triplet spin states decrease from **II.1** [λ_{max} = 34130 ($S = 0$) and 34602 nm ($S = 1$)] to **II.2** [λ_{max} = 29412 ($S = 0$) and 29674 nm ($S = 1$)] (Table II.7), as experimentally observed [λ_{max} = 32468 (**II.1**) and 31646 nm (**II.2**); Table II.3]. Overall, this indicates that the correlation length increases with the number of phenylethyne units in the diphenylethyne (**II.1**) and di(phenylethynyl)phenylene spacers (**II.2**). The deviations between the calculated and experimental values of the bathochromic shift are likely due to the varying loss of π-conjugation among the benzene rings by conformational rotation about the carbon-carbon triple bond ($\psi \neq 0°$), as reported earlier in related theoretical studies on purely organic, amino-terminated OPE derivatives.[15c]

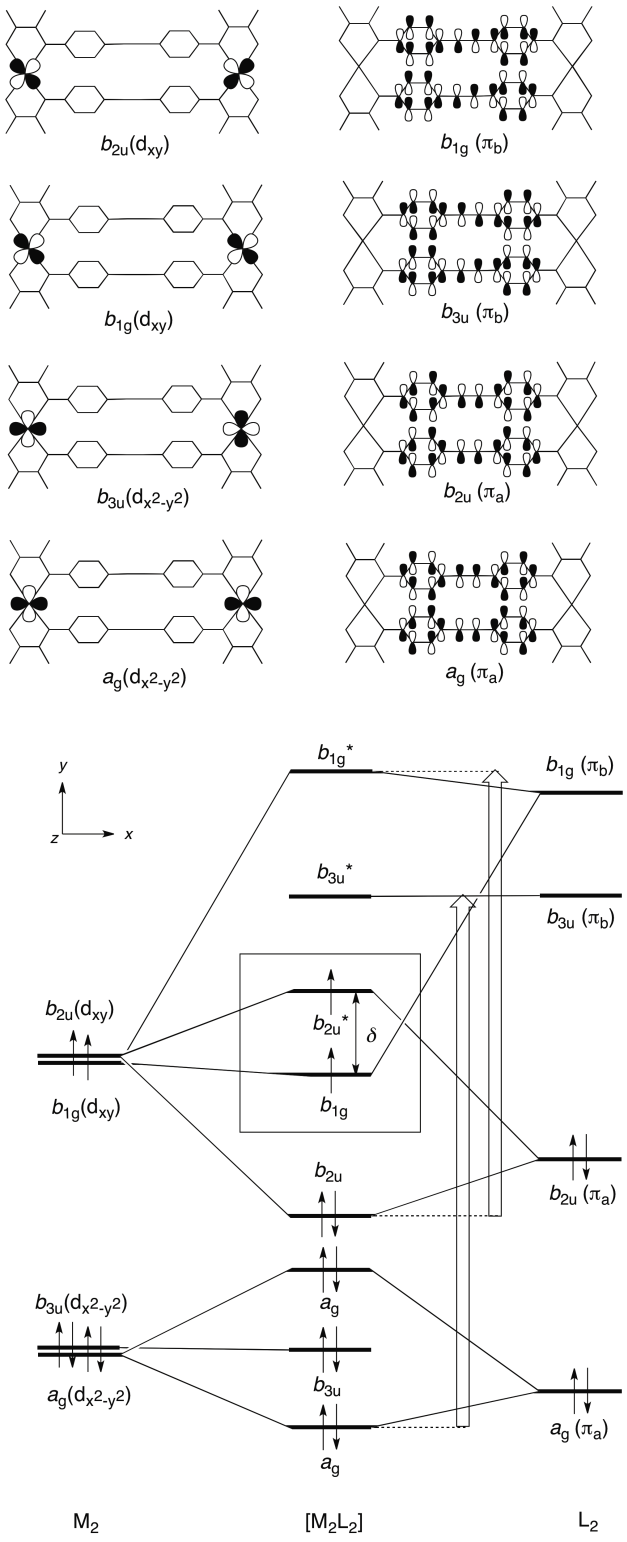

Figure II.16 Simplified MO diagram of the π bonding interaction between the symmetric and antisymmetric combinations of the ligand π_a and π_b and the metal d_{xy} and $d_{x^2-y^2}$ FMOs for **II.1**. The dinuclear metallacyclophane skeleton is shown for the sake of clarity. The open arrows correspond to the intraligand π–π* transitions between the optically active HOMOs and LUMOs. The boxed structure shows the magnetically active SOMOs.

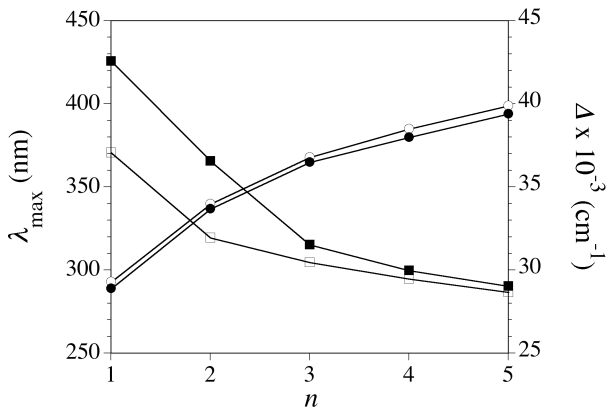

Figure II.17 Dependence of the calculated intraligand transition wavenumber (λ_{max}) for the BS singlet (○) and triplet (●) spin states of **II.1**–**II.5** (data from Table II.7) and the HOMO-LUMO energy gap (Δ) of the two optically active a_g/b_{3u}* (□) and b_{2u}/b_{1g}* (■) pairs for the triplet spin state of **II.1**–**II.5** (data from Figures II.14 and II.15, Supporting Information) with the number of repeating units in the OPE spacers, $-C_6H_4(C{\equiv}CC_6H_4)_n-$ (n = 1–5). The solid lines are guides for the eyes.

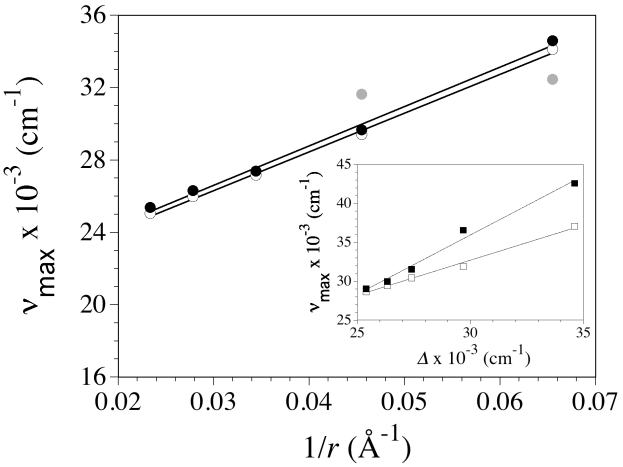

Figure II.18 Decay law of the calculated intraligand transition energy (v_{max}) with the reciprocal intermetallic distance ($1/r$) for the BS singlet (○) and triplet (●) spin states of **II.1**–**II.5** (data from Table II.7). The experimental values of the intraligand transition energy (●) for **II.1** and **II.2** in acetonitrile solution are also shown for comparison (data from Table II.3). The inset shows the linear dependence of the calculated v_{max} values (■) with the HOMO-LUMO energy gap (Δ) of the two optically active a_g/b_{3u}* (□) and b_{2u}/b_{1g}* (■) pairs for the triplet spin state of **II.1**–**II.5** (data from Figures II.15 and II.17). The solid lines correspond to the best-fit curves (see text).

This intense UV band in the calculated electronic spectra of **II.1**–**II.5** have two main contributions corresponding to the IL π–π* transitions from the highest occupied molecular orbitals (HOMOs), a_g and b_{2u} (**II.1**, **II.3**, and **II.5**) or alternatively b_{3u} and b_{1g} (**II.2** and **II.4**), to the lowest unoccupied molecular orbitals (LUMOs), b_{3u}* and b_{1g}* (**II.1**, **II.3**, and **II.5**) or alternatively a_g* and b_{2u}* (**II.2** and **II.4**). The MO composition and energy data of the transitions for the triplet spin state of **II.1**–**II.5** are depicted in Figure II.15.

In terms of the ligand field theory, this situation can be described through the π bonding interaction between the fragment molecular orbitals (FMOs) of the OPE spacers (π_a and π_b) and those of the metal centers (d_{xy} and $d_{x^2-y^2}$), as illustrated for **II.1** in Figure II.16. So, the two optically active HOMO/LUMO pairs of mainly ligand-based nature, noted a_g/b_{3u}* and b_{2u}/b_{1g}*, are composed by the symmetric and antisymmetric combinations of the out-of-plane, filled π_a and unfilled π_b FMOs of the two facing diphenylethyne spacers respectively, which are in turn made up of p_z orbitals of the sp^2- and sp-type carbon atoms from the benzene rings and from the ethyne groups of bonding (π_a) and antibonding (π_b) character. Yet they possess a varyingly small but non-negligible metal contribution resulting from the π-type interaction with the in-plane, filled d_{xy} and half-filled $d_{x^2-y^2}$ FMOs of the copper centers of appropriate symmetry.

The results of the TD-DF calculations on the BS singlet (S = 0) and triplet (S = 1) spin states of the D_{2h}-symmetric model complexes **II.1**–**II.5** with extended π-conjugated OPE spacers, $-C_6H_4(C{\equiv}CC_6H_4)_n-$ (n = 1–5), are shown in Figure II.17 in terms of both transition and MO energy data. The calculated values of the IL π–π* transition wavenumber (λ_{max}) increase asymptotically when increasing the correlation length along this series for both the BS singlet and triplet spin states. As expected, a parallel decrease of the calculated values of the HOMO-LUMO energy gap (Δ) corresponding to the two individual transitions, $a_g \rightarrow b_{3u}$* and $b_{2u} \rightarrow b_{1g}$* (**II.1**, **II.3**, and **II.5**) or alternatively $b_{3u} \rightarrow a_g$* and $b_{1g} \rightarrow b_{2u}$* (**II.2** and **II.4**), occurs for the triplet spin state of **II.1**–**II.5**. The fit of the calculated spectrostructural data for the BS singlet and triplet spin states of **II.1**– **II.5** provides a linear decay law of the IL π–π* transition energy with the reciprocal intermetallic distance as $v_{max} = 1.99 \times 10^4 + 2.15 \times 10^5\ (1/r)$ (S = 0) or $v = 2.01 \times 10^4 + 2.18 \times 10^5\ (1/r)$ (S = 1) (Figure II.18), in such a way that the calculated v_{max} values vary almost linearly with Δ as $v_{max} = 5.7 + 0.90 \times 10^3\Delta$ and $v_{max} = -9.7 + 1.52 \times 10^3\Delta$ (inset of Figure II.18).

This situation reflects the effects of the successive incorporation of additional phenylethyne units on the π-conjugation into the linear OPE spacers, as exemplified by the longer homologue of this series which shows a strong ligand delocalized character for the two pairs of optically active HOMOs and LUMOs (Figure II.15e). So, the pair of HOMOs for the triplet spin state of **II.5**, noted a_g and b_{2u}, are made up by the symmetric and antisymmetric combinations of the bonding π_a orbitals of the two facing OPE spacers, which are weakly mixed with the corresponding combinations of appropriate symmetry of the d_{xy} and $d_{x^2-y^2}$ metal orbitals, respectively. The pair of LUMOs for the triplet spin state of **II.5**, noted b_{3u}* and b_{1g}*, are composed by the symmetric and antisymmetric combinations of the antibonding π_b orbitals of the two facing OPE spacers, which are weakly mixed with the corresponding combinations of appropriate symmetry of the d_{xy} and d_{x2-y2} metal orbitals, respectively. All of them evidence a significant delocalization onto the p_z(C) orbitals of the benzene rings and the ethyne groups that is directly responsible for the proposed molecular wire behavior of extended π-conjugated OPEs.[15c]

II.7 Concluding Remarks

In this paper, we present a density functional study on long-range magnetic and electronic coupling through extended π-conjugated aromatic spacers in a new family of dicopper(II) metallacyclophanes consisting of two square planar bis(oxamato)copper(II) *spin-bearing sites* separated by two linear oligo(*p*-phenylene-ethynylene) (OPE) *spacers*, $-C_6H_4(C{\equiv}CC_6H_4)_n-$ (n = 1–5). Because of their planar configuration, a strong orbital overlap between the p_z-type orbitals of the *para*-substituted benzene rings across the carbon-carbon triple bonds occurs along the *p*-phenylethyne *repeated units* of the OPE spacers, as evidenced by the linear increase of the intraligand (IL) π–π* transition energy with the reciprocal correlation length along this series. Hence, a unusual π-type orbital pathway is available for the propagation of antiferromagnetic interactions between the unpaired electrons occupying the d_{xy}-type orbitals of the two metal centers through the extended π-conjugated OPE spacers, which are disposed perpendicularly to the metal basal planes as a result of the overall orthogonal molecular geometry. On the other hand, the rather low exponential decay of the antiferromagnetic coupling with the intermetallic distance along this series indicates that the electron exchange (EE) through linear OPE spacers follows a spin polarization mechanism. This conclusion is further supported by the presence of non-negligible spin densities of alternating sign on the bridge in the calculations on the broken-symmetry (BS) singlet states. Based on this combined experimental and computational study, we then propose that linear OPE spacers can act as effective antiferromagnetic wires between two Cu^{II} ions separated by up to 3.0 nm.

II.8 Experimental Section

Materials. All chemicals were of reagent grade quality, and they were purchased from commercial sources and used as received. 4,4'-Diphenylethynediamine and 1,4-di(4-phenylethynyl)phenylenediamine were prepared as reported in the literature.[15a]

Preparations. Et_2H_2dpeba: Triethylamine (1.4 mL, 10.0 mmol) and ethyl oxalyl chloride ester (1.2 mL, 10.0 mmol) were added to a solution of 4,4'-diphenylethynediamine (1.0 g, 5.0 mmol) in THF (150 mL) under vigorous stirring. The reaction mixture was heated under reflux for 3 h at 80 ºC. The yellow solid was collected by filtration, washed thoroughly with water to remove the precipitate of Et_3NHCl, and then with acetone and diethyl ether, and dried under vacuum (1.6 g, 78% yield). Anal. Calcd for $C_{22}H_{20}N_2O_6$: C, 64.70; H, 4.94; N, 6.86. Found: C, 64.77; H, 4.97; N, 6.82. ^{1}H NMR (C_2D_6SO): δ 1.31 (t, 6 H, 2 CH_3), 4.30 (q, 4 H, 2 CH_2O), 7.55 (d, 4 H, 2–H, 6–H, 2'–H, and 6'–H), 7.80 (d, 4 H, 3–H, 5–H, 3'–H, and 5'–H), 10.95 (s, 2 H, 2 NH). IR (KBr): 3335 (N–H), 2208 (C≡C), 1729, 1705 cm^{-1} (C=O).

Et_2H_2tpeba: Triethylamine (1.4 mL, 10.0 mmol) and ethyl oxalyl chloride ester (1.2 mL, 10.0 mmol) were added to a solution of 1,4-di(4-phenylethynyl)phenylenediamine (1.5 g, 5.0 mmol) in THF (150 mL) under vigorous stirring. The reaction mixture was heated under reflux for 3 h at 80 ºC. The yellow solid was collected by filtration, washed thoroughly with water to remove the precipitate of Et_3NHCl, and then with acetone and diethyl ether, and dried under vacuum (2.0 g, 80% yield). Anal. Calcd for $C_{30}H_{24}N_2O_6$: C, 70.86; H, 4.76; N, 5.51. Found: C, 70.77; H, 4.82; N, 5.52. ^{1}H NMR (C_2D_6SO): δ 1.33 (t, 6 H, 2 CH_3), 4.33 (q, 4 H, 2 CH_2O), 7.56 (d, 4 H, 2'–H, 6'–H, 2''–H, and 6''–H), 7.81 (d, 4 H, 3'–H, 5'–H, 3''–H, and 5''–H), 10.96 (s, 2 H, 2 NH). IR (KBr): 3335 (N–H), 2217 (C≡C), 1725, 1698 cm^{-1} (C=O).

(nBu$_4$N)$_4$[Cu$_2$(dpeba)$_2$] · 4MeOH · 2Et$_2$O (II.1): A 1.0 M methanolic solution of nBu$_4$NOH (4.0 mL, 4.0 mmol) was added to a suspension of Et_2H_2dpeba (0.41 g, 1.0 mmol) in 20 mL of methanol under gentle warming. A methanol solution (10 mL) of $Cu(ClO_4)_2 \cdot 6H_2O$ (0.37 g, 1.0 mmol) was then added dropwise under stirring. The resulting mixture was filtered to remove the small amount of solid particles and the solvent was removed under vacuum. The dark green solid was recuperated with THF, collected by filtration, washed thoroughly with THF to remove the precipitate of nBu$_4$NClO$_4$, and air dried. Recrystallization from a methanol solution gave dark green prisms of **II.1** suitable for single-crystal X-ray diffraction upon layering of diethyl ether (0.72 g, 70% yield). Anal.: calcd for $C_{100}H_{160}Cu_2N_8O_{12}$: C, 66.97; H, 8.99; N, 6.25. Found: C, 65.31; H, 9.38; N, 6.91. IR (KBr): 2207 (C≡C), 1685, 1648 cm^{-1} (C=O).

(nBu$_4$N)$_4$[Cu$_2$(tpeba)$_2$] · 12H$_2$O (II.2): A 1.0 M methanolic solution of nBu$_4$NOH (4.0 mL, 4.0 mmol) was added to a suspension of Et_2H_2tpeba (0.51 g, 1.0 mmol) in 20 mL of methanol under gentle warming. A methanol solution (10 mL) of $Cu(ClO_4)_2 \cdot 6H_2O$ (0.37 g, 1.0 mmol) was then added dropwise under stirring. The resulting mixture was filtered to remove the small amount of solid particles and the solvent was removed under vacuum. A microcrystalline dark green solid of **II.2** was recuperated with THF, collected by filtration, washed thoroughly with THF to remove the precipitate of nBu$_4$NClO$_4$, and air dried (0.70 g, 65% yield). Anal.: calcd for $C_{116}H_{192}Cu_2N_8O_{24}$: C, 63.05; H, 8.76; N, 5.07. Found: C, 63.37; H, 8.63; N, 4.92. IR (KBr): 2208 (C≡C), 1672, 1655, 1649 cm^{-1} (C=O).

Physical techniques. Elemental analyses (C, H, N) were performed at the Servicio Central de Soporte a la Investigación (SCSIE) at the Universitat de València (Spain). ^{1}H NMR spectra were recorded at room temperature on a Bruker AC 200 (200.1 MHz) spectrometer. Deuterated dimethylsulphoxide was used as solvent and internal standard (δ = 2.50 ppm). FT–IR spectra were recorded on a Nicolet-5700 spectrophotometer as solid KBr pellets. Electronic absorption spectra were recorded on acetonitrile or dimethylsulphoxide solutions at room temperature with an Agilent Technologies-8453 spectrophotometer equipped with a UV–Vis

Chem Station. X-band (ν = 9.47 GHz) EPR spectra were recorded on frozen-matriz acetonitrile solutions at 4.0 K under non-saturating conditions with a Bruker ER 200 D spectrometer equipped with a helium cryostat.

Magnetic measurements. Variable-temperature (2.0–300 K) magnetic susceptibility measurements and variable-field (0–5.0 T) magnetization measurements at 2.0 K were carried out on powdered samples with a SQUID magnetometer. The magnetic susceptibility data at low temperatures (T < 25 K) were measured under a very low applied magnetic field (H = 100 G) in order to avoid saturation effects.

Variable-temperature (2.0–150 K) magnetic susceptibility measurements on frozen-matrix methanol solutions were performed with the same SQUID magnetometer. Two quartz tubes of suprasil quality (8 cm height × 5 mm outer diameter with 0.5 mm wall thickness) were placed together in vertical position, the top tube containing the sample in methanol (8 mm is the height of the solution) and the bottom one being open on both sides. The two tubes fit perfectly in the plastic straw normally used in the SQUID devices. Placing the two tubes one on the top of the other in a vertical manner minimizes their magnetic contribution. At that respect, it is very illustrative that the two empty tubes placed in the plastic straw under an applied magnetic field of 1.0 T gave an almost negligible magnetic signal (less than 5.0×10^{-6} cm^3). The experimental data were corrected for the diamagnetic contributions of the constituent atoms and the sample holder and/or the methanol solvent (24000×10^{-6} cm^3 mol^{-1}), as well as for the temperature-independent paramagnetism (tip) of the two Cu^{II} ions (120×10^{-6} cm^3 mol^{-1}).

Crystal structure data collection and refinement. Single-crystal X-ray diffraction data of **II.1** were collected on a Bruker-Nonius X8APEXII CCD area detector diffractometer using graphite-monochromated Mo-K_α radiation. All calculations for data reduction, structure solution, and refinement were done through the SAINT[19] and SADABS[20] programs. The structure of **II.1** was solved by direct methods and subsequently completed by Fourier recycling using the SHELXTL software package.[21] All non-hydrogen atoms were refined anisotropically. The hydrogen atoms were set in calculated positions and refined as riding atoms. The final geometrical calculations and the graphical manipulations were carried out with PARST97[22] and CRYSTAL MAKER[23] programs, respectively.

Crystallographic data (excluding structure factors) for the structure reported in this paper have been deposited with the Cambridge Crystallographic Data Centre as supplementary publication CCDC no. 831325 (**II.1**). Copies of the data can be obtained free of charge on application to CCDC, 12 Union Road, Cambridge CB21EZ, UK (fax: (+44) 1223-336-033; e-mail: deposit@ccdc.cam.ac.uk).

II.9 Computational Details

The molecular geometries of the model complexes **II.1**–**II.5** with D_{2h} molecular symmetry were not optimized, but their bond lengths and interbond angles were taken from the crystal structure of 1 with an imposed coplanar conformation of the phenylene rings in the OPE spacers (ψ = 0°) and a perpendicular orientation of the phenylene rings with respect to the copper mean basal planes (ϕ = 90°).

Density functional (DF) and time-dependent density functional (TD-DF) calculations were carried out on the broken-symmetry (BS) singlet and triplet spin states of the D_{2h}-symmetric model complexes **II.1**–**II.5** in acetonitrile solution using the hybrid B3LYP method[24] combined with the "broken-symmetry" approach,[25] as implemented in the Gaussian 09 program.[26] The triple- and double-ζ quality basis sets proposed by Ahlrichs and coworkers[27] were used for the metal and non-metal atoms, respectively. The calculated spin density data were obtained from Natural Bond Orbital (NBO) analysis.[28] Solvation effects were introduced using a polarizable continuum model (PCM), where the cavity is created via a series of overlapping spheres,[29] in order to accurately calculate the energy data of the frontier molecular orbitals as well as the transition energy data and transition strength force constants, which were deduced from transition electric dipole moments.

References

[1] a) O. Kahn, *Molecular Magnetism*; VCH Publishers: New York, **1993**. b) *Molecular Electronics*; Jorner, J., Ratner, M., Eds.; Blackwell Science: Oxford, **1997**.

[2] a) J. P. Hay, J. C. Thibeault, R. Hoffmann, *J. Am. Chem. Soc.* **1975**, *97*, 4884. b) R. E. Coffman, G. R. Buettner, *J. Phys. Chem.* **1979**, *83*, 2387. c) O. Kahn, *Angew. Chem., Int. Ed. Engl.* **1985**, *24*, 834. d) J. A. McCleverty, M. D. Ward, *Acc. Chem. Res.* **1998**, *31*, 842. e) T. Terencio, R. Bastardis, N. Suaud, D. Maynau, J. Bonvoisin, J. P. Malrieu, C. J. Calzado, N. Guihéry, *Phys. Chem. Chem. Phys.* **2011**, *13*, 12314.

[3] a) C. Creutz, *Prog. Inorg. Chem.* **1983**, *30*, 1. b) R. J. Crutchley, *Adv. Inorg. Chem.* **1994**, *41*, 273. c) J. P. Launay, *Chem. Soc. Rev.* **2001**, *30*, 386. d) J. P. Launay, C. Coudret, *Electron Transfer in Chemistry*; Wiley-VCH, **2001**, Vol. 5, p 3.

[4] a) C. Joachim, J. K. Gimzewski, A. Aviram, *Nature* **2000**, *408*, 541. b) J. M. Tour, *Acc. Chem. Res.* **2000**, *33*, 791. c) R. R. Caroll, C. B. Gorman, *Angew. Chem., Int. Ed.* **2002**, *41*, 4379. d) W. Liang, M. P. Shores, M. Bockrath, J. R. Long, H. Park, *Nature* **2002**, *417*, 725. e) N. Robertson, C. A. McGowan, *Chem. Soc. Rev.* **2003**, *32*, 96. f) A. Dei, D. Gatteschi, C. Sangregorio, L. Sorace, *Acc. Chem. Res.* **2004**, *37*, 827. g) L. Lafferentz, F. Ample, H. Yu, S. Hecht, C. Joachim, L. Grill, *Science* **2009**, *323*, 1193.

[5] a) M. C. Dul, E. Pardo, R. Lezcouëzec, L. M. Chamoreau, F. Villain, Y. Journaux, R. Ruiz-García, J. Cano, M. Julve,; F. Lloret, J. Pasán, C. Ruiz-Pérez, *J. Am. Chem. Soc*. **2009**, *131*, 14614. b) E. Pardo, J. Ferrando-Soria, M. C. Dul, R. Lezcouëzec,; Y. Journaux, R. Ruiz-García, J. Cano, M. Julve,; F. Lloret, L. Cañadillas-Delgado, J. Pasán, C. Ruiz-Pérez, *Chem. Eur. J.* **2010**, *16*, 12838.

[6] a) M. I. Bruce, P. J. Low, *Adv. Organomet. Chem*. **2004**, *50*, 179. b) P. Aguirre-Etcheverry, D. O'Hare, *Chem. Rev*. **2010**, *110*, 4839.

[7] a) T. R. Felthouse, E. N. Duesler, D. N. Hendrickson, *J. Am. Chem. Soc.* **1978**, *100*, 618. b) T. R. Felthouse, D. N. Hendrickson, *Inorg. Chem.* **1978**, *17*, 2636. c) P. Chaudhuri, K. Oder, K. Wieghardt, S. Gehring, W. Haase, B. Nuber, J. Weiss, *J. Am. Chem. Soc.* **1988**, *110*, 3657. d) K. S. Bürger, P. Chaudhuri, K. Wieghardt, B. Nuber, *Chem. Eur. J.* **1995**, *1*, 583. e) A. M. W. Cargill-Thompson, D. Gatteschi, J. A. McCleverty, J. A. Navas, E. Rentschler, M. D. Ward, *Inorg. Chem.* **1996**, *35*, 2701. f) V. A. Ung, A. M. W. Cargill-Thompson, D. A. Bardwell, D. Gatteschi, J. C. Jeffery, J. A. McCleverty, F. Totti, M. D. Ward, *Inorg. Chem.* **1997**, *36*, 3447. g) J. Cano, G. De Munno, J. L. Sanz, R. Ruiz, J. Faus, F. Lloret, M. Julve, A. Caneschi, *J. Chem. Soc., Dalton Trans.* **1997**, 1915. h) V. A. Ung, S. M. Couchman, J. C. Jeffery, J. A. McCleverty, M. D. Ward, F. Totti, D. Gatteschi, *Inorg. Chem.* **1999**, *38*, 365. i) S. Bayly, J. A. McCleverty, M. D. Ward, D. Gatteschi, F. Totti, *Inorg. Chem.* **2000**, *39*, 1288. j) M. P. Shores, J. R. Long, *J. Am. Chem. Soc.* **2002**, *124*, 3512. k) M. Fabre, J. Bonvoisin, *J. Am. Chem. Soc.* **2007**, *129*, 1434. l) P. F. Hamon, Justaud, O. Cador, P. Hapiot, S. Rigaut, L. Toupet, L. Ouahab, H. Stueger, J. R. Hamon, C. Lapinte, *J. Am. Chem. Soc.* **2008**, *130*, 17372. m) M. Rancan, A. Dolmella, R. Seraglia, S. Orlandi, S. Quici, L. Sorace, D. Gatteschi, L. Armelao, *Inorg. Chem.* **2012**, *51*, 5409.

[8] a) A. Bencini, D. Gatteschi, F. Totti, D. Nieto-Sanz, J. A. McCleverty, M. D. Ward, *J. Phys. Chem. A* **1998**, *102*, 10545. b) E. Ruiz, A. Rodríguez-Fortea, S. Alvarez, *Inorg. Chem.* **2003**, *42*, 4881. c) F. Nunzi, E. Ruiz, J. Cano, S. Alvarez, *J. Phys. Chem. C* **2007**, *111*, 618. d) W. Li, F. Yang, Z. Wang, J. Hu, J. Ma, *J. Phys. Chem. A* **2009**, *113*, 3375. e) R. G. Hadt, V. N. Nemykin, *Inorg. Chem.* **2009**, *48*, 3982. f) J. Ferrando-Soria, M. Castellano, C. Yuste, F. Lloret, M. Julve, O. Fabelo, C. Ruiz-Pérez, S. E. Stiriba, R. Ruiz-García, J. Cano, *Inorg. Chim. Acta* **2010**, *363*, 1666. g) C. Yuste, J. Ferrando-Soria, D. Cangussu, O. Fabelo, C. Ruiz-Pérez, N. Marino, G. De Munno, S. E. Stiriba, R. Ruiz-García, J. Cano, F. Lloret, M. Julve, *Inorg. Chim. Acta* **2010**, *363*, 1984. h) S. Meskaldji, A. Zaiter, L. Belkhiri, A. Boucekkine, *Theor. Chem. Acc.* **2012**, *131*, 1151.

[9] a) E. Pardo, R. Ruiz-García, J. Cano, X. Ottenwaelder, R. Lescouëzec, Y. Journaux, F. Lloret, M. Julve, *Dalton Trans*. **2008**, 2780. b) M. C. Dul, E. Pardo, R. Lezcouëzec, Y. Journaux, J. Ferrando-Soria, R. Ruiz-García, J. Cano, M. Julve, F. Lloret, D. Cangussu, C. L. M. Pereira, H. O. Stumpf, J. Pasán, C. Ruiz-Pérez, *Coord. Chem. Rev*. **2010**, *254*, 2281.

[10] a) A. Mederos, P. Gili, S. Domínguez, A. Benítez, M. S. Palacios, M. Hernández-Padilla, P. Martín-Zarza, M. L. Rodríguez, C. Ruiz-Pérez, F. J. Lahoz, L. A. Oro, F. Brito, J. M. Arrieta, M. Vlassi, G. Germain, *J. Chem. Soc., Dalton Trans.* **1990**, 1477. b) S. Domínguez, A. Mederos, P. Gili, A. Rancel, A. E. Rivero, F. Brito, F. Lloret, X. Solans, C. Ruiz-Pérez, M. L. Rodríguez, I. Brito, *Inorg. Chim. Acta* **1997**, *255*, 367.

[11] a) C. A. Bear, J. M. Waters, T. N. Waters, *J. Chem. Soc. A* **1970**, *17*, 2494. b) D. Y. Jeter, W. E. Hatfield, *Inorg. Chim. Acta* **1972**, *6*, 440. c) R. Hernández-Molina, A. Mederos, P. Gili, S. Domínguez, F. Lloret, J. Cano, M. Julve, C. Ruiz-Pérez, X. Solans, *J. Chem. Soc., Dalton Trans.* **1997**, 4327. d) A. R. Paital, T. Mitra, D. Ray, W. T. Wong, J. Ribas-Ariño, J. J. Novoa, J. Ribas, G. Aromí, *Chem. Commun.* **2005**, 5172. e) A. R. Paital, A. Q. Wu, G. G. Guo, G. Aromí, J. Ribas-Ariño, D. Ray, *Inorg. Chem.* **2007**, *46*, 2947. f) M. Vázquez, A. Taglietti, D. Gatteschi, L. Sorace, C. Sangregorio, A. M. González, M. Maneiro, R. M. Pedrido,; M. R. Bermejo, *Chem. Commun.* **2003**, 1840.

[12] a) M. B. Inoue, E. F. Velázquez, F. Medrano, K. L. Ochoa, J. C. Gálvez, M. Inoue, Q. Fernando, *Inorg. Chem.* **1998**, *37*, 4070. b) M. B. Inoue, I. C. Muñoz, L. Machi, M. Inoue, Q. Fernando, *Inorg. Chim. Acta* **2000**, *311*, 50. c) M. B. Inoue, M. Inoue, R. Sugich-Miranda, L. Machi, E. F. Velázquez, Q. Fernando, *Inorg. Chim. Acta* **2001**, *317*, 181. d) L. V. Mosina, A. V. Raitsimring, M. B. Inoue, Q. Fernando, M. Inoue, *Appl. Magn. Reson.* **2001**, *20*, 249.

[13] a) I. Fernández, R. Ruiz, J. Faus, M. Julve, F. Lloret, J. Cano, X. Ottenwaelder, Y. Journaux, M. C. Muñoz, *Angew. Chem. Int. Ed.* **2001**, *40*, 3039. b) E. Pardo, J. Faus, M. Julve, F. Lloret, M. C. Muñoz, J. Cano, X. Ottenwaelder, Y. Journaux, R. Carrasco, G. Blay, I. Fernández, R. Ruiz-García, *J. Am. Chem. Soc.* **2003**, *125*, 10770. c) E. Pardo, R. Carrasco, R. Ruiz-García, M. Julve, F. Lloret, M. C. Muñoz, Y. Journaux, E. Ruiz, J. Cano, *J. Am. Chem. Soc.* **2008**, *130*, 576. d) E. Pardo, J. Ferrando-Soria, M. C. Dul, R. Lezcouëzec, Y. Journaux, R. Ruiz-García, J. Cano, M. Julve, F. Lloret, L. Cañadillas-Delgado, J. Pasán, C. Ruiz-Pérez, *Chem. Eur. J.* **2010**, *16*, 12838. e) M. Castellano, F. R. Fortéa-Pérez, S.-E. Stiriba, M. Julve, F. Lloret, D. Armentano, G. De Munno, R. Ruiz-García, J. Cano, *Inorg. Chem.* **2011**, *50*, 11279. f) M. Castellano, J. Ferrando-Soria, E. Pardo, M. Julve, F. Lloret, C. Mathonière, J. Pasán, C. Ruiz-Pérez, L. Cañadillas-Delgado, R. Ruiz-García, J. Cano, *Chem. Commun.* **2011**, *47*, 11035.

[14] a) P. F. H. Schwab, M. D. Levin, J. Michl, *Chem. Rev*. **1999**, *99*, 1863. b) S. Szafert, J. A. Gladysz, *Chem. Rev*. **2003**, *103*, 4175. c) P. F. H. Schwab, J. R. Smith, J. Michl, *Chem. Rev*. **2005**, *105*, 1197. d) T. Ren, *Chem. Rev*. **2008**, *108*, 4185.

[15] a) A. J. Deeming, G. Hogarth, M. V. Lee, M. Saha, S. P. Redmond, H. T. Phetmung, A. G. Orpen, *Inorg. Chim. Acta* **2000**, *309*, 109. b) D. G. McLean, J. E. Rogers, T. M. Cooper, *Proc. SPIE-Int. Soc. Opt. Eng.* **2002**, *11*, 4462. c) R. J. Magyar, S. Tretiak, Y. Gao, H.-L. Wang, A. P. Shreve, *Chem. Phys. Lett.* **2005**, *401*, 149. d) C. Kaliginedi, P. Moreno-García, H. Valkenier, W. Hong, V. M. García-Suárez, P. Buiter, J. L. H. Otten, J. C. Hummelen, C. J. Lambert, T. Wandlowski, *J. Am. Chem. Soc.* **2012**, *134*, 5262 and refs. therein.

[16] G. R. Hanson, K. E. Gates, C. J. Noble, M. Griffin, A. Mitchell, S. Benson, *J. Inorg. Biochem*. **2004**, *98*, 903 (*XSOPHE*).

[17] A. Bencini, D. Gatteschi, *EPR of Exchange Coupled Systems*; Springer-Verlag: Berlin, **1990**.

[18] J. Cano, VPMAG package; University of Valencia, Valencia, Spain, 2003.

[19] *SAINT*, version 6.45; Bruker Analytical X-ray Systems: Madison, WI, **2003**.

[20] Sheldrick G.M. *SADABS Program for Absorption Correction*, version 2.10; Analytical X-ray Systems: Madison, WI, **2003**.

[21] *SHELXTL*; Bruker Analytical X-ray Instruments: Madison, WI, **1998**.

[22] M. Nardelli, *J. Appl. Crystallogr.* **1995**, *28*, 659.

[23] D. Palmer, *CRYSTAL MAKER*; Cambridge University Technical Services: Cambridge, **1996**.

[24] A. D. Becke, *J. Chem. Phys.* **1993**, *98*, 5648.

[25] a) E. Ruiz, J. Cano, S. Alvarez, P. Alemany, *J. Comput. Chem.* **1999**, *20*, 1391. b) E. Ruiz, A. Rodriguez-Fortea, J. Cano, S. Alvarez, P. Alemany, *J. Comput. Chem.* **2003**, *24*, 982.

[26] M. J. Frisch, G. W. Trucks, H. B. Schlegel, G. E. Scuseria, M. A. Robb, J. R. Cheeseman, G. Scalmani, V. Barone, B. Mennucci, G. A. Petersson, H. Nakatsuji, M. Caricato, X. Li, H. P. Hratchian, A. F. Izmaylov, J. Bloino, G. Zheng, J. L. Sonnenberg, M. Hada, M. Ehara, K. Toyota, R. Fukuda, J. Hasegawa, M. Ishida, T. Nakajima, Y. Honda, O. Kitao, H. Nakai, T. Vreven, Jr., J. A. Montgomery, J. E. Peralta, F. Ogliaro, M. Bearpark, J. J. Heyd, E. Brothers, K. N. Kudin, V. N. Staroverov, R. Kobayashi, J. Normand, K. Raghavachari, A. Rendell, J. C. Burant, S. S. Iyengar, J. Tomasi, M. Cossi, N. Rega, J. M. Millam, M. Klene, J. E. Knox, J. B. Cross, V. Bakken, C. Adamo, J. Jaramillo, R. Gomperts, R. E. Stratmann, O. Yazyev, A. J. Austin, R. Cammi, C. Pomelli, J. W. Ochterski, R. L. Martin, K. Morokuma, V. G. Zakrzewski, G. A. Voth, P. Salvador, J. J. Dannenberg, S. Dapprich, A. D. Daniels, Ö. Farkas, J. B. Foresman, J. V. Ortiz, J. Cioslowski, D. J. Fox, *Gaussian 09*, revision B.1; Gaussian, Inc.: Wallingford, CT, **2009**.

[27] a) A. Schaefer, H. Horn, R. Ahlrichs, *J. Chem. Phys.* **1992**, *97*, 2571. b) A. Schaefer, C. Huber, R. Ahlrichs, *J. Chem. Phys.* **1994**, *100*, 5829.

[28] a) J. E. Carpenter, F. Weinhold, *J. Mol. Struct.* **1988**, *169*, 41. b) A. E. Reed, L. A. Curtis, F. Weinhold, *Chem. Rev.* **1988**, *88*, 899. c) F. Weinhold, J. E. Carpenter, *The Structure of Small Molecules and Ions*; Plenum, **1988**, p 227.

[29] a) M. Cossi, N. Rega, G. Scalmani, V. Barone, *J. Comp. Chem.* **2003**, *24*, 669. b) J. Tomasi, B. Mennucci, E. Cances, *J. Mol. Struct.-Theochem.* **1999**, *464*, 211.

CHAPTER III

Dicopper(II) Anthraquinophanes as Molecular Magnetic Capacitors

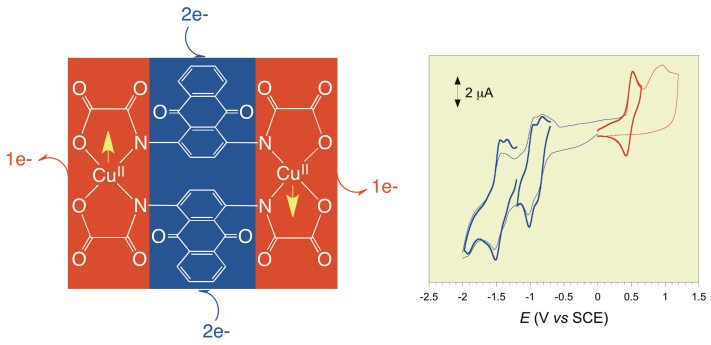

On the road to molecular charge storage devices: a first prototype of dicopper(II) metallacyclophane-based molecular magnetic capacitor is reported which exhibits a dual metal- and ligand-centered, multielectron redox behavior involving 1 e^- oxidation of the antiferromagnetically coupled Cu^{II} ions and 2 e^- reduction of the weakly interacting anthraquinone spacers in a π-stacked *anti* conformation.

III.1 Introductory Aspects

Redox-active ("non-innocent") ligands have long been recognized in coordination chemistry.[1] Dithiolenes, diimines, diamines, and catecholates have a distinctive ability to form radical ligand species when coordinated to transition metal ions.[2] The design and synthesis of new classes of non-innocent aromatic bridging ligands that are able to self-assemble with redox-active, paramagnetic transition metal ions have experienced a renewed interest in supramolecular coordination chemistry (so-called metallosupramolecular chemistry).[3,4]

Metallosupramolecular complexes containing multiple ligand- and/or metal-based, spin containing electrophores are of large interest as potential single-molecule devices for charge storage applications in the emerging field of molecular spintronics.[5] Toward this goal, we are developing new functional metallacyclic complexes of paramagnetic first-row transition metal ions and quinoid-type aromatic dioxamato bridging ligands that would possess both metal- and ligand-centered electrochemical activity because of the strong σ-donor ability (basicity) of the oxamato donor groups[6] and the π-acceptor character of the quinone moieties.[7] In particular, our current studies rely on the well-recognized ability of the non-innocent anthraquinone (AQ) derivatives to impart an additional reducible capacity to the oxidizable metal centers in their oxamato-based metallacyclic complexes.[4] So, the reduction of AQ in aprotic solvents involves two sequential and reversible one-electron transfer steps to give the corresponding semiquinonate-type $ASQ^{\bullet -}$ π-radical anion and catecholate-type $ACAT^{2-}$ dianion (Figure III.1).[8]

Here we report the synthesis, structural and spectroscopic characterization, magnetic and electrochemical properties, and theoretical calculations of two new dinuclear copper(II) metallacyclophanes of formulas $(n\text{Bu}_4\text{N})_4[\text{Cu}^{\text{II}}_2(1,4\text{-quanba})_2] \cdot 2\text{MeCN} \cdot 2\text{Et}_2\text{O}$ (**III.1a**) and $(\text{Ph}_3\text{EtP})_4[\text{Cu}^{\text{II}}_2(1,4\text{-quanba})_2] \cdot 20\text{H}_2\text{O}$ (**III.1b**), where H_4-1,4-quanba is the non-innocent *N,N'*-1,4-bis(oxamic acid)-9,10-anthraquinone bridging ligand (Figure III.1 with X = $NCOCO_2$). Complexes **III.1a** and **III.1b** constitute the first members of a novel class of exchange-coupled, anthraquinone-based dicopper(II) metallacyclophanes, referred to as dicopper(II) anthraquinophanes, which exhibits a multielectron transfer behavior featuring one-electron oxidation of the antiferromagnetically coupled Cu^{II} ions and two-electron reduction of the anthraquinone spacers, as reported in a preliminary communication (see second communication in Appendices).[4d] This dual ligand- and metal-based character of the redox processes in **III.1a** and **III.1b** has been confirmed by density functional (DF) calculations, which allow identifying the nature of the electroactive molecular orbitals in each case.

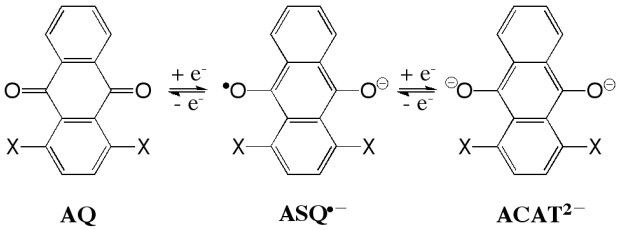

Figure III.1 Redox equilibria of anthraquinone derivatives in aprotic media.

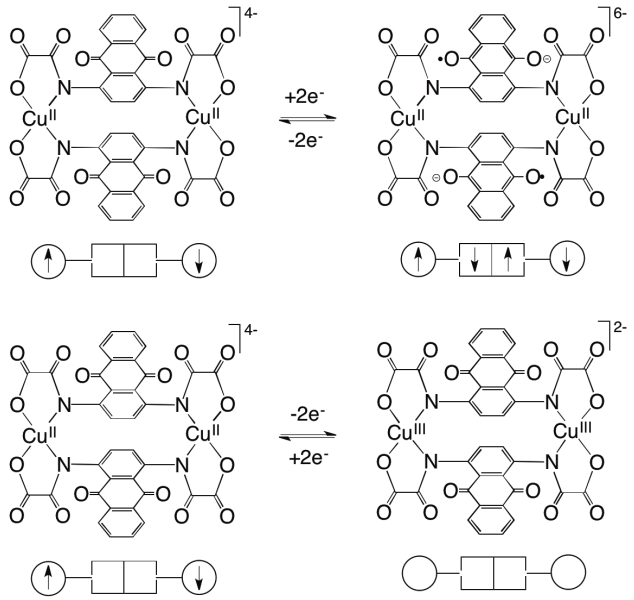

Figure III.2 Illustration of the charge storage magnetic behavior in redox-active dicopper(II) metallacyclophanes featuring 1,4-substituted 9,10-anthraquinonebis(oxamate) π-radical anions as bridging ligands.

Based on these experimental and theoretical exploratory studies, we suggest that dicopper(II) anthraquinophanes can act as effective multielectron reservoirs for the development of a new class of charge storage spintronic devices, referred to as molecular magnetic capacitors (Figure III.2). A molecular magnetic capacitor is defined as an electroactive (oxidable and reducible) molecule with several chemically accessible oxidation levels at the exchange-coupled spin carriers that can store and deliver an electric charge. In this case, the charging and decharging processes can be regarded as the disproportionation equilibrium reaction of the dicopper(II) anthraquinophane. That being so, the overall efficiency of a metallacyclophane-based molecular magnetic capacitor depends on the available number of oxidation (n_{ox}) and reduction equivalents (n_{red}), as well as the magnitude of the comproportionation constant (K_c) (that is, a molecular magnetic capacitor is characterized by small K_c and large n_{ox} and n_{red} values).

III.2 Synthesis of the Ligand and Complexes

The ligand was prepared from the straightforward condensation of the corresponding commercially available 1,4-diamine-9,10-anthraquinone precursor with ethyl oxalyl chloride ester (1:2 molar ratio) in presence of triethylamine as base in tetrahydrofurane (Figure III.3a). It was isolated as the diethyl ester acid

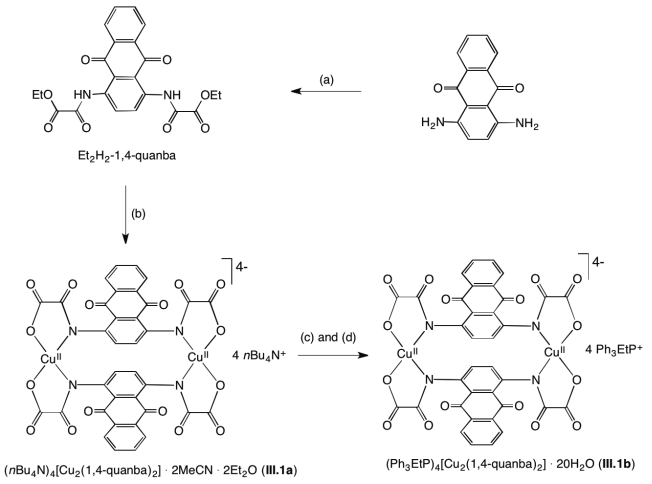

Figure III.3 Synthetic procedure for the Et_2H_2-1,4-qanba proligand and the tetra-*n*-butylammonium and triphenylethylphosphonium salts of the $[Cu^{II}_2(1,4\text{-qanba})_2]^{4-}$ complex: (a) $C_2O_2Cl(OEt)$, Et_3N, THF; (b) nBu_4NOH, $Cu(ClO_4)_2$, CH_3OH; (c) $AgNO_3$, H_2O; (d) Ph_4PCl, H_2O/CH_3CN.

derivative Et_2H_2-1,4-qanba in very good yields (90%) (see Experimental Section).

The corresponding dinuclear copper(II) complexes **III.1a** and **III.1b** were isolated as its tetra-*n*-butylammonium and triphenylethylphosphonium salts, respectively (see Experimental Section). Complex **III.1a** was prepared by the one-step reaction of the corresponding Et_2H_2-1,4-qanba proligand with copper(II) perchlorate (2:2 molar ratio) by using tetra-*n*-butylammonium hydroxide as base in methanol (Figure III.3b). Complex **III.1b** was then synthesized by two successive steps from the metathesis of the tetra-*n*-butylammonium salt **III.1a** with triphenylethylphosphonium bromide in water/acetonitrile through the intermediacy of the silver(I) salt (Figure III.3c and d). Complexes **III.1a** and **III.1b** were soluble in protic solvents like water and methanol but they were sparingly soluble aprotic solvents such as acetonitrile or dichloromethane. X-ray quality single crystals of **III.1a** and **III.1b** were obtained by liquid-vapor diffusion of diethylether over acetronitrile/methanol solutions of the compounds.

The chemical identity of the ligand and complexes was determined by elemental analysis together with ^1H NMR and FTIR spectroscopies (see Experimental Section and Appendices). The structures of **III.1a** and **III.1b** were further confirmed by single-crystal X-ray diffraction. A summary of the crystallographic data of **III.1a** and **III.1b** is given in Table III.1, while selected bond distances and interbond angles are listed in Tables III.2 and III.3, respectively.

III.3 Description of the Structures

The crystal structures of **III.1a** and **III.1b** consist on double-stranded dicopper(II) anions with a crystallographically imposed C_{2h} (**III.1a**) or C_i (**III.1b**) molecular symmetry, $[Cu^{II}_2(\mu\text{-}\kappa^2\text{:}\kappa^2\text{-}1,4\text{-quanba})_2]^{4-}$ (Figures III.4 and III.5), together with tetra-*n*-butylammonium (**III.1a**) or triphenylethylphosphonium (**III.1b**) cations, and highly disordered acetonitrile and diethyl ether molecules of crystallization (**III.1a**) (see Experimental Section).

The Cu(1) atom of **III.1a** and **III.1b** adopts a four-coordinate twisted geometry with alternating helical chiralities (named *RS*-stereoisomers), leading thus to an overall achiral dicopper(II) metallacyclophane of the double mesocate-type (Figures III.4a and III.5a). The values of the tetrahedral twist angle (τ) between

Table III.1 Summary of crystallographic data.

	III.1a	**III.1b**
formula	$C_{112}H_{176}Cu_2N_{10}O_{18}$	$C_{116}H_{132}Cu_2N_4O_{36}P_2$
M (g mol^{-1})	2077.71	2409.22
crystal system	tetragonal	triclinic
space group	$P4_2/m$	$P\text{–}1$
a (Å)	14.8420(10)	12.260(5)
b (Å)	14.8420(10)	14.377(5)
c (Å)	25.8161(18)	19.854(5)
α (°)	90.00	102.024(5)
β (°)	90.00	98.905(5)
γ (°)	90.00	113.657(5)
V (Å^3)	5686.9(7)	3022.1(18)
Z	2	2
ρ_{calc} (g cm^{-3})	1.213	1.324
μ (mm^{-1})	0.441	0.485
T (K)	100(2)	293(2)
indep. reflect.	3281	12467
obs. reflect. [$I > 2\sigma(I)$]	2959	8205
R_1[a] [$I > 2\sigma(I)$] (all)	0.0553 (0.0604)	0.0776 (0.1197)
wR_2[b] [$I > 2\sigma(I)$] (all)	0.1656 (0.1696)	0.2221 (0.2454)
S[c]	1.229	1.504

[a] $R_1 = \sum(|F_o| - |F_c|)/\sum|F_o|$. [b] $wR_2 = [\sum w(|F_o| - |F_c|)^2/\sum w|F_o|^2]^{1/2}$. [c] $S = [\sum w(|F_o| - |F_c|)^2/(N_o - N_p)]^{1/2}$.

Table III.2 Selected bond distances (Å) and interbond angles (°) for **III.1a**.[a,b]

Cu(1)–N(1)	1.963(3)	Cu(1)–O(1)	1.944(2)
N(1)–Cu(1)–N(1)^{II}	109.81(18)	N(1)–Cu(1)–O(1)	83.10(11)
N(1)–Cu(1)–O(1)^{II}	162.40(12)	O(1)–Cu(1)–O(1)^{II}	87.16(15)

[a] The estimated standard deviations are given in parentheses. [b] Symmetry code: (I) = $-x, -y + 1, z$.

Table III.3 Selected bond distances (Å) and interbond angles (°) for **III.1b**.[a,b]

Cu(1)–N(1)	1.995(3)	Cu(1)–N(2)^{I}	1.976(3)
Cu(1)–O(3)^{I}	1.971(3)	Cu(1)–O(6)	1.970(3)
N(1)–Cu(1)–N(2)^{I}	109.31(13)	N(1)–Cu(1)–O(3)^{I}	167.25(12)
N(1)–Cu(1)–O(6)	82.70(13)	N(2)^{I}–Cu(1)–O(3)^{I}	83.15(13)
N(2)^{I}–Cu(1)–O(6)	166.69(13)	O(3)–Cu(1)–O(6)^{I}	85.20(13)

[a] The estimated standard deviations are given in parentheses. [b] Symmetry code: (I) = $-x, -y, -z$.

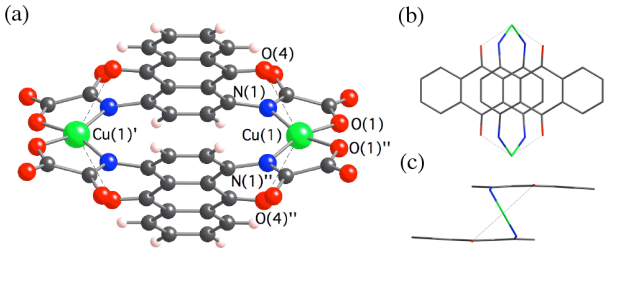

Figure III.4 (a) Perspective view of the anionic dicopper unit of **III.1a** with the atom-numbering scheme of the metal environment [symmetry code: (I) = x, y, $-z$; (II) = $-x$, $-y+1$, z]. (b) Top and (c) side projection views of the metallacyclic anthraquinophane core. The weak axial coordinative interactions are represented by dashed lines.

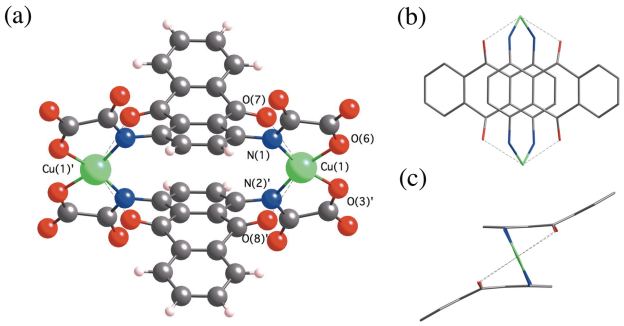

Figure III.5 (a) Perspective view of the anionic dicopper unit of **III.1b** with the atom-numbering scheme of the metal environment [symmetry code: (I) = $-x$, $-y$, $-z$]. (b) Top and (c) side projection views of the metallacyclic anthraquinophane core. The weak axial coordinative interactions are represented by dashed lines.

the Cu(1)N(1)O(1) and Cu(1)N(1)^{II}O(1)^{II} planes are 20.1(1) (**III.1a**) and 7.2(1)º (**III.1b**) (τ = 0 and 90° for ideal square planar and tetrahedral geometries, respectively). The CuN_2O_2 environment at each metal ion is built by two amidate-nitrogen and two carboxylate-oxygen atoms from the chelating oxamato donor groups of the 1,4-quanba^{4-} bridging ligands. The average values of the Cu–N distances [1.963(3) (**III.1a**) and 1.986(3) Å (**III.1b**)] are slightly greater than those of the Cu–O ones [1.944(2) (**III.1a**) and 1.971(3) Å (**III.1b**)], while the values of the N–Cu–N angles [109.81(18) (**III.1a**) and 109.3(1)° (**III.1b**)] are significantly greater than those of the O–Cu–O ones [87.16(15) (**III.1a**) and 85.3(1)° (**III.1b**)]. In addition, there are very weak axial bonding interactions with the two oxygen atoms of the central benzoquinone ring from the anthraquinone spacers of the 1,4-quanba^{4-} bridging ligands [Cu–O = 2.815(3) (**III.1a**) and 2.758(3)/2.921(3) Å (**III.1b**)]

Within the dicoppertetraaza[3.3](1,4)anthraquinophane core, $Cu_2(\mu\text{-}N_2C_{14}H_6O_2)_2$, the anthraquinone spacers connected by the two N–Cu–N linkages have a parallely displaced π-stacked *anti* conformation, being not exactly oriented perpendicular to the copper basal planes (Figures III.4b and III.5b). More likely, the weak axial coordinative interactions with the quinone moieties prevent the adoption of the alternative eclipsed *sin* conformation that maximizes the π–π stacking interactions between the two

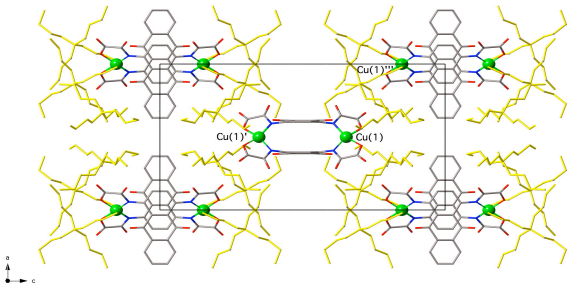

Figure III.6 Crystal packing view of **III.1a** along the crystallographic *b* axis [symmetry code: (I) = x, y, $-z$; (III) = $-1+y$, $-x$, $\frac{1}{2}-z$]. The tetra-*n*-butylammonium countercations are shown in yellow color.

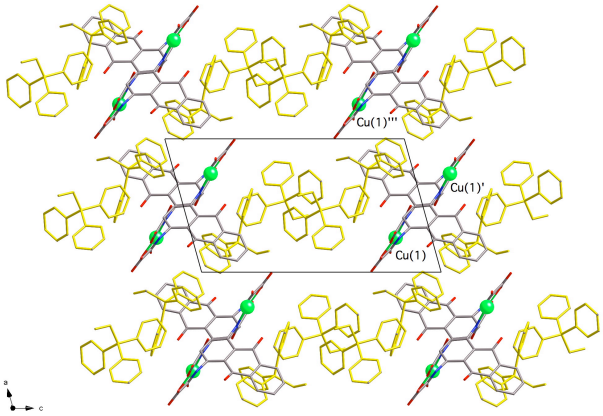

Figure III.7 Crystal packing view of **III.1b** along the crystallographic *b* axis [symmetry code: (I) = x, y, z; (III) = $1+x$, y, z]. The triphenylethylphosphomiumonium countercations are shown in yellow color.

facing anthraquinone spacers. The values of the centroid-centroid distance (h) between the two facing 1,4-substituted benzene rings from each anthraquinone spacer are 3.387(1) (**III.1a**) and 3.425(1) Å (**III.1b**), while the values of the off-set angle (θ) between the centroid-centroid vector and the normal to their planes are 17.2(1) (**III.1a**) and 2.5(1)° (**III.1b**). The values of the torsion angle between the copper basal planes and the mean planes of the facing 1,4-substituted benzene rings around the Cu–N–C–C bonds (ϕ) are 53.7(1) (**III.1a**) and 62.2(3)º (**III.1b**).

On the other hand, the anthraquinone moieties are almost planar in **III.1a** but they deviate significantly from planarity in **III.1b** (Figures III.4c and III.5c). The values of the dihedral angle (φ) between the two lateral benzene ring around the central benzoquinone ring are 3.4(1) (**III.1a**) and 28.4(1)º (**III.1b**) A significant bond length alternation typical of aminoanthraquinone derivatives is observed in the central benzoquinone ring with very short average C=O bond distances [1.240(5) (**III.1a**) and 1.229(4) Å (**III.1b**)] and average short C=C [1.420(1) (**III.1a**) and 1.420(1) Å (**III.1b**)] and long C–C bond distances [1.483(5) (**III.1a**) and 1.505(1) Å (**1b**)], as earlier reported for the related mononuclear copper(II) complex of formula (nBu$_4$N)$_2$[Cu(2,3-quanba)] [2,3-quanba^{4-} = *N,N'*-2,3-bis(oxamate)-9,10-anthraquinone].[9]

In the crystal lattice of **III.1a** and **III.1b**, the dicopper(II) anions are well isolated from each other by the bulky tetra-*n*-butylammonium (**III.1a**) and triphenylethylphosphonium countercations (**III.1b**) (Figures III.6 and III.7). Yet there exist weak edge-to-face π-π stacking interactions between one phenyl substituent from the triphenylethylphosphonium cations and the terminal benzene ring from the anthraquinone spacers in **III.1b**. These intermolecular interactions are likely responsible for the larger deviations from planarity of the anthraquinone moieties in **III.1b**. The intramolecular Cu(1)–Cu(1)^{I} distances (*r*) across the double 9,10-anthraquinone-1,4-diamidate bridge are 7.878(1) (**III.1a**) and 8.008(1) Å (**III.1b**), while the shortest intermolecular Cu(1)–Cu(1)^{III} separations are 11.638(1) (**III.1a**) and 9.306(1) Å (**III.1b**).

III.4 Magnetic Properties

Variable-temperature (2.0–300 K) magnetic susceptibility measurements for **III.1a** and **III.1b** in the form of the χ_M and $\chi_M T$ *vs*. *T* plots (χ_M being the molar magnetic susceptibility per dinuclear unit and *T* the absolute temperature) reveal a magnetic behavior which is typical of moderately strong antiferromagnetically coupled $Cu^{II}{}_2$ pairs (Figure III.8). At room temperature, the $\chi_M T$ values of 0.70 (**III.1a**) and 0.74 cm^3 mol^{-1} K (**III.1b**) are smaller than that expected for two magnetically isolated Cu^{II} ions [$\chi_M T = 2 \times (N\beta^2 g_{Cu}{}^2/3k_B)S_{Cu}(S_{Cu} + 1) = 0.83$ cm^3 mol^{-1} K with $S_{Cu} = ½$ and $g_{Cu} = 2.1$]. Upon cooling, $\chi_M T$ decreases continuously from room temperature and it vanishes around 20 K, while χ_M exhibits a maximum at 70 (**III.1a**) 80 K (**III.1b**) (inset of Figure III.8). This fact unambiguously supports the occurrence of a ground singlet ($S = 0$) spin state resulting from the intramolecular antiferromagnetic coupling between the two Cu^{II} ions through the 1,4-diamidate-9,10-anthraquinone bridges.

The analysis of the magnetic susceptibility data of **III.1a** and **III.1b** was carried out through the appropriate spin Hamiltonian for a dinuclear copper(II) complex (eq III.1 with $S_1 = S_2 = S_{Cu} = ½$), where *J* is the magnetic coupling parameter and *g* is the Zeeman factor of the Cu^{II} ions ($g = g_1 = g_2 = g_{Cu}$). The least-squares fits of the experimental data through the well-known Bleaney-Bowers expression (eq III.2) gave $-J = 84.4(4)$ (**III.1a**) and 90.3(2) cm^{-1} (**III.1b**), $g = 2.10(1)$ (**III.1a**) and 2.09(1) (**III.1b**), and $R = 4.0 \times 10^{-7}$ (**III.1a**) and 2.0×10^{-7} (**III.1b**), where *R* is the agreement factor defined as $\sum[(\chi_M T)_{exp} - (\chi_M T)_{calcd}]^2/\sum[(\chi_M T)_{exp}]^2$ (solid lines in Figure III.8).

$$\mathbf{H} = -J\mathbf{S_1} \cdot \mathbf{S_2} + g\beta(\mathbf{S_1} + \mathbf{S_2})H \qquad \text{(III.1)}$$

$$\chi_M = (2N\beta^2 g^2/k_B T) / [3 + \exp(-J/k_B T)] \qquad \text{(III.2)}$$

The experimental $-J$ values for **III.1a** and **III.1b** are within the range to those reported earlier for related dicopper(II) metallacyclophanes with the related ligand *N,N'*-1,4-phenylenebis(oxamate) ($-J$ = 75–95 cm^{-1}).[4c] This indicates that the π electron accepting nature of the fused benzoquinone moieties does not influence appreciably the propagation of the magnetic exchange interactions between the two Cu^{II} ions through the 1,4-substituted benzene ring. The slightly smaller $-J$ value of **III.1a** when compared to that of **III.1b** are likely due to the greater loss of orthogonality between the copper and the benzene planes [$\phi = 52.7(1)$ (**III.1a**) and 62.1(1)º (**III.1b**)] and/or the larger tetrahedral distortion at the copper centers [$\tau = 20.1(1)$ (**III.1a**) and 7.9(2)º (**III.1b**)], as shown earlier for the 1,4-substituted benzene ancestor.[4c]

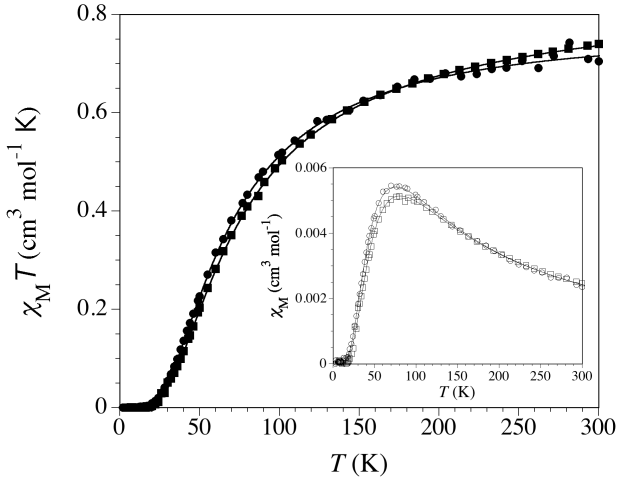

Figure III.8 Temperature dependence of $\chi_M T$ of **III.1a** (●) and **III.1b** (■). The inset shows the χ_M maxima of **III.1a** (○) and **III.1b** (□). The solid lines are the best-fit curves (see text).

III.5 Redox Properties

The cyclic voltammograms (CVs) of **III.1a** and **III.1b** in acetonitrile (25 °C, 0.1 M nBu$_4$NPF$_6$) show identical results independently of the nature of the counteraction (Figure III.9). The CV of **III.1a** show up to four pseudoreversible reduction waves grouped in two pairs at $E_1 = -0.87$ V, $E_2 = -0.98$ V, $E_3 = -1.37$ V, and $E_4 = -1.48$ V *vs*. SCE, with anodic to cathodic peak separation values ($\Delta E_{p,1} = \Delta E_{p,2} = \Delta E_{p,3} = \Delta E_{p,4} = 90$ mV) which are somewhat higher than that of ferrocene under the same conditions [$\Delta E_p(Fc^+/Fc) = 70$ mV (CH_3CN, 0.1 M nBu$_4$NPF$_6$, 25 °C)]. In addition, it exhibits two oxidation waves at $E_5 = +0.47$ V and $E_6 = +0.96$ V *vs*. SCE, being reversible only the first one ($\Delta E_{p,5} = 70$ mV). A perfect linear plot of the peak current against the square root of the scan rate is obtained for the first oxidation wave of **III.1a**, which is then stated to be completely reversible on the voltammetric time-scale.

The first pair of closely spaced reduction waves of **III.1a** ($\Delta E_{12} = E_1 - E_2 = 110$ mV) would correspond to the stepwise one-electron reduction of the weakly interacting 1,4-substituted 9,10-anthraquinone spacers to give the semiquinonate-type π-radical and diradical dicopper(II) species (Figure III.10a). The second pair of closely spaced reduction waves of **III.1a** ($\Delta E_{34} = E_3 - E_4 = 110$ mV) would then correspond to the further stepwise

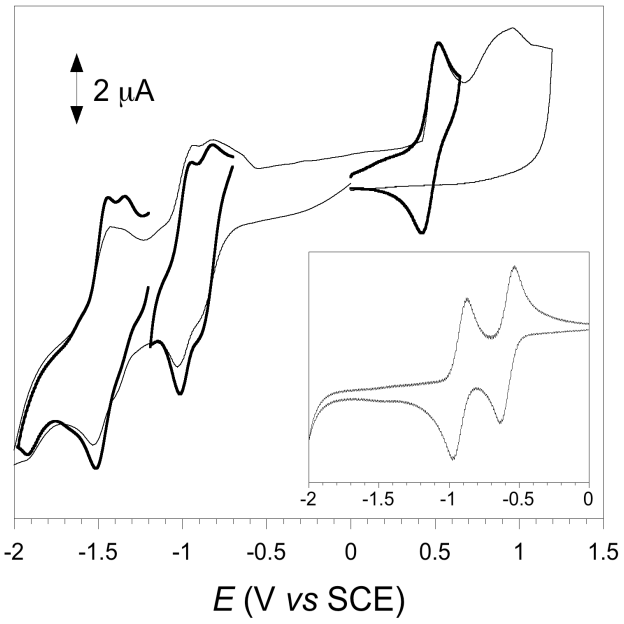

Figure III.9 CVs of **III.1a** in acetonitrile (0.1 M nBu$_4$NPF$_6$, 25 °C). The inset shows the CV of the Et$_2$H$_2$-1,4-quanba proligand in dichloromethane (0.1 M nBu$_4$NPF$_6$, 25 °C).

one-electron reduction of the resulting semiquinonate-type π-diradical dicopper(II) intermediate to give the corresponding catecholate- and bis(catecholate)-type dicopper(II) species (Figure III.10b). The small but nonnegligible separations in the formal potential values for each pair ($\Delta E_{12} = \Delta E_{34} = 110$ mV) is likely due to the weak through-bond interactions across the axially coordinated metal ions. Yet they can obey to the direct interactions between the two facing benzene rings of the *anti* 9,10-anthraquinone spacers in the resulting mixed-valent, quinone/semiquinonate and semiquinonate/catecholate intermediates, respectively (when compared with the expected stronger electronic interactions in the alternative π-stacked *sin* conformation). In both cases, the effect of these interactions is that, once reduced the first ligand, the experienced change in its electronic structure is communicated to the other one, so that its reduction potential is slightly modified.

On the contrary, the two well-separated one-electron oxidation waves of **III.1a** at relatively low positive potentials are likely attributed to the stepwise one-electron oxidation of the metal centers to afford the putative mixed-valent dicopper(II,III) and high-valent dicopper(III,III) species (Figure III.10c). The large separation in the formal potential values ($\Delta E_{56} = E_6 - E_5 = 490$ mV) is related to the ability of the double 9,10-anthraquinone-1,4-diamidate bridge to transmit electronic interactions between the metal centers in the corresponding mixed-valent $Cu^{II/III}{}_2$ intermediate. So that, there is an influence of the firstly oxidized metal ion over the other one, being thus its oxidation potential modified with respect to the first one. Hence, the calculated values of the comproportionation constant ($\log K = \Delta E/59$) for the diverse reduced and oxidized forms of **III.1** ($\log K_{12} = \log K_{34} = 1.86$, $\log K_{23} = 6.61$, and $\log K_{56} = 8.31$) clearly evidence the higher thermodynamic stability of the semiquinonate-type π-diradical dicopper(II) and the mixed-valent dicopper(II,III) species.

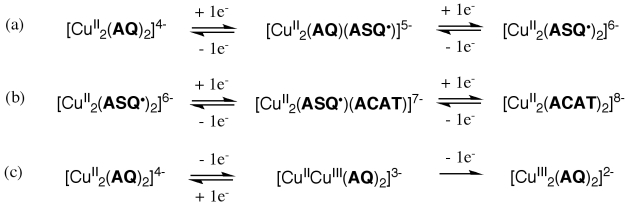

Figure III.10 Proposed redox model for the multielectron transfer series of **III.1a** and **III.1b**.

The stabilization of the trivalent oxidation state of copper in **III.1a** and **III.1b** is explained in terms of the well known strong electron donating character of the oxamato groups, as reported earlier for the dicopper(II) metallacyclophane with the innocent ligand *N,N'*-2-methyl-1,3-phenylenebis(oxamate) ($E_1 = +0.43$ and $E_2 = +0.65$ V *vs*. SCE).[4b] In contrast, this latter complex does not show any reduction at negative potentials up to –2.0 V *vs*. SCE, supporting thus the ligand-based nature of the reduction processes of **III.1a** and **III.1b**.

This is further supported by the CV of the neutral proligand Et$_2$H$_2$-1,4-quanba in dichloromethane (inset of Figure III.9). It shows two sequential and almost reversible one-electron reduction waves at $E_1 = –0.58$ V and $E_2 = –0.92$ V *vs*. SCE to render the corresponding ASQ$^{•–}$ π-radical anion and ACAT$^{2–}$ dianion respectively (see Figure III.1), with anodic to cathodic peak separation values ($\Delta E_{p,1} = \Delta E_{p,2} = 100$ mV) which are identical to that of ferrocene under the same conditions [$\Delta E_p(Fc^+/Fc) = 100$ mV (CH_2Cl_2, 0.1 M nBu$_4$NPF$_6$, 25 °C)]. The overall dislocation by *ca.* 0.5 V toward higher negative potentials for the two pairs of reduction waves of **III.1a** and **III.1b** is as expected given the tetraanionic nature of the 1,4-quanba$^{4–}$ bridging ligands which makes their reduction more difficult. In contrast to **III.1a** and **III.1b**, the CV of the Et$_2$H$_2$-1,4-quanba proligand with a markedly π electron accepting nature does not show any oxidation at positive potentials up to +1.8 V *vs*. SCE (data not shown).

III.6 Spectroscopic Properties

The stable singly oxidized dicopper(II,III) species was prepared by chemical oxidation of **III.1a** with excess of bromine in acetonitrile [$E(Br_2/Br^–) = +0.47$ V *vs*. SCE] and it was characterized by X-band EPR spectroscopy. Unfortunately, the doubly oxidized dicopper(III,III) species as well as the doubly and quadruply reduced, semiquinonate- and catecholate-type dicopper(II) forms respectively, are not stable enough to be spectroscopically characterized.

The X-band EPR spectrum of a frozen acetonitrile solution of **III.1a** shows a rhombic signal with a well-resolved seven-line

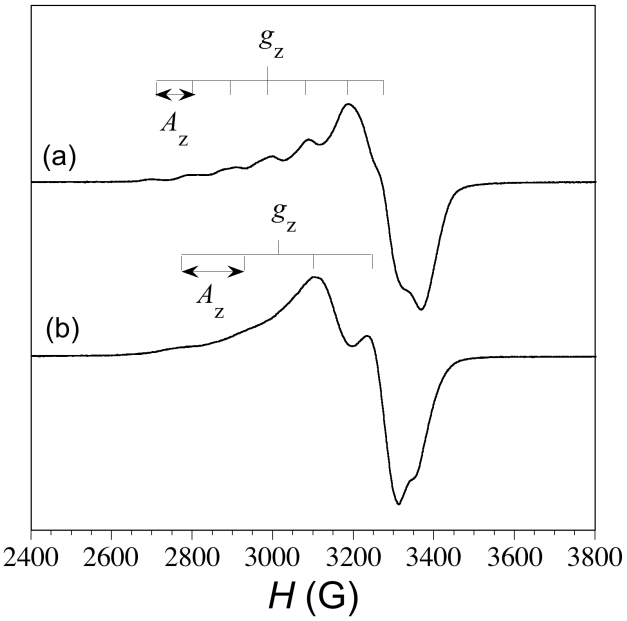

Figure III.11 X-band EPR spectra of **III.1a** (a) and the monoxidized species (b) in acetonitrile at 77 K and 4 K, respectively.

splitting of the g_z signal due to the hyperfine coupling with the nuclear spin of the two Cu^{II} ions ($2nI_{Cu} + 1 = 7$ with $n = 2$ and $I_{Cu} = 3/2$) whose intensity decreases when lowering the temperature, as expected for an antiferromagnetically coupled Cu^{II}_2 complex (Figure III.11a). On the contrary, the X-band EPR spectrum of a frozen acetonitrile solution of the *in situ* prepared, deep brown singly oxidized species exhibits a simpler four-line splitting typical of a localized mixed-valent $Cu^{II,III}_2$ complex with a doublet ground spin state ($2nI_{Cu} + 1 = 4$ with $n = 1$ and $I_{Cu} = 3/2$) whose intensity increases when lowering the temperature, as expected for a metal-centered oxidation (Figure III.11b). Moreover, the calculated value of the hyperfine coupling constant of the singly oxidized species ($A_z = 165$ G) is almost twice that of **III.1a** ($A_z = 95$ G), as expected from the different $S = 1/2$ $Cu^{II,III}_2$ ($A = A_{Cu}$) and $S = 1$ Cu^{II}_2 formulations ($A = 1/2A_{Cu}$).

III.7 Theoretical Calculations

Molecular geometry optimizations. The optimized molecular geometry for the ground broken-symmetry (BS) singlet spin state of **III.1** in acetonitrile solution shows large structural similarities, in terms of both bond lengths and interbond angles, with the actual structures of **III.1a** and **III.1b** determined by single crystal X-ray diffraction (see Computational Details). As a matter of fact, the deviation from planarity of the anthraquinone spacers in **III.1** is intermediate between that found experimentally in **III.1a** and **III.1b** [φ = 12.8 (**III.1**), 3.4 (**III.1a**), and 28.4° (**III.1b**); Table III.4]. Yet the optimized molecular geometry of **III.1** evidence a larger deviation from perpendicularity between the copper basal planes and the anthraquinone spacers and a larger tetrahedral distortion of the metal environment than those found experimentally in **III.1a** and **III.1b** [ϕ = 52.5 (**III.1**), 53.7 (**III.1a**), and 62.2° (**III.1b**); τ = 29.4 (**III.1**), 20.1 (**III.1a**), and 7.2° (**III.1b**); Table III.4].

Table III.4 Selected calculated structural and energy data.[a]

	III.1a	**III.1b**	**III.1**
φ[b] (°)	3.4	28.4	12.8
ϕ[c] (°)	53.7	62.2	52.5
τ[d] (°)	20.1	7.2	29.4
ΔE_{ST}[e] (cm^{-1})	46.5 (84.4)	58.3 (90.3)	52.3
$E(b_{2u})$[f] (a.u.)	–0.12168	–0.12531	–0.13153
$E(b_{1g})$[f] (a.u.)	–0.11647	–0.11808	–0.12479
$E(b_{1g}^*)$[f] (a.u.)	–0.11434	–0.11326	–0.11655
$E(b_{2u}^*)$[f] (a.u.)	–0.09597	–0.10311	–0.10361
$E_{M\text{-}L}$[g] (cm^{-1})	467	1058	1809
δ[h] (cm^{-1})	1144	1587	1479
δ^*[i] (cm^{-1})	4032	2228	2840

[a] DF calculations were performed on the ground BS singlet ($S = 0$) and triplet ($S = 1$) states of the actual molecular geometries of **III.1a** and **III.1b**, as well as on the optimized molecular geometry of **III.1**, in acetonitrile solution (see Computational Details). [b] Dihedral angle between the lateral benzene ring around the central benzoquinone ring from each anthraquinone spacer. [c] Torsion angle between the copper basal planes and the 1,4-substituted benzene rings from the anthraquinone spacers. [d] Tetrahedral twist angle at the copper atoms. [e] Singlet-triplet energy gap ($\Delta E_{ST} = -J$). The experimental J values are given in parentheses. [f] Molecular orbital energy. [g] Energy gap between the high- and low-lying SOMO and LUMO for the triplet spin state [$E_{M\text{-}L} = E(b_{1g}^*) - E(b_{1g})$]. [h] Energy gap between the two SOMOs for the triplet spin state [$\delta = E(b_{1g}) - E(b_{2u})$]. [i] Energy gap between the two LUMOs for the triplet spin state [$\delta^* = E(b_{2u}^*) - E(b_{1g}^*)$].

Energy calculations. DF energy calculations on the actual geometries of **III.1a** and **III.1b** in acetonitrile solution show a ground broken-symmetry (BS) singlet ($S = 0$) spin state lying well below the excited triplet ($S = 1$) spin state (see Computational Details). The calculated values of the singlet-triplet energy gap [$\Delta E_{ST} = -J = 46.5$ (**III.1a**) and 58.3 cm^{-1} (**III.1b**)] are, however, somewhat smaller than the experimental ones obtained from the fit of the magnetic susceptibility data in the solid state [$-J = 84.4$ (**III.1a**) and 90.3 cm^{-1} (**III.1b**)] (Table III.4). Yet they conform with DF energy calculations on the optimized geometry of **III.1** in acetonitrile solution, which shows an intermediate value of the calculated singlet-triplet energy gap to those of **1a** and **1b** ($\Delta E_{ST} = -J = 52.3$ cm^{-1}; Table III.4).

The dependence of the magnetic coupling parameter with some relevant structural data for **III.1**, **III.1a**, and **III.1b** is illustrated in Figure III.12. In general, the calculated $-J$ values increase with the dihedral angles between the central benzoquinone ring and the lateral benzene ring from each anthraquinone spacer (φ) and that between the copper basal planes and the 1,4-substituted benzene rings from the anthraquinone spacers (ϕ), while they decrease with the tetrahedral twist angle at the copper atoms (τ), in agreement with the observed experimental trend for **III.1a** and **III.1b**. So, the increase of the calculated $-J$ values according to **III.1a** < **III.1** < **III.1b** is likely due to the larger loss of planarity of the anthraquinone spacers as well as the smaller distortion from orthogonality between the copper and the benzene

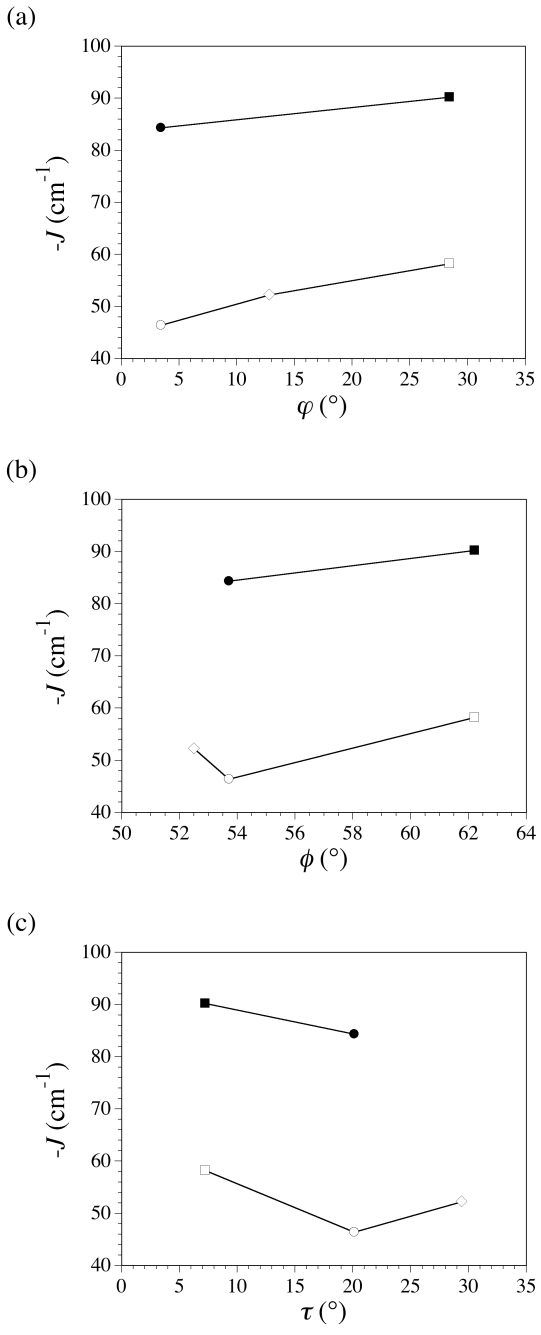

Figure III.12 Plots of the calculated values of the magnetic coupling parameter (–*J*) with (a) the dihedral angle between the central benzoquinone ring and the lateral benzene ring from each anthraquinone spacer (φ), (b) the torsion angle between the copper basal planes and the 1,4-substituted benzene rings from the anthraquinone spacers (ϕ), and (c) the tetrahedral twist angle at the copper atoms (τ) for the actual molecular geometries of **III.1a** (○) and **III.1b** (□) and the optimized molecular geometry of **III.1** (◇)in acetonitrile solution (data from Table III.4). The experimental –*J* values of **III.1a** (●) and **III.1b** (■) are also shown for comparison. The solid lines are only eye-guides.

planes and/or the smaller tetrahedral distortion of the copper center along this series, as evidenced by the crystal structures of **III.1a** and **III.1b**.

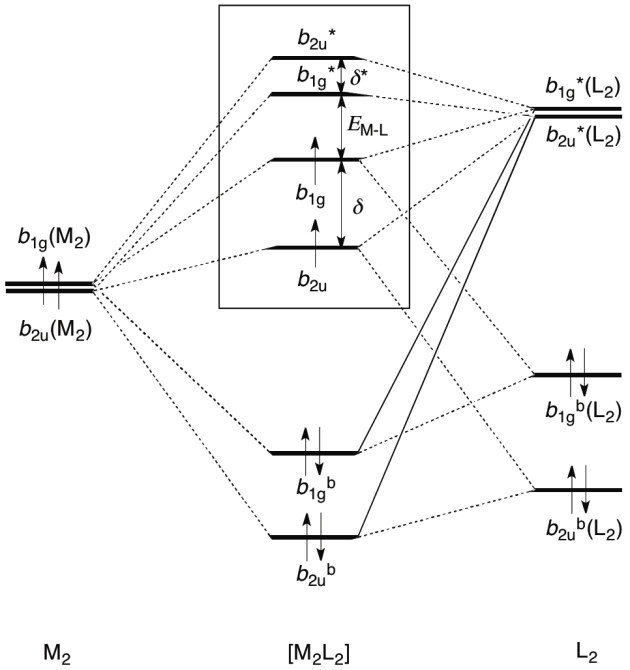

Figure III.13 Simplified energy level diagram of the frontier MOs of the optimized molecular geometry in acetonitrile solution of **III.1**. The boxed structure shows the electrochemically active LUMOs and SOMOs.

Overall, this indicates that the exchange coupling interaction along this series is governed by both structural and electronic factors associated with the steric requirements and electron acceptor properties of the anthraquinone group. Hence, the spin delocalization and spin polarization effects onto the ligand π-conjugated electron system are maximized when the basal planes of the square planar metal ions are disposed perpendicularly to the two 1,4-substituted 9,10-anthraquinone spacers. This particular orthogonal geometry ensures a unusual π-type pathway for the exchange interaction between the unpaired electrons of the two Cu^{II} ions through the double aromatic bridge. Contrarily, the electron acceptor character of the benzoquinone ring is more important in planar anthraquinone, minimizing thus the spin delocalization and spin polarization onto the fused 1,4-substituted benzene rings when compared to the non-planar situation. Hence, the –*J* values must reach a maximum for ϕ = 90º and τ = 0º, whereas they would be minimum for φ = 0º along this series of dicopper(II) anthraquinophanes.

Molecular orbital calculations. DF molecular orbital (MO) calculations for the triplet spin state of the optimized molecular geometry of **III.1** in acetonitrile solution are consistent with the proposed dual, ligand- and metal-based redox behavior for **III.1a** and **III.1b**. So, the energy diagram of the frontier MOs of **III.1** is typical of strong antiferromagnetically coupled dicopper(II) metallacyclophanes with weakly interacting 1,4-substituted 9,10-anthraquinonebis(oxamate) bridging ligands of large σ-field strength and distinctly π electron accepting nature (Figure III.13).

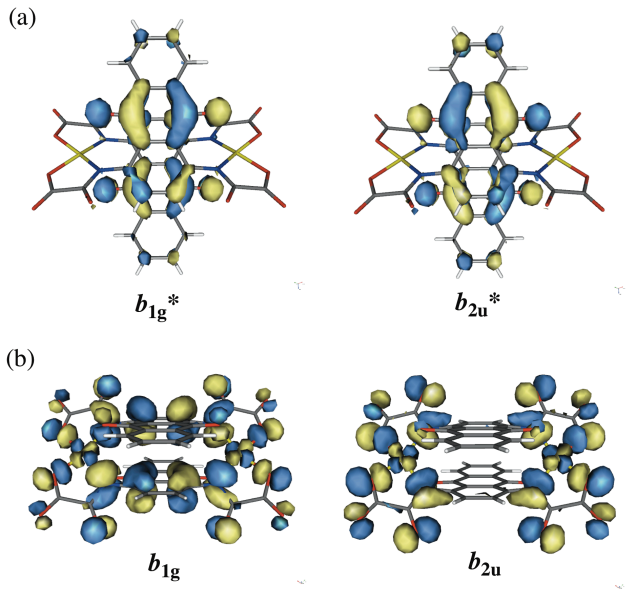

Figure III.14 Perspective views of the calculated electroactive LUMOs (a) and SOMOs (b) for the triplet spin configuration of the optimized molecular geometry in acetonitrile solution of **III.1**. The isodensity surface corresponds to a cutoff value of 0.001 e bohr^{-3}.

In fact, there exists a pair of lowest unoccupied molecular orbitals (LUMOs) of ligand-based π-nature, noted b_{1g}^* and b_{2u}^*, which are very close in energy to the pair of singly occupied molecular orbitals (SOMOs) of mainly metal-based σ-nature, noted b_{1g} and b_{2u} (Figure III.14). The relatively small value of the SOMO–LUMO energy gap of **III.1** [$E_{M-L} = E(b_{1g}^*) - E(b_{1g})$ = 0.00824 a.u. = 1809 cm^{-1}; Table III.4] results from both the electron π-acceptor character of the quinone group, which causes the stabilization of the π-ligand LUMOs, and the electron σ-donor character of the oxamato groups, which leads instead to the destabilization of the σ-metal SOMOs.

The pair of low-lying b_{1g}^* and b_{2u}^* LUMOs of mainly non-bonding nature of **III.1** are energetically close but non-degenerated [$\delta^* = E(b_{2u}^*) - E(b_{1g}^*)$ = 0.01294 a.u. = 2840 cm^{-1}; Table III.4]. They are made up by the symmetric and antisymmetric combinations of the two π-type orbitals from the electron accepting 9,10-anthraquinone spacers (Figure III.14a). Indeed, they have a large contribution from the p_z(O) and p_z(C) orbitals of the central benzoquinone ring which would be the ultimately responsible for the semiquinonate- and catecholate-type nature of the resulting ligand-reduced dicopper(II) species of **III.1a** and **III.1b**.

The pair of b_{1g} and b_{2u} SOMOs of markedly antibonding nature of **III.1** are energetically close but non-degenerated [$\delta = E(b_{1g}) - E(b_{2u})$ = 0.00674 a.u. = 1479 cm^{-1}; Table III.4]. They are mainly composed by the symmetric and antisymmetric combinations of the $d_{x^2-y^2}$ orbitals of the Cu^{II} ions mixed with the corresponding combinations of appropriate symmetry of the two σ-type orbitals of the electron donating oxamato groups (Figure III.14b). The large mixing of the $d_{x^2-y^2}$(Cu) orbitals with the

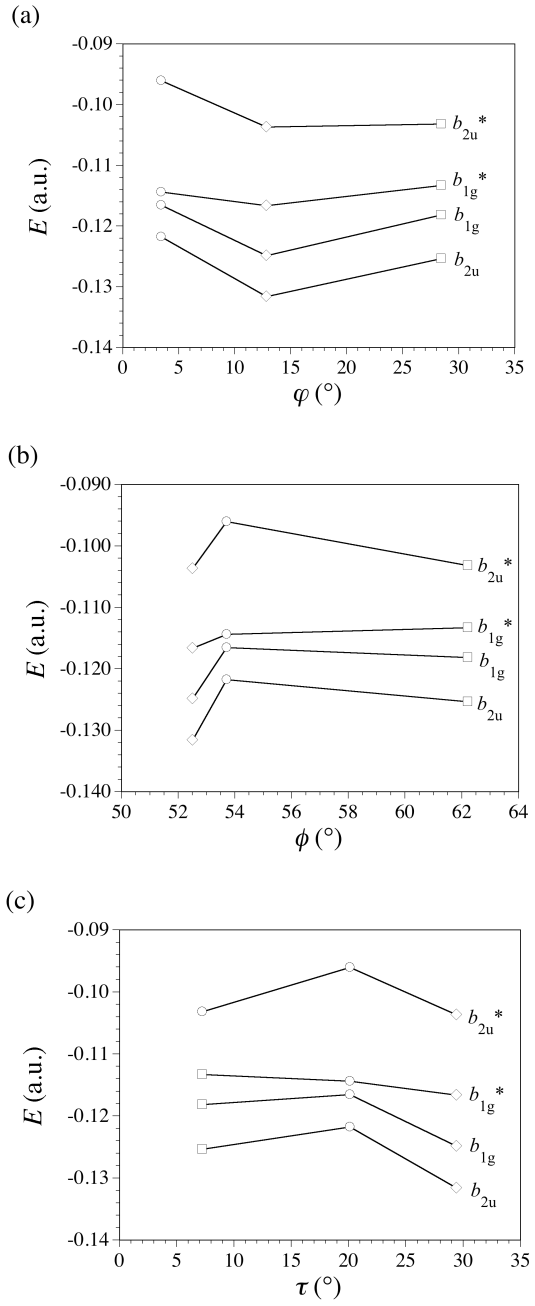

Figure III.15 Plots of the calculated values of the frontier MO energies (E) with (a) the dihedral angle between the central benzoquinone ring and the lateral benzene ring from each anthraquinone spacer (φ), (b) the torsion angle between the copper basal planes and the 1,4-substituted benzene rings from the anthraquinone spacers (ϕ), and (c) the tetrahedral twist angle at the copper atoms (τ) for the triplet spin state of the actual molecular geometries of **III.1a** (○) and **III.1b** (□) and the optimized molecular geometry of **III.1** (◇) in acetonitrile solution (data from Table III.4). The solid lines are only eye-guides.

p_x(N/O) and p_y(N/O) orbitals causes a destabilization of the σ-metal SOMOs that would account for the accessibility of the trivalent metal oxidation state in the resulting metal-oxidized dicopper(II,III) and dicopper(III) species of **III.1a** and **III.1b**. They also evidence a significant delocalization onto the p_z(C) orbitals of the proximal 1,4-substituted benzene rings, which is directly

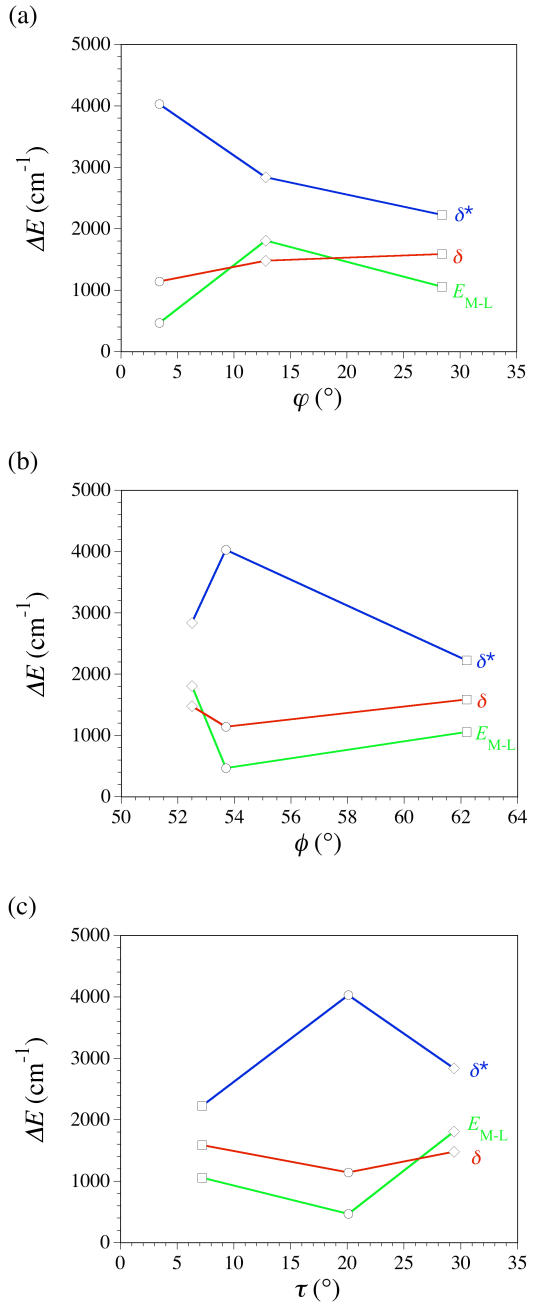

Figure III.16 Plots of the calculated values of the frontier MO energy gaps (ΔE) between the high- and low-lying SOMO and LUMO ($E_{M\text{-}L}$), the two SOMOs (δ), and the two LUMOs (δ^*) with (a) the dihedral angle between the central benzoquinone ring and the lateral benzene ring from each anthraquinone spacer (φ), (b) the torsion angle between the copper basal planes and the 1,4-substituted benzene rings from the anthraquinone spacers (ϕ), and (c) the tetrahedral twist angle at the copper atoms (τ) for the triplet spin state of the actual molecular geometries of **III.1a** (○) and **III.1b** (□) and the optimized molecular geometry of **III.1** (◇) in acetonitrile solution (data from Table III.4). The solid lines are only eye-guides.

responsible for the observed moderately strong antiferromagnetic coupling found experimentally in **III.1a** and **III.1b**.

Finally, it is possible to extract useful information about the molecular and electronic structures of this series of dicopper(II)

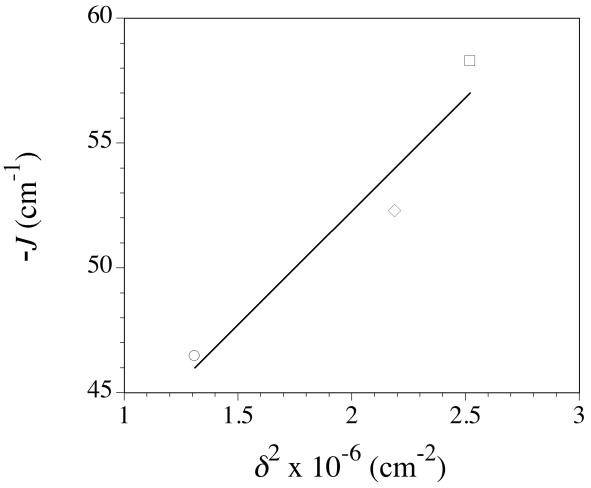

Figure III.17 Linear dependence of the calculated $-J$ values for the actual molecular geometries of **III.1a** (○) and **III.1b** (□) and the optimized molecular geometry of **III.1** (◇) in acetonitrile solution with the square of the energy gap (δ) between the two SOMOs (data from Table III.4). The solid line corresponds to the linear fit curve (see text).

anthraquinophanes by representing the calculated energy values of the frontier MOs for **III.1**, **III.1a**, and **III.1b** against some relevant structural parameters (Figures III.15 and III.16).

The calculated δ^* values for **III.1**, **III.1a**, and **III.1b** show a strong dependence with the structural parameters that have an indirect influence over the "through-space" interactions between the p_z(C/O) orbitals from the two facing 9,10-anthraquinone spacers in the corresponding b_{1g}^* and b_{2u}^* LUMOs (Figure III.14b). An overall decrease of δ^* with φ and ϕ is shown in Figures III.16a and III.16b respectively, while Figure III.16c shows an overall increase of δ^* with τ. A maximum value of δ would be reached for φ = 0º for which the intramolecular π–π stacking interactions between the two facing 9,10-anthraquinone spacers would be maximum because of their planar conformation. In contrast, a minimum δ^* value would be reached for ϕ = 90º and τ = 0º, where the 1,4-substituted benzene rings from the two facing 9,10-anthraquinone spacers in an *anti* conformation are eclipsed to each other. In this situation, the major contributions resulting from the overlapping between the p_z(C) orbitals of the electron accepting benzoquinone and the electron donor 1,4-substituted benzene rings from the two facing 9,10-anthraquinone spacers would be minimum.

Conversely, the calculated δ values for **III.1**, **III.1a**, and **III.1b** show a strong dependence with the structural parameters that have a direct influence over the "through-bond" interactions between the $d_{x^2-y^2}$(Cu) orbitals of the metal ions and the p_z(C/N) orbitals of the 1,4-substituted benzenediamidate group from each anthraquinonedioxamato bridging ligand in the corresponding b_{1g} and b_{2u} SOMOs (Figure III.14b), the $-J$ values being proportional to the square of δ according to the simpler MO models of the electron exchange interaction (Figure III.17). An overall increase of δ with φ and ϕ is shown in Figures III.16a and III.16b respectively, while Figure III.16c shows an overall decay of δ with τ. A minimum value of δ would be reached for φ = 0º, where

the electron withdrawing effects of the quinone group would be maximum. In contrast, a maximum δ value would be reached for $\phi = 90º$ and $\tau = 0º$, whereby the metal-ligand interaction would be maximum. In this situation, the 9,10-anthraquinone spacers are orthogonal to the basal planes of the square planar metal ions and consequently, the mixing between the p_z(C/N) orbitals and the $d_{x^2-y^2}$(Cu) orbitals would be maximum.

In spite of the clear trends showed by all of these data, it is important to remark that the considered structural parameters φ, ϕ, and τ are more or less correlated, and particularly these two latter ones, so that there is not easy to separate the influence of their distinct effects over the orbital energy differences. In addition, it should be noticed that we focus only on **III.1**, **III.1a**, and **III.1b** to build the showed structural-energy correlations, so that the random component of the observed tendencies may be important.

III.8 Concluding Remarks

In this work, we present a complementary experimental and theoretical study on magnetic coupling and multielectron transfer in a new class of dicopper(II) metallacyclophanes with redox-active anthraquinone spacers. The new anthraquinone-based dicopper(II) metallacyclophanes resulting from the side-by-side self-assembly of the 1,4-quanba^{4-} ligands with Cu^{II} ions possess a dual metal- and ligand-centered redox behavior featuring stepwise one-electron oxidation of the antiferromagnetically coupled Cu^{II} ions and two-electron reduction of the anthraquinone spacers in a π-stacked *anti* conformation. Hence, the non-innocent 1,4-quanba^{4-} ligands and the Cu^{II} ions function as electron reservoirs for reduction and oxidation respectively, to impart multielectron redox (charge storage) properties to this novel antiferromagnetically coupled dicopper(II) anthraquinophane to be used as molecular magnetic capacitor. This unique charge storage magnetic behavior ultimately result from the large σ-field strength and distinctly π electron accepting nature of the 1,4-substituted 9,10-anthraquinonebis(oxamate) bridging ligands, as substantiated from both experimental and theoretical studies. Quinone functionalization in this metallacyclic system constitutes thus a unique example of ligand design for the supramolecular control of the magnetic properties and electrochemical reactivity.

III.9 Experimental Section

Materials. All chemicals were of reagent grade quality. They were purchased from commercial sources and used as received, except those for electrochemical measurements. The nBu$_4$NPF$_6$ salt was recrystallized twice from ethyl acetate/diethyl ether, dried at 80 °C under vacuum, and kept in an oven at 110 °C. Acetonitrile and dichloromethane were purified by distillation from calcium hydride on activated 3 Å molecular sieves and stored under argon. Elemental analyses (C, H, N) were performed at the Servicio Central de Soporte a la Investigación (SCSIE) at the Universitat de València (Spain).

Preparations of the ligands. *N,N′*-1,4-bis(oxamic acid ethyl ester)-9,10-anthraquinone (Et_2H_2-1,4-quanba): Ethyl oxalyl chloride ester (2.8 mL, 24 mmol) was poured into a solution of 1,4-diamino-9,10-anthraquinone (2.9 g, 12 mmol) and triethylamine (3.4 mL, 24 mmol) in THF (150 mL) under vigorous stirring at 0 °C on an ice-bath. The reaction mixture was then refluxed for 1 h. The deep orange solid was collected by filtration after cooling, washed thoroughly with water to remove the white precipitate of Et_3NHCl and then with diethyl eter, and dried under vacuum (4.5 g, 85% yield). Anal.: calcd for $C_{22}H_{18}N_2O_8$ (438.2 g mol^{-1}): C, 60.27; H, 4.15; N, 6.39%. Found: C, 59.18; H, 4.28; N, 5.69%; ^{1}H NMR ($CDCl_3$): δ = 1.46 (t, 6 H, 2 CH_3), 4.46 (q, 4 H, 2 CH_2O), 7.83 (dd, 2 H, 6–H and 7–H of $C_{14}H_6O_2$), 8.34 (dd, 2 H, 5–H and 8–H of $C_{14}H_6O_2$), 9.21 (s, 2 H, 2–H and 3–H of $C_{14}H_6O_2$), 13.84 (s, 2 H, 2 NH); IR (KBr): ν = 3125 (N–H), 1721, 1642 cm^{-1} (C=O).

Preparations of the complexes. (nBu$_4$N)$_4$[Cu$_2$(1,4-quanba)$_2$] · 2MeCN · 2Et$_2$O (III.1a): A 1.0 M methanolic solution of nBu$_4$NOH (8.0 mL, 8.0 mmol) was added to a suspension of Et_2H_2-1,4-quanba (0.88 g, 2.0 mmol) in 20 mL of methanol under gentle warming. $Cu(ClO_4)_2 \cdot 6H_2O$ (0.75 g, 2.0 mmol) dissolved in methanol (10 mL) was then added dropwise under stirring. The resulting deep purple solution was filtered to separate the small amount of solid particles and the solvent was removed under vacuum. The solid was recovered with THF, collected by filtration, washed thoroughly with THF to remove the precipitate of nBu$_4$NClO$_4$, and air dried. Recrystallization from an acetonitrile/methanol solution solution (4:1 v/v) gave X-ray quality dark purple tiny prisms of **III.1a** upon slow vapor difussion of diethyl ether (1.3 g, 70% yield). Anal.: calcd for $C_{112}H_{176}Cu_2N_{10}O_{18}$ (2077.7 g mol^{-1}): C, 64.74; H, 8.54; N, 6.74%. Found: C, 64.24; H, 8.60; N, 6.76%; IR (KBr): ν = 3432 (O–H), 1648, 1607 cm^{-1} (C=O).

(Ph$_3$EtP)$_4$[Cu$_2$(1,4-quanba)$_2$] · 20H$_2$O (III.1b): An aqueous solution (10 mL) of $AgNO_3$ (0.34 g, 2.0 mmol) was added to an aqueous solution (20 mL) of **III.1a** (0.92 g, 0.5 mmol) under stirring at room temperature. The dark red solid that appeared was collected by filtration, suspended in water (10 mL), and then charged with an acetonitrile solution (5 mL) of Ph_3EtPBr (0.74 g, 2.0 mmol). The reaction mixture was further stirred for 30 min under gentle warming and then filtered to remove the precipitate of AgBr. Slow diffusion of diethyl ether over the filtered solution in acetonitrile gave dark red prisms of **III.1b** suitable for single-crystal X-ray diffraction after several days in the open air at room temperature (4.2 g, 90% yield). Anal. Calcd for $C_{116}H_{132}Cu_2N_4O_{36}P_4$ (2411): C, 57.83; H, 5.52; N, 2.33%. Found: C, 58.62; H, 5.38; N, 2.44%. IR (KBr): ν = 1648, 1603 cm^{-1} (C=O).

Physical techniques. ^{1}H NMR spectra were recorded at room temperature on a Bruker AC 200 (200.1 MHz) spectrometer. Chemical shifts are reported in δ (ppm) *vs*. TMS. $CDCl_3$ was used as solvent and internal standard (δ = 7.27 ppm). FTIR spectra

were recorded on a Nicolet-5700 spectrophotometer as KBr pellets.

X-ray crystallographic data collection and structure refinement. Single-crystal X-ray diffraction data of **III.1a** and **III.1b** were collected on a Bruker-Nonius X8APEXII CCD area detector diffractometer using graphite-monochromated Mo-K_α radiation at T = 100 (**III.1a**) and 293 K (**III.1b**). Due to the poor crystal quality of **III.1a**, a lower θ_{max} of diffraction was obtained even if all possible steps were undertaken to ensure that the experiment has been able to extract the best diffracting power from the sample. Low temperature measurements for **III.1a** were also used in order to enhance the reflection intensities and the extent of the "observed" data. Unfortunately, all our attempts to grow single crystals of better quality were unsuccessful. All calculations for data reduction, structure solution, and refinement of **III.1a** and **III.1b** were done through the SAINT[10] and SADABS[11] programs.

The structures of **III.1a** and **III.1b** were solved by Patterson method and subsequently completed by Fourier recycling using the SHELXTL software package.[12] The final geometrical calculations and the graphical manipulations were carried out with WinGX[13] and CRYSTALMAKER[14] programs, respectively. All non-hydrogen atoms of **III.1a** and **III.1b** were refined anisotropically. The hydrogen atoms were set in calculated positions and refined as riding atoms. However, it was not possible to find a reasonable model for the highly disordered acetonitrile and diethyl ether molecules of crystallization in the refinement of the structure of **III.1a**. The contribution to the diffraction pattern from the crystallization solvent molecules, which are located in the channels of the lattice (17.2% percentage void volume of the unit cell), were subtracted from the observed data by using the "SQUEEZE" method, as implemented in PLATON.[15] In fact, the SQUEEZE-Bypass method described therein is widely used in the crystallographic analysis of compounds containing substantial amounts of disordered solvent and/or counterions that cannot be located accurately from diffraction data. So, the values of the residual agreement factors for the reflections with $I > 2\sigma(I)$ of **III.1a** were R_1 = 0.1085 and wR_2 = 0.3058 before SQUEEZE, or R_1 = 0.0553 and wR_2 = 0.1656 after SQUEEZE (see Table III.1). The final formulation of **III.1a** is now in agreement with the residual electron density and cell volume.

Crystallographic data (excluding structure factors) for the structures reported in this paper have been deposited with the Cambridge Crystallographic Data Centre as supplementary publication CCDC no. 919043 (**III.1a**) and 948414 (**III.1b**). Copies of the data can be obtained free of charge on application to CCDC, 12 Union Road, Cambridge CB21EZ, UK (fax: (+44) 1223-336-033; e-mail: deposit@ccdc.cam.ac.uk).

Magnetic measurements. Variable-temperature (2.0–300 K) magnetic susceptibility measurements were carried out with a SQUID magnetometer under an applied field of 10 kOe ($T \geq 50$ K) and 100 Oe ($T < 50$ K). The experimental data were corrected for the diamagnetic contributions of the constituent atoms and the sample holder as well as for the temperature-independent paramagnetism (tip) of the Cu^{II} ion (60×10^{-6} cm^3 mol^{-1}).

Electrochemical measurements. The electrochemical studies were performed using a PAR 273A scanning potentiostat operating at a scan rate of 10–1000 mV s^{-1}. Cyclic voltammograms were carried out using 0.1 M nBu$_4$NPF$_6$ as supporting electrolyte and 1.0 mM of the Et_2H_2-1,4-quanba proligand and the complexes **III.1a** and **III.1b** in dichloromethane and acetonitrile, respectively. The working electrode was a glassy carbon disk (0.32 cm^2) that was polished with 1.0 μm diamond powder, sonicated, washed with absolute ethanol and acetone, and air dried. The reference electrode was $AgClO_4$/Ag separated from the test solution by a salt bridge containing the solvent/supporting electrolyte, with platinum as auxiliary electrode. All experiments were performed in standard electrochemical cells at 25 °C under argon. The investigated potential range was in the range of –2.00 to +1.80 V *vs*. SCE. The formal potentials were measured at a scan rate of 100 mV s^{-1} and were referred to the saturated calomel electrode (SCE). Ferrocene (Fc) was added as internal standard at the end of the measurements. The measured formal potential values of ferrocene are $E(Fc^+/Fc)$ = +0.46 (CH_2Cl_2, 0.1 M nBu$_4$NPF$_6$, 25 °C) and +0.40 V *vs*. SCE (CH_3CN, 0.1 M nBu$_4$NPF$_6$, 25 °C).[16] The values of the anodic to cathodic peaks separation of ferrocene are $\Delta E_p(Fc^+/Fc)$ = 100 (CH_2Cl_2, 0.1 M nBu$_4$NPF$_6$, 25 °C) and 70 mV (CH_3CN, 0.1 M nBu$_4$NPF$_6$, 25 °C)].

Chemical oxidation procedures and spectroscopic measurements. The monooxidized species was obtained by addition of a 0.01 M acetonitrile solution of bromine (0.1 mL) to a 1.0 mM acetonitrile solution of **III.1a** (0.1 mL) at –40 °C. X-band EPR spectra (ν = 9.47 GHz) of frozen-matrix acetonitrile solutions were recorded under non-saturating conditions on a Bruker ER 200 D spectrometer equipped with a helium cryostat.

III.10 Computational Details

Density functional (DF) calculations were carried out on the actual geometries of **III.1a** and **III.1b**, as well as on the optimized geometry of **III.1** in acetonitrile solution with the hybrid B3LYP functional[17] combined with the "broken-symmetry" (BS) approach,[18] as implemented in the Gaussian 09 program.[19] The triple- and double-ζ quality basis sets proposed by Ahlrichs and co-workers[20] were used for the metal and non-metal atoms, respectively. Solvation effects were introduced using a polarizable continuum model (PCM), where the cavity is created via a series of overlapping spheres.[21]

References

[1] a) G. N. Schrauzer, V. Mayweg, *J. Am. Chem. Soc.* **1962**, *84*, 3221. b) H. B. Gray, R. Williams, I. Bernal, E. Billig, *J. Am. Chem. Soc.* **1962**, *84*, 3596. c) H. B. Gray, E. Billig, *J. Am. Chem. Soc.* **1963**, *85*, 2019. d) A. Davison, N. Edelstein, R. H. Holm, A. H. Maki, *J. Am. Chem. Soc.* **1963**, *85*, 2029. e) E. Billig, R. Williams, I. Bernal, J. H. Waters, H. B. Gray, *Inorg. Chem.* **1964**, *3*, 663. f) C. K. Jorgensen, *Coord. Chem. Rev.* **1966**, *1*, 164. g) A. Davison, N. Edelstein, R. H. Holm, A. H. Maki, *Inorg. Chem.* **1963**, *2*, 1227. h) J. A. McCleverty, *Prog. Inorg. Chem.* **1968**, *10*, 49.

[2] a) M. D. Ward, J. A. McCleverty, *J. Chem. Soc. Dalton Trans.* **2002**, 275. b) K. Ray, T. Petrenko, K. Wieghardt, F. Neese, *Dalton Trans.* **2007**, 1552. c) R. Eisenberg, H. B. Gray, *Inorg. Chem.* **2011**, *50*, 9741. d) W. Kaim, *Inorg. Chem.* **2011**, *50*, 9752. e) C. G. Pierpont, *Inorg. Chem.* **2011**, *50*, 9766.

[3] a) A. Dei, D. Gatteschi, C. Sangregorio, L. Sorace, M. G. F. Vaz, *Inorg. Chem.* **2003**, *42*, 1701. b) A. Dei, D. Gatteschi, C. Sangregorio, L. Sorace, M. G. F. Vaz, *Chem. Phys. Lett.* **2003**, *368*, 162. c) S. Mukherjee, E. Rentschler, T. Weyhermüller, K. Wieghardt, P. Chaudhuri, *Chem. Commun.* **2003**, 1828. d) S. Mukherjee, T. Weyhermüller, E. Bothe, K. Wieghardt, P. Chaudhuri, *Dalton Trans.* **2004**, 3842.

[4] a) M. C. Dul, E. Pardo, R. Lezcouëzec, L. M. Chamoreau, F. Villain, Y. Journaux, R. Ruiz-García, J. Cano, M. Julve, F. Lloret, J. Pasán, C. Ruiz-Pérez, *J. Am. Chem. Soc.* **2009**, *131*, 14614. b) E. Pardo, J. Ferrando-Soria, M. C. Dul, R. Lezcouëzec, Y. Journaux, R. Ruiz-García, J. Cano, M. Julve, F. Lloret, L. Cañadillas-Delgado, J. Pasán, C. Ruiz-Pérez, *Chem. Eur. J.* **2010**, *16*, 12838. c) J. Ferrando-Soria, M. Castellano, R. Ruiz-García, J. Cano, M. Julve, F. Lloret, J. Pasán, C. Ruiz-Pérez, L. Cañadillas-Delgado, Y. Li, Y. Journaux, E. Pardo, *Chem. Commun.,* **2012**, *48*, 8401. d) M. Castellano, R. Ruiz-García, J. Cano, M. Julve, F. Lloret, Y. Journaux, G. De Munno, D. Armentano, *Chem. Commun.,* **2013**, *49*, 3534.

[5] a) J. M. Lehn, *Angew. Chem. Int. Ed.* **2004**, *43*, 3644. b) L. K. Thompson, O. Waldman, *Coord. Chem. Rev.* **2005**, *249*, 2677. c) T. Moriuchi, T. Hirao, *Acc. Chem. Res.* **2012**, *45*, 347.

[6] a) R. Ruiz, C. Surville-Barland, A. Aukauloo, E. Anxolabèhere-Mallart, Y. Journaux, J. Cano, M. C. Muñoz, *J. Chem. Soc., Dalton Trans.* **1997**, 745. b) B. Cervera, J. L. Sanz, M. J. Ibáñez, G. Vila, F. Lloret, M. Julve, R. Ruiz, X. Ottenwaelder, A. Aukauloo, S. Poussereau, Y. Journaux, M. C. Muñoz, *J. Chem. Soc., Dalton Trans.* **1998**, 781. c) X. Ottenwaelder, R. Ruiz-García, G. Blondin, R. Carrasco, J. Cano, D. Lexa, Y. Journaux and A. Aukauloo, *Chem. Commun.* **2004**, 504. d) X. Ottenwaelder, A. Aukauloo, Y. Journaux, R. Carrasco, J. Cano, B. Cervera, I. Castro, S. Curreli, M. C. Muñoz, A. L. Roselló, B. Soto, R. Ruiz-García, *Dalton Trans.* **2005**, 2516. e) R. Carrasco, J. Cano, X. Ottenwaelder, A. Aukauloo, Y. Journaux, R. Ruiz-García, *Dalton Trans*. **2005**, 2527.

[7] a) W. S. Durfee, C. G. Pierpont, *Inorg. Chem.* **1993**, *32*, 493. b) J. M. Mallwitz, N. L. Alkire, W. S. Durfee, *J. Coord. Chem.* **2002**, *55*, 641.

[8] a) J.-M. Savéant, Elements of Molecular and Biomolecular Electrochemistry: An Electrochemical Approach to Electron Transfer Chemistry, John Wiley & Sons, **2006**. b) K. Izutsu, Electrochemistry in Nonaqueous Solution, Wiley VCH, 2nd edn, **2009**.

[9] T. Rüffer, B. Bräuer, F. E. Meva, B. Walfort, *Dalton Trans.* **2008**, 5089.

[10] *SAINT*, version 6.45, Bruker Analytical X-ray Systems, Madison, WI, **2003**.

[11] G.M. Sheldrick, *SADABS Program for Absorption Correction*, version 2.10, Analytical X-ray Systems, Madison, WI, **2003**.

[12] *SHELXTL*, Bruker Analytical X-ray Instruments, Madison, WI, **1998**.

[13] L.J. Farrugia, *J. Appl. Cryst.* **1999**, *32*, 837.

[14] D. Palmer, *CRYSTALMAKER,* Cambridge University Technical Services, Cambridge, **1996**.

[15] a) A. L. Spek, *Acta Cryst.*, **1990**, *A46,* C34. b) P. Van der Sluis, A. L. Spek, *Acta Cryst.* **1990**, *A46,* 194.

[16] N. G. Connelly, W. E. Geiger, *Chem. Rev.* **1996**, *96*, 877.

[17] A. D. Becke, *J. Chem. Phys.* **1993**, *98*, 5648.

[18] a) E. Ruiz, J. Cano, S. Alvarez, P. Alemany, *J. Comput. Chem.* **1999**, *20*, 1391. b) E. Ruiz, A. Rodriguez-Fortea, J. Cano, Alvarez, P. Alemany, *J. Comput. Chem.,* **2003**, *24*, 982.

[19] M. J. Frisch, G. W. Trucks, H. B. Schlegel, G. E. Scuseria, M. A. Robb, J. R. Cheeseman, G. Scalmani, V. Barone, B. Mennucci, G. A. Petersson, H. Nakatsuji, M. Caricato, X. Li, H. P. Hratchian, A. F. Izmaylov, J. Bloino, G. Zheng, J. L. Sonnenberg, M. Hada, M. Ehara, K. Toyota, R. Fukuda, J. Hasegawa, M. Ishida, T. Nakajima, Y. Honda, O. Kitao, H. Nakai, T. Vreven, Jr., J. A. Montgomery, J. E. Peralta, F. Ogliaro, M. Bearpark, J. J. Heyd, E. Brothers, K. N. Kudin, V. N. Staroverov, R. Kobayashi, J. Normand, K. Raghavachari, A. Rendell, J. C. Burant, S. S. Iyengar, J. Tomasi, M. Cossi, N. Rega, J. M. Millam, M. Klene, J. E. Knox, J. B. Cross, V. Bakken, C. Adamo, J. Jaramillo, R. Gomperts, R. E. Stratmann, O. Yazyev, A. J. Austin, R. Cammi, C. Pomelli, J. W. Ochterski, R. L. Martin, K. Morokuma, V. G. Zakrzewski, G. A. Voth, P. Salvador, J. J. Dannenberg, S. Dapprich, A. D. Daniels, Ö. Farkas, J. B. Foresman, J. V. Ortiz, J. Cioslowski, D. J. Fox, *Gaussian 09*, revision B.1; Gaussian, Inc.: Wallingford, CT, **2009**.

[20] a) A. Schaefer, H. Horn, R. Ahlrichs, *J. Chem. Phys.* **1992**, *97*, 2571. b) A. Schaefer, C. Huber, R. Ahlrichs, *J. Chem. Phys.,* **1994**, *100*, 5829.

[21] a) M. Cossi, N. Rega, G. Scalmani, V. Barone, *J. Comp. Chem.* **2003**, *24*, 669. b) J. Tomasi, B. Mennucci and E. Cances, *J. Mol. Struct.-Theochem.* **1999**, *464*, 211.

CHAPTER IV

Permethylated Dicopper(II) Paracyclophanes as Molecular Magnetic Electroswitches

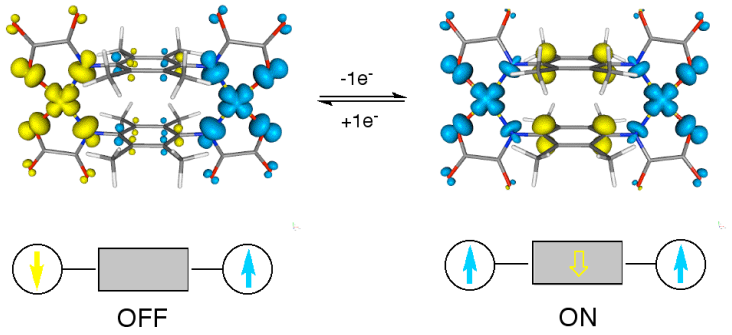

On the road to molecular electroswitches: upon reversible one-electron ligand oxidation of a permethylated dicopper(II) paracyclophane, the spin alignment of the two Cu^{II} ions (S_{Cu} = ½) changes from antiparallel (OFF) to parallel (ON) in the resulting dicopper(II) π-radical cation species. This new member of the family of oxamato-based dinuclear copper(II) metallacyclophanes illustrates an attractive design concept for molecular magnetic electroswitches incorporating two metal-based spin carriers and a redox-active ('non-innocent') bridging ligand.

IV.1 Introductory Aspects

The control of the electronic (redox, conducting, and/or magnetic) properties of polymetallic complexes by ligand design continues to attract attention in organometallic and coordination chemistry.[1,2] Besides their interest as models for the fundamental research on electron exchange (EE) and electron transfer (ET) phenomena between distant metal centers through extended π-conjugated organic ligands, homo- and heterovalent dimetallic complexes could be also of great importance due to their potential application in electronic and magnetic devices.[3]

The design and synthesis of redox-active ('non-innocent') aromatic bridging ligands that are able to connect two paramagnetic transition metal ions to form exchange-coupled, metal-radical or mixed-valent dinuclear complexes, depending on the locus of oxidation/reduction, are a major goal in the field.[2] A well-known example is the non-innocent *p*-phenylenediamine ligand which has been earlier demonstrated to act as efficient bridge for the transmission of EE interactions between two Cu^{II} ions.[4] In fact, the *N,N,N',N'*-tetramethyl-*p*-phenylenediamine (TMPD) is easily oxidized to the corresponding π-radical iminium cation ($TMPD^{\bullet+}$), referred to as Wurster blue, which is one of the oldest known stable π-radical organic cations (Figure IV.1a).[5] This work has been recently extended to related π-stacked radical (**I**) and diradical iminium cations (**II**) resulting from the stepwise two-electron oxidation of doubly polymethylene-bridged bis(*p*-phenylenediamines) which belong to the class of *N,N',N'',N'''*-tetraalkyl-substituted tetraza[*n*.*n*]para-cyclophanes (*n* = 5 and 7 with R = Me, Et, and *i*Pr), so-called Wurster blue cyclophanes (Figure IV.1b).[6]

Metallacyclic complexes containing multiple redox-active, either metal- or ligand-based paramagnetic centers are a current challenge in the multidisciplinary field of metallosupramolecular chemistry which lies at the interface of several disciplines, including supramolecular electrochemistry and magnetochemistry.[7] Moreover, they are of large interest as potential candidates to molecular magnetic electroswitches.[8,9] Our strategy in this field consists of using non-innocent, polymethyl-substituted *p*-phenylenebis(oxamato) bridging ligands which self-assemble with square-planar Cu^{II} ions to give the corresponding double-stranded dinuclear copper(II) paracyclophanes (**IV.1**–**IV.3**, Figure IV.2).[10] Complex **IV.3** shows an intriguing electroswitching magnetic behavior upon reversible one-electron oxidation of one of the two facing permethylated *p*-phenylene spacers to give the putative metallo-π-radical cation species **IV.3'**, as reported in a preliminay

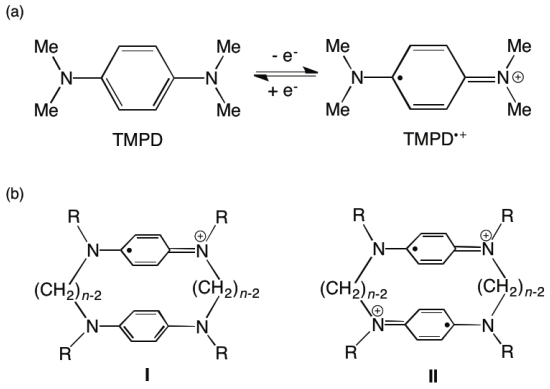

Figure IV.1 Redox equilibrium in *N,N,N',N'*-tetramethyl-*p*-phenylenediamine (a) and redox forms of polymethylene-bridged paracyclophane derivatives (b).

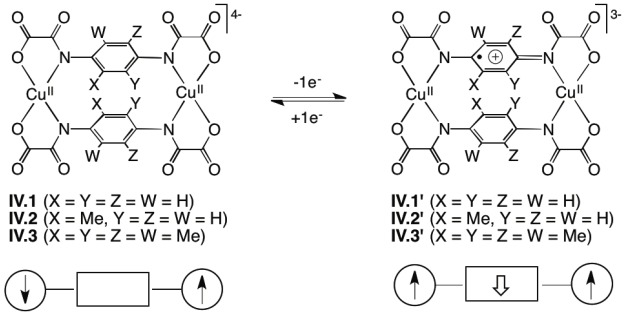

Figure IV.2 Illustration of the redox-triggered magnetic switching in dicopper(II) paracyclophanes featuring polymethyl-substituted *p*-phenylenebis(oxamate) π-radical cations as bridging ligands.

communication (see third communication in Appendices).[10b] Indeed, the redox pair **IV.3**/**IV.3'** presents very different molecular and electronic structures, as supported by preliminary spectroscopic (UV–vis–NIR and EPR) measurements and density functional (DF) calculations.

Herein we report the complete synthesis, structural and spectroscopic characterization, magnetic and redox properties of this series of dinuclear copper(II) paracyclophanes (**IV.1**–**IV.3**) with the parent *N,N'-p*-phenylenebis(oxamate) ligand (ppba) and its 2-methyl- (Meppba) and 2,3,5,6-tetramethyl-substituted (Me_4ppba) derivatives (Figure IV.2). The influence of the number of electron donating methyl substituents in the benzene ring on their unique structural and electronic (magnetic and redox) properties has been analyzed and discussed with the aid of theoretical calculations. Hence, DF calculations have been carried out on **IV.1**–**IV.3** to elucidate the mechanism of the EE interaction and to examine the influence of steric and/or electronic effects on magnetic coupling along this series. Moreover, DF calculations have been performed on the oxidized product of the permethylated derivative **IV.3'** in order to give further support to the putative ligand-based oxidation chemistry which is ultimately responsible for the electroswitching magnetic behavior (Figure IV.2).

IV.2 Syntheses of the Ligands and Complexes

The ligands were isolated as the diethyl ester acid derivatives of general formula Et_2H_2L (L = ppba, Meppba, and Me_4ppba) (see Experimental Section). The Et_2H_2ppba and $Et_2H_2Me_4$ppba proligands were prepared from the straightforward condensation of the corresponding *p*-phenylenediamine and 2,3,5,6-tetramethyl-*p*-phenylenediamine precursors with ethyl oxalyl chloride ester (1:2 molar ratio) in tetrahydrofurane (Figure IV.3a). The Et_2H_2Meppba proligand was instead synthesized from the reaction of the commercially available 2-methyl-*p*-phenylenediamine dihydrogen sulfate with ethyl oxalyl chloride ester (1:2 molar ratio) in presence of triethylamine as base in tetrahydrofurane (Figure IV.3b).

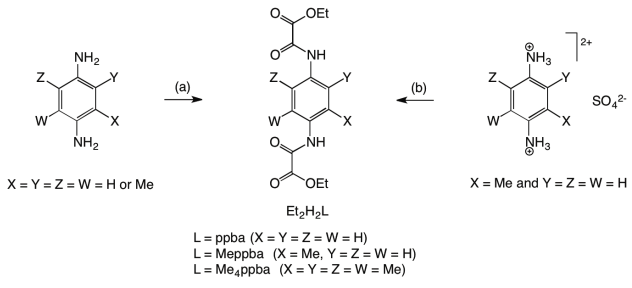

Figure IV.3 Synthetic procedure for the Et_2H_2L proligands (L = ppba, Meppba, and Me_4ppba): (a) $C_2O_2Cl(OEt)$, THF; (b) $C_2O_2Cl(OEt)$, Et_3N, THF.

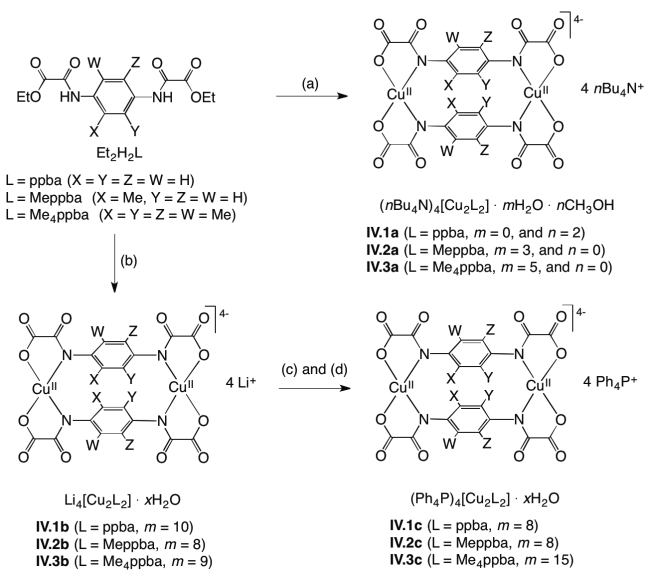

Figure IV.4 Synthetic procedure for the the tetra-*n*-butylammonium, lithium(I), and tetraphenylphosphonium salts of the $[Cu^{II}_2L_2]^{4-}$ complexes (L = ppba, Meppba, and Me_4ppba): (a) nBu_4NOH, $Cu(ClO_4)_2$, CH_3OH; (b) $LiOH \cdot H_2O$, $Cu(NO_3)_2 \cdot 3H_2O$, H_2O; (c) $AgNO_3$, H_2O; (d) Ph_4PCl, H_2O/CH_3CN.

Complexes **IV.1–IV.3** were isolated as their tetra-*n*-butylammonium, lithium(I), and tetraphenylphosphonium salts (see Experimental Section). The tetra-*n*-butylammonium salts of general formula $(nBu_4N)_4[Cu_2L_2] \cdot xH_2O \cdot yCH_3OH$ [L = ppba (x = 0 and y = 2) (**IV.1a**), Meppba (x = 3 and y = 0) (**IV.2a**), and Me_4ppba (x = 5 and y = 0) (**IV.3a**)] were prepared by the one-step reaction of the corresponding Et_2H_2L proligands with copper(II) perchlorate (2:2 molar ratio) by using tetra-*n*-butylammonium hydroxide as base in methanol (Figure IV.4a). Alternatively, the lithium(I) salts of general formula $Li_4[Cu_2L_2] \cdot xH_2O$ [L = ppba (x = 10) (**IV.1b**), Meppba (x = 7) (**IV.2b**), and Me_4ppba (x = 9) (**IV.3b**)] were obtained from the reaction of the corresponding Et_2H_2L proligands with copper(II) nitrate (2:2 molar ratio) by using lithium(I) hydroxide as base in water (Figure IV.4b). The tetraphenylphosphonium salts of general formula $(Ph_4P)_4[Cu_2L_2] \cdot xH_2O$ [L = ppba (x = 8) (**IV.1c**), Meppba (x = 8) (**IV.2c**), and Me_4ppba (x = 15) (**IV.3c**)] were then synthesized by two successive steps from the metathesis of the lithium(I) salts with tetraphenylphosphonium chloride in water/acetonitrile through the intermediacy of the silver(I) salts (Figures IV.4c and IV.4d). The inorganic lithium(I) salts of **IV.1– IV.3** were only soluble in water, while the organic tetra-*n*-butylammonium and tetraphenylphosphonium salts were also soluble in organic solvents like acetonitrile or dichloromethane. X-ray quality single crystals of **IV.1–IV.3** as their tetra-*n*-butylammonium (**IV.1a**), lithium(I) (**IV.2b**), and tetraphenylphosphonium (**IV.3c**) salts were obtained by layering of either diethyl ether or methanol into the methanol or water solutions of **IV.1a** and **IV.2b** respectively, or by slow evaporation from the water/acetronitrile solutions of **IV.3c**.

The chemical identity of the ligands and complexes was determined by elemental analysis together with ^{1}H NMR and FTIR spectroscopies (see Experimental Section and Appendices).

IV.3 Description of the Structures

Single-crystal X-ray diffraction of **IV.1a**, **IV.2b**, and **IV.3c** confirmed the expected metallacyclic dicopper(II)tetraaza[3.3]paracyclophane structure that was earlier observed for the related complex $Na_4[Cu_2(ppba)_2] \cdot 11H_2O$ (Figures IV.5–IV.10).[10a] A summary of the crystallographic data is given in Table IV.1, while selected bond distances and interbond angles are listed in Tables IV.2–IV.4.

Table IV.1 Summary of crystallographic data.

	IV.1a	**IV.2b**	**IV.3c**
formula	$C_{86}H_{160}Cu_2N_8O_{14}$	$C_{22}H_{26}Cu_2Li_4N_4O_{19}$	$C_{124}H_{134}Cu_2N_4O_{27}P_4$
M (g mol^{-1})	1657.30	805.31	2363.31
crystal system	triclinic	monoclinic	triclinic
space group	*P*–1	*C*2/*c*	*P*–1
a (Å)	10.6798(15)	18.3550(10)	13.5320(10)
b (Å)	13.9059(18)	18.4560(10)	15.7080(10)
c (Å)	18.099(2)	13.4790(10)	15.8360(10)
α (°)	69.861(5)		71.2170(10)
β (°)	74.331(6)	131.5100(10)	70.9200(10)
γ (°)	75.581(6)		68.9650(10)
V (Å^3)	2393.4(5)	3419.3(4)	2888.2(3)
Z	1	4	1
ρ_{calc} (g cm^{-3})	1.150	1.564	1.359
μ (mm^{-1})	0.504	1.326	0.501
T (K)	296(2)	100(2)	100(2)
indep. reflect.	8422	3670	9167
obs. reflect. [$I > 2\sigma(I)$]	7479	3180	9045
R^a [$I > 2\sigma(I)$]	0.0513	0.1020	0.0412
wR^b [$I > 2\sigma(I)$]	0.1482	0.3297	0.1104
S^c	1.084	1.537	1.036

^{a} $R = \sum(|F_o| - |F_c|)/\sum|F_o|$. ^{b} $wR = [\sum w(|F_o| - |F_c|)^2/\sum w|F_o|^2]^{1/2}$. ^{c} $S = [\sum w(|F_o| - |F_c|)^2/(N_o - N_p)]^{1/2}$.

Table IV.2 Selected bond distances (Å) and interbond angles (°) for **IV.1a**.[a,b]

Cu(1)–N(1)	1.9832(18)	Cu(1)–N(2)^I	1.9775(18)
Cu(1)–O(1)	1.9693(17)	Cu(1)–O(4)^I	1.9611(16)
N(1)–Cu(1)–N(2)^I	108.79(7)	N(1)–Cu(1)–O(1)	83.43(7)
N(1)–Cu(1)–O(4)^I	164.81(7)	N(2)^I–Cu(1)–O(1)	164.10(7)
N(2)^I–Cu(1)–O(4)^I	83.45(7)	O(1)–Cu(1)–O(4)^I	86.34(7)

[a] The estimated standard deviations are given in parentheses. [a] Symmetry code: (I) = $-x+2, -y+1, -z+1$.

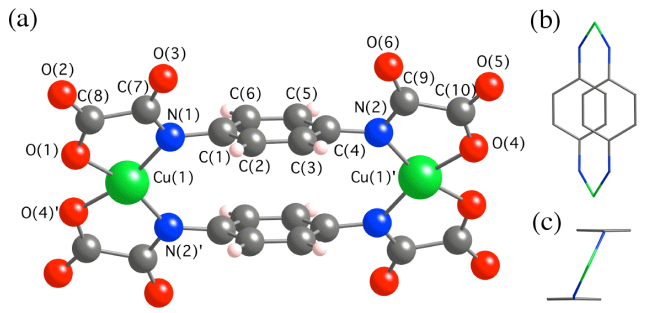

Figure IV.5 (a) Perspective view of the centrosymmetric anionic dicopper unit of **IV.1a** with the atom-numbering scheme [symmetry code: (I) = $-x+2, -y+1, -z+1$]. (b) Top and (c) side projection views of the metallacyclic core of **IV.1a**.

Table IV.3 Selected bond distances (Å) and interbond angles (°) for **IV.2b**.[a,b]

Cu(1)–N(1)	1.946(5)	Cu(2)–N(2)	1.950(5)
Cu(1)–O(1)	1.941(4)	Cu(2)–O(4)	1.934(5)
Cu(1)–O(1w)	2.77(1)	Cu(2)–O(2w)	2.84(2)
N(1)–Cu(1)–N(1)^{I}	105.5(3)	N(2)–Cu(2)–N(2)^{I}	106.7(3)
N(1)–Cu(1)–O(1)	85.2(2)	N(2)–Cu(2)–O(4)	85.1(2)
N(1)–Cu(1)–O(1)^{I}	168.4(2)	N(2)–Cu(2)–O(4)^{I}	168.1(2)
O(1)–Cu(1)–O(1)^{I}	84.5(3)	O(4)–Cu(2)–O(4)^{I}	83.3(3)
N(1)–Cu(1)–O(1w)	92.9(3)	N(2)–Cu(2)–O(2w)	90.8(4)
N(1)^{I}–Cu(1)–O(1w)	96.8(2)	N(2)^{I}–Cu(2)–O(2w)	90.8(4)
O(1)–Cu(1)–O(1w)	77.9(3)	O(4)–Cu(2)–O(2w)	86.9(4)
O(1)^{I}–Cu(1)–O(1w)	90.1(3)	O(4)^{I}–Cu(2)–O(2w)	91.1(4)

[a] The estimated standard deviations are given in parentheses. [b] Symmetry code: (I) = $-x+1, y, -z+3/2$.

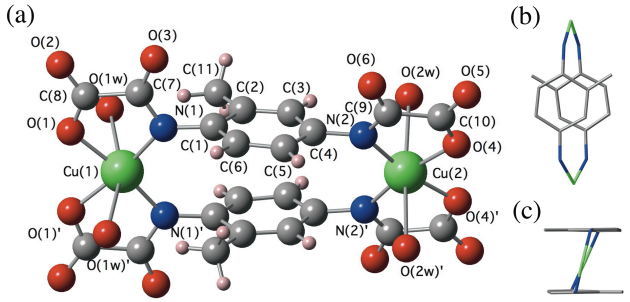

Figure IV.6 (a) Perspective view of the two-fold symmetric anionic dicopper unit of **IV.2b** with the atom-numbering scheme [symmetry code: (I) = $-x+1, y, -z+3/2$] (b) Top and (c) side projection views of the metallacyclic core of **IV.2b**.

The double-stranded dinuclear $[Cu^{II}_2L_2]^{4-}$ anions of **IV.1a** (L = ppba) and **IV.3c** (L = Me_4ppba) are centrosymmetric (Figures IV.5a and IV.7a). The two centrosymmetrically-related Cu(1) and Cu(1)^{I} atoms of **IV.1a** and **IV.3c** have an essentially square planar coordination environment, CuN_2O_2, which is formed by two amidate-nitrogen [Cu–N = 1.9775(18) – 1.9832(18) (**IV.1a**) and 1.9624(19)–1.9639(19) Å (**IV.3c**)] and two carboxylate-oxygen atoms [Cu–O = 1.964(2)–1.969(2) (**1a**) and 1.9413(16) – 1.9793(16) Å (**IV.3c**)] from two oxamato donor groups [mean plane deviations from the metal basal plane of ±0.199(1) (**IV.1a**) and ±0.029 Å (**IV.3c**) for N(1) and N(2)^{I}, and of ±0.166(1) (**IV.1a**) and ±0.034 Å (**IV.3c**) for O(1) and O(4)^{I}]. The values of the tetrahedral twist angle (τ) between the Cu(1)N(1)O(1) and Cu(1)N(2)^{I}O(4)^{I} mean planes are 16.1(1) (**IV.1a**) and 5.0(1)° (**IV.3c**), indicating thus a stronger tetrahedral distortion for the metal coordination site in the unsubstituted ancestor **IV.1a** when compared to the permethylated derivative **IV.3c**. In contrast, the double-stranded dinuclear $[Cu^{II}_2L_2(H_2O)_2]^{4-}$ anions of **IV.2b** (L = Meppba) have a crystallographically imposed two-fold symmetry with the C_2 molecular axis running along the metal-metal vector (Figure IV.6a). The two crystallographically independent Cu(1) and Cu(2) atoms of **IV.2b** possess an axially elongated octahedral geometry, $CuN_2O_2(Ow)_2$, whereby two amidate-nitrogen [Cu–N = 1.946(4)–1.950(5) Å] and two carboxylate-oxygen atoms [Cu–O = 1.934(6)–1.941(4) Å] from two oxamato donor groups build the copper basal plane [mean plane deviations of ±0.07 and ±0.09 Å for N(1) and O(1) at Cu(1), and of ±0.03 and ±0.04 Å for N(2) and O(4) at Cu(2)] while two weakly coordinated, disordered water molecules with half occupancy factor occupy the axial positions [Cu–Ow = 2.77(1)–2.84(2) Å].

Table IV.4 Selected bond distances (Å) and interbond angles (°) for **IV.3c**.[a,b]

Cu(1)–N(1)	1.9639(19)	Cu(1)–N(2)^{I}	1.9624(19)
Cu(1)–O(1)	1.9793(16)	Cu(1)–O(4)^{I}	1.9413(16)
N(1)–Cu(1)–N(2)^{I}	106.91(8)	N(1)–Cu(1)–O(1)	82.40(7)
N(1)–Cu(1)–O(4)^{I}	170.08(7)	N(2)^{I}–Cu(1)–O(1)	169.36(7)
N(2)^{I}–Cu(1)–O(4)^{I}	82.86(7)	O(1)–Cu(1)–O(4)^{I}	87.71(7)

[a] The estimated standard deviations are given in parentheses. [b] Symmetry code: (I) = $-x+2, -y+1, -z$.

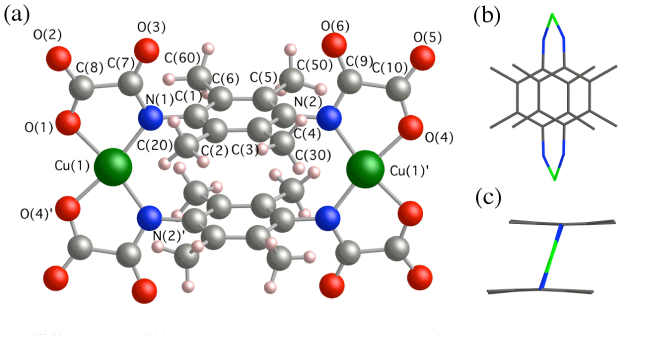

Figure IV.7 (a) Perspective view of the centrosymmetric anionic dicopper unit of **IV.3c** with the atom-numbering scheme [symmetry code: (I) = $-x+2, -y+1, -z$]. (b) Top and (c) side projection views of the metallacyclic core of **IV.3c**.

Within the dicopper(II) paracyclophane cores, $Cu_2(p\text{-}N_2C_6Me_n)_2$ [n = 0 (**IV.1a**), 1 (**IV.2b**), and 4 (**IV.3c**)], the polymethyl-substituted *p*-phenylene spacers which are connected by the two N–Cu–N linkages have a parallel-displaced π-stacked conformation (Figures IV.5b–IV.7b). The values of the centroid-centroid inter-ring distance (h) between the two benzene rings are 3.435(2) (**IV.1a**), 3.267(1) (**IV.2b**), and 3.349(2) Å (**IV.3c**), while the values of the angle between the centroid-centroid vector and their normal (θ) are 23.27(4) (**IV.1a**), 18.5(2) (**IV.2b**), and 17.56(5)° (**IV.3c**) (Figures IV.5c–IV.7c). Hence, the entire metallacyclophane molecule has approximate C_{2h} symmetry in **IV.1a** and **IV.3c**, where the copper basal planes are not exactly oriented perpendicular to the benzene planes (Figure IV.5c and IV.7c). The values of the dihedral angle (ϕ) between the benzene and the copper basal planes are 58.72(7) (**IV.1a**) and 73.67(5)° (**IV.3c**). This reflects a significantly larger deviation from the ideal D_{2h} symmetry corresponding to the alternative eclipsed π-stacked, orthogonal conformation (ϕ = 90°) in the unsubstituted ancestor **IV.1a** than in the permethylated derivative **IV.3c** (Figure IV.5b and IV.7b). This situation is likely explained by the electron donating nature of the methyl substituents, which favors the inter-ring π-π stacking interactions between the two facing benzene rings in spite of the steric hindrance among their methyl substituents. Instead, the metallacyclophane core of **IV.2b** has a reduced C_2 symmetry because of the pseudo-*meta* configuration of the 2-methyl substituents from the two facing benzene rings (Figure IV.6b). This situation reflects on the smaller deviations from perpendicularity between the benzene planes and the copper basal planes for the metal atom closer to the methyl groups in **IV.2b** [ϕ = 79.2(3) and 64.2(3)° at Cu(1) and Cu(2), respectively] (Figure IV.6c). In addition, the facing benzene planes are not exactly parallel to each other as in **IV.1a** and **IV.3c**, while the copper basal planes also deviate slightly from coplanarity. The value of the dihedral angle (γ) between the benzene planes and that

between the copper basal planes (φ) in **IV.2b** are 2.7(3) and 15.0(3)°, respectively.

In the crystal lattice, the $[Cu^{II}_2L_2]^{4-}$ anions of **IV.1a** (L = ppba) and **IV.3c** (L = Me_4ppba) establish weak hydrogen bonds with the crystallization solvent molecules of methanol (**IV.1a**) and water (**IV.3c**) through the carbonyl- and/or carboxylate-oxygen atoms from the oxamato groups [O···O = 2.772(5) Å (**IV.1a**) and O···Ow = 2.812(2)–2.919(2) Å (**IV.3c**)]. This situation gives rise to either discrete (**IV.1a**) or extended layers of hydrogen-bonded anionic dicopper(II) units (**IV.3c**) (Figures IV.8a and IV.10a), which are well separated from each other by the bulky tetra-*n*-butylammonium (**IV.1a**) or tetraphenylphosphonium (**IV.3c**) cations (Figures IV.8b and IV.10b). On the contrary, the $[Cu^{II}_2L_2(H_2O)_2]^{4-}$ anions of **IV.2b** (L = Meppba) are differently bound to the partially hydrated Li(1) and Li(3) atoms through the carboxylate- and carbonyl-oxygen atoms from the oxamato groups respectively, while a coordinated water molecule acts as bridge between the Li(1) and Li(2) atoms [Li–O = 1.970(11)–2.083(9) Å and Li–Ow = 1.997(11)–2.23(2) Å] (Figure IV.9a). This situation leads to heterobimetallic lithium(I)-copper(II) rectangular layers of "brick-wall" topology (Figure IV.9b). The adjacent $Li^{II}_4Cu^{II}_2$ layers of **IV.2b** closely stack above each other to give an infinite array of parallely displaced (not eclipsed) corrugated layers along the crystallographic *a* axis (Figure IV.9c). The intramolecular Cu–Cu distances (*r*) across the double polymethyl-substituted *p*-phenylenediamidate bridges are 8.002(2) (**IV.1a**), 7.939(2) (**IV.2b**), and 7.944(2) Å (**IV.3c**), while the

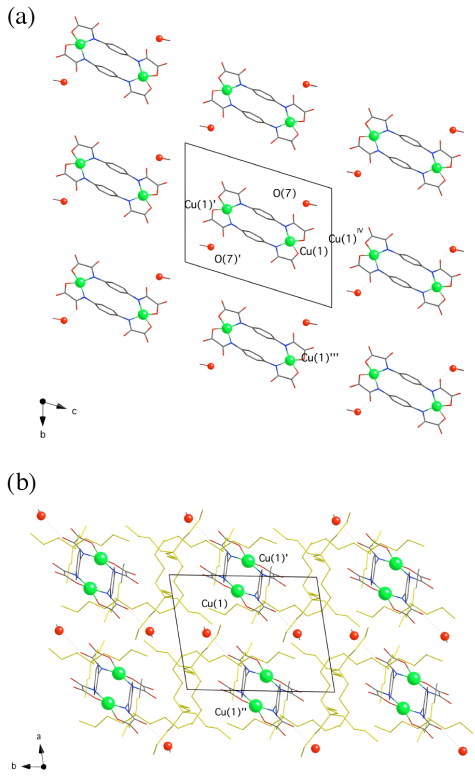

Figure IV.8 (a) Projection view of the discrete anionic dicopper units of **IV.1a** along the [100] direction [symmetry code: (I) = – *x* + 2, – *y* + 1, – *z* + 1; (II) = *x* – 1, *y*, *z* + 1; (III) = *x* – 1, *y* – 1, *z*; (IV) = – *x* + 1, – *y* + 1, – *z* + 2]. The hydrogen bonds with the crystallization methanol molecules are represented by dotted lines. (b) Crystal packing view of **IV.1a** along the [001] direction. The *n*-tetrabutylammonium cations are shown in yellow color (hydrogen atoms have been omitted for clarity).

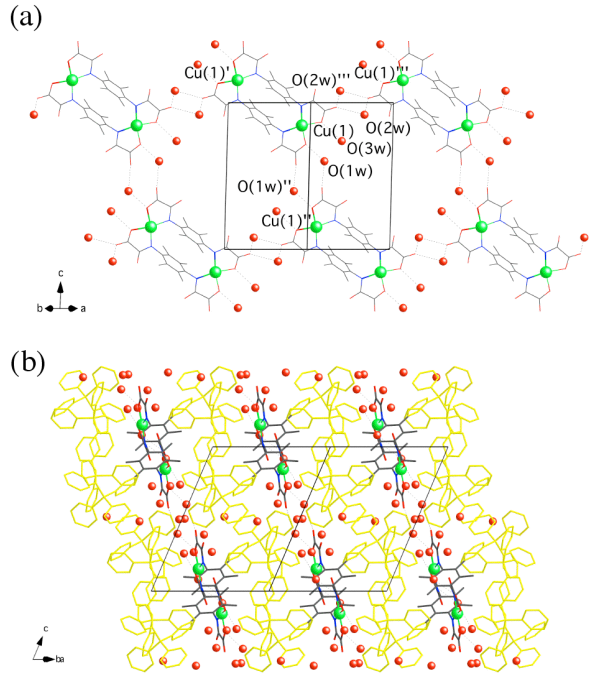

Figure IV.10 (a) Projection view of a layer of hydrogen-bonded anionic dicopper units of **3c** along the [110] direction [symmetry code: (I) = – *x* + 2, – *y* + 1, – *z*; (II) = – *x* + 1, – *y* + 1, – *z* + 1; (III) = – *x* + 1, – *y* + 1, – *z*]. The hydrogen bonds with the crystallization water molecules are represented by dotted lines. (b) Crystal packing view of **IV.3c** along the [–110] direction. The tetraphenylphosphonium cations are shown in yellow color (hydrogen atoms have been omitted for clarity).

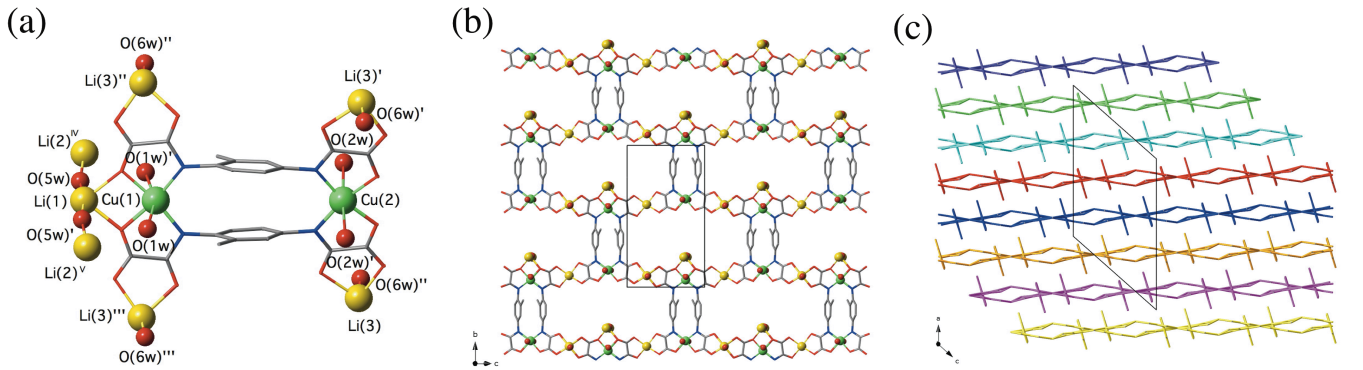

Figure IV.9 (a) Perspective view of the asymmetric unit of **IV.2b** with the metal atom numbering scheme (hydrogen atoms have been omitted for clarity) [symmetry code: (I) = – *x* + 1, *y*, – *z* + 3/2; (II) = *x* – 1/2, *y* + 1/2, *z* – 1; (III) = – *x* + 3/2, *y* + 1/2, – *z* + 5/2; (IV) = – *x* + 1, – *y*, – *z* + 2; (V) = *x*, – *y*, *z* – 1/2]. (b) Projection view of a brick-wall rectangular layer of lithium-coordinated anionic dicopper units of **IV.2b** along the crystallographic *a* axis. (c) Crystal packing view of the lithium(I)-copper(II) layers of **IV.2b** along the crystallographic *b* axis. The adjacent heterobimetallic layers are shown in different colors.

Table IV.5 Least-squares fitting magnetic data.

Complex	$-J^a$ (cm^{-1})	g^b	$R^c \times 10^5$
IV.1a	75	2.05	3.0
IV.1b	95	2.05	1.1
IV.1c	94	2.06	0.7
IV.2a	112	2.05	1.0
IV.2b	100	2.04	0.4
IV.2c	124	2.08	0.4
IV.3a	128	2.04	1.5
IV.3b	130	2.06	0.5
IV.3c	144	2.10	2.7

[a] Magnetic coupling parameter. [b] Landé factor. [c] Agreement factor defined as $R = \sum[(\chi_M T)_{exp} - (\chi_M T)_{calcd}]^2/\sum[(\chi_M T)_{exp}]^2$.

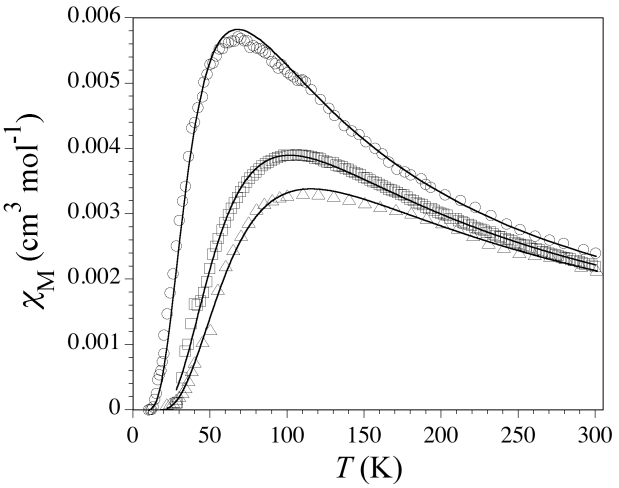

Figure IV.11 Temperature dependence of χ_M for **IV.1a** (○), **IV.2a** (□), and **IV.3a** (△). The solid lines are the best-fit curves (see Table IV.5).

shortest intermolecular Cu–Cu distances are 10.680(1) (**IV.1a**), 7.009(1) (**IV.2b**), and 10.650(2) Å (**IV.3c**).

IV.4 Magnetic Properties

The magnetic properties of the tetra-*n*-butylammonium, lithium(I), and tetraphenylphosphonium salts of **IV.1**–**IV.3** in the form of the χ_M *vs*. T plots (χ_M being the molar magnetic susceptibility per dinuclear unit and T the temperature) are typical of antiferromagnetically coupled Cu^{II}_2 pairs (Figures IV.11–IV.13). In fact, the presence of χ_M maxima in the ranges of 65–85 (**IV.1**), 90–110 (**IV.2**), and 115–130 K (**IV.3**) indicates a ground singlet ($S = 0$) spin state resulting from the antiferromagnetic coupling between the unpaired electron of each Cu^{II} ion ($S_{Cu} = ½$). The qualitatively similar magnetic behavior with variation in the countercation for **IV.1**–**IV.3** demonstrates the unambiguously intramolecular nature of the magnetic coupling in origin, the intermolecular interactions through the Li^I ions, if any, being negligible.

The magnetic susceptibility data of the tetra-*n*-butylammonium, lithium(I), and tetraphenylphosphonium salts of **IV.1**–**IV.3** were analyzed according to the spin Hamiltonian for a dinuclear model (eq IV.1 with $S_1 = S_2 = S_{Cu} = ½$), where J is the magnetic coupling parameter and g is the Landé factor of the Cu^{II} ions. The least-squares fits of the experimental data through the Bleaney-Bowers expression (eq IV.2 where N is the Avogadro number, β is the Bohr magneton, and k_B is the Boltzmann constant] gave $-J$ values in the ranges of 75–95 (**IV.1**), 100–124 (**IV.2**), and 128–144 cm^{-1} (**IV.3**) (Table IV.5).

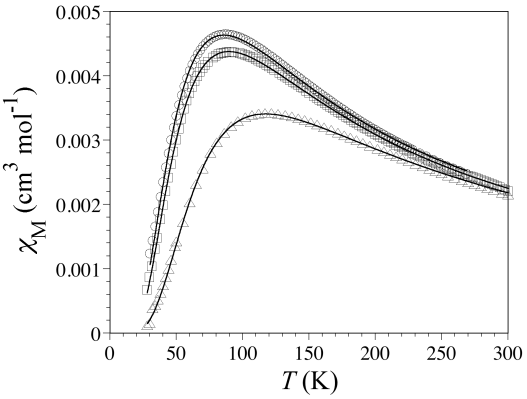

Figure IV.12 Temperature dependence of χ_M for **IV.1b** (○), **IV.2b** (□), and **IV.3b** (△). The solid lines are the best-fit curves (see Table IV.5).

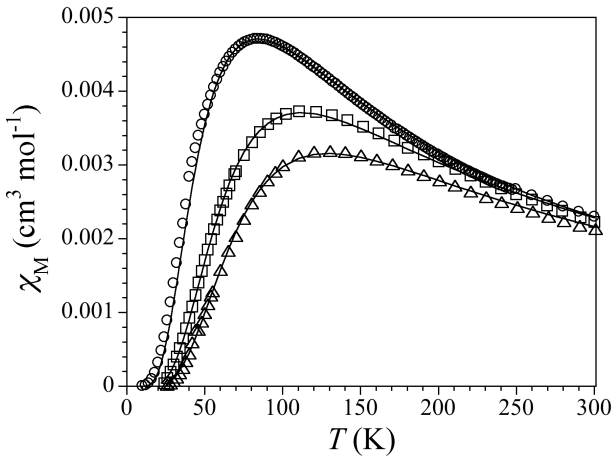

Figure IV.13 Temperature dependence of χ_M for **IV.1c** (○), **IV.2c** (□), and **IV.3c** (△). The solid lines are the best-fit curves (see Table IV.5).

$$\mathbf{H} = -J\mathbf{S_1}\cdot\mathbf{S_2} + g(\mathbf{S_1} + \mathbf{S_2})\beta H \qquad \text{(IV.1)}$$

$$\chi_M = (2N\beta^2 g^2/k_B T) / [3 + \exp(-J/k_B T)] \qquad \text{(IV.2)}$$

The moderately strong intramolecular antiferromagnetic coupling for **IV.1**–**IV.3** despite the relatively large intramolecular Cu–Cu separation ($r \approx 8.0$ Å) evidences that the EE interaction between the two Cu^{II} ions is mainly transmitted through the π-bond system of the polymethyl-substituted *p*-phenylenediamidate bridges.[10a] Moreover, the overall strengthening of the antiferromagnetic coupling with the number of methyl substituents along this series is remarkable and, more importantly, it agrees with the theoretical calculations (see discussion below).

IV.5 Redox Properties

The cyclic voltammograms (CVs) of the tetra-*n*-butylammonium and tetraphenylphosphonium salts of **IV.1**–**IV.3** in acetonitrile (25 °C, 0.1 M nBu$_4$NPF$_6$) show identical results independently of the nature of the countercation. They exhibit two well-separated one-electron oxidation waves at $E_1 = +0.33$ (**IV.1**), +0.24 (**IV.2**), and +0.15 V (**IV.3**) *vs*. SCE, and $E_2 = +0.79$ (**IV.1**), +0.80 (**IV.2**), and +0.86 V (**IV.3**) *vs*. SCE (Table IV.6), only the first one being reversible (Figure IV.14). Indeed, the values of the anodic peak to cathodic peak separation of the first redox wave for **IV.1**–**IV.3** are comparable to that of the ferricinium/ferrocene couple [$\Delta E(Fc^+/Fc) = 70$ mV]. A perfect linear plot of the peak current against the square root of the scan rate is obtained for the

Table IV.6 Selected electrochemical data.[a]

Complex	E_1[b] (V)	E_2[b] (V)	K_c[c]
IV.1	+0.33 (80)	+0.79 (i)	0.6×10^8
IV.2	+0.24 (80)	+0.80 (i)	0.3×10^{10}
IV.3	+0.15 (70)	+0.86 (i)	1.1×10^{12}

[a] In acetonitrile (25 °C, 0.1 M nBu$_4$NPF$_6$) with a scan rate of 100 mV s^{-1}. [b] All formal potential (E) values were taken as the half-wave potentials *vs*. SCE, except for the irreversible (i) waves for which the anodic peak potentials were given. The values of the peak-to-peak separation (ΔE / mV) between the anodic and cathodic peak potentials are given in parentheses. [c] The values of the comproportionation constant (K_c) were calculated from the difference in the formal potential values between the two one-electron oxidation waves ($\Delta E_{12} = E_2 - E_1$) through the expression $\log K_c = \Delta E_{12}/0.059$.

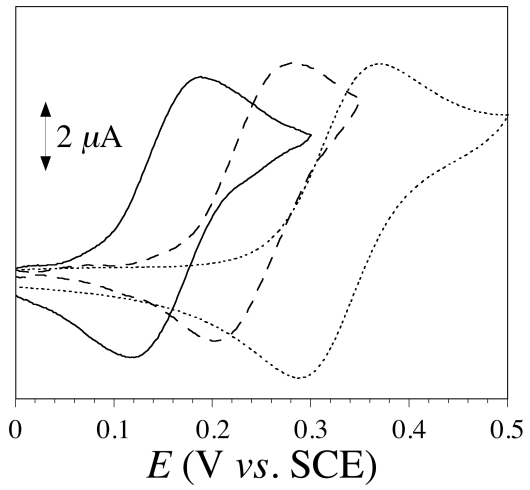

Figure IV.14 CVs of **IV.1** (dotted line), **IV.2** (dashed line), and **IV.3** (solid line) in acetonitrile at 25 ˚C (0.1 M nBu$_4$NPF$_6$) with a scan rate of 100 mV s^{-1}.

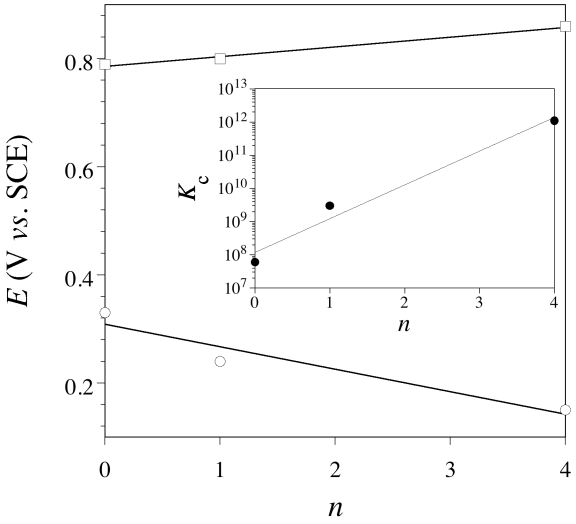

Figure IV.15 Plot of the E_1 (○) and E_2 (□) values with the number of methyl substituents (n) for **IV.1**– **IV.3**. The inset show the exponential dependence of the calculated K_c values (●) (data from Table IV.6). The solid lines correspond to the best-fit curves (see text).

first redox wave of **IV.3**, which is then stated to be completely reversible on the voltammetric time-scale.

Table IV.7 Selected kinetic data for the decomposition of **IV.3'**.[a]

T (˚C)	c_0[b] × 10^4 (M)	k[b] (M^{-1} s^{-1})	$t_{1/2}$[c] (h)
5	1.00(1)	0.295(3)	9.4
15	0.64(2)	0.598(6)	7.3
25	0.48(4)	1.86(2)	3.1

[a] In acetonitrile. [b] The initial concentration (c_0) and second-order rate constant (k) values were calculated from the reciprocal of the absorbance at λ_{max} = 875 nm ($1/A_{875}$) *vs* time (t) plots through the expression $(1/c) = (1/c_0) + kt$ with $c = A_{875}/(l \times \varepsilon_{875})$, where l is the path length (l = 1 cm) and ε_{875} is the molar extinction cofficient at λ_{max} = 875 nm (ε_{875} = 5660 M^{-1} cm^{-1}). [c] The half-life ($t_{1/2}$) is the time required for the concentration to fall from c_0 to $c_0/2$ [$t_{1/2} = (1/c_0)(1/k)$].

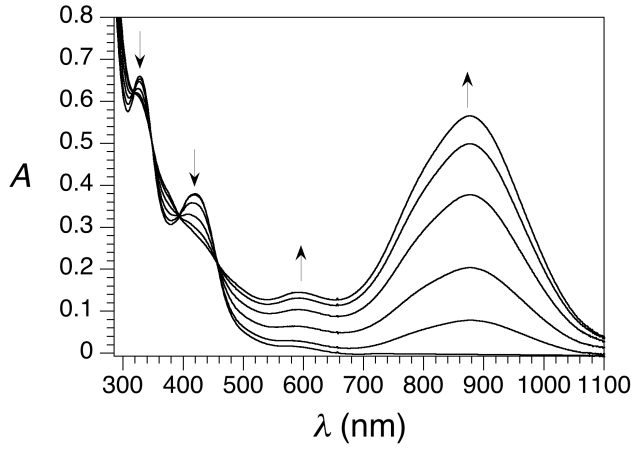

Figure IV.16 UV–Vis–NIR spectral changes for the chemical oxidation of **IV.3** with Br_2 in acetonitrile at 5 ˚C. The arrows indicate the course of the reaction.

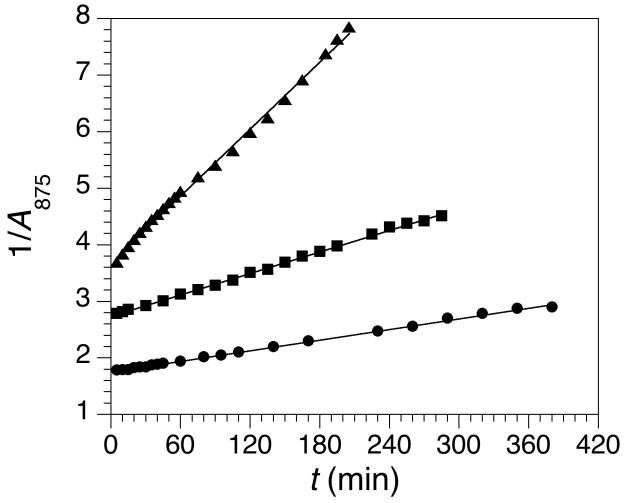

Figure IV.17 Time evolution of the reciprocal of the absorbance at λ_{max} = 875 nm ($1/A_{875}$) for the decomposition of **IV.3'** in acetonitrile at 5 (●), 15 (■), and 25 ˚C (▲). The solid lines correspond to the bes-fit curves (see Table IV.7).

These two redox processes for **IV.1**–**IV.3** would correspond to the stepwise ligand-centered oxidation of each of the two facing polymethyl-substituted *p*-phenylenediamidate bridges. Hence, the resulting dicopper(II) π-radical and diradical species are the metallacyclic analogues of forms **I** and **II** from the *N,N',N'',N'''*-tetramethyl-tetraza[7.7]paracyclophane, which shows similar values of the formal potentials to those of **IV.3** (E_1 = +0.08 and E_2 = +0.69

Table IV.8 Selected UV–Vis–NIR[a] and calculated EPR[b] spectral data.

Complex	λ_{max} [c] (nm)	ν [d] (cm^{-1})	g_x [e]	g_y [e]	g_z [e]
IV.3	325 (6450)	30770	2.005 (20)	2.085 (15)	2.239 (93)
	420 (3810)	23810			
	575 (180)	17390			
IV.3'	595 (1460)	16805	2.012 (30)	2.065 (20)	2.250 (108)
	875 (5660)	11430			

[a] In acetonitrile at 5 °C. [b] In acetonitrile at 77 (**IV.3**) and 4 K (**IV.3'**). [c] The values of the molar extinction cofficient (ε / M^{-1} cm^{-1}) are given in parentheses. [d] The wavenumber is defined as $\nu = 1/\lambda_{max}$. [e] The values of the Landé factors (g_i) and the hyperfine coupling constants (A_i) associated with the *x*, *y*, and *z* components of the allowed $M_s = 0 \rightarrow M_s = \pm 1$ transitions of the excited triplet ($S = 1$) spin state for **IV.3**, and the corresponding ones of the $M_s = -1/2 \rightarrow M_s = +1/2$ transition of the ground doublet ($S = 1/2$) spin state for **IV.3'** were calculated by using the *XSOPHE* program. The values of the calculated hyperfine coupling constants (A_i / G) are given in parentheses.

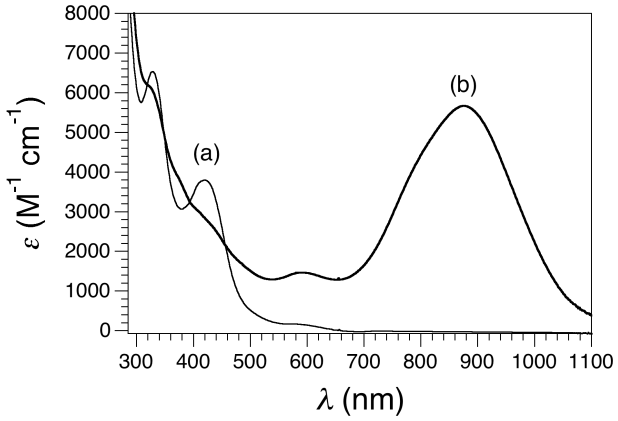

Figure IV.18 Electronic spectra of **IV.3** (a) and **IV.3'** (b) in acetonitrile at 5 °C.

V *vs*. SCE).[6a] The observed linear decrease of the E_1 values according to **IV.1** > **IV.2** > **IV.3** indicates that the oxidation of the polymethyl-substituted *p*-phenylenediamidate bridge is favored as the number of electron donating methyl substituents increases (Figure IV.15). On the contrary, the linear increase of the E_2 values along this series reflects the higher thermodynamic stability of the one-electron oxidized dicopper(II) π-radical species according to **IV.1'** < **IV.2'** < **IV.3'** (Figure IV.15). Hence, the estimated values of the comproportionation constant [$K_c = 0.6 \times 10^8$ (**IV.1'**), 0.3×10^{10} (**IV.2'**), and 1.1×10^{12} (**IV.3'**), Table IV.7] follow an almost perfect exponential increase with the number of methyl substituents (*n*) onto the *p*-phenylenediamidate bridges (inset of Figure IV.15).

IV.6 Spectroscopic Properties

Complex **IV.3'** was prepared by chemical oxidation of the tetraphenylphosphonium salt of **IV.3** with bromine in acetonitrile [$E(Br_2/Br^-) = +0.47$ V *vs*. SCE] (Figure IV.16) The *in situ* prepared, deep blue dicopper(II) π-radical species is fairly stable in acetonitrile solution at 5 °C but progressively decomposes when going up to room temperature (see Experimental Section). The decomposition reaction for **IV.3'** follows a second–order kinetics (more probably, a disproportionation reaction) with calculated half-life ($t_{1/2}$) values of 9.4, 7.3, and 3.1 h at 5, 15, and 25 °C, respectively (Table IV.7 and Figure IV.17).

The electronic absorption spectrum of **IV.3'** shows two intense bands in the vis–NIR region at λ_{max} = 595 and 875 nm (ε = 1460 and

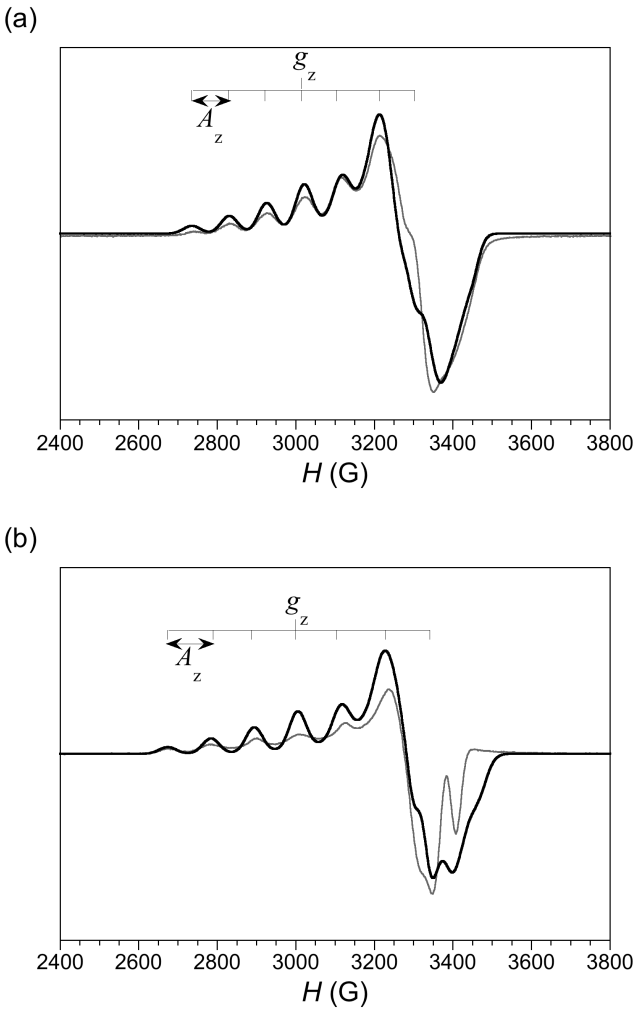

Figure IV.19 X-band EPR spectra of **IV.3** (a) and **IV.3'** (b) in acetonitrile at 77 and 4 K, respectively. The bold lines are the simulated spectra (see Table IV.8).

5660 M^{-1} cm^{-1}, respectively) with a shoulder at λ_{max} = 790 nm (Table IV.8 and Figure IV.18). In contrast, **IV.3** exhibits two intense UV–Vis bands at λ_{max} = 325 and 420 nm (ε = 6450 and 3810 M^{-1} cm^{-1}, respectively), together with a Vis band of lower intensity at λ_{max} = 575 nm (ε = 180 M^{-1} cm^{-1}) which corresponds to the typical d-d transitions of square planar Cu^{II} ion, as earlier found in related mononuclear oxamate copper(II) complexes (Table IV.8 and Figure IV.18).[11] Because of their greater intensity, the unique Vis–NIR spectral features of **3'** would mainly correspond to either metal-to-ligand (MLCT) or ligand-to-metal charge transfer (LMCT) transitions. Yet a partial contribution from inter-ligand charge transfer (ILCT) transitions cannot be discarded, by analogy with those found in fully delocalized, π-stacked radical cation species of Wurster blue cyclophanes (see Theoretical Calculations below).[6d]

The X-band EPR spectra of frozen acetonitrile solutions of **IV.3** and **IV.3'** at 77 (**IV.3**) and 4 K (**IV.3'**) show a rhombic signal with a complex multiline splitting pattern (Figure IV.19). These spectral features would be associated with either the excited triplet (S = 1) spin state of the moderately strong antiferromagnetically coupled dicopper(II) pair (**IV.3**) or the ground doublet (S = 1/2) spin state of the very strong antiferromagnetically coupled dicopper(II)-π-radical triad (**IV.3'**), as confirmed by the temperature dependence of the X-band EPR spectra of **IV.3** and **IV.3'** in frozen acetonitrile solutions (Figure IV.20). So, the double integral of the intensity of the EPR

(a)

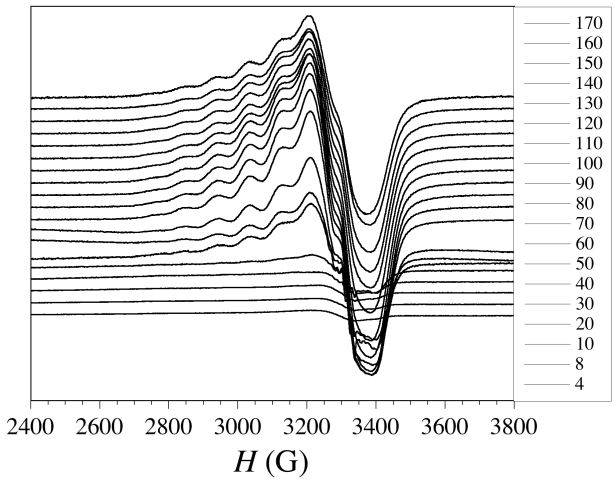

(b)

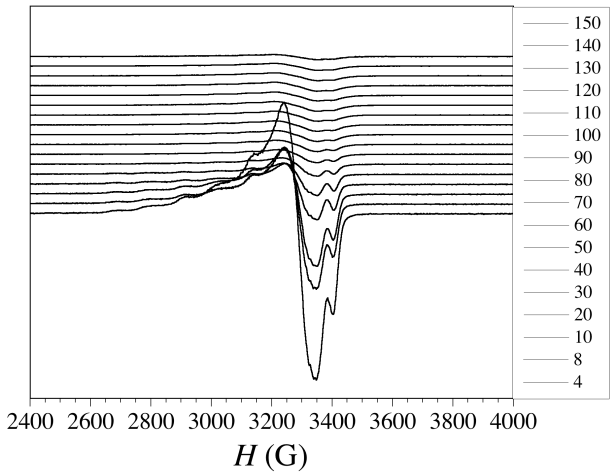

Figure IV.20 Temperature dependence of the X-band EPR spectra of **IV.3** (a) and **IV.3'** (b) in acetonitrile.

signal for **IV.3** exhibits a maximum at *ca.* 80 K, whereas it increases continuously as the temperature decreases for **IV.3'** (Figure IV.21), in agreement with the postulated magnetic switching behavior for the redox pair of permethylated derivatives **IV.3**/**IV.3'** (see Figure IV.2). The least-squares fit of the double integrated EPR signal intensity (DI) in arbitrary units of **IV.3** through the Bleaney-Bowers expression gave J = –91 cm^{-1} (solid line in Figure IV.21), as expected for a moderately strong antiferromagnetically coupled dicopper(II) species. This value is however somewhat smaller than that obtained from the fit of the magnetic susceptibility data of the structurally characterized tetraphenylphosphonium salt of **IV.3** (J = –144 cm^{-1}), reflecting thus the small variations of the molecular geometry in acetonitrile solution and in the solid state. On the other hand, the double integrated EPR signal intensity of **IV.3'** follows a Curie law behavior (solid line in Figure IV.21), as expected for a very strong antiferromagnetically coupled dicopper(II)-π-radical species (see theoretical calculations below).

The EPR spectra of **IV.3** and **IV.3'** were then simulated by using the *XSOPHE* program[12] that diagonalizes the full Hamiltonian matrix within the basis of the three S = 1 spin functions (M_s = 0, ±1) for **IV.3** or the two S = 1/2 spin functions (M_s = ±1/2) for **IV.3'** (bold lines in Figure IV.19). The calculated values of the Landé

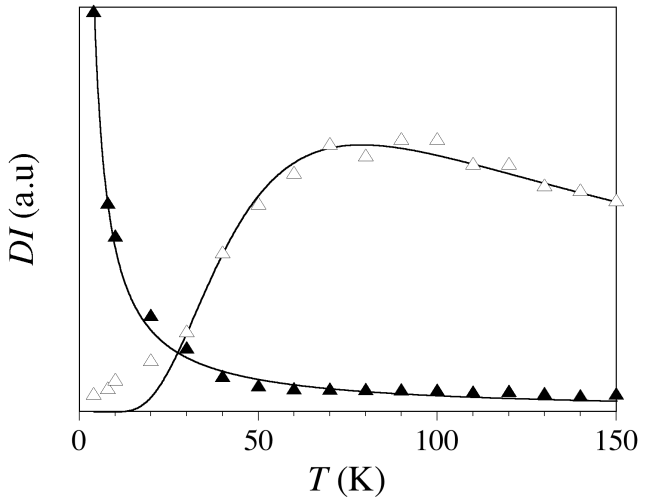

Figure IV.21 Temperature dependence of the double integrated EPR signal intensity for **IV.3** (△) and **IV.3'** (▲). The solid lines are the best-fit curves (see text).

factors are g_x = 2.005 (**IV.3**) and 2.012 (**IV.3'**), g_y = 2.085 (**IV.3**) and 2.065 (**IV.3'**), and g_z = 2.239 (**IV.3**) and 2.250 (**IV.3'**), while those of the hyperfine coupling constants are A_x = 20 (**IV.3**) and 30 G (**IV.3'**), A_y = 15 (**IV.3**) and 20 G (**IV.3'**), and A_z = 93 (**IV.3**) and 108 G (**IV.3'**) (Table IV.8). The most remarkable feature of the X-band EPR spectra of **IV.3** and **IV.3'** is the well-resolved seven-line splitting of the g_z signal due to the hyperfine coupling with the nuclear spin of the two Cu^{II} ions ($2nI_{Cu}$ + 1 = 7 with n = 2 and I_{Cu} = 3/2) (Figure IV.19). This situation clearly contrasts with that expected for a metal-centered oxidation that would give a simple four-line splitting typical of a localized dicopper(II,III) species for **IV.3'** ($2nI_{Cu}$ + 1 = 4 with n = 1 and I_{Cu} = 3/2). Although an alternative delocalized dicopper(II,III) description cannot be definitely discarded for **IV.3'**, this situation better agrees with that expected for an antiferromagnetically coupled dicopper(II)-π-radical species resulting from a ligand-centered oxidation. In fact, the calculated A_z value of **IV.3'** is almost four thirds that of **IV.3** [A_z = 93 (**IV.3**) and 108 G (**IV.3'**)], as expected from the different S = 1 Cu$^{II}_2$ (**IV.3**) and S = 1/2 Cu$^{II}_2$-π-radical (**IV.3'**) formulations [$A(S$ = 1/2) = 4/3$A(S$ = 1) with $A(S$ = 1) = 1/2A_{Cu}]. In contrast, the calculated A_z value of a delocalized S = 1/2 Cu$^{II,III}_2$ mixed-valent formulation for **IV.3'** [$A(S$ = 1/2) = 1/2A_{Cu}] would be identical to that of a S = 1 Cu$^{II}_2$ one for **IV.3** [$A(S$ = 1) = 1/2A_{Cu}], both of them being half the value found for a localized S = 1/2 Cu$^{II,III}_2$ mixed-valent formulation [$A(S$ = 1/2) = A_{Cu}].

IV.7 Theoretical Calculations

Energy and molecular orbital calculations. DF energy calculations on the model complexes **IV.1**–**IV.3** with an imposed planar conformation of the copper basal planes (τ = 0°) and a perpendicular orientation of the copper basal planes with respect to the benzene rings (ϕ = 90°) are summarized in Table IV.9 (see Computational Details). All four possible configurations of the methyl substituents from the two facing benzene rings were considered for **IV.2** (Figure IV.22). For all these orthogonal model complexes with polymethyl-substituted benzene spacers, –$C_6H_{(4-n)}Me_n$– [n = 0 (**IV.1**), 1 (**IV.2**), and 4 (**IV.3**)], the energy calculations show a ground broken-symmetry (BS) singlet (S = 0) spin state lying well below the excited triplet (S = 1) spin state. The calculated value of the singlet-triplet energy gap ($\Delta E_{ST} = -J$) for **IV.1** and **IV.3** increases with the number of methyl substituents from 130 (**IV.1**) to

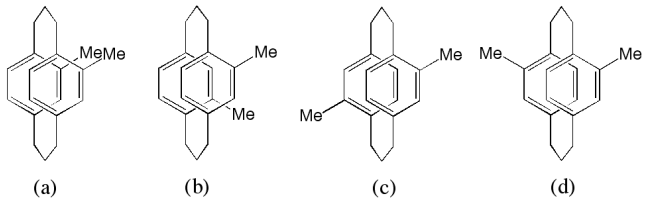

Figure IV.22 Illustration of the metallacyclic core for the pseudo-*gem* (a), -*ortho* (b), -*para* (c), and -*meta* (d) isomers of **IV.2**.

Table IV.9 Selected calculated energy data for the orthogonal model complexes **IV.1**– **IV.3**.

	Molecular symmetry	ΔE_{ST} [a] (cm^{-1})	δ [b] (cm^{-1})
IV.1	D_{2h}	130 (106)	2992 (2702)
IV.2 (pseudo-*gem*)	C_s	131	3057
IV.2 (pseudo-*ortho*)	C_2	128	3008
IV.2 (pseudo-*para*)	C_i	128	3017
IV.2 (pseudo-*meta*)	C_2	129 (115)	3025 (2831)
IV.3	D_{2h}	139 (124)	3250 2976)

[a] The calculated singlet-triplet energy gap ($\Delta E_{ST} = -J$) of the optimized molecular geometries in acetonitrile solution are given in parentheses. [b] The calculated energy gap between the two singly occupied molecular orbitals (SOMOs) for the triplet spin state of the optimized molecular geometries in acetonitrile solution are given in parentheses.

139 cm^{-1} (**IV.3**), while they vary in the narrow range of 128–131 cm^{-1} for the pseudo-*gem*, -*ortho*, -*para*, and -*meta* isomers of **IV.2**, being closer to that of **IV.1** than to that of **IV.3**. However, the calculated $-J$ values for the orthogonal model complexes (ϕ = 90° and τ = 0°) significantly differ from the experimental ones, as illustrated in Figure IV.23. The larger deviations among the calculated and experimental values in **IV.1** when compared to those in **IV.3** are likely due to the greater loss of orthogonality between the copper and the benzene planes and/or the larger tetrahedral distortion of the copper center when decreasing the number of methyl substituents, as evidenced by the crystal structures of **IV.1a** and **IV.3c**.

DF energy calculations on the optimized molecular geometries of **IV.1**, **IV.2** (pseudo-*meta* isomer), and **IV.3** in acetonitrile solution show a much better agreement with the experimental data (see Computational Details). Hence, the calculated $-J$ values [$-J$ = 106 (**IV.1**), 115 (**IV.2**), and 124 cm^{-1} (**IV.3**), Table IV.9] are close to the experimental ones obtained from the fit of the magnetic susceptibility data in the solid state [$-J$ = 75–95 (**IV.1a**–**IV.1c**), 100–124 (**IV.2a**–**IV.2c**), and 128–144 cm^{-1} (**IV.3a**– **IV.3c**), Table IV.5]. This situation reflects the structural similarities among the optimized molecular geometries [τ = 8.5 (**IV.1**), 6.3 (**IV.2**), and 1.9° (**IV.3**); ϕ = 63.9 (**IV.1**), 73.0 (**IV.2**), and 75.2° (**IV.3**)] and the experimental ones [τ = 16.1(1) (**IV.1a**), 5.4(2) (**IV.2b**), and 5.0(1)° (**IV.3c**); ϕ = 58.72(7) (**IV.1a**), 71.7(3) (**IV.2b**), and 73.67(5)° (**IV.3c**)]. As a matter of fact, the optimization geometry calculations evidence a significantly lesser tetrahedral distortion of the metal environment and a smaller deviation from the ideal D_{2h} symmetry corresponding to the orthogonal conformation when going from the unsubstituted ancestor (**IV.1**) to the methyl-substituted (**IV.2**) and then to the tetramethyl-substituted derivatives (**IV.3**), as observed experimentally. More importantly, the calculated $-J$ values for the optimized molecular geometries of **IV.1**, **IV.2** (pseudo-*meta* isomer), and **IV.3** in acetonitrile solution increase continuously with

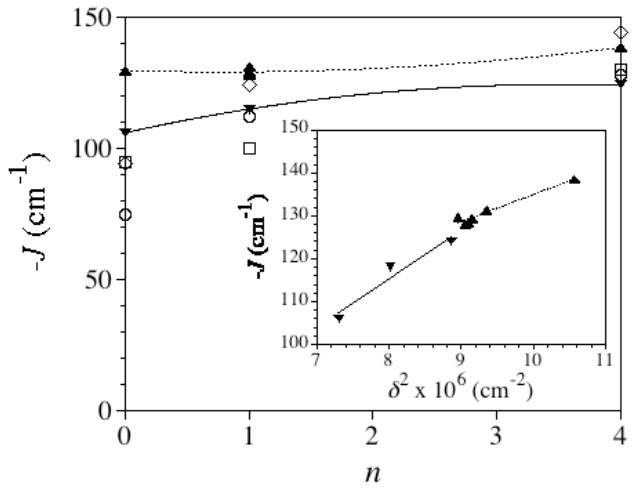

Figure IV.23 Plot of the calculated values of the magnetic coupling parameter ($-J$) with the number of methyl substituents (n) for the orthogonal model complexes (▲) and the optimized molecular geometries in acetonitrile solution of **IV.1**–**IV.3** (▼) (data from Table IV.9). The dotted and solid lines correspond to the second polynomial fit curves. The experimental $-J$ values for the tetra-*n*-butylammonium (○), lithium(I) (□), and tetraphenylphosphonium salts (◇) of **IV.1**–**IV.3** are also shown for comparison (data from Table IV.5). The inset shows the linear dependence of the calculated $-J$ values for the orthogonal model complexes (▲) and the optimized molecular geometries in acetonitrile solution of **IV.1**–**IV.3** (▼) with the square of the energy gap (δ) between the two SOMOs (data from Table IV.9). The dotted and solid lines correspond to the linear fit curves (see text).

the increasing number of methyl substituents (n) from 0 (**IV.1**) to 1 (**IV.2**) and 4 (**IV.3**) in agreement with the observed experimental trend. This indicates that the magnetic coupling along this series is governed by both electronic and structural factors associated with the electron donor properties and steric requirements of the methyl group (Figure IV.23).

DF molecular orbital (MO) calculations on the optimized molecular geometries of **IV.1**, **IV.2** (pseudo-*meta* isomer), and **IV.3** in acetonitrile solution reveal a parallel increase in the calculated energy separation between the two singly occupied molecular orbitals (SOMOs) [δ = 2702 (**IV.1**), 2831 (**IV.2**), and 2976 cm^{-1} (**IV.3**), Table IV.9]. In fact, the calculated $-J$ values vary almost linearly with the square of δ for both orthogonal and nonorthogonal models of **IV.1**– **IV.3**, in agreement with the simplest orbital models of the EE interaction (inset of Figure IV.23).[13] This is explained by the electron donor character of the methyl group which increases the energy of the two π ligand orbitals involved in the EE mechanism, favoring thus the metal-ligand orbital mixing because of their smaller energy separation relative to the 3d metal orbitals [ΔE_{M-L} and (ΔE_{M-L} + ΔE_L)] (Figure IV.24). This fact ultimately leads to an increased delocalization of the unpaired electrons of the Cu^{II} ions onto the π-conjugated electron system of the *p*-phenylene spacers with the increasing number of methyl substituents (n) for **IV.1**– **IV.3**. This situation is clearly reflected on the two calculated SOMOs for the triplet spin state of **IV.3**, which show a high metal-ligand covalency and strongly ligand delocalized character (Figure IV.25). These two SOMOs, noted b_g* and b_u*, are composed by the symmetric and antisymmetric combinations respectively, of the $d(x^2-y^2)$ orbitals of the square-planar Cu^{II} ions mixed with the corresponding combinations of appropriate symmetry of the two π-type orbitals of the tetramethyl-*p*-phenylenediamidate bridges, which are in turn made up of p(z) orbitals of the carbon and nitrogen atoms (Figure IV.24).

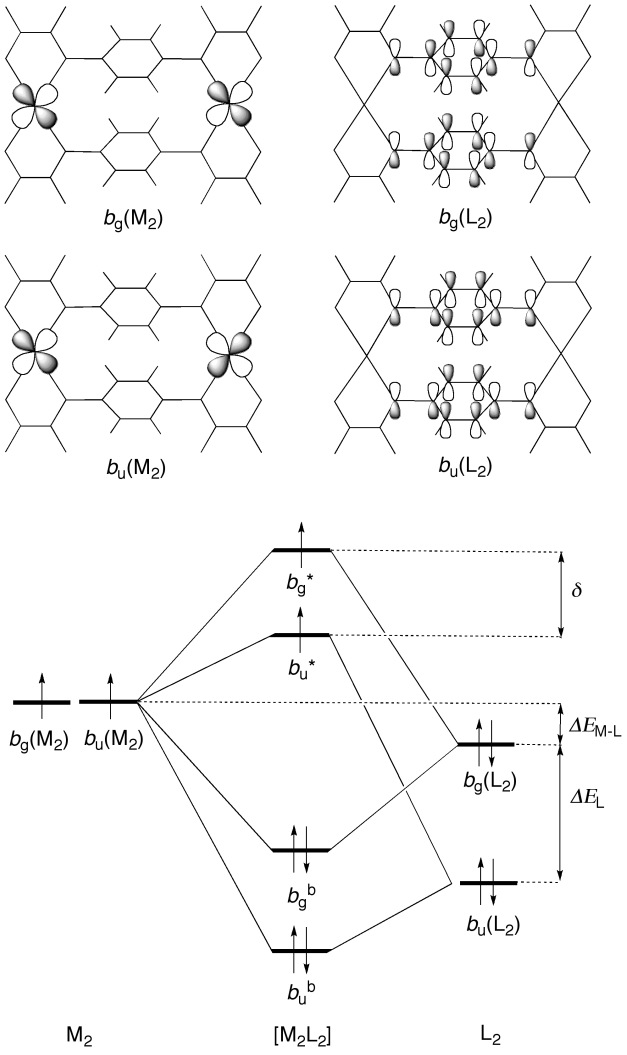

Figure IV.24 Simplified energy level diagram of the EE interaction in dicopper(II) paracyclophanes with polymethyl-substituted *p*-phenylenebis(oxamate) bridging ligands. The dinuclear metallacyclophane skeleton is shown for the sake of clarity.

DF energy calculations on the optimized molecular geometries of **IV.3** and **IV.3'** in acetonitrile solution show ground BS singlet (S = 0) and doublet (S = 1/2) spin states, respectively (see Computational Details). Several electronic configurations were checked for **IV.3'**, even by modifying the starting geometrical parameters to stabilize them, but in all cases the geometry optimization leads to a unique geometry which corresponds to a S = 1/2 Cu^{II}_2-π-radical configuration resulting from the one-electron oxidation of the double tetramethyl-*p*-phenylenediamidate bridge skeleton. This ground doublet (S = 1/2) spin state of **IV.3'**, labeled $|\uparrow\downarrow\uparrow>$, would result from the antiferromagnetic coupling between the central π-radical (S_R = 1/2) cation and the two peripheral Cu^{II} (S_{Cu} = 1/2) ions within the Cu^{II}_2-π-radical triad. In addition, there are two excited doublet (S = 1/2) and quartet (S = 3/2) spin states, labeled ($|\uparrow\uparrow\downarrow>$) and ($|\uparrow\uparrow\uparrow>$), which are located at 1897 and 5550 cm^{-1} respectively, well above the ground doublet (S = 1/2) spin state. The metal-radical magnetic coupling parameter can then be calculated from the energy gap between the two low-lying doublet spin configurations [$\Delta E = E(|\uparrow\uparrow\downarrow>) - E(|\uparrow\downarrow\uparrow>) = -J'$]. The calculated $-J'$ value of 1897 cm^{-1} for **IV.3'** is very large, ensuring thus that only the ground doublet (S = 1/2) spin state is thermally populated with essentially no population of the excited doublet (S = 1/2) and quartet (S = 3/2) spin states, as deduced from the EPR spectroscopic data of **IV.3'** in acetonitrile solution. This situation is that expected for a direct antiferromagnetic exchange interaction between the unpaired electrons occupying the $d(x^2-y^2)$ orbitals of the square-planar Cu^{II} ions and that occupying the π-type orbital of the tetramethyl-*p*-phenylene radical cation. By comparison, the ground BS singlet (S = 0) spin state of **IV.3** resulting from the antiferromagnetic coupling between the two Cu^{II} (S_{Cu} = 1/2) ions within the Cu^{II}_2 pair lies at only 124 cm^{-1} below the excited triplet (S = 1) spin state. The magnetic coupling parameter can be calculated from the singlet-triplet energy gap between these two spin configurations, labeled $|\uparrow\downarrow>$ and $|\uparrow\uparrow>$, respectively [$\Delta E = E(|\uparrow\uparrow>) - E(|\uparrow\downarrow>) = -J$]. The calculated $-J$ value of 124 cm^{-1} for **IV.3** is close to the experimental one obtained from the fit of the EPR spectroscopic data in acetonitrile solution (J = –91 cm^{-1}). This situation corresponds to an indirect (through-bond) antiferromagnetic exchange interaction between the unpaired electrons occupying the $d(x^2-y^2)$ orbitals of the square-planar Cu^{II} ions through the diamagnetic tetramethyl-*p*-phenylene spacers.

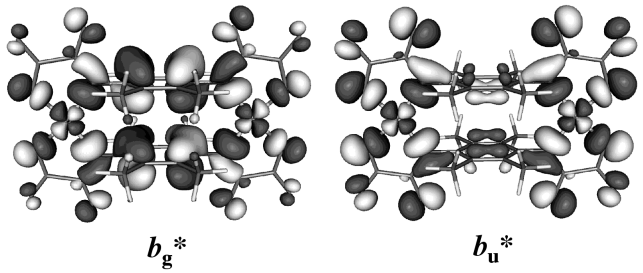

Figure IV.25 Perspective views of the calculated SOMOs for the triplet spin state of **IV.3**. The isoelectronic surface corresponds to a cutoff value of 0.003 e $bohr^{-3}$.

Table IV.10 Selected structural data for the optimized geometries in acetonitrile solution of the ground BS singlet and doublet spin states of **IV.3** and **IV.3'**, respectively.

	IV.3[a]	**IV.3'**
C–N (Å)	1.436 (1.427)	1.411
	1.436 (1.431)	1.411
C–C(Me) (intra-ring) (Å)	1.417 (1.398)	1.426
	1.417 (1.401)	1.426
	1.424 (1.401)	1.434
	1.424 (1.402)	1.434
C(Me)–C(Me) (intra-ring) (Å)	1.415 (1.394)	1.405
	1.417 (1.401)	1.407
C···C (inter-ring) (Å)	3.456 (3.290)	3.245
	3.456 (3.290)	3.245
C(Me)···C(Me) (inter-ring) (Å)	3.540 (3.359)	3.338
	3.540 (3.359)	3.338
	3.544 (3.399)	3.338
	3.544 (3.399)	3.338
ϕ^b (°)	75.23 (73.67)	80.91

[a] The experimental structural data of **IV.3c** are given in parentheses. [b] Dihedral angle between the copper basal planes and the benzene planes.

Molecular geometry optimizations. The optimized molecular geometries for the ground BS singlet (**IV.3**) and doublet (**IV.3'**) spin states in acetonitrile solution are consistent with the generation of a fully delocalized (mixed-valent), π-stacked monoradical ligand upon one-electron oxidation of the double tetramethyl-*p*-phenylenediamidate bridging skeleton (Table IV.10). The validity of this approach is confirmed by the structural similarities, in terms of both bond lengths and interbond angles, between the optimized structure in acetonitrile solution of **IV.3** and that of its tetraphenylphosphonium salt (**IV.3c**), which was experimentally

Table IV.11 Selected calculated atomic spin density data for the optimized geometries in acetonitrile solution of the ground BS singlet and doublet spin states of **IV.3** and **IV.3'**, respectively.[a,b]

	IV.3	IV.3'
Cu(1)	±0.5553	+0.4915
N(1)	–0.1027	+0.0390
N(2)	+0.1021	+0.0389
O(1)	–0.0947	+0.0815
O(2)	–0.0078	+0.0086
O(3)	–0.0068	–0.0017
O(4)	+0.0946	+0.0813
O(5)	+0.0077	+0.0086
O(6)	+0.0067	–0.0018
C(1)	+0.0401	–0.1121
C(2)	–0.0346	+0.0039
C(3)	+0.0345	+0.0037
C(4)	–0.0401	–0.1121
C(5)	+0.0344	–0.0027
C(6)	–0.0343	–0.0030
C(7)	+0.0026	–0.0045
C(8)	+0.0067	–0.0055
C(9)	–0.0025	–0.0045
C(10)	–0.0068	–0.0055
C(20)	+0.0026	+0.0006
C(30)	–0.0025	+0.0006
C(50)	–0.0025	+0.0017
C(60)	+0.0025	+0.0017

[a] The calculated values of the atomic spin density (ρ_X) are given in e units. [b] The atom-numbering scheme is given in Figure IV.7a.

determined in the solid state by single-crystal X-ray diffraction (Table IV.10).

A small but non-negligible bond alternation is observed within the two equivalent benzene rings of **IV.3'**, with average short and long intra-ring C(Me)–C(Me) and C–C(Me) distances of 1.406 and 1.430 Å respectively, whereas **IV.3** shows no appreciable bond alternation, with a mean value of the intra-ring C(Me)–C(Me) and C–C(Me) distances of 1.416 and 1.420 Å, respectively. Moreover, the amidate substituents of the benzene rings in **IV.3'** have a common value of the C–N distance of 1.411 Å which is significantly shorter than that of 1.436 Å in **IV.3**, indicating thus the development of a partial double bond character typical of imines. Overall, these small but non-negligible bond length changes evidence a iminoquinonoid character for both tetramethyl-*p*-phenylenediamidate bridges of **IV.3'**, in rather good agreement with the recently reported X-ray crystal structure of the fully delocalized, π-stacked radical iminium cation (form **I**) of the 2,2-dimethylpropylene-bridged *N,N',N'',N'''*-tetramethyl-tetraza[5.5]paracyclophane [CH–CH = 1.364(4)–1.376(4) Å, C–CH = 1.399(4)–1.420(4) Å, and C–N = 1.374(4)–1.386(4) Å].[9d]

The most salient structural feature for **IV.3'** is, however, the inter-ring C···C and C(Me)···C(Me) distances of 3.245 and 3.338 Å respectively, values which are significantly shorter than the Van der Waals contact (3.40 Å). By comparison, the average inter-ring C···C and C(Me)···C(Me) distances for **IV.3** are 3.456 and 3.542 Å, respectively. The approach of the benzene rings is accompanied by slightly smaller deviations from the eclipsed π-stacked, orthogonal molecular conformation on going from **IV.3** (ϕ = 75.23°) to **IV.3'** (ϕ = 80.91°). These inter-ring close contacts reveal the occurrence of an incipient π-π long-bond formation between the two facing tetramethyl-*p*-phenylene spacers within the metallacyclophane core of **IV.3'**, as expected from the ligand delocalized nature of this monooxidized metallacyclic radical species. This situation has also been found in the fully delocalized, π-stacked radical iminium cation (form **I**) of the 2,2-dimethylpropylene-bridged *N,N',N'',N'''*-tetramethyl-tetraza[5.5]paracyclophane, which have similar inter-ring π-stacking bonding interactions [C···C = 3.188(4)–3.448(4) Å and CH···CH = 3.216(4)–3.492(4) Å].[9d]

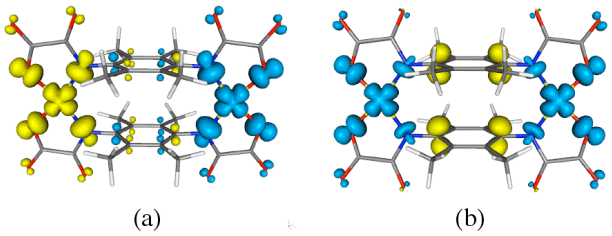

Figure IV.26 Perspective views of the calculated spin density distribution for the ground BS singlet and doublet spin configurations of **IV.3** (a) and **IV.3'** (b), respectively. Blue and yellow contours represent positive and negative spin densities, respectively. The isodensity surface corresponds to a cutoff value of 0.003 e bohr^{-3}.

Spin density analysis. Spin densities obtained by NBO analysis on the ground BS singlet (**IV.3**) and doublet (**IV.3'**) spin states in acetonitrile solution agree with a switch from antiparallel to parallel alignment of the local spin moments of the Cu^{II} ions by the presence of the delocalized π-radical cation generated upon one-electron oxidation of the double tetramethyl-*p*-phenylenediamidate bridge skeleton (Table IV.11 and Figure IV.26). So, the spin density distribution for the ground BS singlet spin state of **IV.3** shows spin densities of opposite sign at the metal atoms (ρ_M = ±0.5553 e), together with small but non-negligible spin densities of alternating sign at the adjacent carbon atoms of the benzene rings resulting from spin polarization effects by the amidate nitrogen atoms (Figure IV.26a). On the contrary, the spin density distribution for the ground doublet spin state of **IV.3'** reflects spin densities of the same sign at the metal atoms (ρ_M = +0.4915 e), alongside a large amount of spin density of opposite sign mainly delocalized along each of the four benzene carbon atoms directly attached to the amidate nitrogen ones (ρ_C = –0.1122 e) (Figure IV.26b). This picture nicely corresponds to that expected for a metallacyclic analogue of the purely organic Wurster blue cyclophanes, which would be described by the four equivalent resonance forms **I** of a fully delocalized, π-stacked radical iminium cation species.

IV.8 Concluding Remarks

In this paper, we present a combined experimental and theoretical study on a novel family of electroactive, antiferromagnetically coupled dicopper(II) paracyclophanes with polymethyl-substituted benzene spacers, $-C_6H_{(4-n)}Me_n-$ [*n* = 0, 1, and 4]. The overall strengthening of the antiferromagnetic coupling along this series is due to an increased delocalization of the unpaired electrons of the Cu^{II} ions onto the π-conjugated electron system of the *p*-phenylene spacers with the increasing number of electron donating methyl substituents. This phenomenon is ultimately responsible for the higher stability of the one-electron oxidized dicopper(II) π-radical species resulting from the oxidation of the polymethyl-substituted *p*-phenylenediamidate bridge as the number of electron donating methyl substituents increases. Interestingly, the permethylated dicopper(II) paracyclophane exhibits a unique magnetic electroswitching (ON/OFF) behavior, as shown both experimentally and theoretically. The magnetic bistability obeys to the change from antiparallel (OFF) to parallel (ON) spin alignment of the metal centers by the π-stacked delocalized monoradical ligand generated upon one-electron oxidation of the double tetramethyl-*p*-

phenylenediamidate bridge skeleton. Permethylation in this metallacyclic system constitutes thus a unique example of ligand design for the supramolecular control of magnetic properties and electrochemical reactivity.

IV.9 Experimental Section

Materials. All chemicals were of reagent grade quality. They were purchased from commercial sources and used as received, except those for electrochemical measurements. The nBu$_4$NPF$_6$ salt was recrystallized twice from ethyl acetate/diethyl ether, dried at 80 °C under vacuum, and kept in an oven at 110 °C. Acetonitrile was purified by distillation from calcium hydride on activated 3 Å molecular sieves and stored under argon.

Physical techniques. Elemental analyses (C, H, N) were performed at the Servicio Central de Soporte a la Investigación (SCSIE) at the Universitat de València (Spain). ^{1}H NMR spectra were recorded at room temperature on a Bruker AC 200 (200.1 MHz) spectrometer. Chemical shifts are reported in δ (ppm) *vs*. SiMe$_4$. C$_2$D$_6$SO was used as solvent and internal standard (δ = 2.50 ppm). FTIR spectra were recorded on a Nicolet-5700 spectrophotometer as KBr pellets.

Preparation of the ligands. Et$_2$H$_2$ppba: Ethyl oxalyl chloride ester (14.0 mL, 120 mmol) was poured into a solution of 2,3,5,6-tetramethyl-*p*-phenylenediamine (6.5 g, 60 mmol) in THF (250 mL) under vigorous stirring at 0 °C on an ice-bath. The reaction mixture was then refluxed for 1 h. After cooling, the solid was collected by filtration, washed with diethyl eter, and dried under vacuum (15.7 g, 85% yield). Anal. Calcd for $C_{14}H_{16}N_2O_6$ (308): C, 54.55; H, 5.19; N, 9.09%. Found: C, 54.42; H, 5.21; N, 9.21%. ^{1}H NMR (C$_2$D$_6$SO): 1.28 (t, 6 H, 2 CH$_3$), 4.29 (q, 4 H, 2 CH$_2$O), 7.71 (s, 4H, C$_6$H$_4$), 10.79 (s, 2 H, 2 NH). IR (KBr): 3250 (N–H), 1733, 1685 cm^{-1} (C=O).

Et$_2$H$_2$Meppba: Ethyl oxalyl chloride ester (14.0 mL, 120 mmol) was poured into a solution of 2-methyl-*p*-phenylenediamine dihydrogen sulfate (13.2 g, 60 mmol) and triethylamine (16.8 mL, 120 mmol) in THF (250 mL) under vigorous stirring at 0 °C on an ice-bath. The reaction mixture was then refluxed for 1 h. After cooling, the solid was collected by filtration, washed thoroughly with water to remove the precipitate of (Et$_3$NH)$_2$SO$_4$ and then with diethyl eter, and dried under vacuum (15.5 g, 80% yield). Anal. Calcd for $C_{15}H_{18}N_2O_6$ (322): C, 55.90; H, 5.59; N, 8.70%. Found: C, 55.87; H, 5.29; N, 8.91%. ^{1}H NMR (C$_2$D$_6$SO): 1.28 (t, 6 H, 2 CH$_3$), 2.16 (s, 3H, CH$_3$ of C$_6$H$_3$CH$_3$), 4.28 (q, 4 H, 2 CH$_2$O), 7.30 (d, 1 H, 5–H of C$_6$H$_3$CH$_3$), 7.53 (d, 1 H, 4–H of C$_6$H$_3$CH$_3$), 7.62 (s, 1 H, 3–H of C$_6$H$_3$CH$_3$), 10.26 (s, 1 H, 1 NH), 10.74 (s, 1 H, 1 NH). IR (KBr): 3237 (N–H), 1752, 1734, 1693 cm^{-1} (C=O).

Et$_2$H$_2$Me$_4$ppba: Ethyl oxalyl chloride ester (14.0 mL, 120 mmol) was poured into a solution of 2,3,5,6-tetramethyl-*p*-phenylenediamine (9.9 g, 60 mmol) in THF (250 mL) under vigorous stirring at 0 °C on an ice-bath. The reaction mixture was then refluxed for 1 h. After cooling, the solid was collected by filtration, washed with diethyl eter, and dried under vacuum (19.7 g, 90% yield). Anal. Calcd for $C_{18}H_{24}N_2O_6$ (364): C, 59.33; H, 6.64; N, 7.68%. Found: C, 58.98; H, 6.67; N, 7.74%. ^{1}H NMR (C$_2$D$_6$SO): 1.29 (t, 6 H, 2 CH$_3$), 2.02 (s, 12H, 4 CH$_3$ of C$_6$(CH$_3$)$_4$), 4.30 (q, 4 H, 2 CH$_2$O), 10.39 (s, 2 H, 2 NH). IR (KBr): 3246 (N–H), 1728, 1677 cm^{-1} (C=O).

Preparation of the complexes. (nBu$_4$N)$_4$[Cu$_2$(ppba)$_2$] · 2CH$_3$OH (IV.1a): A 1.0 M methanol solution of nBu$_4$NOH (20 mL, 20.0 mmol) was added all at once to a suspension of H$_2$Et$_2$ppba (1.6 g, 5.0 mmol) in methanol (50 mL). A methanol solution (10 mL) of Cu(ClO$_4$)$_2$ · 6H$_2$O (1.85 g, 5.0 mmol) was then added dropwise under stirring at room temperature to the reaction mixture. The deep green solution was filtered to eliminate the small amount of solid particles and the solvent was removed under vacuum. The green solid was recuperated with acetone, collected by filtration, washed thoroughly with tetrahydrofuran to remove the precipitate of nBu$_4$NClO$_4$, and air dried. Recrystallization from a methanol solution gave green prisms of **IV.1a** suitable for single-crystal X-ray diffraction upon layering of diethyl ether (3.3 g, 80% yield). Anal. Calcd for $C_{86}H_{160}Cu_2N_8O_{14}$ (1657): C, 62.32; H, 9.73; N, 6.76%. Found: C, 61.98; H, 9.51; N, 6.74%. IR (KBr): 1654, 1612 cm^{-1} (C=O).

Li$_4$[Cu$_2$(ppba)$_2$] · 10H$_2$O (IV.1b): An aqueous solution (10 mL) of Cu(NO$_3$)$_2$ · 3H$_2$O (1.2 g, 5.0 mmol) was added dropwise to an aqueous solution (50 mL) of Et$_2$H$_2$ppba (1.5 g, 5.0 mmol) and LiOH · H$_2$O (0.8 g, 20.0 mmol) under stirring at room temperature. The resulting deep green solution was then filtered, and the solvent was reduced under vacuum until a solid appeared. The light green solid of **IV.1b** was collected by filtration, washed with acetone and diethyl ether, and air dried (1.6 g, 75% yield). Anal. Calcd for $C_{20}H_{28}Cu_2Li_4N_4O_{22}$ (831): C, 28.88; H, 3.37; N, 6.74%. Found: C, 28.75; H, 3.28; N, 6.67%. IR (KBr): 1624, 1616 cm^{-1} (C=O).

(Ph$_4$P)$_4$[Cu$_2$(ppba)$_2$] · 8H$_2$O (IV.1c): An aqueous solution (10 mL) of AgNO$_3$ (1.4 g, 8.0 mmol) was added to an aqueous solution (20 mL) of **IV.1b** (1.7 g, 2.0 mmol) under stirring at room temperature. The dark green solid that appeared was collected by filtration, suspended in water (10 mL), and then charged with an acetonitrile solution (5 mL) of Ph$_4$PCl (3.0 g, 8.0 mmol). The reaction mixture was further stirred for 30 min under gentle warming and then filtered to remove the precipitate of AgCl. Slow evaporation of the filtered deep green solution gave dark green crystals of **IV.1c** not suitable for single-crystal X-ray diffraction after several days in the open air at room temperature (4.2 g, 95% yield). Anal. Calcd for $C_{116}H_{104}Cu_2N_4O_{20}P_4$ (2123): C, 65.56; H, 4.89; N, 2.63%. Found: C, 65.65; H, 4.82, N 2.47%. IR (KBr): 1644, 1603 cm^{-1} (C=O).

(nBu$_4$N)$_4$[Cu$_2$(Meppba)$_2$] · 3H$_2$O (IV.2a): A 1.0 M methanol solution of nBu$_4$NOH (20 mL, 20.0 mmol) was added all at once to a suspension of H$_2$Et$_2$Meppba (1.6 g, 5 mmol) in methanol (50 mL). A methanol solution (10 mL) of Cu(ClO$_4$)$_2$ · 6H$_2$O (1.85 g, 5.0 mmol) was then added dropwise under stirring at room temperature to the reaction mixture. The deep brown solution was filtered to eliminate the small amount of solid particles and the solvent was removed under vacuum. The dark brown solid of **IV.2a** was recuperated with acetone, collected by filtration, washed thoroughly with tetrahydrofuran to remove the precipitate of nBu$_4$NClO$_4$, and air dried (3.4 g, 80% yield). Anal. Calcd for $C_{88}H_{162}Cu_2N_8O_{15}$ (1700): C, 61.65; H, 9.75; N, 6.69%. Found: C, 61.53; H, 9.61; N, 6.51%. IR (KBr): 1649, 1602 cm^{-1} (C=O).

$Li_4[Cu_2(Meppba)_2] \cdot 7H_2O$ (IV.2b): An aqueous solution (10 mL) of $Cu(NO_3)_2 \cdot 3H_2O$ (1.2 g, 5.0 mmol) was added dropwise to an aqueous solution (50 mL) of $Et_2H_2Meppba$ (1.6 g, 5.0 mmol) and $LiOH \cdot H_2O$ (0.8 g, 20.0 mmol) under stirring at room temperature. The resulting deep brown solution was then filtered, and the solvent was reduced under vacuum until a solid appeared. The dark brown solid was collected by filtration, washed with acetone and diethyl ether, and dried under vacuum. Recrystallization from an aqueous solution gave dark brown prisms of **IV.2b** suitable for single-crystal X-ray diffraction upon layering of methanol (1.7 g, 85% yield). Anal. Calcd for $C_{22}H_{26}Cu_2Li_4N_4O_{19}$ (804): C, 32.81; H, 3.25; N, 6.96%. Found: C, 31.34; H, 3.20; N, 6.89%. IR (KBr): 1645, 1618 cm^{-1} (C=O).

$(Ph_4P)_4[Cu_2(Meppba)_2] \cdot 8H_2O$ (IV.2c): An aqueous solution (10 mL) of $AgNO_3$ (1.4 g, 8.0 mmol) was added to an aqueous solution (20 mL) of **IV.2b** (1.6 g, 2.0 mmol) under stirring at room temperature. The dark brown solid that appeared was collected by filtration, suspended in water (10 mL), and then charged with an acetonitrile solution (5 mL) of Ph_4PCl (3.0 g, 8.0 mmol). The reaction mixture was further stirred for 30 min under gentle warming and then filtered to remove the precipitate of AgCl. Slow evaporation of the filtered deep brown solution gave dark brown crystals of **IV.2c** not suitable for single-crystal X-ray diffraction after several days in the open air at room temperature (3.9 g, 90% yield). Anal. Calcd for $C_{118}H_{108}Cu_2N_4O_{20}P_4$ (2151): C, 65.82; H, 5.06; N, 2.60%. Found: C, 65.45; H, 4.99; N, 2.77%. IR (KBr): 3425 (O–H), 1642, 1617 cm^{-1} (C=O).

$(n\mathrm{Bu_4N})_4[Cu_2(Me_4ppba)_2] \cdot 5H_2O$ (IV.3a): A 1.0 M methanol solution of $n\mathrm{Bu_4NOH}$ (20 mL, 20.0 mmol) was added all at once to a suspension of $H_2Et_2Me_4ppba$ (1.8 g, 5.0 mmol) in methanol (50 mL). A methanol solution (10 mL) of $Cu(ClO_4)_2 \cdot 6H_2O$ (1.85 g, 5.0 mmol) was then added dropwise under stirring at room temperature to the reaction mixture. The deep brown solution was filtered to eliminate the small amount of solid particles and the solvent was removed under vacuum. The dark brown solid of **IV.3a** was recuperated with acetone, collected by filtration, washed thoroughly with tetrahydrofuran to remove the precipitate of $n\mathrm{Bu_4NClO_4}$, and air dried (3.9 g, 85% yield). Anal. Calcd for $C_{94}H_{178}Cu_2N_8O_{17}$ (1820): C, 61.54; H, 9.99; N, 6.24%. Found: C, 61.91; H, 9.90; N, 5.99%. IR (KBr): 1647, 1597 cm^{-1} (C=O).

$Li_4[Cu_2(Me_4ppba)_2] \cdot 9H_2O$ (IV.3b): An aqueous solution (10 mL) of $Cu(NO_3)_2 \cdot 3H_2O$ (1.2 g, 5.0 mmol) was added dropwise to an aqueous solution (50 mL) of $Et_2H_2Me_4ppba$ (1.8 g, 5.0 mmol) and $LiOH \cdot H_2O$ (0.8 g, 20.0 mmol) under stirring at room temperature. The resulting deep brown solution was then filtered, and the solvent was reduced under vacuum until a solid appeared. The dark brown solid of **IV.3b** was collected by filtration, washed with acetone and diethyl ether, and air dried (2.0 g, 85% yield). Anal.: calcd for $C_{28}H_{42}Cu_2Li_4N_4O_{21}$ (924): C, 36.34; H, 4.57; N, 6.05%. Found: C, 36.63; H, 4.40; N, 6.03%; IR (KBr): ν = 3473 (O–H), 1634, 1605 cm^{-1} (C=O).

$(Ph_4P)_4[Cu_2(Me_4ppba)_2] \cdot 15H_2O$ (IV.3c): An aqueous solution (10 mL) of $AgNO_3$ (1.4 g, 8.0 mmol) was added to an aqueous solution (20 mL) of **IV.3b** (1.9 g, 2.0 mmol) under stirring at room temperature. The dark brown solid that appeared was collected by filtration, suspended in water (10 mL), and then charged with an acetonitrile solution (5 mL) of Ph_4PCl (3.0 g, 8.0 mmol). The reaction mixture was further stirred for 30 min under gentle warming and then filtered to remove the precipitate of AgCl. Slow evaporation of the filtered solution gave dark brown prisms of **IV.3c** suitable for single-crystal X-ray diffraction after several days in the open air at room temperature (4.2 g, 90% yield). Anal. Calcd for $C_{124}H_{134}Cu_2N_4O_{27}P_4$ (2363): C, 63.02; H, 5.71; N, 2.37%. Found: C, 63.99; H, 5.59; N, 2.46%. IR (KBr): 3413 (O–H), 1637, 1604 cm^{-1} (C=O).

Chemical oxidation procedures and spectroscopic measurements. Variable-temperature (5–25 °C) UV–vis–NIR spectra of acetonitrile solutions were recorded on an Agilent Technologies-8453 spectrophotometer equipped with a thermostated Chem Station. Varying amounts of a 0.01 M solution of bromine (0–15 µL) were added stepwise to a 0.1 mM solution of **IV.3c** in acetonitrile (2.5 mL) at 5, 15, and 25 °C. In each case, the course of the decomposition reaction of the monooxidized species was followed by measuring the absorbance at λ_{max} = 875 nm as a function of time.

Variable-temperature (4.0–150 K) X-band EPR spectra (ν = 9.47 GHz) of frozen-matrix acetonitrile solutions were recorded under non-saturating conditions on a Bruker ER 200 D spectrometer equipped with a helium cryostat. The monooxidized species was obtained by addition of an excess of Br_2 to a 0.1 M solution of **IV.3c** in acetonitrile (0.5 mL) at –40 °C.

Magnetic measurements. Variable-temperature (2.0–300 K) magnetic susceptibility measurements were carried out on powdered samples with a SQUID magnetometer under an applied field of 10 kOe ($T \geq 50$ K) and 100 Oe ($T < 50$ K). The experimental data were corrected for the diamagnetic contributions of the constituent atoms and the sample holder as well as for the temperature-independent paramagnetism (tip) of the Cu^{II} ion (60×10^{-6} cm^3 mol^{-1}).

Electrochemical measurements. The cyclic voltammetry measurements were performed using a PAR 273A scanning potentiostat operating at a scan rate of 10–1000 mV s^{-1}. Cyclic voltammograms were carried out in acetonitrile using 0.1 M $n\mathrm{Bu_4NPF_6}$ as supporting electrolyte and 1.0 mM of either **IV.1a**–**IV.3a** or **IV.1c**–**IV.3c**. The working electrode was a glassy carbon disk (0.32 cm^2) that was polished with 1.0 µm diamond powder, sonicated, washed with absolute ethanol and acetone and air dried. The reference electrode was $AgClO_4$/Ag separated from the test solution by a salt bridge containing the solvent/supporting electrolyte, with platinum as auxiliary electrode. All experiments were performed in standard electrochemical cells at 25 °C under argon. The potential range investigated was between –2.00 and +1.80 V *vs*. SCE. The formal potentials were measured at a scan rate of 100 mV s^{-1} and were referred to the saturated calomel electrode (SCE), which was consistently measured as –0.26 V *vs*. the $AgClO_4$/Ag electrode. Ferrocene (Fc) was added as internal standard at the end of the measurements [$E(Fc^+/Fc)$ = +0.40 V *vs*. SCE].

Crystal structure data collection and refinement. The X-ray diffraction data of **IV.1a** were collected with graphite-monochromated Mo-K_α radiation (λ = 0.7107 Å) using a Bruker-Nonius X8APEXII CCD area detector diffractometer, while those of **IV.2b** and **IV.3c** were collected using synchrotron radiation [λ =

0.7380 (**IV.2b**) and 0.7513 Å (**IV.3c**)] at the BM16-CRG beamline in the ESRF (Grenoble, France). Although several crystals of **IV.2b** were tested, their small size and poor diffraction power precluded the achievement of an optimal $\sin(\theta)/\lambda$ ratio. In fact, we are totally conscious of the poor quality of the data for **IV.2b** with high *R*, *wR*, and *S* values (see Table IV.1). The program *TwinRotMat* included in the *PLATON* package[14] indicates that **IV.2b** was composed of two crystal domains related by a rotation of 180° each other. A twin law was created and included in the *SHELXL* refinement together with the corresponding *BASF* parameter, the best refinement value being 0.173. The statistical weight factor was also included in the last cycles of the refinement. A detailed model for the crystal refinement can be seen in the "refine_special_details" section of the CIF file. Although the disorder in the region of the benzene ring is complicated, the proposed model does lead to a clear positioning of the methyl substituents. In spite of all these disorder problems, the metallacyclic molecular structure and the essential heterobimetallic layered network and crystal packing features of **IV.2b** could be realisticaly discussed and reasonably established.

The X-ray diffraction data of **IV.2b** and **IV.3c** were indexed, integrated and scaled using the *HKL2000* program.[15] All calculations for data reduction, structure solution, and refinement were done through the *SAINT* and *SADABS* programs[16] (**IV.1a**) or through the *WINGX*[17] program (**IV.2b** and **IV.3c**). The structures were solved by direct methods and refined with full-matrix least-squares technique on F^2 using the SHELXTL software package[18] (**IV.1a**) or the *SHELXS-97* and *SHELXL-97* programs (**IV.2b** and **IV.3c**).[19] All non-hydrogen atoms of **IV.1a**, **IV.2b**, and **IV.3c** were refined anisotropically except for the C(2), C(3), C(5), C(6), and C(11) atoms from the benzene ring of **IV.2b**, which are greatly disordered and consequently, they were refined with occupancy factors of 0.76 and 0.24 by using isotropic thermal parameters at the later of these two sites. In addition, soft restraints were used to fix the planarity and the bond distances within the benzene ring of **IV.2b**. The O(1w), O(2w), and O(5w) atoms from the weakly coordinated water molecules of **IV.2b** were somewhat disordered as well as the O(3w) and O(4w) atoms from the crystallization water molecules, and they were all refined anisotropically with an occupancy factor of 0.5. Some thermal disorder was also observed for the *n*-butyl chains of the $n\text{Bu}_4\text{N}^+$ cations in **IV.1a**. The hydrogen atoms from the benzene ring of **IV.1a**, **IV.2b**, and **IV.3c** were calculated and refined with isotropic thermal parameters, while those of the crystallization water molecules were neither found nor calculated. The final geometrical calculations and the graphical manipulations were carried out with *PARST97* and *CRYSTALMAKER* programs, respectively.[20]

Crystallographic data (excluding structure factors) for the structures reported in this paper have been deposited with the Cambridge Crystallographic Data Centre as supplementary publication CCDC no. 911161 (**IV.1a**), 901378 (**IV.2b**), and 856597 (**IV.3c**). Copies of the data can be obtained free of charge on application to CCDC, 12 Union Road, Cambridge CB21EZ, UK (fax: (+44) 1223-336-033; e-mail: deposit@ccdc.cam.ac.uk).

IV.10 Computational Details

Density functional (DF) calculations were carried out on the broken-symmetry (BS) singlet and triplet spin states of the orthogonal model complexes **IV.1**–**IV.3** using the hybrid B3LYP functional[21] combined with the BS approach,[22] as implemented in the Gaussian 09 program.[23] Triple- and double-ζ quality basis sets proposed by Ahlrichs and co-workers were used for the metal and non-metal atoms, respectively.[24] All four possible configurations of the methyl substituents from the two facing benzene rings were considered for **IV.2**. The molecular geometries of the model complexes **IV.1** and **IV.3** with D_{2h} molecular symmetry as well as those of the pseudo-*gem*, -*ortho*, -*para*, and -*meta* isomers of **IV.2** with C_s, C_2, C_i, and C_2 molecular symmetries respectively, were not optimized but their metal bond lengths and metal interbond angles were taken from the crystal structure of **3c** with an imposed planar conformation of the copper basal planes ($\tau = 0°$) and a perpendicular orientation of the copper basal planes with respect to the benzene rings ($\phi = 90°$).

DF calculations were also performed on the optimized molecular geometries of **IV.1**– **IV.3** and **IV.3'** in acetonitrile solution. A pseudo-*meta* configuration of the methyl substituents from the two facing benzene rings was only considered for **IV.2**, as observed in the X-ray crystal structure of **IV.2b**. Different ground electronic configurations are available for **IV.3'** depending on the oxidized center (metal or ligand-based oxidation) and the overall spin state (doublet or quartet). That being so, the starting geometry was modified in each case to come closer to those experimentally observed in either copper(III) complexes or copper(II)-radical ligands. However, a unique result was found in all cases during the geometry optimization process. In fact, the $S = 1/2$ Cu^{II}_2-π-radical configuration is the most stable one and moreover, there is no energy barrier with other possible electronic configurations. Solvation effects were introduced using a polarizable continuum model (PCM), where the cavity is created via a series of overlapping spheres.[25] The calculated spin density data for **IV.3** and **IV.3'** were obtained from natural bond orbital (NBO) analysis.[26]

References

[1] a) J. A. McCleverty, M. D. Ward, *Acc. Chem Res.* **1998**, *31*, 842; b) F. Paul, C. Lapinte, *Coord. Chem. Rev*. **1998**, *178–180*, 431; c) B. S. Brunschwig, N. Sutin, *Coord. Chem. Rev*. **1999**, *187*, 233; d) W. Kaim, A. Klein, M. Cloeckle, *Acc. Chem. Res.* **2000**, *33*, 755; e) K. D. Demadis, C. M. Hartshorn, T. J. Meyer, *Chem. Rev*. **2001**, *101*, 2655; f) M. D. Ward, J. A. McCleverty, *Dalton Trans.* **2002**, 275; g) M. I. Bruce, P. J. Low, *Adv. Organomet. Chem*. **2004**, *50*, 179; h) K. Ray, T. Petrenko, K. Weighardt, F. Neese, *Dalton Trans.* **2007**, 1552; i) P. Aguirre-Etcheverry, D. O'Hare, *Chem. Rev*. **2010**, *110*, 4839.

[2] a) A. M. W. Cargill-Thompson, D. Gatteschi, J. A. McCleverty, J. A. Navas, E. Rentschler, M. D. Ward, *Inorg. Chem.* **1996**, *35*, 2701; b) T. Weyland, K. Costaus, A. Mari, J.-F. Halet, C. Lapinte, *Organometallics* **1998**, *17*, 5569; c) S. W. Gordon-Wylie, B. L. Claus, C. P. Horwitz, Y. Leychkis, J. M. Workman, A. J. Marzec, G. R. Clark, C. E. F. Rickard, B. J. Conklin, S. Sellers, G. T. Yee, T. J. Collins, *Chem. Eur. J.* **1998**, *4*, 2173; d) A. Aukauloo, X. Ottenwaelder, R. Ruiz, S. Possereau, Y. Pei, Y. Journaux, P. Fleurat, F. Volatron, B. Cervera, M. C. Muñoz, *Eur. J. Inorg. Chem*. **1999**, 1067; e) I. Fernández, R. Ruiz, J. Faus, M. Julve, F. Lloret, J. Cano, X. Ottenwaelder, Y. Journaux, M. C. Muñoz, *Angew. Chem. Int. Ed.* **2001**, *40*, 3039; f) A. Caneschi, A. Dei, H. Lee, D. A. Shultz, L. Sorace, *Inorg. Chem.* **2001**, *40*, 408; g) A. Caneschi, A. Dei, C. P. Mussari, D. A. Shultz, L. Sorace, K. E. Vostrikova, *Inorg. Chem*. **2002**, *41*, 1086; h) T. Glaser, M. Gerenkamp, R. Frölich, *Angew. Chem. Int. Ed.* **2002**, *41*, 3823; i) M. P. Shores, J. R. Long, *J. Am. Chem. Soc.* **2002**, *124*, 3512; j) U. Beckmann, E. Bill, T. Weyhermüller, K. Wieghardt, *Eur. J. Inorg. Chem*. **2003**, 1768; k) W. Kaim, N. Doslik, S. Frantz, T. Sixt, M. Wanner, F. Baumann, G. Deninger, H.-J. Kümmerer, C. Duboc-Toia, J. Fiedler, S. Zalis, *J. Mol. Struct.* **2003**, *656*, 183; l) F. Michel, S. Torelli, F. Thomas, C. Duboc, C. Philouze, C. Belle, S. Hamman, E. Saint-Aman, J.-L. Pierre, *Angew. Chem. Int. Ed.* **2005**, *44*, 438; m) M. Fabre, J. Bonvoisin, *J. Am. Chem. Soc.* **2007**, *129*, 1434; n) K. S. Min, A. G. Di Pasquale, J. A. Golen, A. L. Rheingold, J. S. Miller, *J. Am. Chem. Soc.* **2007**, *129*, 2360; o) T. Glaser, M. Heidemeier, J. B. H. Strautmann, H. Bögge, A. Stammler, E. Krickemeyer, R. Huenerbein, S. Grimme, E. Bothe, E. Bill, *Chem. Eur. J.* **2007**, *13*, 9191; p) P. Hamon, F. Justaud, O. Cador, P. Hapiot, S. Rigaut, L. Toupet, L. Ouahab, H. Stueger, J.-R. Hamon, C. Lapinte, *J. Am. Chem. Soc.* **2008**, *130*, 17372; q) M. L. Kirk, D. A. Shultz, R. D. Schmidt, D. Habel-Rodriguez, H. Lee, J. Lee, *J. Am. Chem. Soc.* **2009**, *131*, 18304; r) M. C. Dul, X. Ottenwaelder, E. Pardo, R. Lescouëzec, Y. Journaux, L. M. Chamoreau, R. Ruiz-García, J. Cano, M. Julve, F. Lloret, *Inorg. Chem.* **2009**, *48*, 5244; s) A. Mondal, T. Weyhermüller, K. Wieghardt, *Chem. Commun.* **2009**, 6098; t) M. A. Fox, B. Le Guennic, R. L. Roberts, D. A. Brue, D. S. Yufit, J. A. K. Howard, G. Manca, J. F. Halet, F. Hartl, P. J. Low, *J. Am. Chem. Soc*. **2011**, *133*, 18433; u) K. Motoyama, H. Li, T. Koike, M. Hatakeyama, S. Yokojima, S. Nakamura, M. Akita, *Dalton Trans.* **2011**, *40*, 10643; v) A. Hildebrandt, H. Lang, *Dalton Trans.* **2011**, *40*, 11831.

[3] a) A. Caneschi, D. Gatteschi, P. Rey, R. Sessoli, *Acc. Chem. Res.* **1989**, *22*, 392; b) J.-P. Launay, C. Coudret, in *Electron Transfer in Chemistry*, Vol. 5, Wiley-VCH, **2001**, p. 3; c) J.-P. Launay, *Chem. Soc. Rev.* **2001**, *30*, 386; d) A. Dei, D. Gatteschi, C. Sangregorio, L. Sorace, *Acc. Chem. Res.* **2004**, *37*, 827.

[4] a) T. R. Felthouse, E. N. Duesler, D. N. Hendrickson, *J. Am. Chem. Soc.* **1978**, *100*, 618; b) T. R. Felthouse, D. N. Hendrickson, *Inorg. Chem.* **1978**, *17*, 2636; c) J. Ferrando-Soria, M. Castellano, C. Yuste, F. Lloret, M. Julve, O. Fabelo, C. Ruiz-Pérez, S.-E. Stiriba, R. Ruiz-García, J. Cano, *Inorg. Chim. Acta* **2010**, *363*, 1666; d) C. Yuste, J. Ferrando-Soria, D. Cangussu, O. Fabelo, C. Ruiz-Pérez, N. Marino, G. De Munno, S.-E. Stiriba, R. Ruiz-García, J. Cano, F. Lloret, M. Julve, *Inorg. Chim. Acta* **2010**, *363*, 1984;

[5] L. Michaelis, M. P. Schubert, S. Granick, *J. Am. Chem. Soc.* **1939**, *61*, 1981.

[6] a) K. Takemura, K. Takehara, M. Ata, *Eur. J. Org. Chem.* **2004**, 4936; b) S. F. Nelsen, G. Li, K. P. Schultz, I. A. Guzei, H. Q. Tran, D. A. Evans, *J. Am. Chem. Soc.* **2008**, *130*, 11620; c) A. S. Jalilov, G. Li, S. F. Nelsen, I. A. Guzei, Q. Wu, *J. Am. Chem. Soc.* **2010**, *132*, 6176; d) A. S. Jalilov, S. F. Nelsen, I. A. Guzei, Q. Wu, *Angew. Chem. Int. Ed*. **2011**, *50*, 6860.

[7] a) M. Fujita, in *Comprehensive Supramolecular Chemistry*, Vol. 9 (Eds.: J. P. Sauvage, M. W. Hosseini), Elsevier, **1996**, p. 253; b) G. F. Swiegers, T. J. Malefetse, *Chem. Rev.* **2000**, *100*, 3483; c) L. K. Thompson, *Coord. Chem. Rev.* **2002**, *233–234*, 193; d) J. M. Lehn, *Angew. Chem. Int. Ed.* **2004**, *43*, 3644; e) M. Ruben, J. M. Lehn, P. Müller, *Chem. Soc. Rev.* **2006**, *35*, 1056; f) E. Pardo, R. Ruiz-García, J. Cano, X. Ottenwaelder, R. Lescouëzec, Y. Journaux, F. Lloret, M. Julve, *Dalton Trans*. **2008**, 2780; g) L. N. Dawe, T. S. M. Abedin, L. K. Thompson, *Dalton Trans.* **2008**, 1661; h) M. C. Dul, E. Pardo, R. Lezcouëzec, Y. Journaux, J. Ferrando-Soria, R. Ruiz-García, J. Cano, M. Julve, F. Lloret, D. Cangussu, C. L. M. Pereira, H. O. Stumpf, J. Pasán, C. Ruiz-Pérez, *Coord. Chem. Rev*. **2010**, *254*, 2281; i) R. Chakrabarty, P. S. Mukherjee, P. J. Stang, *Chem. Rev.* **2011**, *111*, 6810.

[8] a) A. Dei, D. Gatteschi, C. Sangregorio, L. Sorace, M. G. F. Vaz, *Inorg. Chem.* **2003**, *42*, 1701; b) A. Dei, D. Gatteschi, C. Sangregorio, L. Sorace, M. G. F. Vaz, *Chem. Phys. Lett.* **2003**, *368*, 162; c) S. Mukherjee, E. Rentschler, T. Weyhermüller, K. Wieghardt, P. Chaudhuri, *Chem. Commun*. **2003**, 1828; d) S. Mukherjee, T. Weyhermüller, E. Bothe, K. Wieghardt, P. Chaudhuri, *Dalton Trans.* **2004**, 3842.

[9] a) M. C. Dul, E. Pardo, R. Lezcouëzec, L. M. Chamoreau, F. Villain, Y. Journaux, R. Ruiz-García, J. Cano, M. Julve, F. Lloret, J. Pasán, C. Ruiz-Pérez, *J. Am. Chem. Soc*. **2009**, *131*, 14614; b) E. Pardo, J. Ferrando-Soria, M. C. Dul, R. Lezcouëzec, Y. Journaux, R. Ruiz-García, J. Cano, M. Julve, F. Lloret, L. Cañadillas-Delgado, J. Pasán, C. Ruiz-Pérez, *Chem. Eur. J.* **2010**, *16*, 12838.

[10] a) E. Pardo, J. Faus, M. Julve, F. Lloret, M. C. Muñoz, J. Cano, X. Ottenwaelder, Y. Journaux, R. Carrasco, G. Blay, I. Fernández, R. Ruiz-García, *J. Am. Chem. Soc.* **2003**, *125*, 10770. b) J. Ferrando-Soria, M. Castellano, R. Ruiz-García, J. Cano, M. Julve, F. Lloret, J. Pasán, C. Ruiz-Pérez, L. Cañadillas-Delgado, Y. Li, Y. Journaux, E. Pardo, *Chem. Commun.* **2012**, *48*, 8401.

[11] a) R. Ruiz, C. Surville-Barland, A. Aukauloo, E. Anxolabèhere-Mallart, Y. Journaux, J. Cano, M. C. Muñoz, *J. Chem. Soc., Dalton Trans.* **1997**, 745; b) B. Cervera, J. L. Sanz, M. J. Ibañez, G. Vila, F. Lloret, M. Julve, R. Ruiz, X. Ottenwaelder, A. Aukauloo, S. Poussereau, Y. Journaux, M. C. Muñoz, *J. Chem. Soc., Dalton Trans.* **1998**, 781.

[12] G. R. Hanson, K. E. Gates, C. J. Noble, M. Griffin, A. Mitchell, S. Benson, *J. Inorg. Biochem*. **2004**, *98*, 903 (*XSOPHE*).

[13] J. P. Hay, J. C. Thibeault, R. Hoffmann, *J. Am. Chem. Soc.* **1975**, *97*, 4884.

[14] A. L. Speck, *Acta Cryst*. **2009**, *D65*, 148.

[15] Z. Otwinowski, W. Minor, *Processing of X-ray Diffraction Data Collected in Oscillation Mode,* in *Methods in Enzymology: Macromolecular Crystallography, Part A*, Vol. 276 (Eds.: C. W. Jr., Carter, R. M. Sweet), **1997**, p. 307.

[16] a) *SAINT*, version 6.45, Bruker Analytical X-ray Systems, Madison, WI, **2003**; b) G.M. Sheldrick, *SADABS Program for Absorption Correction*, version 2.10, Analytical X-ray Systems, Madison, WI, **2003**.

[17] L. J. Farrugia, *J. Appl. Crystallogr*. **1999**, *32*, 837 (*WINGX*).

[18] *SHELXTL*, Bruker Analytical X-ray Instruments, Madison, WI, **1998.**

[19] G. M. Sheldrick, *SHELX97*, *Programs for Crystal Structure Analysis, release 97-2*, Institüt für Anorganische Chemie der Universität Göttingen, Göttingen, **1998**.

[20] a) M. Nardelli, *J. Appl. Crystallogr.* **1995**, *28*, 659; b) D. Palmer, *CRYSTALMAKER,* Cambridge University Technical Services, Cambridge, **1996**.

[21] A. D. Becke, *J. Chem. Phys.* **1993**, *98*, 5648.

[22] a) E. Ruiz, J. Cano, S. Alvarez, P. Alemany, *J. Am. Chem. Soc.* **1998**, *120*, 11122; b) E. Ruiz, J. Cano, S. Alvarez, P. Alemany, *J. Comput. Chem.* **1999**, *20*, 1391; c) E. Ruiz, A. Rodriguez-Fortea, J. Cano, Alvarez, P. Alemany, *J. Comput. Chem.* **2003**, *24*, 982; d) E. Ruiz, V. Polo, J. Cano, S. Alvarez, *J. Chem. Phys.* **2005**, *123*, 164110.

[23] M. J. Frisch, G. W. Trucks, H. B. Schlegel, G. E. Scuseria, M. A. Robb, J. R. Cheeseman, G. Scalmani, V. Barone, B. Mennucci, G. A. Petersson, H. Nakatsuji, M. Caricato, X. Li, H. P. Hratchian, A. F. Izmaylov, J. Bloino, G. Zheng, J. L. Sonnenberg, M. Hada, M. Ehara, K. Toyota, R. Fukuda, J. Hasegawa, M. Ishida, T. Nakajima, Y. Honda, O. Kitao, H. Nakai, T. Vreven, Jr., J. A. Montgomery, J. E. Peralta, F. Ogliaro, M. Bearpark, J. J. Heyd, E. Brothers, K. N. Kudin, V. N. Staroverov, R. Kobayashi, J. Normand, K. Raghavachari, A. Rendell, J. C. Burant, S. S. Iyengar, J. Tomasi, M. Cossi, N. Rega, J. M. Millam, M. Klene, J. E. Knox, J. B. Cross, V. Bakken, C. Adamo, J. Jaramillo, R. Gomperts, R. E. Stratmann, O. Yazyev, A. J. Austin, R. Cammi, C. Pomelli, J. W. Ochterski, R. L. Martin, K. Morokuma, V. G. Zakrzewski, G. A. Voth, P. Salvador, J. J. Dannenberg, S. Dapprich, A. D. Daniels, Ö. Farkas, J. B. Foresman, J. V. Ortiz, J. Cioslowski, D. J. Fox, *Gaussian 09*, revision B.1; Gaussian, Inc.: Wallingford, CT, **2009**.

[24] a) A. Schaefer, H. Horn, R. Ahlrichs, *J. Chem. Phys.* **1992**, *97*, 2571; b) A. Schaefer, C. Huber, R. Ahlrichs, *J. Chem. Phys.* **1994**, *100*, 5829.

[25] a) M. Cossi, N. Rega, G. Scalmani, V. Barone, *J. Comp. Chem.* **2003**, *24*, 669; b) J. Tomasi, B. Mennucci, E. Cances, *J. Mol. Struct.-Theochem.* **1999**, *464*, 211.

[26] a) J. E. Carpenter, F. Weinhold, *J. Mol. Struct.* **1988**, *169*, 41; b) A. E. Reed, L. A. Curtis, F. Weinhold, *Chem. Rev.* **1988**, *88*, 899; c) F. Weinhold, J. E. Carpenter, *The Structure of Small Molecules and Ions*, Plenum, **1988**, p. 227.

CHAPTER V

Dicopper(II) Oligoacenophanes as Molecular Magnetic Photoswitches

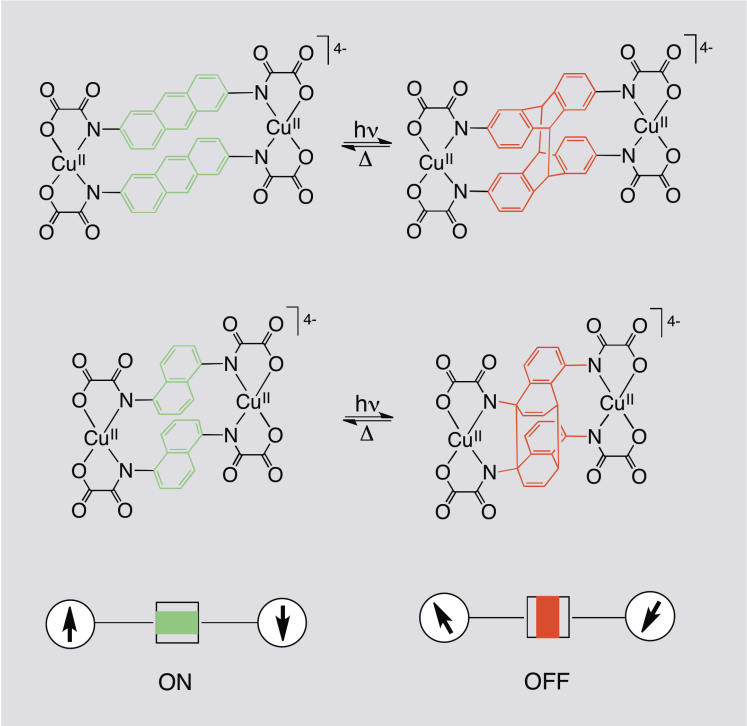

On the road to molecular photoswitches: upon UV light irradiation, the two Cu^{II} ions (S_{Cu} = 1/2) that are moderately strong antiferromagnetically coupled in the dicopper(II) 2,6-anthraceno- and 1,5-naphthalenophanes (ON state) become magnetically uncoupled in the corresponding [4+4] photocycloaddition products (OFF state), as shown both experimentally and theoretically.

V.1 Introductory Aspects

The supramolecular control of photochemical reactivity and photophysical (optical, electronic, and magnetic) properties of polymetallic complexes is a current challenge in coordination chemistry which lies at the interface of several disciplines, including photochemistry and magnetochemistry.[1–3] In particular, the design and synthesis of photoactive aromatic bridging ligands that are able to self-assemble with paramagnetic transition metal ions to form photoswitchable exchange-coupled, dinuclear metallacyclic complexes, so-called metallacyclophanes, constitute a largely unexplored subject in this multidisciplinary field of supramolecular coordination chemistry (metallosupramolecular chemistry).[1] Besides their interest as models for the fundamental research on electron exchange phenomena between distant metal centers through extended π-conjugated aromatic spacers, photoswitchable metallacyclophanes could be also of great importance in the "bottom-up" approach to nanometer-scale electronic and photonic devices.[4,5] So, they appear as potential alternatives to metal-based molecular magnetic photoswitches, in contrast to earlier examples reported by Irie and others which are purely organic diradicals or hybrid metal-organic radicals with photoactive stilbene, azobenzene, diarylethene, and diarylanthracene bridges.[6,7]

Our strategy in this field consists of using oxamato-based dinuclear copper(II) metallacyclophanes with potentially photoactive *α,α'*- and *β,β'*-disubstituted oligoacene spacers such as 1,5-naphthalene or 2,6-anthracene (Scheme 1).[8] In fact, oligoacenes possess a well-recognized and rich photochemical reactivity that includes both uni- and bimolecular reactions, either in solution or in the solid state.[9] In particular, the [4+4] photodimerization of anthracene and its 1- and 2-substituted derivatives through the more reactive carbon atoms at the 9,10 and 9',10' (*meso*) positions of the central benzene rings to give the corresponding cyclodimer is one of the oldest known photochemical reactions which has been extensively investigated from synthetic and mechanistic viewpoints (Figure V.1a).[10] However, naphtalenes are much less photoreactive than anthracenes such as less is known about their photodimerization, which is largely dependent on the substittion pattern.[11] So, although naphthalene itself does not react upon irradiation, its 1- and 2-substituted derivatives undergo a [4+4] photodimerization reaction through the more reactive carbon atoms at the 1,4 and 1',4' positions of the substituted benzene rings (Figure V.1b).[11a,b] In the former case, however, the resulting [4+4] cyclodimer can experience a subsequent Cope rearrangement to the corresponding [2+2] cyclodimer (Figure V.1c).[11c,d]

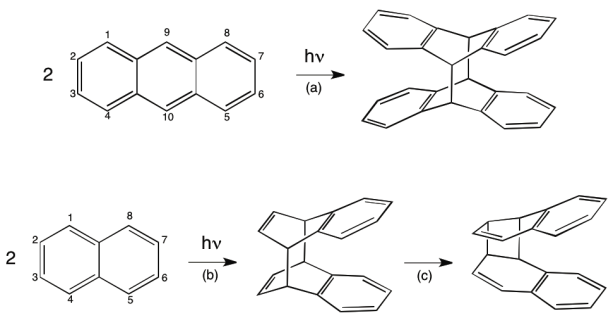

Figure V.1 Photodimerization of anthracene (a), 2- (b) and 1-substituted (c) naphthalene derivatives.

We recently demonstrated that the 2,6-anthracenebis(oxamate) bridging ligand can act as thermally reversible, photoswitchable magnetic wire for the transmission of EE interactions between the two square planar Cu^{II} ions, as reported in a preliminary communication (see fourth communication in Appendices).[8b] In the solid state, the moderately strong antiferromagnetically coupled dicopper(II) anthracenophane converts to the corresponding magnetically uncoupled dicopper(II) product resulting from the intramolecular ("pseudo-bimolecular") [4+4] photocycloaddition reaction of the two facing 2,6-anthracene spacers (Figure V.2a).[8b] As an extension of this previous work, we have also investigated the photodimerization of the moderately strong antiferromagnetically coupled dicopper(II) naphthalenophane with the bridging ligand *N,N'*-1,5-naphthalenebis(oxamate). In this case, a similar photomagnetic switching behavior is expected upon conversion to the putative magnetically uncoupled dicopper(II) product resulting from the [4+4] photocycloaddition reaction of the two facing 1,5-naphthalene spacers (Figure V.2b).

Here we report a complete study concerning the synthesis, X-ray crystal structures, solution spectrophotochemical and solid-state photomagnetic properties of the two novel dicopper(II) oligoacenophanes of formula $(n\text{Bu}_4\text{N})_4[\text{Cu}_2(2,6\text{-anba})_2]$ (**V.1**) and $(n\text{Bu}_4\text{N})_4[\text{Cu}_2(1,5\text{-naba})_2] \cdot 4\text{H}_2\text{O}$ (**V.2**) [$n\text{Bu}_4\text{N}^+$ = tetra-*n*-butylammonium cation, H_4-2,6-anba = *N,N'*-2,6-anthracenebis(oxamic acid), and H_4-1,5-naba = *N,N'*-1,5-naphthalenebis(oxamic acid)]. In order to give further support to the photomagnetic switching behavior observed experimentally, we have performed accurate density functional (DF) calculations for the photocycloaddition of **V.1** and **V.2** to the corresponding metallacyclic cyclodimers **V.*c*-1(9,10)** and **V.*c*-2(1,4)** (Figure V.2).

V.2 Synthesis of the Ligands and Complexes

The proligands *N,N'*-2,6'-anthracenebis(oxamic acid) (H_4-2,6-anba) and *N,N'*-1,5-naphthalenebis(oxamic acid) (H_4-1,5-naba) were synthesized from the straightforward condensation of 2,6-anthracene- and 1,5-naphthalenediamine respectively, with ethyl oxalyl chloride ester (1:2 ratio) in THF in the presence of triethylamine (Figure V.3), and they were isolated as the diethyl

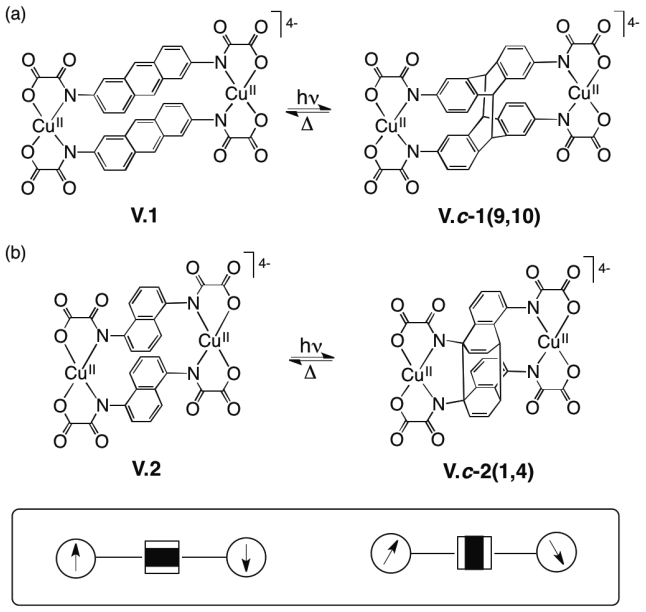

Figure V.2 Illustration of the postulated photomagnetic switching in oxamato-based dicopper(II) 2,6-anthracenophanes (a) and 1,5-naphthalenophanes (b).

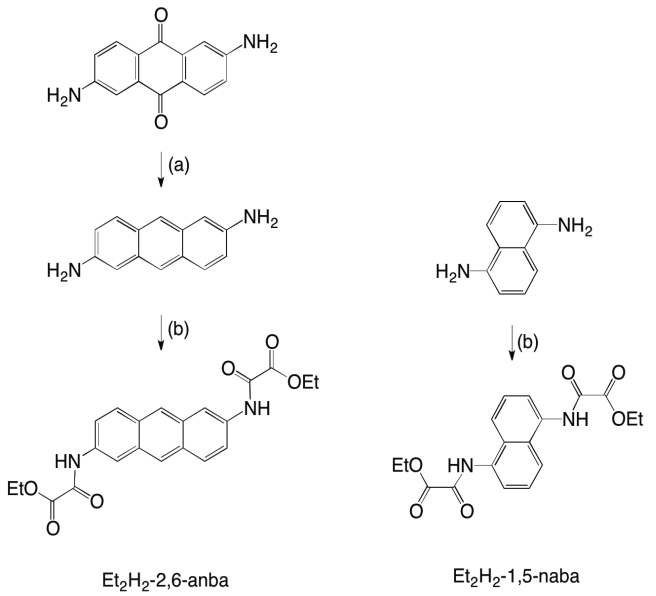

Figure V.3 Synthetic procedure for the Et_2H_2-2,6-anba and Et_2H_2-1,5-naba proligands: (a) Zn, NaOH, H_2O; (b) $C_2O_2Cl(OEt)$, Et_3N, THF.

ester derivatives in very good yields (80–85%). In the former case, the 2,6-anthracenediamine was not commercially available and it was prepared by reduction of the commercially available 2,6-anthraquinone with zinc in basic water solution, as reported earlier.[8b]

The tetraanionic dinuclear copper(II) complexes were synthesized by reaction of the diethyl ester derivatives of H_4-1,5-naba and H_4-2,6-anba respectively, with $CuCl_2$ (2:2 ratio) in a water-methanol solution by using nBu$_4$OH as base. They were isolated as the tetra-*n*-butylammonium salts of formula $(n\text{Bu}_4\text{N})_4[\text{Cu}_2(2,6\text{-anba})_2]$ (**V.1**) and $(n\text{Bu}_4\text{N})_4[\text{Cu}_2(1,5\text{-naba})_2] \cdot 4\text{H}_2\text{O}$ (**V.2**) in very good yields (90%) after extraction with dichloromethane and subsequent recrystallization from acetonitrile/methanol. The chemical identity of the complexes was obtained from elemental analysis and FTIR spectroscopies (see Experimental Section and Appendices).

Table V.1 Summary of crystallographic data.

	V.1	**V.2**
formula	$C_{100}H_{160}Cu_2N_8O_{12}$	$C_{92}H_{164}Cu_2N_8O_{16}$
M (g mol^{-1})	1793.44	1765.39
crystal system	orthorhombic	triclinic
space group	*P*bca	*P*–1
a (Å)	23.490(5)	11.6909(14)
b (Å)	16.875(3)	14.6859(13)
c (Å)	24.537(5)	16.241(3)
α (°)	90.00	70.160(10)
β (°)	90.00	75.453(9)
γ (°)	90.00	77.602(8)
V (Å^3)	9726(3)	2513.1(6)
Z	4	1
ρ_{calc} (g cm^{-3})	1.225	1.166
μ (mm^{-1})	0.500	0.485
T (K)	100(2)	293(2)
indep. reflect.	9873	9321
obs. reflect. [$I > 2\sigma(I)$]	9057	4985
R^a [$I > 2\sigma(I)$]	0.0641	0.0756
wR^b [$I > 2\sigma(I)$]	0.1804	0.1324
S^c	0.957	1.028

[a] $R = \sum(|F_o| - |F_c|)/\sum|F_o|$. [b] $wR = [\sum w(|F_o| - |F_c|)^2/\sum w|F_o|^2]^{1/2}$. [c] $S = [\sum w(|F_o| - |F_c|)^2/(N_o - N_p)]^{1/2}$.

V.3 Description of the Structures

Single-crystal X-ray diffraction analysis of **V.1** and **V.2** confirmed the double-stranded dicoppertetraaza[3.3](2,6)anthracenophane (**V.1**) and dicoppertetraaza[3.3](1,5)naphthalenophane (**V.2**) metallacyclic structures of the dicopper(II) anions that were earlier proposed or actually observed respectively, for the related tetraphenylphosphonium salts of formula for $(Ph_4P)_4[Cu_2(anba)_2] \cdot 4H_2O$ for $(Ph_4P)_4[Cu_2(1,5\text{-naba})_2] \cdot 8H_2O$ (Figures V.4 and V.5).[8a] A summary of the crystallographic data of **V.1** and **V.2** is given in Table V.1, while selected bond distances and interbond angles are listed in Tables V.2 and V.3, respectively.

The two centrosymmetrically related Cu(1) and Cu(1)^I atoms of **V.1** and **V.2** are essentially square planar (Figures V.4a and V.5a). The CuN_2O_2 environment is formed by two amidate-nitrogen and two carboxylate-oxygen atoms from two oxamato donor groups of the bis(chelating) bridging ligands. The values of the tetrahedral twist angle (τ) between the Cu(1)N(1)O(3) and Cu(1)N(2)^{I}O(6)^I mean planes are 14.30(5) (**V.1**) and 13.30(5)° (**V.2**), indicating thus a similar small tetrahedral distortion for the metal environment in **V.1** and **V.2**. The average values of the Cu–N distances [1.9609(16) (**V.1**) and 1.965(3) Å (**V.2**)] are slightly greater than those of the Cu–O one [1.9432(15) (**V.1**) and 1.936(3) Å (**V.2**)], while the values of the N–Cu–N angles [107.89(7) (**V.1**) and 107.40(14)° (**V.2**)] are significantly greater than those of the O–Cu–O ones [85.42(5) (**V.1**) and 86.31(14)° (**V.2**)]. The overall Cu–N bond lengthening and the N–Cu–N interbond broadening for **V.1** and **V.2** can obey to the π–π stacking interactions between the two facing oligoacene spacers within the metallacyclic core.

Within the dinuclear metallacyclophane cores, $Cu_2(2,6\text{-}N_2C_{14}H_8)_2$ (**V.1**) and $Cu_2(1,5\text{-}N_2C_{10}H_6)_2$ (**V.2**), the oligoacene spacers connected by the two N–Cu–N linkages are not exactly planar in **V.1** but they are slightly bent outwards (Figures V.4b and V.5b). The values of the dihedral angle between the fused benzene

Table V.2 Selected bond distances (Å) and interbond angles (°) for **V.1**.[a,b]

Cu(1)–N(1)	1.9571(16)	Cu(1)–N(2)^I	1.9647(16)
Cu(1)–O(3)	1.9453(14)	Cu(1)–O(6)^I	1.9410(15)
N(1)–Cu(1)–N(2)^I	107.89(7)	N(1)–Cu(1)–O(3)	84.53(6)
N(1)–Cu(1)–O(6)^I	165.92(6)	N(2)^I–Cu(1)–O(3)	164.44(7)
N(2)^I–Cu(1)–O(6)^I	83.78(6)	O(3)–Cu(1)–O(6)^I	85.42(5)

[a] The estimated standard deviations are given in parentheses. [b] Symmetry code: (I) = $-x + 1, -y + 1, -z$.

Table V.3 Selected bond distances (Å) and interbond angles (°) for **V.2**.[a,b]

Cu(1)–N(1)	1.956(3)	Cu(1)–N(2)^I	1.973(3)
Cu(1)–O(3)	1.948(3)	Cu(1)–O(6)^I	1.924(3)
N(1)–Cu(1)–N(2)^I	107.40(14)	N(1)–Cu(1)–O(3)	83.40(14)
N(1)–Cu(1)–O(6)^I	167.01(14)	N(2)^I–Cu(1)–O(3)	168.13(14)
N(2)^I–Cu(1)–O(6)^I	83.62(14)	O(3)–Cu(1)–O(6)^I	86.31(14)

[a] The estimated standard deviations are given in parentheses. [b] Symmetry code: (I) = $-x, -y, -z + 1$.

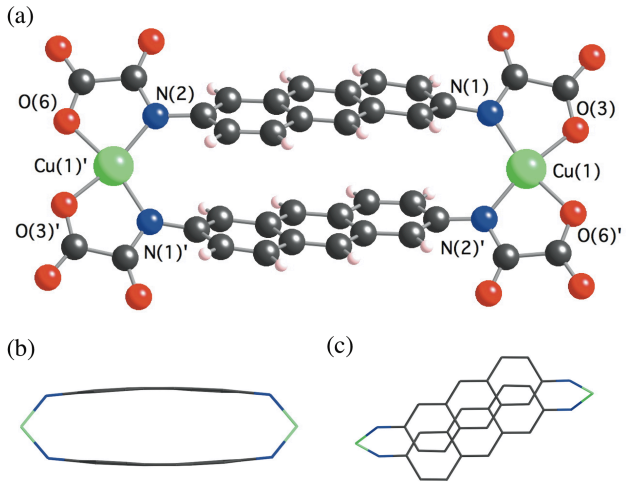

Figure V.4 (a) Perspective view of the centrosymmetric anionic dicopper unit of **V.1** with the atom-numbering scheme of the metal environments [symmetry code: (I) = –*x* + 1, –*y* + 1, –*z*]. (b) Front and (c) top projection views of the metallacyclic core of **V.1**.

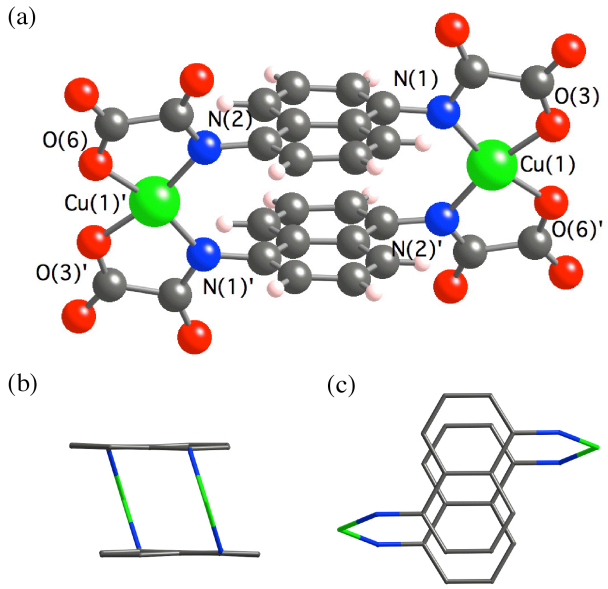

Figure V.5 (a) Perspective view of the centrosymmetric anionic dicopper unit of **V.2** with the atom-numbering scheme of the metal environments [symmetry code: (I) = –*x*, –*y*, –*z* + 1]. (b) Side and (c) top projection views of the metallacyclic core of **V.2**.

rings within each oligoacene spacer (φ) are 3.44(5) (**V.1**) and 0.44(5)° (**V.2**). A small but nonnegligible bond length alternation is observed in the anthracene (**V.1**) and naphthalene (**V.2**) spacers which is typical of oligoacene molecules. The average values for the short C–C distances are 1.375(3) (**V.1**) and 1.360(8) Å (**V.2**), while the average values for the long C–C distances are 1.423(3) (**V.1**) and 1.414(8) Å (**V.2**). The average values of the torsion angle (ϕ) around the Cu–N–C–C bonds (ϕ) are 58.5(2) (**V.1**) and 70.9(2)° (**V.2**), reflecting thus an appreciable larger distortion from perpendicularity between the copper basal planes and the oligoacene spacers in **V.1**. For symmetry reasons, the copper basal planes are parallel to each other in **V.1** and **V.2**, so that the value of the angle between the copper basal planes (ψ) are exactly 0°. Deviations from the ideal C_{2h} molecular symmetry corresponding

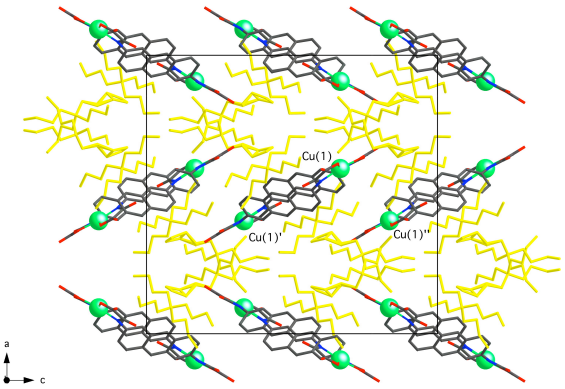

Figure V.6 Crystal packing view of **V.1** along the *b* axis [symmetry code: (I) = –*x* + 1, –*y* + 1, –*z*; (II) = –*x* + 1, *y* + ½, –*z* + ½]. The *n*-tetrabutylammonium cations are shown in yellow color (hydrogen atoms have been omitted for clarity).

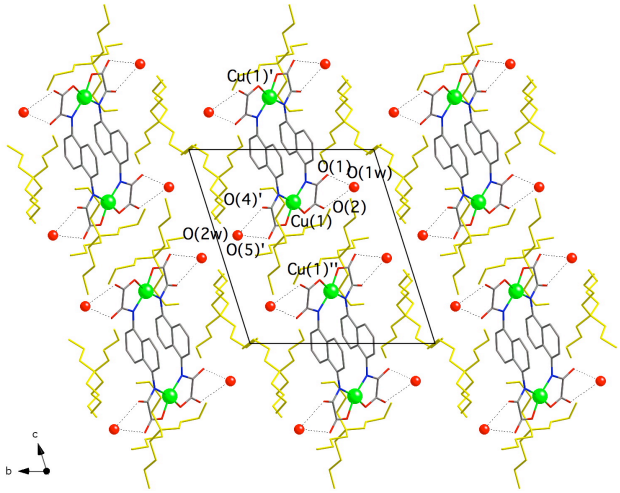

Figure V.7 Crystal packing view of **V.2** along the crystallographic *a* axis [symmetry code: (I) = –*x*, –*y*, –*z* + 1; (II) = –*x*, –*y*, –*z*]. The *n*-tetrabutylammonium cations are shown in yellow color (hydrogen atoms have been omitted for clarity). The hydrogen bonds with the crystallization water molecules are represented by dotted lines.

to an eclipsed π-stacked orthogonal conformation (ϕ = 90°) may be originated from the favorable π-π interactions in the diagonal- (**V.1**) or parallel-displaced (**V.2**) conformation of the two facing oligoacene spacers (Figures 1c and 2c). The average values of the centroid-centroid inter-ring distance (*h*) between the equivalent benzene rings are 3.678(3) (**V.1**) and 3.429(4) Å (**V.2**), while the average values of the angle between the centroid-centroid vector from the equivalent benzene rings and their normal (θ) are 23.04(4) (**V.1**) 17.15(5)° (**V.2**).

In the crystal lattice, the dicopper(II) anions of **V.1** and **V.2** are well separated from each other by the bulky tetra-*n*-butylammonium cations (Figures V.6 and V.7). The discrete dicopper(II) anions of **V.2** establish, however, weak hydrogen bonds with the crystallization water molecules through the free carbonyl- and carboxylate-oxygen atoms from the oxamato groups [O···Ow = 2.790(2)–2.949(2) Å]. The value of the intramolecular Cu(1)–Cu(1)^{I} distance (*r*) across the double 2,6-anthracenediamidate bridge in **V.1** is 12.477(2) Å, whereas that through the double 1,5-naphthalenediamidate bridge in **V.2** is

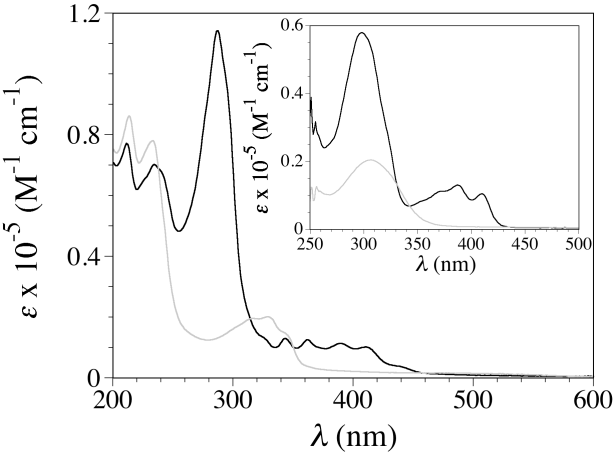

Figure V.8 UV–Vis spectra of **V.1** (black) and **V.2** (grey) in acetonitrile solution. The inset shows the spectra of the corresponding proligands Et_2H_2-2,6-anba (black) and Et_2H_2-1,5-naba (grey) in dimethylsulphoxide.

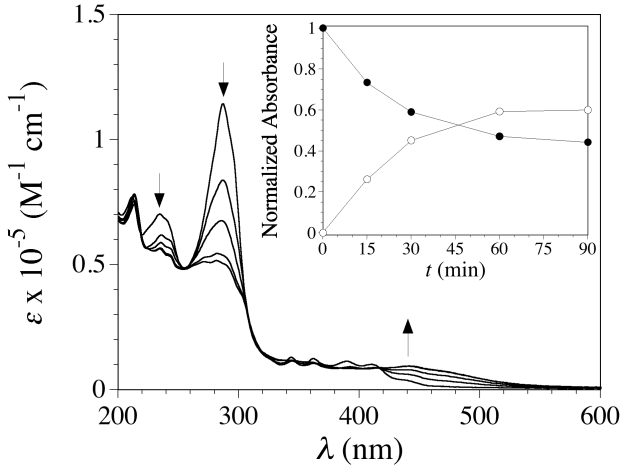

Figure V.9 Electronic absorption spectra of an acetonitrile solution of **V.1** (0.01 mM) after UV light irradiation (λ_{max} = 308 nm) at room temperature under Ar. The arrows indicate the course of the photochemical reaction. The inset shows the time evolution of the normalized absorbance at 287 (●) and 440 nm (○). The solid lines are onle eye-guides.

8.368(2) Å. The values of the shortest intermolecular Cu(1)–Cu(1)^{II} separation are 10.387(2) (**V.1**) and 8.988(2) Å (**V.2**).

V.4 Spectrophotochemical Properties

The electronic absorption spectra of **V.1** and **V.2** in acetonitrile consist of several intense and fairly narrow bands in the far UV region, together with a less intense and much broader largely splitted band in the near UV region with a shoulder that extends into the visible zone (Figure V.8). The high-energy UV bands located at 211, 234, and 287 nm for **V.1** (ε = 70450–114500 M^{-1} cm^{-1}) or at 213 and 232 nm for **V.2** (ε = 78200–86300 M^{-1} cm^{-1}) are commonly assigned to intraligand (IL) π–π* transitions within the anthracene and naphthalene spacers, respectively.[10] The low-energy UV band with up to five peaks centered at 325, 343, 361, 389, and 410 nm for **V.1** (ε = 10400–13250 M^{-1} cm^{-1}) or at 290, 298, 316, 330, and 342 nm for **V.2** (ε = 14050–20330 M^{-1} cm^{-1}), alongside a distinct visible shoulder located around 435 (**V.1**) and 430 nm (**V.2**), can be attributed to IL and metal-to-ligand charge transfer (MLCT) transitions, respectively. So, the unique fivefold vibronic splitting of this low-energy UV band [average energy splitting of *ca.* 1570 (**V.1**) and 1310 cm^{-1} (**V.2**)] is typical of anthracene and naphthalene derivatives,[10] namely that corresponding to the π–π* transition between the ground S_0 and first exited S_1 singlet states. In fact, this $S_0 \rightarrow S_1$ transition band is also present at 387 and 306 nm in somewhat perturbed yet identifiable form in the spectra of the proligands Et_2H_2-2,6-anba and Et_2H_2-1,5-naba in dimethylsulphoxide, respectively (inset of Figure V.8). The overall batochromic shift in the position of this low-energy UV band for both the proligands and the complexes is as expected for the increase in the effective π-conjugation length when going from naphthalene to anthracene.

The electronic absorption spectra recorded upon irradiation at room temperature of a deaerated 0.01 mM acetonitrile solution of **V.1** and **V.2** with UV light (λ_{max} = 308 nm) during 90 min are shown in Figures V.9 and V.10, respectively. In both cases, the low-energy vibronically splitted UV band centered at 361 (**V.1**) and 316 nm (**V.2**) disappears with irradiation time, while a distinct visible band at 440 (**V.1**) and 450 nm (**V.2**) progressively develops in the low-energy side of this IL π–π* transition band. Likewise, a progressive fading of the high-energy UV bands at 234 and 287 nm (**V.1**) or at 213 and 232 nm (**V.2**) occurs, concomitantly with the

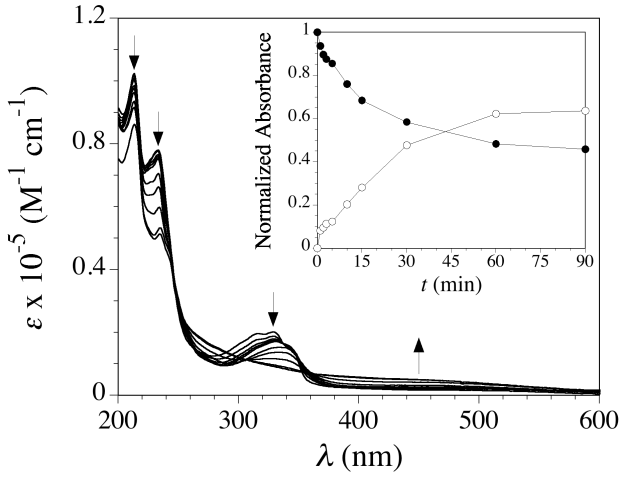

Figure V.10 Electronic absorption spectra of an acetonitrile solution of **V.2** (0.01 mM) after UV light irradiation (λ_{max} = 308 nm) at room temperature under Ar. The arrows indicate the course of the photochemical reaction. The inset shows the time evolution of the normalized absorbance at 330 (●) and 450 nm (○). The solid lines are onle eye-guides.

appearance of two distinct shoulders around 270 and 300 nm (**V.1**) or around 225 and 245 nm (**V.2**).

The electronic absorption spectra of deaerated 0.02 mM dimethylsulfoxide solutions of the proligands Et_2H_2-2,6-anba and Et_2H_2-1,5-naba were also recorded upon UV light (λ_{max} = 308 nm) irradiation at room temperature during 180 min (Figures V.11 and V.12). Although no spectral changes were observed in the UV band at 306 nm of Et_2H_2-1,5-naba upon irradiation (Figure V.12), Et_2H_2-2,6-anba shows however a gradual disappearence of both the low-energy vibronically splitted UV band centered at 387 nm and the high-energy UV band at 298 nm, to give a single UV band at 276 nm (Figure V.11). The dramatically different photochemical behaviour of Et_2H_2-2,6-anba and Et_2H_2-1,5-naba agrees with those earlier reported for anthracene and naphthalene themselves.[10,11]

The presence of clear isosbestic points for **V.1** suggests an equilibrium between only two species up to the attainment of the photostationary state (Figure V.9). This is supported by the

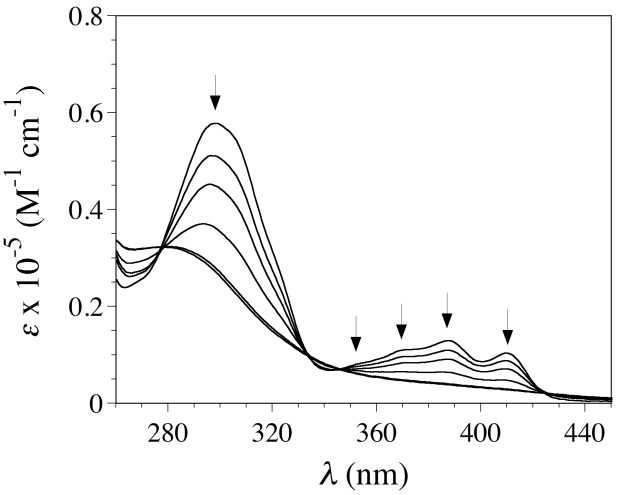

Figure V.11 Electronic absorption spectra of a dimethylsulphoxide solution of Et_2H_2-2,6-anba (0.02 mM) after UV light irradiation (λ_{max} = 308 nm) at room temperature of during 15, 30, 60, 120, and 180 min under Ar. The arrows indicate the course of the photochemical reaction.

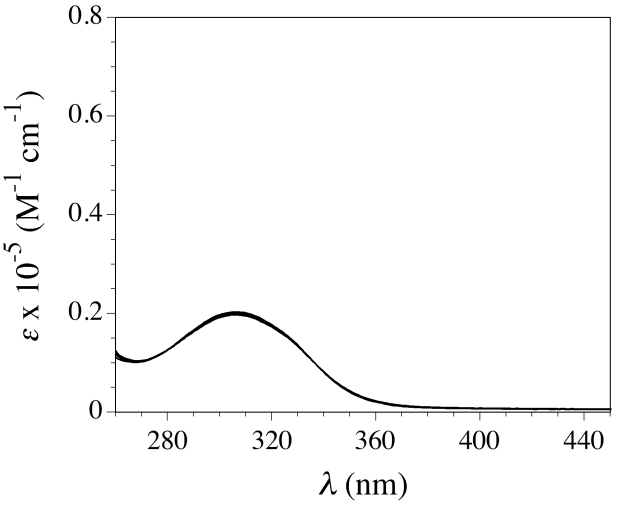

Figure V.12 Electronic absorption spectra of a dimethylsulphoxide solution of Et_2H_2-1,5-naba (0.02 mM) after UV light irradiation (λ_{max} = 308 nm) at room temperature of during 15, 30, 60, 120, and 180 min under Ar. The arrows indicate the course of the photochemical reaction.

representation of the normalized absorbance values at 287 and 440 nm with irradiation time for **V.1**, which shows a crossing point of the two curves at an ordinate value of 0.5, with a final conversion value of up to 0.6 (inset of Figure V.9). In contrast, the appearance of isosbestic points characteristic of an equilibrium between two species is preceded by a short induction period during the first 5 min of irradiation for **V.2** (Figure V.10). This may indicate that an intermediate rapidly forms in a preequilibrium process and that it converts to the final product. Yet the curves of the normalized absorbance values at 333 and 450 nm with irradiation time for **V.2** also shows a crossing point at an ordinate value close to 0.5, with a final conversion value of up to 0.6 (inset of Figure V.10). Once the photostationary state was reached for both **V.1** and **V.2**, no further spectral changes were observed upon standing for several hours at room temperature without irradiation, suggesting thus a very slow (if any) thermal relaxation in solution for the photocycloaddition products of these dicopper(II) metallacyclophanes, as shown for the

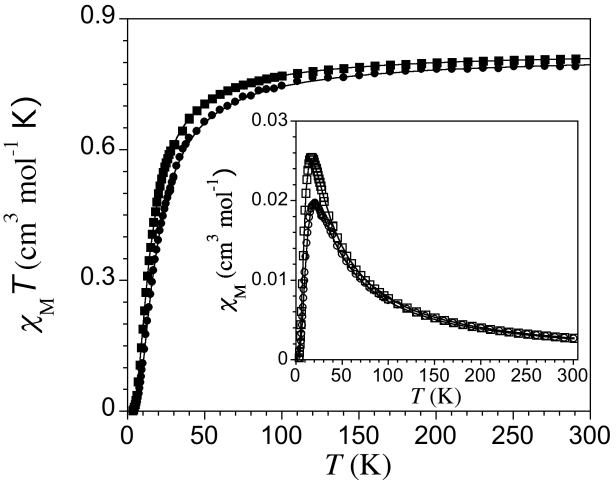

Figure V.13 Temperature dependence of $\chi_M T$ of **V.1** (●) and **V.2** (■). The inset shows the χ_M maxima of **V.1** (○) and **V.2** (□). The solid lines are the best-fit curves (see text).

9,10:9',10' photocycloaddition product of the proligand Et_2H_2-2,6-anba.

These unique spectral changes upon irradiation of **V.1** and **V.2** would be likely related to the formation of the corresponding cyclodimers **V.*c*-1(9,10)** and **V.*c*-2(1,4)** (Figure V.2). Hence, the disparition of the low-energy vibronically splitted IL π–π* transition evidence the loss of the aromatic character within the resulting [4+4] photocycloaddition products, as reported earlier for the photodimerization of anthracene and 2-substituted naphthalenes (Figure V.1a and b).[10,11a,11b] That being so, the presence of a visible band for **V.*c*-1(9,10)** and **V.*c*-2(1,4)** is accordingly attributed to a metal-to-ligand charge transfer (MLCT) transition from the Cu^{II} ions to the benzene rings of the anthracene and naphthalene photodimer moieties respectively, supporting thus the integrity of the dicopper(II) photocycloaddition products in solution. However, the complex photoreaction kinetics found for **V.2** does not exclude that a facile Cope rearrangement of the cyclodimer **V.*c*-2(1,4)** to the corresponding [2+2] photocycloaddition product would occur in solution, as reported earlier for the photodimerization of 1-substituted naphthalenes (Figure V.1c).[11c,11d]

V.5 Photomagnetic Properties

The magnetic properties of **V.1** and **V.2** in the form of the χ_M and $\chi_M T$ *vs*. *T* plots (χ_M being the molar magnetic susceptibility per dinuclear unit and *T* the absolute temperature) are typical of moderately strong antiferromagnetically coupled Cu^{II}_2 pairs (Figure V.13). At room temperature, the $\chi_M T$ values of 0.79 (**V.1**) and 0.81 $cm^3\ mol^{-1}\ K$ (**V.2**) are close to that expected for two magnetically isolated Cu^{II} ions [$\chi_M T = 2 \times (N\beta^2 g_{Cu}^2/3k_B) S_{Cu}(S_{Cu} + 1) = 0.83\ cm^3\ mol^{-1}\ K$ with S_{Cu} = ½ and g_{Cu} = 2.1]. Upon cooling, $\chi_M T$ continuously decreases for both **V.1** and **V.2** and vanishes at *ca.* 4 K, whereas χ_M exhibits a characteristic maximum at 21 (**V.1**) and 17 K (**V.2**) which unambiguously indicates a ground singlet ($S = 0$) spin state resulting from the antiferromagnetic intramolecular coupling between the two Cu^{II} ions through the 2,6-anthracene- (**V.1**) and 1,5-naphthalenediamidate (**V.2**) bridges (inset of Figure V.13).

The least-squares fit of the experimental data of **V.1** and **V.2** through the Bleaney-Bowers expression (eq V.1) for a dinuclear copper(II) complex [$\boldsymbol{H} = -J\boldsymbol{S_1} \cdot \boldsymbol{S_2} + g\beta H(\boldsymbol{S_1} + \boldsymbol{S_2})$ with $S_1 = S_2 =$

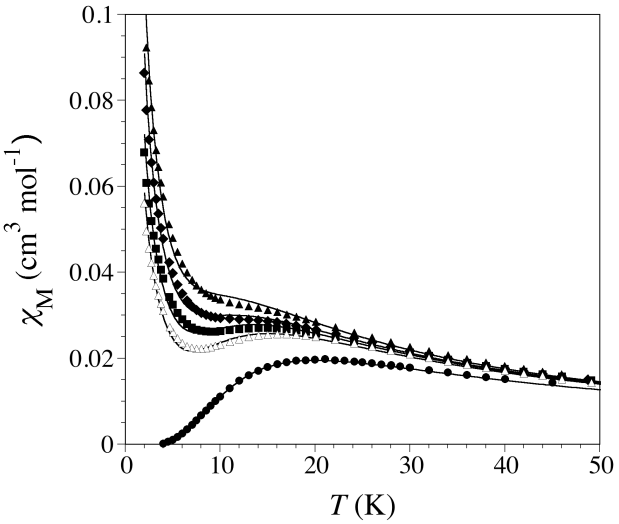

Figure V.14 Temperature dependence of χ_M for **V.1** under dark (●) and after UV light irradiation (λ_{max} = 308 nm) at room temperature during 6 (■), 12 (◆), and 24 h (▲) under Ar and subsequent thermal relaxation by heating at 75 °C during 1h (Δ). The solid lines are the best-fit curves (see text).

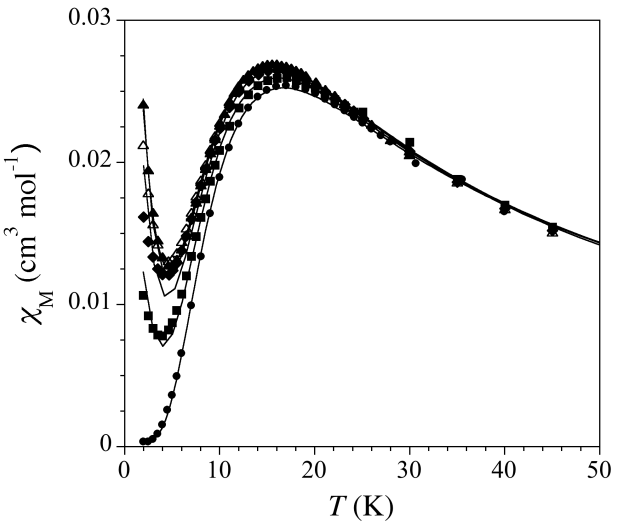

Figure V.15 Temperature dependence of χ_M for **V.2** under dark (●) and after UV light irradiation (λ_{max} = 308 nm) at room temperature during 6 (■), 12 (◆), and 24 h (▲) under Ar and subsequent thermal relaxation by heating at 75 °C during 1h (Δ). The solid lines are the best-fit curves (see text).

S_{Cu} = ½ and $g = g_{Cu}$] gave J = –23.9(1) (**V.1**) and –18.6(1) cm^{-1} (**V.2**) and g = 2.089(1) (**V.1**) and 2.101(1) (**V.2**), with $R = 1.2 \times 10^{-5}$ (**V.1**) and 0.7×10^{-5} (**V.2**) ($R = \sum[(\chi_M T)_{exp} - (\chi_M T)_{calcd}]^2/\sum[(\chi_M T)_{exp}]^2$). The theoretical curves reproduce perfectly well the experimental data (solid lines in Figure V.13). The calculated –J values of **V.1** and **V.2** are similar to those found earlier for their lithium(I) and tetraphenylphosphonium salts of formulas $Li_4[Cu_2(2,6\text{-anba})_2] \cdot 12H_2O$ and $(Ph_4P)_4[Cu_2(2,6\text{-anba})_2] \cdot 4H_2O$ (–J = 21.2 and 23.0 cm^{-1}, respectively) or $Li_4[Cu_2(1,5\text{-naba})_2] \cdot 12H_2O$ and $(Ph_4P)_4[Cu_2(1,5\text{-naba})_2] \cdot 8H_2O$ (–J = 20.5 and 20.7 cm^{-1}, respectively).[8a] As stated earlier, the somewhat greater –J value for **V.1** compared to **V.2** [–J = –23.9 (**V.1**) and 18.6 cm^{-1} (**V.2**)] is quite remarkable given the larger Cu–Cu separation through the double 2,6-anthracenediamidate bridge compared to that through the 1,5-naphthalenediamidate one [r = 12.477(2) (**V.1**) and 8.368(2) Å (**V.2**)]. Once again, this situation clearly evidences the better efficiency of β,β'- over α,α'-substitution pattern on long-range magnetic coupling across extended π-conjugated oligoacene spacers, as we demonstrated earlier, both experimentally and theoretically.[8a]

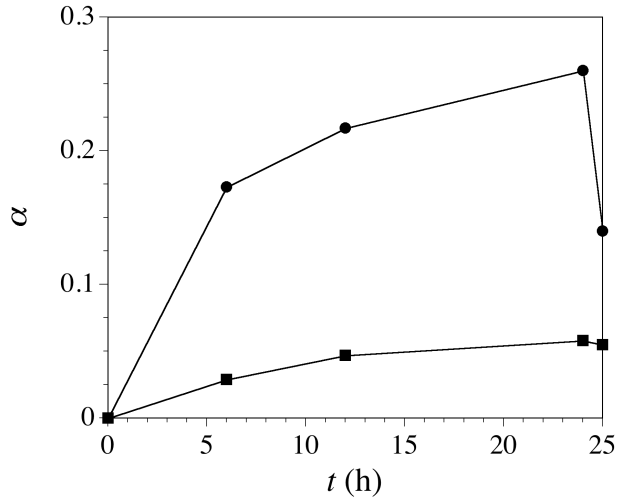

Figure V.16 Time evolution of the calculated α values for the photocycloaddition of **V.1** (●) and **V.2** (■) after UV light irradiation (λ_{max} = 308 nm) during 24 h under Ar at room temperature and subsequent decay upon thermal relaxation by heating at 75 °C during 1h. The solid lines are only eye-guides.

$$\chi_M = (2N\beta^2g^2/k_BT) / [3 + \exp(-J/k_BT)] \qquad (V.1)$$

The magnetic properties recorded after irradiation at room temperature of powdered samples of **V.1** and **V.2** with UV light (λ_{max} = 308 nm) in a Pyrex tube in the absence of dioxygen reveal the occurrence of a slow and incomplete, solid-state photochemical reaction to give the putative [4+4] cycloaddition products **V.*c*-1(9,10)** and **V.*c*-2(1,4)** (Figure V.2). So, the χ_M *vs*. T plots of the irradiated samples of **V.1** and **V.2** for 6, 12, and 24 h show a progressive disappearence of the χ_M maximum at 20 (**V.1**) and 17 K (**V.2**) characteristic of the moderately strong antiferromagnetically coupled dicopper(II) oligoacenophanes, concomitantly with the development of a low-temperature χ_M tail corresponding to the magnetically uncoupled dicopper(II) photocycloaddition products (Figures V.14 and V.15). Moreover, **V.*c*-1(9,10)** slowly relaxes upon heating at 75 ºC for 1h to render **V.1**, as evidenced by the partial disappearence of the low-temperature χ_M tail with the concurrently recovery of the χ_M maximum, suggesting thus that the changes in the magnetic properties upon irradiation of **V.1** are not due to a photodegradation product. This thermally reversible photomagnetic switching is accompanied by a peculiar photo- and thermochromic behavior in the solid state. So, upon irradiation of **V.1** with UV light (λ_{max} = 308 nm) at room temperature during 24 h, a gradual color change from green to brown occurred, the transformation being reversible as evidenced by the partial recovery of the original green color by heating at 75 ºC for 1 h.

Satisfactory least-squares fits of the experimental data for the irradiated samples of **V.1** and **V.2** were obtained by taken into account the presence of a variable amount (α) of a magnetically uncoupled dinuclear copper(II) complex alongside the original antiferromagnetically coupled one [eq V.2 with fixed –J values of 23.9 (**V.1**) and 18.6 cm^{-1} (**V.2**)] (solid lines in Figure V.14 and V.15).

$$\chi_M = \alpha\,(N\beta^2g^2/2k_BT) +$$

Table V.4 Selected experimental and calculated structural data for the optimized molecular geometries of **V.1** using different functionals.[a]

	B97D	PBE	B3LYP	CAMB3LYP	Exp.
Cu–N[b] (Å)	1.998	1.985	1.989	1.972	1.9609(16)
Cu–O[b] (Å)	2.026	1.999	1.965	1.954	1.9432(15)
N–Cu–N[c] (°)	111.5	113.4	113.6	110.5	107.89(7)
O–Cu–O[c] (°)	86.5	84.3	91.3	85.2	85.42(5)
φ[d] (°)	0.9	2.8	5.1	2.7	3.44(5)
ϕ[e] (°)	60.0	57.0	36.9	61.5	58.5(2)
τ[f] (°)	21.1	26.5	49.5	12.9	14.30(5)

[a] The calculated structural data correspond to the BS singlet state of the optimized molecular geometries in acetonitrile solution. [b] Average values of the bond legths at the copper atoms. [c] Average values of the interbond angles at the copper atoms. [d] Dihedral angle between the fused benzene rings from each anthracene spacer. [e] Torsion angle between the copper basal planes and the lateral benzene rings from each anthracene spacer. [f] Tetrahedral twist angle at the copper atoms.

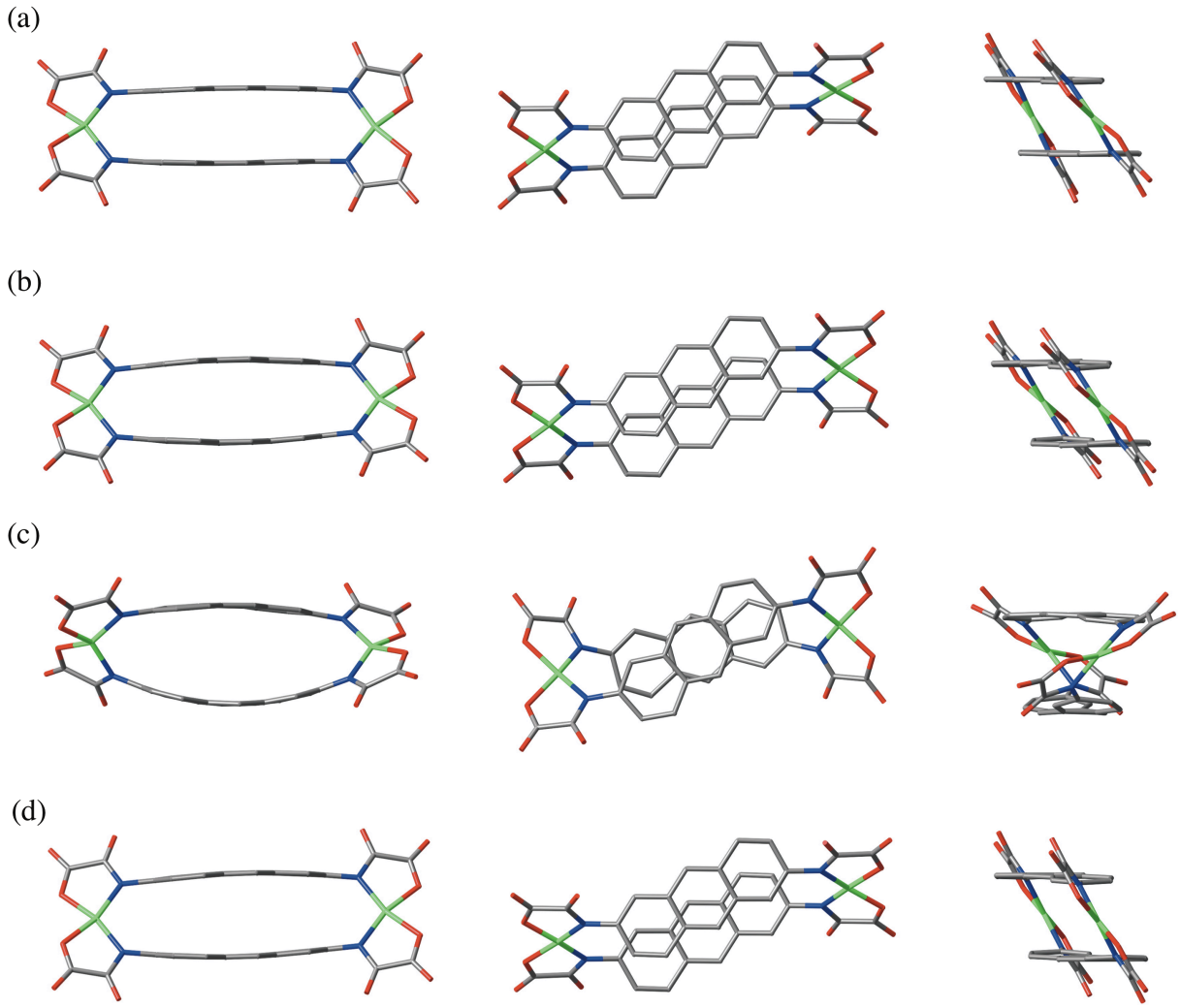

Figure V.17 Front, top, and side projection views of the optimized molecular geometries of **V.1** using the B97D (a), PBE (b), B3LYP (c), and CAMB3LYP (d) functionals (hydrogen atoms have been omitted for clarity).

$$(1 - \alpha)\,(2N\beta^2 g^2/k_B T)\,/\,[3 + \exp(-J/k_B T)] \qquad (V.2)$$

The calculated α values for the photocycloaddition and subsequent decay of **V.1** and **V.2** evidence a lower photochemical efficiency and thermal reversibility for the intramolecular ("pseudo-bimolecular") photodimerization of **V.2** (Figure V.16). This situation agrees with that previously reported for the photodimerization of anthracene and naphthalene themselves and their derivatives.[10,11] Yet they are comparable to those reported for the intramolecular [4+4] photocycloaddition of purely organic anthracenophane and naphthalenophane analogues,[9b,14] reflecting thus the importance of the steric constraints associated with the rigid cyclic or metallacyclic structures.

V.6 Theoretical Calculations

Molecular geometry optimizations. Geometry optimizations of **V.1** and **V.2** were performed in acetonitrile solution using the B97D, PBE, B3LYP, and CAMB3LYP functionals (Figures V.17 and V.18). The validity of the CAMB3LYP functional over other commonly used hybrid functionals was confirmed by the stronger

Table V.5 Selected experimental and calculated structural data for the optimized molecular geometries of **V.2** using different functionals.[a]

	B97D	PBE	B3LYP	CAMB3LYP	Exp.
Cu–N[b] (Å)	1.995	1.986	1.971	1.971	1.965(3)
Cu–O[b] (Å)	2.026	2.003	1.956	1.956	1.936(3)
N–Cu–N[c] (°)	110.0	111.2	109.6	109.6	107.40(14)
O–Cu–O[c] (°)	86.5	84.6	86.0	86.0	86.31(14)
φ[d] (°)	1.1	0.9	0.6	0.5	0.44(5)
ϕ[e] (°)	69.1	70.7	76.1	68.0	70.9(2)
τ[f] (°)	3.3	4.4	1.7	2.7	13.30(5)

[a] The calculated structural data correspond to the BS singlet state of the optimized molecular geometries in acetonitrile solution. [b] Average values of the bond legths at the copper atoms. [c] Average values of the interbond angles at the copper atoms. [d] Dihedral angle between the fused benzene rings from each naphthalene spacer. [e] Torsion angle between the copper basal planes and the lateral benzene rings from each naphthalene spacer. [f] Tetrahedral twist angle at the copper atoms

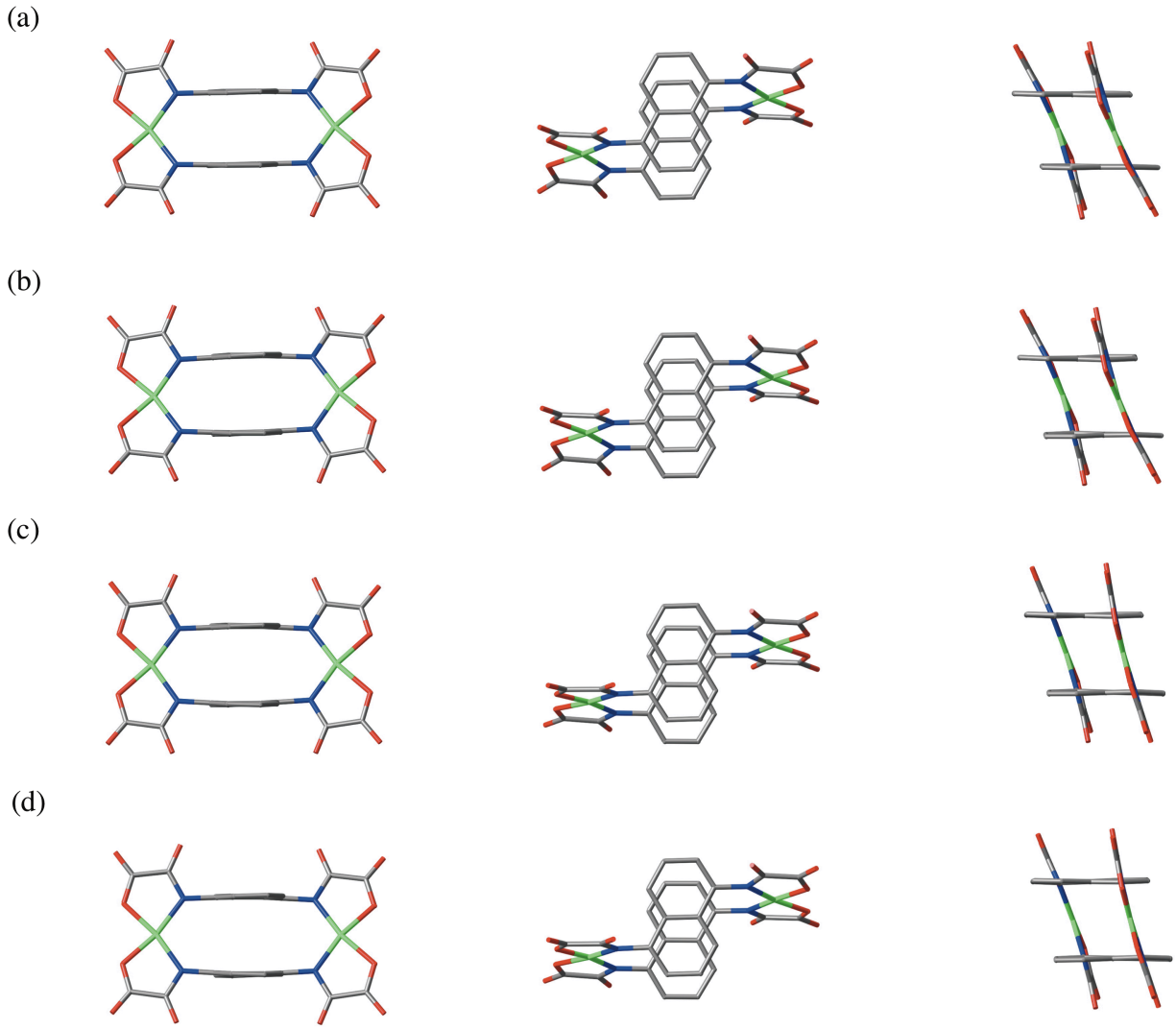

Figure V.18 Front, top, and side projection views of the optimized molecular geometries of **V.2** using the B97D (a), PBE (b), B3LYP (c), and CAMB3LYP (d) functionals (hydrogen atoms have been omitted for clarity).

structural and conformational similarities, in terms of both bond lengths and interbond and torsion angles, between the optimized molecular geometries in acetonitrile solution of **V.1** and **V.2** and those experimentally determined in the solid state by single-crystal X-ray diffraction (Tables V.4 and V.5). Geometry optimizations of the putative cyclodimers, **V.*c*-1(9,10)**, **V.*c*-2(1,4)**, **V.*c*-2(1,2)**, and **V.*c*-2(3,4)**, as well as the corresponding intermediates, **V.*i*-1(9)** and **V.*i*-2(4)**, and transition states, **V.*c*-1(9,10)**[#], **V.*c*-2(1,4)**[#], and **V.*c*-2(3,4)**[#], were then performed in acetonitrile solution using the CAMB3LYP functional (Figures V.19 and V.20). Selected calculated structural data for the titled complexes are summarized in Tables V.6 and V.7.

The optimized molecular geometries in acetonitrile solution of the cyclodimers, **V.*c*-1(9,10)**, ***c*-V.2(1,4)**, **V.*c*-2(1,2)**, and **V.*c*-2(3,4)**, reveal the occurrence of a significant bond length alternation within the two directly connected cyclohexadiene rings in the oligoacenophane photodimer bridge skeleton. So, the two short and four long intra-ring C–C distances with average values of 1.41 [**V.*c*-1(9,10)**]/1.37 [**V.*c*-2(1,4)**]/1.38 [**V.*c*-2(1,2)**]/1.38 Å [**V.*c*-

2(3,4)] and 1.52 [**V.*c*-1(9,10)**]/1.53 [**V.*c*-2(1,4)**]/1.51 [**V.*c*-2(1,2)**]/1.51 Å [**V.*c*-2(3,4)**] respectively, correspond to those expected for double and single carbon-carbon bonds (Tables V.6 and V.7). In contrast, **V.1** and **V.2** show no appreciable bond alternation within the benzene rings, with mean values of 1.42 (**V.1**)/1.41 Å (**V.2**) for the six intra-ring C–C distances (Tables V.6 and V.7). Yet the most salient structural feature of the cyclodimers is the rather long inter-ring C–C distances of 1.65 [**V.*c*-1(9,10)**]/1.66 [**V.*c*-2(1,4)**]/1.62 [**V.*c*-2(1,2)**]/1.60 Å [**V.*c*-2(3,4)**] for the two newly formed single carbon-carbon bonds, which are however shorter than the corresponding inter-ring C–C separations of 3.80 (**V.1**)/3.44 Å (**V.2**) in the reactants (Tables V.6 and V.7). This situation agrees with that previously reported for the X-ray crystal structure of the 9,10:9',10' anthracene photodimer, which also shows long inter-ring single carbon-carbon bonds [C–C = 1.62 Å].[12]

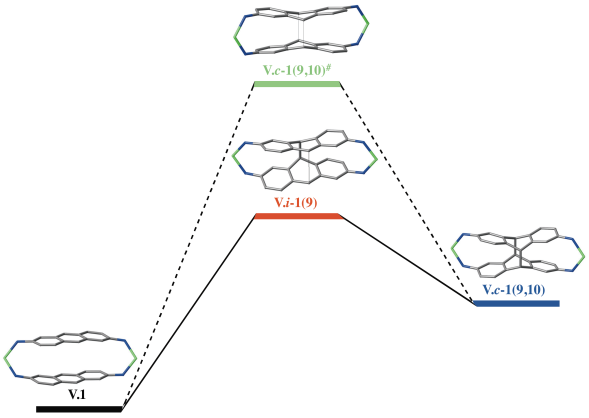

Figure V.19 Reaction pathway for the photocycloaddition of **V.1** showing the metallacyclic cores for the optimized molecular geometries in acetonitrile solution of the reactant (black), the cyclodimer product (blue), the intermediate (red), and the transition state (green).

In addition, the fused benzene rings from the oligoacene spacers are considerably bent in the cyclodimers **V.*c*-1(9,10)** and **V.*c*-2(1,4)**, as a result of the pronounced boat conformation of the directly connected cyclohexadiene rings (Figures V.19 and V.20). By comparison, the cyclodimers **V.*c*-2(1,2)** and **V.*c*-2(3,4)** show smaller deviations from planarity of the two naphthalene halves because of the almost planar conformation of the directly connected cyclohexadiene rings (Figure V.19). So, the values of the dihedral angle beween the cyclohexadiene and fused benzene ring from each oligoacene spacer (φ) are 43.7 [**V.*c*-1(9,10)**]/46.9 [**V.*c*-2(1,4)**]/5.7 [**V.*c*-2(1,2)**]/4.9° [**V.*c*-2(3,4)**] (Tables V.6 and V.7). Yet the φ value is slightly smaller for **V.*c*-1(9,10)** than that found in the 9,10:9',10' anthracene photodimer itself (φ = 46°),[12] more likely due to the steric constraints of the rigid metallacyclic core structure. Overall, these structural features are consistent with a complete loss of the aromatic character of the two facing 2,6-anthracene and 1,5-naphthalene spacers of **V.1** and **V.2** upon intramolecular [4+4] photocycloaddition through the more reactive carbon atoms at the 9,10/9',10' and 1,4/1',4' positions, respectively. A partial recovery of the aromatic character of the naphtalene spacers would then occur upon the putative intramolecular Cope rearrangement to the corresponding [2+2] photocycloaddition products.

On the other hand, the optimized molecular geometries in acetonitrile solution of the intermediates, **V.*i*-1(9)** and **V.*i*-2(4)**, and the transition states, **V.*c*-1(9,10)$^{\#}$** and **V.*c*-2(1,4)$^{\#}$**, which are involved in the [4+4] photocycloaddition of **V.1** and **V.2** to **V.*c*-1(9,10)** and **V.*c*-2(1,4)** agree with those expected for concerted (synchronous) and non-concerted (asynchronous) pathways (Figures V.19 and V.20). So, the intermediates with a ligand biradical character show short and long inter-ring C–C distances of

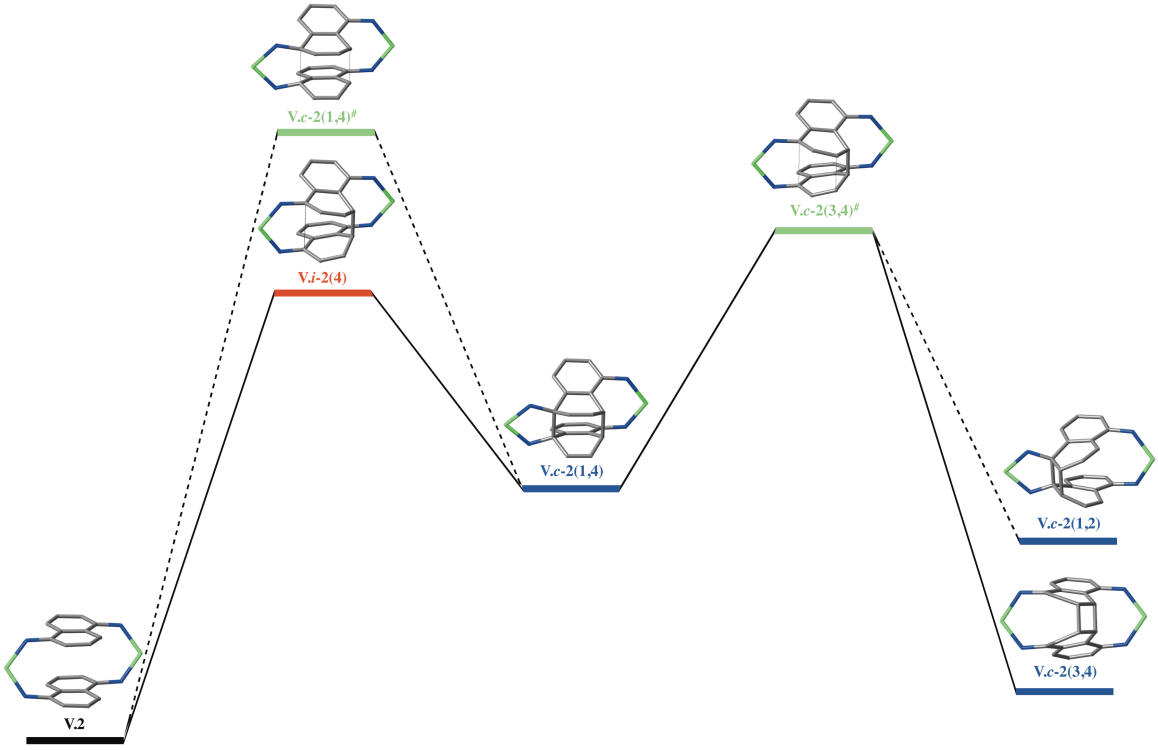

Figure V.20 Reaction pathway for the photocycloaddition of **V.2** showing the metallacyclic cores for the optimized molecular geometries in acetonitrile solution of the reactant (black), the cyclodimer products (blue), the intermediate (red), and the transition states (green).

1.69 [**V.*i*-1(9)**]/1.65 Å [**V.*i*-2(4)**] and 3.39 [**V.*i*-1(9)**]/3.04 Å [**V.*i*-2(4)**] respectively, for the two successively forming, asymmetric single carbon-carbon bonds, whereas the non-radical transition states exhibit intermediate inter-ring C–C distances of 2.30 [**V.*c*-1(9,10)**$^{\#}$]/2.21 Å [**V.*c*-2(1,4)**$^{\#}$] for the two simultaneously forming, symmetric single carbon-carbon bonds (Tables V.6 and V.7).

Instead, the transition state **V.*c*-2(3,4)**$^{\#}$ that is involved in the intramolecular Cope rearrangement of the [4+4] photocycloaddition product **V.*c*-2(1,4)** to the corresponding [2+2] photocycloaddition product **V.*c*-2(3,4)** shows intermediate and long inter-ring C–C distances of 2.25 and 2.90 Å for the two simultaneously forming/breaking single carbon-carbon bonds at the 3/3' and 1/1' positions respectively, together with a relatively short inter-ring C–C distance of 1.59 Å for the remaining single carbon-carbon bond at the 4/4' position (Table V.7). All these inter-ring C–C separations are indeed shorter than the Van der Waals contact (3.40 Å), revealing thus the occurrence of incipient single carbon-carbon bond formation and breaking between the two facing cyclohexadiene rings from each naphthalene spacer.

Energy calculations. DF energy calculations were performed on the BS singlet (S = 0) and triplet (S = 1) states of the optimized molecular geometries in acetonitrile solution of **V.1** and **V.2** and the putative cyclodimers, **V.*c*-1(9,10)**, **V.*c*-2(1,4)**, **V.*c*-2(1,2)**, and **V.*c*-2(3,4)**, as well as the corresponding intermediates, **V.*i*-1(9)** and **V.*i*-2(4)**, and transition states, **V.*c*-1(9,10)**$^{\#}$, **V.*c*-2(1,4)**$^{\#}$, and **V.*c*-2(3,4)**$^{\#}$, using the CAMB3LYP functional (see Computational Details). Selected calculated structural energy data for the titled complexes are summarized in Table V.8.

The calculated values of the standard free energy of **V.*c*-1(9,10)** and **V.*c*-2(1,4)** relative to those of the reactants (ΔG) clearly indicate that the [4+4] photocycloaddition product of the dicopper(II) naphthalenophane are more thermodinamically unfavored than that of the dicopper(II) anthracenophane (Table V.8). This agrees with the photomagnetic studies of **V.1** and **V.2** in the solid state, which also reveals a less efficiency of the photocycloaddition reaction in the latter case (Figure V.16).

In both cases, however, the calculated ΔG values of **V.*i*-1(9)** and **V.*i*-2(4)** are lower than those of **V.*c*-1(9,10)**$^{\#}$ and **V.*c*-2(1,4)**$^{\#}$ (Table V.8), indicating that the dicopper(II) biradical intermediates possessing a single carbon-carbon bond at the 9/9' and 4/4' positions respectively, are much more stable than the alternative dicopper(II) non-radical transition states with two incipient carbon-carbon bonds at the 9,10/9',10' and 1,4/1',4' positions, respectively. This situation conforms with a non-concerted (asynchronous) against a concerted (synchronous) mechanism of double carbon-carbon bond formation (solid and dashed lines respectively, in Figures V.19 and V.20), in agreement with recent reaction path calculations on the photodimerization of simpler oligoacenes.[13] Yet the rather high ΔG values for the singly carbon-carbon bonded, dicopper(II) biradical intermediates, **V.*i*-1(9)** and **V.*i*-2(4)**, when compared to those of the dicopper(II) cyclodimers, **V.*c*-1(9,10)** and **V.*c*-2(1,4)**, agree with the experimental results concerning the unfavorable thermal relaxation in solution of the [4+4] photocycloaddition product at room temperature (RT = 0.6 kcal mol^{-1} at 298.15 K) or in the solid state by heating. So, the calculated values of the energy barrier, $\Delta\Delta G = \Delta G$[**V.*i*-1(9)**] – ΔG[**V.*c*-1(9,10)**] and ΔG[**V.*i*-2(4)**] – ΔG[**V.*c*-2(1,4)**], are 18.9 and 8.8 kcal mol^{-1}, respectively. This situation is also in agreement with earlier experimental and theoretical investigations on purely organic anthracenophanes, which evidence the occurrence of a bond dissociation of the anthracenophane photodimer only at high pressures.[14]

Table V.6 Selected calculated structural data for the photocycloaddition of **V.1**.[a]

	V.1	**V.*c*-1(9,10)**	**V.*c*-1(9,10)**$^{\#}$	**V.*i*-1(9)**
C–C (intra-ring)[b] (Å)	1.401 (1.393)	1.406	1.428	1.425
	1.404 (1.397)	1.406	1.428	1.428
	1.405 (1.397)	1.515	1.452	1.429
	1.405 (1.401)	1.516	1.452	1.432
	1.440 (1.433)	1.516	1.452	1.511
	1.442 (1.435)	1.517	1.453	1.512
C–C (inter-ring)[c] (Å)	3.797 (3.700)	1.653	2.300	1.687
	3.797 (3.700)	1.653	2.300	3.393
φ[d] (°)	2.7 (3.4)	43.7	26.7	19.4
ϕ[e] (°)	61.5 (58.5)	80.7	83.6	82.3
τ[f] (°)	12.9 (14.3)	3.3	3.0	3.4

[a] The calculated structural data correspond to the BS singlet state of the optimized molecular geometries in acetonitrile solution using the CAMB3LYP functional (see Computational Details). The experimental structural data are given in parentheses. [b] Distances between the carbon atoms of the central benzene ring from each anthracene spacer. [c] Distances between the equivalent carbon atoms of the central benzene rings from the two facing anthracene spacers. [d] Dihedral angle between the fused rings from each anthracene spacer. [e] Average torsion angle between the copper basal planes and the lateral benzene rings from each anthracene spacer. [f] Tetrahedral twist angle at the copper atoms.

Table V.7 Selected calculated structural data for the photocycloaddition of **V.2**.[a]

	V.2	**V.*c*-2(1,4)**	**V.*c*-2(1,2)**	**V.*c*-2(3,4)**	**V.*c*-2(1,4)**$^{\#}$	**V.*c*-2(3,4)**$^{\#}$	**V.*i*-2(4)**
C–C (intra-ring)[b] (Å)	1.378 (1.359)	1.337	1.345	1.347	1.361	1.393	1.372
	1.383 (1.363)	1.408	1.415	1.416	1.422	1.398	1.423
	1.417 (1.402)	1.513	1.471	1.489	1.453	1.419	1.420
	1.424 (1.414)	1.519	1.494	1.494	1.466	1.475	1.457
	1.431 (1.422)	1.525	1.518	1.505	1.468	1.517	1.510
	1.438 (1.430)	1.541	1.576	1.561	1.487	1.534	1.516
C–C (inter-ring)[c] (Å)	3.371 (3.353)	1.624	1.593	1.594	2.205	1.585	1.650
	3.501 (3.473)	1.699	1.640	1.607	2.205	2.245	3.043
						2.903	
φ[d] (°)	3.2 (0.4)	46.9	5.7	4.9	28.0	27.3	25.3
ϕ[e] (°)	68.0 (70.9)	69.8	76.3	73.3	75.6	73.4	72.5
τ[f] (°)	2.7 (13.3)	1.4	1.7	1.8	1.1	3.5	2.4

[a] The calculated structural data correspond to the BS singlet state of the optimized molecular geometries in acetonitrile solution using the CAMB3LYP functional (see Computational Details). The experimental structural data are given in parentheses. [b] Distances between the carbon atoms of the proximal benzene ring from each naphthalene spacer. [c] Distances between the equivalent carbon atoms of the proximal benzene rings from the two facing naphthalene spacers. [d] Dihedral angle between the fused rings from each naphthalene spacer. [e] Average torsion angle between the copper basal planes and the benzene ring from each naphthalene spacer. [f] Average tetrahedral twist angle at the copper atoms.

Table V.8 Selected calculated energy data for the photocycloaddition of **V.1** and **V.2**.[a]

Complex	E^b (a.u.)	ΔH^c (kcal mol^{-1})	ΔG^d (kcal mol^{-1})	$\Delta E_{ST}{}^e$ (cm^{-1})
V.1	–5781.5473	0	0	–18.8 (–23.9)
V.*c*-1(9,10)	–5781.5105	23.1	27.6	+0.9
V.*c*-1(9,10)$^{\#}$	–5781.4391	67.9	68.8	
V.*i*-1(9)	–5781.4736	46.2	46.5	
V.2	–5474.7404	0	0	–19.0 (–18.6)
V.*c*-2(1,4)	–5474.6673	45.9	49.6	+0.8
V.*c*-2(1,2)	–5474.6683	45.2	47.4	+3.3
V.*c*-2(3,4)	–5474.6671	46.0	42.9	–7.8
V.*c*-2(1,4)$^{\#}$	–5474.6082	83.0	81.8	
V.*c*-2(3,4)$^{\#}$	–5474.6392	63.5	64.5	
V.*i*-2(4)	–5474.6459	59.3	58.4	

[a] DF energy calculations were performed on the ground BS singlet ($S = 0$) state of the optimized molecular geometries in acetonitrile solution using the CAMB3LYP functional (see Computational Details). [b] Potential energy minimum. [c] Standard enthalpy values relative to those of the reactants. [d] Standard free energy values relative to those of the reactants. [e] Singlet-triplet energy gap ($\Delta E_{ST} = J$). The experimental J values are given in parentheses.

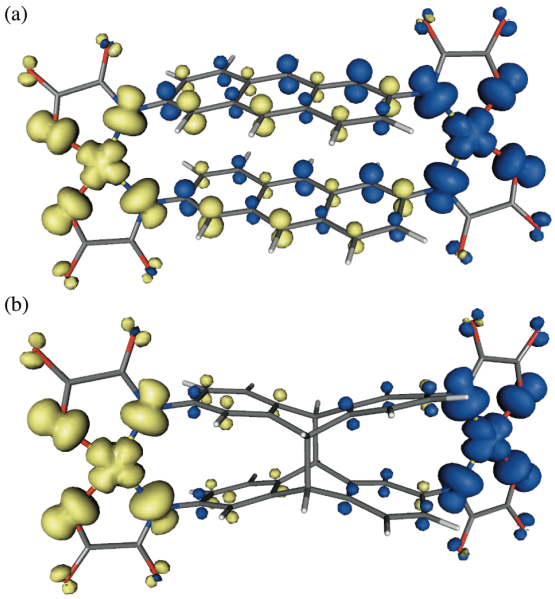

Figure V.21 Perspective views of the calculated spin density distribution for the BS singlet spin states of **V.1** (a) and **V.*c*-1(9,10)** (b). Yellow and blue contours represent positive and negative spin densities, respectively. The isodensity surface corresponds to a value of 0.0015 e bohr^{-3}.

On the other hand, the calculated ΔG values of **V.*c*-2(1,2)** and **V.*c*-2(3,4)** indicate a small but significant stabilization when compared to **V.*c*-2(1,4)** (Table V.8), the more stable cyclodimer being **V.*c*-2(3,4)** in agreement with related reaction pathway calculations on the photodimerization of naphthanene itself.[13] However, DF energy calculations reveal the presence of a dicopper(II) transition state with two incipient carbon-carbon bonds at the 3,4/3',4' positions, **V.*c*-2(3,4)$^{\#}$**, which is somewhat less stable than the dicopper(II) biradical intermediate, **V.*i*-2(4)**, possessing a single carbon-carbon bond at the 4/4' positions (Table V.8). Overall, this indicates that the Cope rearrangement of the initial [4+4] photocycloaddition product, **V.*c*-2(1,4)**, to give the corresponding [2+2] photocycloaddition product, **V.*c*-2(3,4)**, is kinetically unfavored over the thermal relaxation to the original dicopper(II) naphthalenophane precursor (Figure V.19).

More importantly, the DF energy calculations on the BS singlet and triplet spin states of the optimized geometries in acetonitrile solution of the reactants, **V.1** and **V.2**, and the cyclodimers, **V.*c*-1(9,10)** and **V.*c*-2(1,4)**, are consistent with the occurrence of a switch from a moderately strong antiferromagnetic coupling in the dicopper(II) oligoacenophane precursors to the lack of magnetic coupling in the corresponding [4+4] photocycloaddition products. So, the calculated values of the singlet-triplet energy gap for **V.*c*-1(9,10)** and **V.*c*-2(1,4)** are almost negligible ($\Delta E_{ST} = J = +0.9$ [**V.*c*-1(9,10)**] and +0.8 cm^{-1} [**V.*c*-2(1,4)**]; Table V.8), as expected due to the complete loss of aromatic character of the oligoacene spacers in the [4+4] photocycloaddition products. Yet the calculated J values for **V.1** and **V.2** are similar [$J = -18.8$ (**V.1**) and –19.0 cm^{-1} (**V.2**); Table V.8], in spite of the largely different values of the intermetallic distance resulting from the inclusion of an additional fused benzene ring in the oligoacene spacer [r = 12.453 (**V.1**) and 8.295 Å (**V.2**)]. Moreover, they are very close to the experimental ones [J = –23.9 (**V.1**) and –18.6 cm^{-1} (**V.2**) with r = 12.477(2) (**V.1**) and 8.368(2) Å (**V.2**)].

On the other hand, the DF energy calculations on the BS singlet and triplet spin states of the optimized geometries in acetonitrile solution of the cyclodimers **V.*c*-2(1,2)** and **V.*c*-2(3,4)** evidence the occurrence of a small but nonnegligible, either ferro- or antiferromagnetic coupling respectively, which contrast with the almost negligible ferromagnetic coupling found for the cyclodimer **V.*c*-2(1,4)** (J = +0.8 [**V.*c*-2(1,4)**]/+3.3 [**V.*c*-2(1,2)**]/–7.8 cm^{-1} [**V.*c*-2(3,4)**]; Table V.8). This situation agrees with the aforementioned partial recovery of aromatic character of the naphthalene spacers in the putative [2+2] photocycloaddition products resulting from the putative intramolecular Cope rearrangement of the [4+4] photocycloaddition product and, in turn, it clearly discards the occurrence of a solid-state intramolecular Cope rearrangement of **V.*c*-2(1,4)** to give neither **V.*c*-2(1,2)** nor **V.*c*-2(3,4)**.

Spin density analysis. Spin densities obtained by natural bond orbital (NBO) analysis on the BS singlet state of the optimized molecular structures in acetonitrile solution of **V.1** and **V.2** and the cyclodimers **V.*c*-1(9,10)** and **V.*c*-2(1,4)** conform to the interruption of the π-conjugation upon [4+4] photocycloaddition of the two facing oligoacene spacers (Figures V.21 and V.22). As stated earlier,[8a] the spin polarization and spin delocalization effects into the extended π-conjugated oligocenediamidate bridges lead to significant values of the spin density of opposite sign at the adjacent carbon atoms of the fused benzene rings in **V.1** and **V.2** (Figures V.21a and V.22a). On the contrary, the spin polarization and spin delocalization effects across the non-conjugated oligoacenediamidate photodimer bridge skeleton in **V.*c*-1(9,10)** and **V.*c*-2(1,4)** are restricted to the benzene rings, the values of the spin density at the tertiary bridgehead carbon atoms of the fused cyclohexadiene rings being strictly zero (Figures V.21b and V.22b). Hence, a net decrease of the exchange interaction between the unpaired electrons occupying the $d_{x^2-y^2}$ orbitals ('magnetic orbitals') of each square planar Cu^{II} ion results for **V.*c*-1(9,10)** and **V.*c*-2(1,4)** relative to **V.1** and **V.2** respectively, which is ultimately responsible for the photomagnetic switching behavior observed experimentally in the solid state.

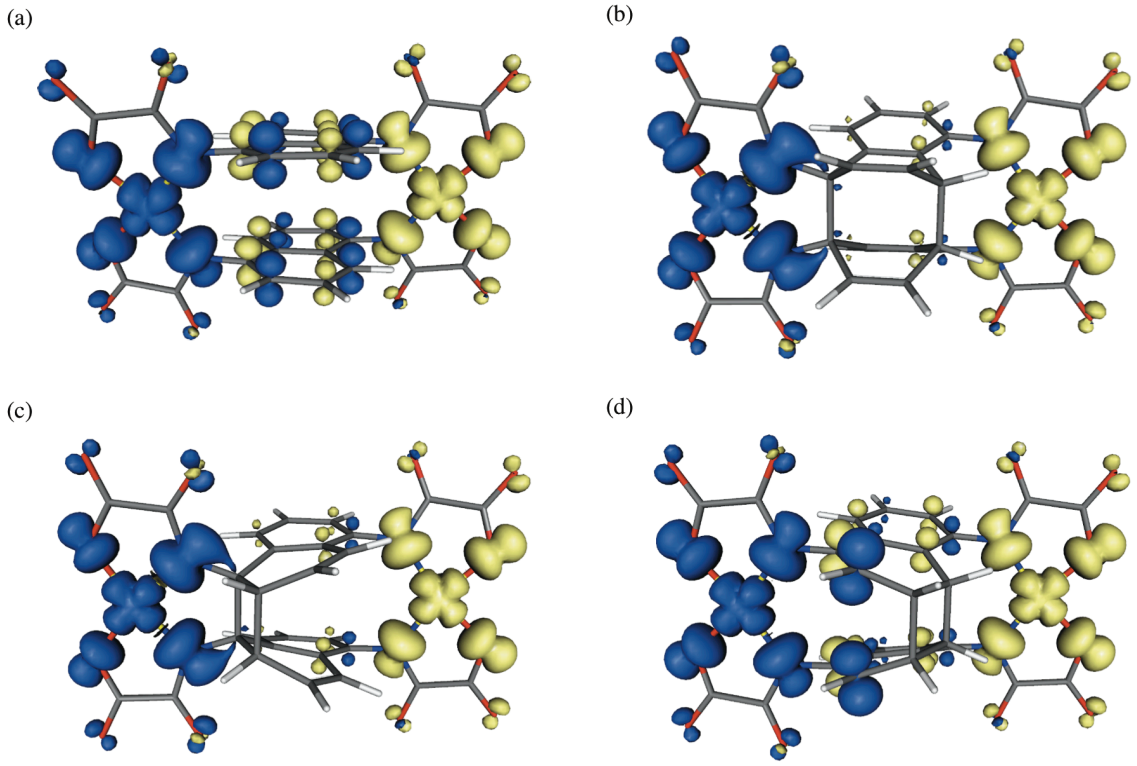

Figure V.22 Perspective views of the calculated spin density distribution for the BS singlet spin states of **V.2** (a), **V.*c*-2(1,4)** (b), **V.*c*-2(1,2)** (c), and **V.*c*-2(3,4)** (d). Yellow and blue contours represent positive and negative spin densities, respectively. The isodensity surface corresponds to a value of 0.0015 e bohr^{-3}.

At this regards, the spin densities obtained by NBO analysis on the BS singlet state of the optimized molecular structure in acetonitrile solution of the cyclodimer **V.*c*-2(3,4)** agree with the partial recovery of the π-conjugation into the dicopper(II) naphthalenophane photodimer bridge skeleton upon intramolecular Cope rearrangement of the [4+4] photocycloaddition product to the corresponding [2+2] photocycloaddition product. In fact, the spin polarization by the amidate nitrogen atoms leads to significant values of the spin density of opposite sign at the directly attached sp^2-hybridized carbon atoms of the fused cyclohexadiene rings, which are ultimately reponsible for the small antiferromagnetic coupling in **V.*c*-2(3,4)** (Figure V.22d). In contrast, the spin delocalization effects by the amidate nitrogen atoms dominate over the spin polarization ones leading to relatively small values of the spin density of the same sign at the directly attached sp^3-hybridized carbon atoms of the cyclohexadiene rings in both **V.*c*-2(1,4)** and **V.*c*-2(1,2)**, which explain the almost negligible to small ferromagnetic coupling (Figures V.22b and V.22c).

V.7 Concluding Remarks

In this work, we present a complementary experimental and theoretical study on long-range magnetic coupling in a family of dinuclear copper(II) metallacyclophanes with extended π-conjugated oligoacene spacers as new examples of photoswitchable magnetic wires. The oxamato-based dicopper(II) 2,6-anthraceno- and 1,5-naphthalenophanes resulting from the self-assembly of the ligands 2,6-anba and 1,5-naba with Cu^{II} ions exhibit an antiferromagnetically coupled to magnetically uncoupled (ON/OFF) switching behavior upon UV light irradiation and heating in the solid state. This photomagnetic bistability results from a putative [4+4] photocycloaddition of the two facing anthracene and naphthalene spacers through the more reactive carbon atoms at the 9,10/9',10' and 1,4/1',4' positions of the central and lateral benzene rings respectively, as supported by molecular and electronic structure calculations. Energy calculations on the relative stability of the dicopper(II) photocycloaddition products evidence that there do not exist severe steric constraints associated to the metallacyclic structure that preclude the formation of the resulting [4+4] photodimer of anthracene and naphthalene. Moreover, they allow explaining the lower photochemical efficiency and thermal reversibility for the photodimerization of the dicopper(II) naphthalenophane while excluding the subsequent Cope rearrengement to the corresponding [2+2] photodimer. Finally, the calculations on the energetics and reaction pathway of the [4+4] photocycloaddition reaction support the singly carbon-carbon bonded, biradical ligand nature of the dicopper(II) intermediate against the alternative doubly carbon-carbon bonded, dicopper(II) transition state for a non-concerted *vs*. concerted mechanism of double carbon-carbon bond formation, respectively. This intramolecular ("pseudo-bimolecular") reaction constitutes a unique example of coordination-driven self-assembly for the supramolecular control of photochemical reactivity and photophysical properties, both in solution and in the solid state.

V.8 Experimental Section

Materials. All chemicals were of reagent grade quality. They were purchased from commercial sources and used as received. 2,6-Anthracenediamine was prepared as reported in the literature.[8b]

Physical techniques. Elemental analyses (C, H, N) were performed at the Servicio Central de Soporte a la Investigación (SCSIE) at the Universitat de València (Spain). FT-IR spectra were recorded on a Nicolet-5700 spectrophotometer as KBr pellets. The irradiation experiments were carried out in a photoreactor equipped with eight UVB lamps (λ in the range of 281–315 nm, λ_{max}

centered at 308 nm). UV-vis spectra were recorded on an Agilent Technologies-8453 spectrophotometer equipped with a UV-vis Chem Station. Variable-temperature (2.0–300 K) magnetic susceptibility measurements were carried out with a SQUID magnetometer under an applied field of 10 kOe ($T \geq 50$ K) and 100 Oe ($T < 50$ K). The experimental data were corrected for the diamagnetic contributions of the constituent atoms and the sample holder as well as for the temperature-independent paramagnetism (tip) of the Cu^{II} ion (60×10^{-6} cm^3 mol^{-1}).

Preparations of the ligands. Et_2H_2-2,6-anba: Ethyl oxalyl chloride ester (2.3 mL, 20 mmol) was added all at once to a solution of 2,6-anthracenediamine (2.08 g, 10 mmol) in THF (250 mL) under vigorous stirring at 0 °C on an ice-bath. The reaction mixture was charged with triethylamine (2.8 mL, 20 mmol) and it was heated to reflux for 3 h under argon. The light yellow solid was collected by filtration after cooling, washed thoroughly with water to eliminate the precipitate of Et_3NHCl, and dried under vacuum (3.3 g, 80% yield). Anal. Calcd for $C_{22}H_{20}N_2O_6$: C, 64.71; H, 4.90; N, 6.86. Found: C, 65.03; H, 4.78; N, 6.98. ^{1}H NMR (C_2D_6SO): δ = 1.31 (t, J = 7.2 Hz, 6 H, 2 CH_3), 4.33 (q, J = 7.2 Hz, 4–H, 2 CH_2O), 7.79 (d, J = 7.7 Hz, 2 H, 3–H and 7–H of $C_{14}H_8N_2$), 8.04 (d, J = 9.2 Hz, 2 H, 4–H and 8–H of $C_{14}H_8N_2$), 8.46 (s, 2 H, 1–H and 5–H of $C_{14}H_8N_2$), 8.56 (s, 2 H, 9–H and 10–H of $C_{14}H_8N_2$), 10.99 (s, 2 H, 2–NH). IR (KBr): ν = 3222 (NH), 1735, 1693 cm^{-1} (CO).

Et_2H_2-1,5-naba: Ethyl oxalyl chloride ester (7.0 mL, 60 mmol) was added all at once to a solution of 1,5-naphthalenediamine (5.75 g, 30 mmol) in THF (250 mL) under vigorous stirring at 0 °C on an ice-bath. The reaction mixture was charged with triethylamine (2.8 mL, 20 mmol) and it was heated to reflux for 1 h. The light grey solid was collected by filtration after cooling, washed thoroughly with water to eliminate the precipitate of Et_3NHCl, and dried under vacuum (9.25 g, 85% yield). Anal. Calcd for $C_{18}H_{18}N_2O_6$: C, 60.34; H, 5.03; N, 7.82. Found: C, 60.77; H, 5.17; N, 7.52. ^{1}H NMR (C_2D_6SO): δ = 1.34 (t, J = 7.2 Hz, 6 H, 2 CH_3), 4.36 (q, J = 7.2 Hz, 4 H, 2 CH_2O), 7.59 (dd, J = 7.2 and 2.8 Hz, 2 H, 4–H and 8–H of $C_{10}H_6N_2$), 7.60 (t, J = 7.2 Hz, 2 H, 3–H and 7–H of $C_{10}H_6N_2$), 7.91 (dd, J = 6.3 and 2.8 Hz, 2 H, 2–H and 6–H of $C_{10}H_6N_2$), 10.96 (s, 2 H, 2 NH). IR (KBr): ν = 3207 (NH), 1738, 1689 cm^{-1} (CO).

Preparations of the complexes. (nBu$_4$N)$_4$[Cu$_2$(2,6-anba)$_2$] (V.1): A 1.0 M methanolic solution of nBu$_4$NOH (4.0 mL, 4.0 mmol) was added to an aqueous suspension (20 mL) of H_2Et_2-2,6-anba (0.41 g, 1.0 mmol). An aqueous solution (25 mL) of $CuCl_2 \cdot 2H_2O$ (0.17 g, 1.0 mmol) was then added dropwise under stirring. The resulting green mixture was filtered to remove the rest of solid particles and then it was extracted with dichloromethane. The organic phase was separated from the mixture and dried over a molecular sieve to give a deep green solution. Solvent was removed under vacuum and the resulting dark green solid was recovered with tetrahydrofuran, collected by filtration, washed with acetone and diethyl eter, and dried under vacuum. Recrystallization from an acetonitrile/methanol mixture (10:1, v/v) afforded X-ray quality crystals of **V.1** as green tiny prisms upon slow vapor diffusion of acetone in a closed flask (0.81 g, 90% yield). Anal. Calcd for $C_{100}H_{160}Cu_2N_8O_{12}$: C, 66.97; H, 8.99; N, 6.25%. Found: C, 65.81; H, 9.08; N, 6.12%. IR (KBr): ν = 1650, 1604 cm^{-1} (CO).

(nBu$_4$N)$_4$[Cu$_2$(1,5-naba)$_2$]·4H$_2$O (V.2): A 1.0 M methanolic solution of nBu$_4$NOH (4.0 mL, 4.0 mmol) was added to an aqueous suspension (20 mL) of H_2Et_2-2,6-anba (0.41 g, 1.0 mmol). An aqueous solution (25 mL) of $CuCl_2 \cdot 2H_2O$ (0.17 g, 1.0 mmol) was then added dropwise under stirring. The resulting green mixture was filtered to remove the rest of solid particles and then it was extracted with dichloromethane. The organic phase was separated from the mixture and dried over a molecular sieve to give a deep green solution. Solvent was removed under vacuum and the resulting dark green solid was recovered with tetrahydrofuran, collected by filtration, washed with acetone and diethyl eter, and dried under vacuum. Recrystallization from an acetonitrile/methanol mixture (10:1, v/v) afforded X-ray quality crystals of **V.2** as green tiny prisms upon slow vapor diffusion of acetone in a closed flask (0.81 g, 90% yield). Anal. Calcd for $C_{100}H_{160}Cu_2N_8O_{12}$: C, 66.97; H, 8.99; N, 6.25%. Found: C, 65.81; H, 9.08; N, 6.12%. IR (KBr): ν = 1625, 1601 cm^{-1} (CO).

Spectrophotochemical measurements. Solutions of the proligands Et_2H_2-2,6-anba and Et_2H_2-1,5-naba and complexes **V.1** and **V.2** in dimethylsulfoxide and acetonitrile respectively, were degassed with Ar in a sealed quartz cell designed for solution studies under inert atmosphere prior to carry out the irradiation experiments at room temperature. The electronic absorption spectra of the deaerated irradiated solutions were measured at regular time intervals until the photostationary state was reached, and they were then measured without irradiation to check for possible thermal relaxation effects at room temperature.

Photomagnetic measurements. Powdered samples of **V.1** and **V.2** were stored in a sealed Pyrex tube saturated with Ar during the course of the irradiation experiments at room temperature. The magnetic properties of the irradiated powdered samples were immediately measured after different irradiation times, and they were then measured after heating *in situ* at 75 ºC for 1 h without irradiation to check for possible thermal relaxation effects.

Crystal structure data collection and refinement. The X-ray diffraction data of **V.1** were collected at 100(2) K using synchrotron radiation (λ = 0.7513 Å) at the BM16-CRG beamline in the ESRF (Grenoble, France), while those of **V.2** were collected at 293(2) K with graphite-monochromated Mo-K$_\alpha$ radiation using a Bruker Nonius Kappa CCD diffractometer. The data of **V.1** were indexed, integrated and scaled using the *HKL2000* program,[15] while the data collection and data reduction of **V.2** were done with the *COLLECT* and *EVALCCD* programs.[16] All calculations for the structure solution and refinement of **V.1** and **V.2** were done by standard procedures using the *WINGX* program.[17] The structures of **V.1** and **V.2** were solved by direct methods and refined with full-matrix least-squares technique on F^2 using the *SHELXS-97* and *SHELXL-97* programs.[18] All non-hydrogen atoms of **V.1** and **V.2** were refined anisotropically. The hydrogen atoms from the organic ligands of **V.1** and **V.2** were set on calculated positions and refined with a riding model, while those of the crystallization water molecules of **V.2** were neither found nor calculated. The final geometrical calculations and the graphical manipulations of **V.1** and **V.2** were carried out with *PARST97* and *CRYSTAL MAKER* programs, respectively.[19]

Crystallographic data (excluding structure factors) for the structures reported in this paper have been deposited with the Cambridge Crystallographic Data Centre as supplementary publication CCDC no. 828222 (**V.1**) and 949613 (**V.2**). Copies of the data can be obtained free of charge on application to CCDC, 12 Union Road, Cambridge CB21EZ, UK (fax: (+44) 1223-336-033; e-mail: deposit@ccdc.cam.ac.uk).

V.9 Computational Details

Geometry optimizations of **V.1** and **V.2** were performed in acetonitrile solution using the B97D, PBE, B3LYP, and CAMB3LYP functionals[20] combined with the broken-symmetry (BS) approach,[21] as implemented in the Gaussian 09 program.[22] DF energy calculations were then performed on the BS singlet and triplet spin states of the optimized molecular geometries in acetonitrile solution of the reactants, **V.1** and **V.2**, the intermediates, **V.*i*-1(9), V.*i*-2(1)**, and **V.*i*-2(4)**, the photocycloaddition products, **V.*c*-1(9,10), V.*c*-2(1,4)**, **V.*c*-2(1,2)**, and **V.*c*-2(3,4)**, and the corresponding transition states, **V.*c*-1(9,10)$^{\#}$, V.*c*-2(1,4)$^{\#}$**, and **V.*c*-2(3,4)$^{\#}$**, with the hybrid CAMB3LYP functional. Solvation effects were introduced using a polarizable continuum model (PCM), where the cavity is created via a series of overlapping spheres.[23] Triple- and double-ζ quality basis sets proposed by Ahlrichs and co-workers were used for the metal and non-metal atoms, respectively.[24] The calculated spin density data were obtained from natural bond orbital (NBO) analysis.[25]

References

[1] a) J. M. Lehn, *Supramolecular Chemistry: Concepts and Perspectives*, VCH, Weinheim, Germany, **1995**; b) G. F. Swiegers, T. J. Malefetse, *Chem. Rev.* **2000**, *100*, 3483.

[2] a) N. J. Turro, *Modern Molecular Photochemistry*, University Sience Books, Sausalito, Californy, USA, **1991**; b) L. R. MacGillivray, G. S. Papaefstathiou, T. Friscic, T. D. Hamilton, D. K. Buar, Q. Chu, D. B. Varshney, I. G. Georgiev, *Acc. Chem. Res*. **2008**, *41*, 280.

[3] a) O. Kahn, *Molecular Magnetism*, VCH, New York, USA, **1993**; b) M. C. Dul, E. Pardo, R. Lezcouëzec, Y. Journaux, J. Ferrando-Soria, R. Ruiz-García, J. Cano, M. Julve, F. Lloret, D. Cangussu, C. L. M. Pereira, H. O. Stumpf, J. Pasán, C. Ruiz-Pérez, *Coord. Chem. Rev*. **2010**, *254*, 2281.

[4] a) B. L. Feringa, *Molecular Switches,* VCH, New York, USA, **2001**; b) M. Irie, *Chem. Rev*. **2000**, *100*, 1685.

[5] a) Y. Tanaka, A. Inagaki, M. Akita, *Chem. Commun.* **2007**, 1169; b) Y. F. Liu, C. Lagrost, K. Constuas, N. Touchar, H. Le Bozac, S. Rigaut, *Chem. Commun.* **2008**, 6117; c) Y. Lin, J. J. Yuan, M. Hu, J. Cheng, J. Yin, S. Jin, S. H. Liu, *Organometallics,* **2009**, *28*, 6402; d) K. A. Green, M. P. Cifuentes, T. C. Corkery, M. Samoc, M. G. Humphrey, *Angew. Chem. Int. Ed.* **2009**, *48*, 7867; e) Y. Tanaka, T. Ishisaka, A. Inagaki, T. Koike, C. Lapinte, M. Akita, *Chem. Eur. J.* **2010**, *16*, 4762; f) K. Motoyama, H. Li, T. Koike, M. Hatakeyama, S. Yokojima, S. Nakamura, M. Akita, *Dalton Trans.* **2011**, *40*, 10643.

[6] a) K. Matsuda, M. Irie, *J. Am. Chem. Soc*. **2000**, *122*, 7195; b) K. Matsuda, M. Irie, *J. Am. Chem. Soc*. **2000**, *122*, 8309; c) K. Matsuda, M. Irie, *J. Am. Chem. Soc.* **2001**, *123*, 9896; d) K. Matsuda, M. Irie, *Chem. Eur. J*. **2001**, *7*, 3466; e) K. Takayama, K. Matsuda, M. Irie, *Chem. Eur. J*. **2003**, *9*, 5605; f) N. Tanufuji, M. Irie, K. Matsuda, *J. Am. Chem. Soc*. **2005**, *127*, 13344.

[7] a) T. Mitsumori, N. Koga, H. Iwamura, *J. Phys. Org. Chem*. **1994**, *7*, 43; b) T. Mitsumori, K. Inoue, N. Koga, H. Iwamura, *J. Am. Chem. Soc.* **1995**, *117*, 2467; c) K. Hamachi, K. Matsuda, T. Itoh, H. Iwamura, *Bull. Chem. Soc. Jpn.* **1998**, *71*, 2937; d) Y. Teki, S. Miyamoto, K. Iimura, M. Nakatsuji, Y. Miura, *J. Am. Chem. Soc*. **2000**, *122*, 984; e) Y. Teki, *Polyhedron* **2001**, *20*, 1163.

[8] a) E. Pardo, R. Carrasco, R. Ruiz-García, M. Julve, F. Lloret, M. C. Muñoz, Y. Journaux, E. Ruiz, J. Cano, *J. Am. Chem. Soc.* **2008**, *130*, 576; b) M. Castellano, J. Ferrando-Soria, E. Pardo, M. Julve, F. Lloret, C. Mathonière, J. Pasán, C. Ruiz-Pérez, L. Cañadillas-Delgado, R. Ruiz-García, J. Cano, *Chem. Commun.* **2011**, *47*, 11035.

[9] a) J. J. McCullough, *Chem. Rev*. **1987**, *87*, 811; b) H. D. Becker, *Chem. Rev*. **1993**, *93*, 145; c) H. Bouas-Laurent, A. Castellan, J.-P. Desvergne, R. Lapouyade, *Chem. Soc. Rev*. **2000**, *29*, 43.

[10] a) J. Fritsche, *J. Prakt. Chem*. **1867**, *101*, 333; b) E. J. Bowen, *Adv. Photochem*. **1963**, *1*, 23; c) A. Castellan, R. Lapouyade, H. Bouas-Laurent, *Bull. Soc. Chim. Fr*. **1976**, 210; d) H. Bouas-Laurent, A. Castellan, J.-P. Desvergne, *Pure Appl. Chem*. **1980**, *52*, 2633.

[11] a) J. S. Bradshaw, G. S. Hammond, *J. Am. Chem. Soc*. **1963**, *85*, 3953; b) B. K. Selinger, M. Sterns, *J. Chem. Soc*., *Chem. Commun.* **1969**, 978; c) R. A. Caldwell, *J. Am. Chem. Soc*. **1980**, *102*, 4004; d) T. Noh, Y. Jeong, D. Kim, *J. Chem. Soc*., *Perkin Trans.* **1998**, 2501.

[12] Ehrenberg, M. *Acta Crystallogr.* **1966**, *20*, 177.

[13] S. S. Zade, N. Zamoshchik, A. R. Reddy, G. Fridman-Marueli, D. Sheberla, M. Bendikov, *J. Am. Chem. Soc.* **2011**, *133*, 10803.

[14] S. R. Jezowski, L. Zhu, Y. Wang, A. P. Rice, G. W. Scott, C. J. Bardeen, E. L. Chronister, *J. Am. Chem. Soc.* **2012**, *134*, 7459.

[15] Z. Otwinowski, W. Minor, Processing of X-ray Diffraction Data Collected in Oscillation Mode, in Methods in Enzymology: Macromolecular Crystallography, Part A, Vol. 276 (Eds.: C. W. Jr., Carter, R. M. Sweet), **1997**, p. 307.

[16] a) R. W. W. Hooft, *COLLECT*, Nonius BV, Delft, The Netherlands, **1999**; b) A. J. M. Duisenberg, L. M. J. Kroon-Batenburg, A. M. M. Schreurs, *J. Appl. Crystallogr.* **2003**, *36*, 220 (*EVALCCD*).

[17] L. J. Farrugia, *J. Appl. Crystallogr*. **1999**, *32*, 837 (*WINGX*).

[18] G. M. Sheldrick, *SHELX97*, *Programs for Crystal Structure Analysis, release 97-2*, Institüt für Anorganische Chemie der Universität Göttingen, Göttingen, **1998**.

[19] a) M. Nardelli, *J. Appl. Crystallogr.* **1995**, *28*, 659; b) D. Palmer, *CRYSTAL MAKER,* Cambridge University Technical Services, Cambridge, **1996**.

[20] A. D. Becke, *J. Chem. Phys.* **1993**, *98*, 5648.

[21] a) E. Ruiz, J. Cano, S. Alvarez, P. Alemany, *J. Am. Chem. Soc.* **1998**, *120*, 11122; b) E. Ruiz, J. Cano, S. Alvarez, P. Alemany, *J. Comput. Chem.* **1999**, *20*, 1391; c) E. Ruiz, A. Rodriguez-Fortea, J. Cano, Alvarez, P. Alemany, *J. Comput. Chem.* **2003**, *24*, 982; d) E. Ruiz, V. Polo, J. Cano, S. Alvarez, *J. Chem. Phys.* **2005**, *123*, 164110.

[22] M. J. Frisch, G. W. Trucks, H. B. Schlegel, G. E. Scuseria, M. A. Robb, J. R. Cheeseman, G. Scalmani, V. Barone, B. Mennucci, G. A. Petersson, H. Nakatsuji, M. Caricato, X. Li, H. P. Hratchian, A. F. Izmaylov, J. Bloino, G. Zheng, J. L. Sonnenberg, M. Hada, M. Ehara, K. Toyota, R. Fukuda, J. Hasegawa, M. Ishida, T. Nakajima, Y. Honda, O. Kitao, H. Nakai, T. Vreven, Jr., J. A. Montgomery, J. E. Peralta, F. Ogliaro, M. Bearpark, J. J. Heyd, E. Brothers, K. N. Kudin, V. N. Staroverov, R. Kobayashi, J. Normand, K. Raghavachari, A. Rendell, J. C. Burant, S. S. Iyengar, J. Tomasi, M. Cossi, N. Rega, J. M. Millam, M. Klene, J. E. Knox, J. B. Cross, V. Bakken, C. Adamo, J. Jaramillo, R. Gomperts, R. E. Stratmann, O. Yazyev, A. J. Austin, R. Cammi, C. Pomelli, J. W. Ochterski, R. L. Martin, K. Morokuma, V. G. Zakrzewski, G. A. Voth, P. Salvador, J. J. Dannenberg, S. Dapprich, A. D. Daniels, Ö. Farkas, J. B. Foresman, J. V. Ortiz, J. Cioslowski, D. J. Fox, *Gaussian 09*, revision B.1; Gaussian, Inc.: Wallingford, CT, **2009**.

[23] a) A. Schaefer, H. Horn, R. Ahlrichs, *J. Chem. Phys.* **1992**, *97*, 2571; b) A. Schaefer, C. Huber, R. Ahlrichs, *J. Chem. Phys.* **1994**, *100*, 5829.

[24] a) J. E. Carpenter, F. Weinhold, *J. Mol. Struct.* **1988**, *169*, 41; b) A. E. Reed, L. A. Curtis, F. Weinhold, *Chem. Rev.* **1988**, *88*, 899; c) F. Weinhold, J. E. Carpenter, *The Structure of Small Molecules and Ions*, Plenum, **1988**, p. 227.

[25] a) M. Cossi, N. Rega, G. Scalmani, V. Barone, *J. Comp. Chem.* **2003**, *24*, 669; b) J. Tomasi, B. Mennucci, E. Cances, *J. Mol. Struct.-Theochem.* **1999**, *464*, 211.

CHAPTER VI

Conclusions and Outlook: From Single-Molecules to Molecule-Based Materials for Applications in Nanospintronic Devices

Molecular spintronics is a new and emergent field of spintronics which can benefit from the well-stablished developments in molecular magnetism and molecular electronics.[1,2] As occurs in these two related fields, molecular spintronics can be divided into two areas, namely single-molecule spintronics and molecule-based spintronics.[2a] The first area focuses on the study of the spin-dependent electron transport through a single molecule and the use of these individual molecules as active components of spintronic circuits.[2b,c] The second area deals with the design and synthesis of new materials from molecular precursors ('molecule-based materials') that can mimic the unique magnetic and electronic properties exhibited by the existing 'conventional' inorganic materials used in spintronics.[2d]

At this regard, **metallosupramolecular chemistry** is an outstanding research area in the field of supramolecular chemistry which offers convenient tools for the evolution from molecular magnetism and molecular electronics toward molecular spintronics.[3,4] The spectacular development of metallasupramolecular chemistry in the late eighties and nineties has set up the guiding principles for the self-assembly of well-defined multimetallic coordination architectures of increasing structural complexity based on metal-ligand interactions.[3] Discrete zero-dimensional (0D) polynuclear coordination compounds,[4] as well as infinite, one- (1D), two- (2D), or three-dimensional (3D) coordination polymers,[5] referred to as **metal-organic clusters** (MOCs) and **metal-organic frameworks** (MOFs) respectively, are included in this category.

At the beginning of this new century, the introduction of functionality into these MOCs and MOFs has become one of the aims of a large number of research groups[6,7] They take advantage from the chemical reactivity (redox or photochemical) and electronic properties (conducting, magnetic or optical) of the metal ions and eventually the organic ligands, as well as from the particular level of organization created by the metal-ligand coordinative interaction. In general, the unique properties exhibited by these hybrid inorganic-organic systems are not the sum of those from the individual components but they derive from the cooperative interactions between the metal ions through the organic bridging ligands. The study of the supramolecular structure-function correlations will then orientate the rational design and synthesis of self-assembled supramolecular functional materials. They display interesting physicochemical properties that could be exploited in supramolecular recognition and catalysis[6] and supramolecular photo-, electro-, and magnetochemistry.[7]

In pursuing molecular spintronic materials,[8] the ligand design is crucial both to organize the paramagnetic metal ions in a desired topology and to efficiently transmit electron exchange interactions between the metal ions in a controlled manner.[9,10] This basic principle is impressively demonstrated by our recent work on the rich supramolecular coordination chemistry of a novel family of aromatic polyoxalamide (APOXA) ligands with first-row transition metal ions which has allowed to get on one step further in the rational design of metallosupramolecular assemblies of increasing structural and magnetic complexity.[11-21]

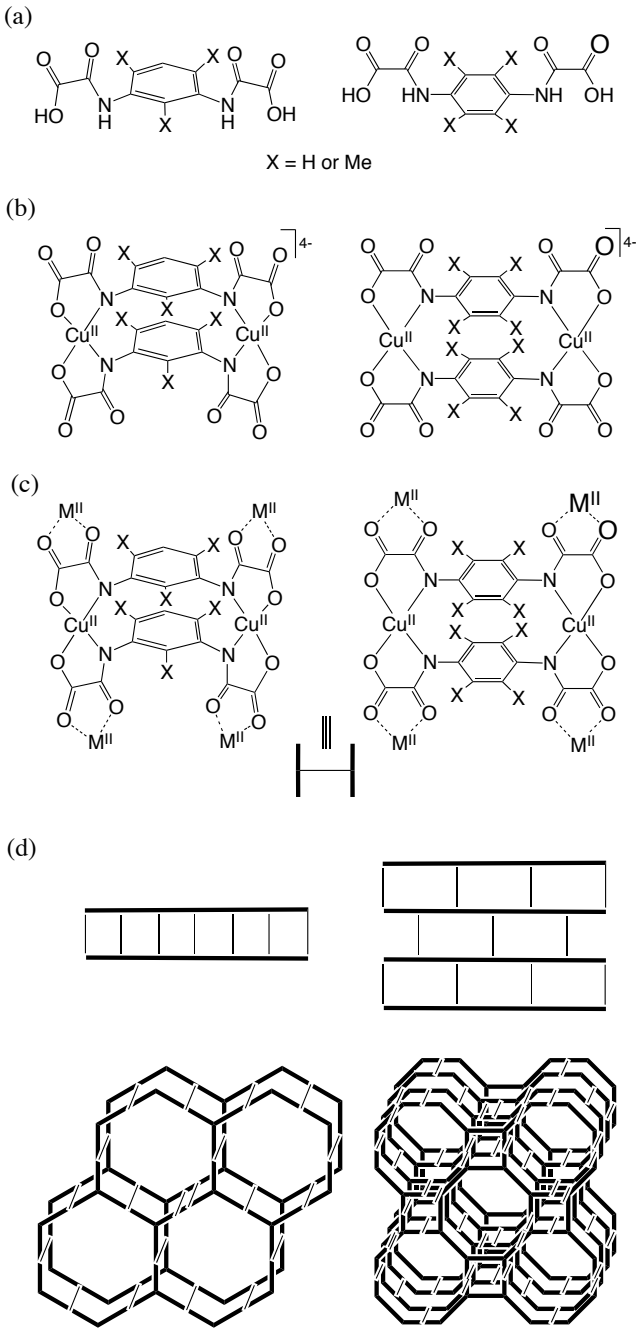

Figure VI.1 Illustration of the molecular-programmed strategy for the rational design of MOCs (c) and MOFs (d) from self-assembling dicopper(II) metallacyclophanes (b) with APOXA ligands (a).

APOXA ligands with multiple oxamato donor groups, from one to up to four, separated by more or less hindered, polymethyl-substituted phenylene spacers of varying substitution pattern, offer a kind of double programming according to the terminology of metallosupramolecular chemistry.[11] The first level of ligand programming allows the coordination to transition metal ions (M = Cu^{II}, Ni^{II}, and Co^{II}) through the bidentate *N,O*-oxamato donor sets to give double- or triple-stranded oligonucler complexes, from mono- to tetranuclear.[13-15] The second level of ligand programming resides precisely on the free *cis* carbonyl oxygen atoms of the oxamato donor groups, which allow these self-assembled metallacyclic species to be used as ligands

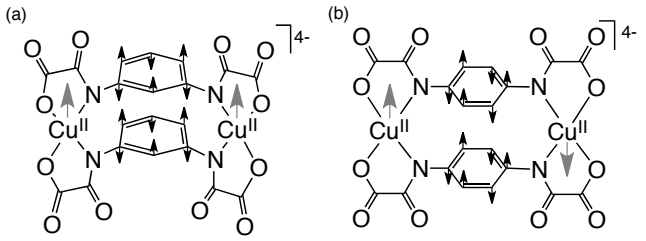

Figure VI.2 Chemical structure of the oxamato-based dicopper(II) meta- and paracyclophanes showing the different spin alignment resulting from the alternance of the spin densities on the (a) *meta*- and (b) *para*-substituted phenylene spacer.

(metalloligands) toward other alkaline, alkaline earth, and transition metal ions (M' = Li^{I}, Na^{I}, Mg^{II}, Ca^{II}, Sr^{II}, Cu^{II}, Ni^{II}, Co^{II}, and Mn^{II}). This molecular-programmed approach based on ligand design allows the rational preparation of a variety of molecular magnetic materials with predictable structures and magnetic properties.[16-21]

In particular, MOCs and MOFs of variable nuclearity and dimensionality have been designed and synthesized from self-assembled dicopper(II) metallacyclophanes with polymethyl-substituted 1,3- and 1,4-phenylene dioxamato bridging ligands (Figure VI.1). In the former case, both homo- and heterobimetallic, penta- and hexanuclear complexes were obtained when using blocking ligands in the coordination sphere of the coordinated metal ion to preclude polymerization (Figure VI.1c).[16] These latter hexanuclear complexes constitute the basic structural units for the construction of the corresponding homo- and heterobimetallic *n*D (*n* = 1–3) coordination polymers, whose topology would depend on both the coordination mode and steric requirements of the Cu^{II}_2 metalloligand and the stereochemical preferences of the M^{II} ion, as well as the templating effects of the organic or inorganic countercation. They include 1D ladders , 2D brick-wall monolayers and hexagonal bilayers, and 3D square-octogonal pillared nets (Figure VI.1d).[20]

In this thesis, we have developed new oxamato-based dicopper(II) metallacyclophanes with potential photo or redox activity at the aromatic ligand counterpart. This will provide us with appropriate building blocks for the elaboration of molecular spintronic materials for future applications in materials science and nanotechnology. Let us briefly develop this point in the following two sections by including a summary of our major achievements, together with an advancement of our preliminary results in this area.

VI.1 Redox and Photo Control of the Magnetic Properties through Ligand Design

The design and synthesis of ligands which are able to self-assemble spontaneously with paramagnetic metal ions to form exchange-coupled polymetallic complexes of predetermined nuclearity and topology are one of the major goals in molecular magnetism and molecular spintronics. Our strategy in this field has been based on the use of polytopic ligands possessing multiple oxamato donor groups, separated by aromatic spacers. These aromatic polyoxalamide (APOXA) ligands coordinate to the late first-row transition metal ions, from copper to cobalt, to afford stable oligonuclear metallacyclic complexes.[11]

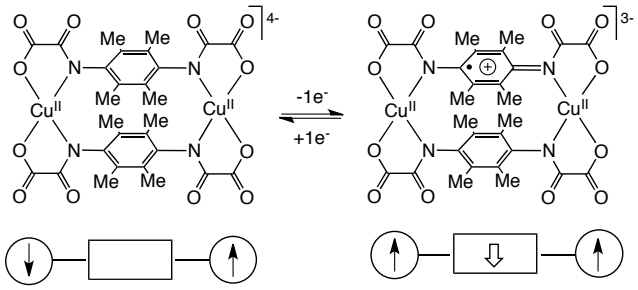

Figure VI.3 Illustration of the magnetic electroswitching in oxamato-based permethylated dicopper(II) paracyclophanes.

Overall, we have shown that aromatic spacers are really effective to transmit exchange interactions between paramagnetic metal centers separated by relatively long intermetallic distances in discrete metallacyclic entities. Furthermore, we have demonstrated that the appropriate choice of the electronic configuration of the metal ion and the topology of the bridging ligand allows to control the nature and magnitude of the magnetic coupling between the metal centers through the aromatic spacers in the corresponding dinuclear metallacyclic complexes.

Earlier investigations of our research group on the unique pair of dicopper(II) metallacyclophanes with 1,3- and 1,4-phenylene spacers has provided deeper insights on the fundamental knowledge of the distinct spin delocalization and spin polarization effects that govern the magnetic coupling through extended π-conjugated aromatic spacers.[13a,b] Thus, the ferromagnetic or antiferromagnetic nature of the electron exchange interaction in the corresponding dicopper(II) meta- and paracyclophanes results from a spin polarization mechanism through the extended π-conjugated bond system of the phenylene spacers, as supported by theoretical calculations (Figure VI.2).

In this thesis, we have investigated a novel family of electroactive, antiferromagnetically coupled dicopper(II) paracyclophanes with polymethyl-substituted 1,4-phenylene spacers, $-C_6H_{(4-n)}Me_n-$ (*n* = 0, 1, and 4) (see Chapter IV). The overall strengthening of the antiferromagnetic coupling along this series is due to an increased delocalization of the unpaired electrons of the Cu^{II} ions onto the π-conjugated electron system of the *p*-phenylene spacers with the increasing number of electron donating methyl substituents. This phenomenon is ultimately responsible for the higher stability of the one-electron oxidized dicopper(II) π-radical species resulting from the oxidation of the polymethyl-substituted *p*-phenylenediamidate bridge as the number of electron donating methyl substituents increases.

Interestingly, the permethylated dicopper(II) paracyclophane exhibits a unique magnetic electroswitching (ON/OFF) behavior, as shown both experimentally and theoretically.[13f] The magnetic bistability obeys to the change from antiparallel (OFF) to parallel (ON) spin alignment of the metal centers by the π-stacked delocalized monoradical ligand generated upon one-electron oxidation of the double tetramethyl-*p*-phenylenediamidate bridge skeleton (Figure VI.3). Permethylation in this metallacyclic system constitutes thus a unique example of ligand design for the supramolecular control of magnetic properties and electrochemical reactivity.

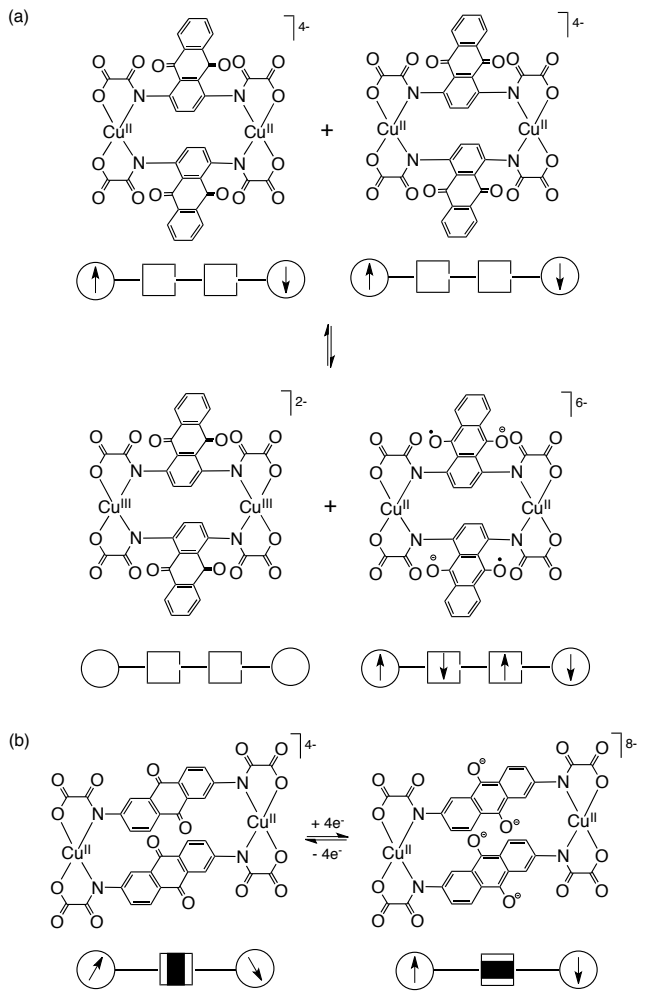

Figure VI.4 Illustration of the magnetic charge storage (a) and electroswitching (b) in oxamato-based dicopper(II) anthraquinophanes.

In this thesis, we have also explored an alternative way to electroactive oxamato-based dicopper(II) metallacyclophanes by incorporating anthraquinone spacers possessing higher electrochemical stability, both thermodynamic and kinetic (see Chapter III). In the former case, the redox non-innocent 1,4-anthraquinone spacers and the Cu^{II} ions function as electron reservoirs for reduction and oxidation respectively, to impart a dual multielectron redox (charge storage) behavior to this novel antiferromagnetically coupled dicopper(II) 1,4-anthraquinophane to be used as magnetic capacitor, *i.e.,* electroactive (oxidizable and reducible) molecules with several chemically accessible oxidation levels at the exchange-coupled spin carriers that can store and deliver an electric charge. In this case, the charging and decharging processes of the magnetic capacitor can be regarded as the disproportionation equilibrium reaction of the dicopper(II) 1,4-anthraquinophane (Figure VI.4a). That being so, the overall efficiency depends on the available number of oxidation (n_{ox}) and reduction equivalents (n_{red}), as well as the magnitude of the comproportionation constant (K_c), that is, small K_c and large n_{ox} and n_{red} values.

We can go have gone one step further in this study by developing new oxamato-based dicopper(II) metallacyclophanes with 2,6-anthraquinone spacers as new prototypes of magnetic electroswitches in the emerging field of molecular spintronics. In this latter case, the spins of the Cu^{II} ions are magnetically isolated

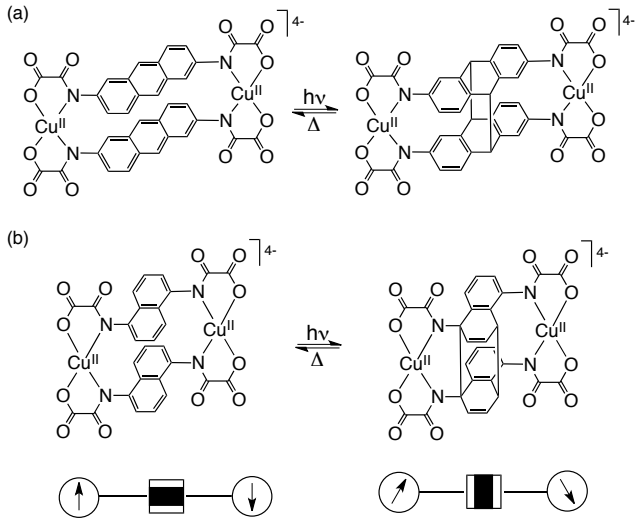

Figure VI.5 Illustration of the magnetic photoswitching in oxamato-based dicopper(II) naphthalenophanes (a) and anthracenophanes (b).

accross the non-conjugated 2,6-anthraquinone spacers ('OFF' state), whereas they are weak antiferromagnetically coupled through the extended π-conjugated spacers in the fully reduced bis(catecholate)-type dicopper(II) species ('ON' state) (Figure VI.4b).[13h] Quinone functionalization in this metallacyclic system constitutes thus a unique example of ligand design for the supramolecular control of the magnetic properties and electrochemical reactivity.

This work has directed our research efforts toward other dicopper(II) metallacyclophane molecules with extended π-conjugated aromatic spacers that were earlier investigated by our research group, such as linear oligophenylenes (OPs) and oligoacenes (OAs).[13b,c] At this respect, OAs are very appealing candidates as molecular wires because of their unique electronic properties and photochemical reactivity which have received much attention from both experimental and theoretical points of view.[22] As a matter of fact, the design and synthesis of novel bridging ligands which can act as effective molecular wires to transmit spin coupling effects over long distances are a major achievement in the field of molecular spintronics.[13c] In contrast to conventional charge transport-based molecular wires, these so-called "magnetic molecular wires" (MMWs) may offer a new design concept for the transfer of information over long distances based on purely electron exchange interactions (EE) and without current flow.

In this thesis, we have further demonstrated that OAs can act as thermally reversible photoswitchable magnetic wires for the transmission of EE interactions between the two square planar Cu^{II} ions in the corresponding dicopper(II) metallacyclophanes (see Chapter V).[13d] However, rather low photochemical efficiencies and thermal reversibilities are obtained for the conversion of the moderately strong antiferromagnetically coupled dicopper(II) 1,5-naphthaleno- and 2,6-anthracenophanes to the corresponding magnetically uncoupled dicopper(II) products resulting from the [4+4] photocycloaddition of the two facing oligoacene spacers (Figure VI.5). This intramolecular ("pseudo-bimolecular") reaction constitutes a unique example of coordination-driven self-assembly for the supramolecular control of photochemical reactivity and photophysical properties, both in solution and in the solid state.

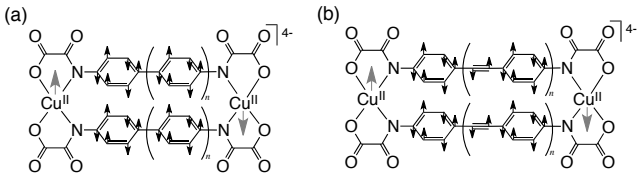

Figure VI.6 Chemical structure of the oxamato-based dicopper(II) oligophenylenophanes (a) and oligophenylethinophanes showing the alternance of the spin densities on the spacer resulting from the spin polarization mechanism.

Oligo(*p*-phenyleneethyne) (OPE) spacers are also very appealing candidates as molecular magnetic wires due to their potential extended π-conjugation.[23] In this thesis, we have shown that the rigid rod-like OPEs allow for a stronger magnetic communication between very distant metal centers in the corresponding dicopper(II) oligophenyleneethynophanes, when compared with their dicopper(II) oligophenylenophane ancestors (see Chapter II).[13e] Because of the planar configuration of the OPE spacers, a strong orbital overlap between the p_z-type orbitals of the *para*-substituted benzene rings across the carbon-carbon triple bonds occurs along the *p*-phenylethyne repeat units. Moreover, the rather low exponential decay of the antiferromagnetic coupling with the intermetallic distance indicates that the electron exchange (EE) through linear OPE spacers follows a spin polarization mechanism. This conclusion is further supported by the presence of non-negligible spin densities of alternating sign on the bridge in the calculations on the broken-symmetry (BS) singlet states, as earlier found for the dicopper(II) oligophenylenophane analogues (Figure VI.6). Based on this combined experimental and theoretical study, we then propose that linear OPE spacers can act as effective antiferromagnetic wires between two Cu^{II} ions separated by up to 3.0 nm.

In turn, the related oligo(*p*-phenylenevinylidene) (OPV) and oligo(*p*-azobenzene) (OAB) spacers, like stilbene and azobenzene, are very appealing candidates as photoswitchable magnetic wires because of their well known rich photochemical reactivity that includes intramolecular [2+2] cycloadition and *cis-trans* geometric isomerization, respectively (Figure VI.7).[24] So, compared with dicopper(II) oligoacenophanes, our preliminary studies show that higher photochemical efficiencies and thermal reversibilities are found for the conversion of the weak antiferromagnetically coupled dicopper(II) stilbenophane ('ON' state) to the corresponding magnetically uncoupled dicopper(II) photocycloaddition product ('OFF' state) resulting from the intramolecular [2+2] photocycloaddition reaction of the two facing stilbene spacers (Figure VI.7a).[13i] Moreover, a complete photochemical reversivility has been achieved in dicopper(II) azobenzenophanes after irradiation with UV and visible light. The spins of the Cu^{II} ions are weak antiferromagnetically coupled through the planar *trans*-azobenzene spacers ('ON' state), whereas they are magnetically isolated accross the non-planar *cis*-azobenzene spacers ('OFF' state) (Figure VI.7b).[13j]

We are currently investigating these novel series of electro- and photo-active, oxamato-based dicopper(II) metallacyclophanes as prototypes of molecular magnetic devices as well as potential precursors for molecular spintronic materials. Indeed, these simple molecules were revealed as ideal experimental and theoretical models for the fundamental study on electron- and photo-triggered

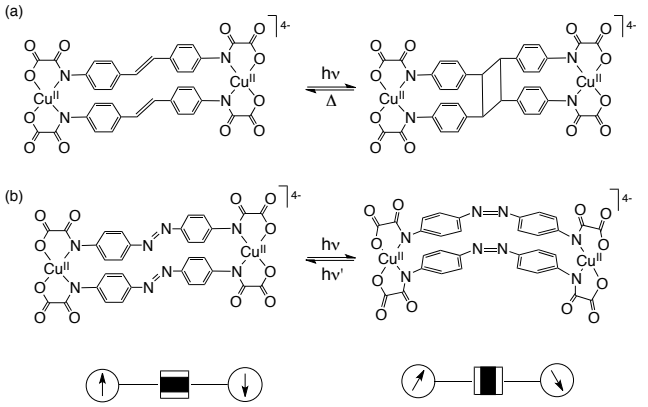

Figure VI.7 Illustration of the magnetic photoswitching in oxamato-based dicopper(II) stilbenophanes (a) and azobenzenophanes (b).

EE processes, which are two central topics in the emerging area of molecular spintronics. Because of their nanoscopic size and feasible "addressing" over a variety of substrates (electrodes, surfaces, porous materials, etc.), they thus appear as very promising candidates to get single-molecule spintronic devices. They include those facilitating the spin communication ("magnetic molecular wires", MMWs) or exhibiting multistable spin behavior ("magnetic molecular switches", MMSs) for future applications in information processing and storage. Moreover, they could bring an external photo- and redox-control over the magnetic properties of MOCs and MOFs when used as precursors to prepare molecule-based spintronic materials.

VI.2 Metalloligand Approach in the Design of Molecular Spintronic Materials

The design and synthesis of simple paramagnetic molecules that are able to self-assemble through metal–ligand interactions to form more complex aggregates (supermolecules) with prefixed dimensionality, nuclearity, and/or topology is a major target in molecular magnetism and molecular spintronics. Our strategy in this field has been based on the use of oxamato-based metallacyclic complexes as ligands (metalloligands) toward either coordinatively unsaturated metal complexes or fully solvated transition metal ions affording discrete polynuclear coordination compounds (metal-organic clusters, MOCs) or infinite coordination polymers (metal-organic frameworks, MOFs), respectively.

This well-known metalloligand approach allowed controlling the overall magnetic properties of the resulting *n*D (*n*D = 0–3) multidimensional compound through the appropriate choice of the precursor (substitution pattern and steric requirements of the bridging ligand) and the coordinated metal ion or metal complex (electronic configuration and local anisotropy). The development of this unique family of oxamato-bridged MOCs and MOFs expands on the reported examples of multidimensional magnetic materials.[11] Our target dicopper(II) metallacyclophanes developed in this thesis also contained predetermined information as to act as metalloligands towards other metal ions in order to generate clusters and high dimensionality arrays. The pursuit of our goal is allowing us to modify their magnetic properties under electro- and photochemical control.

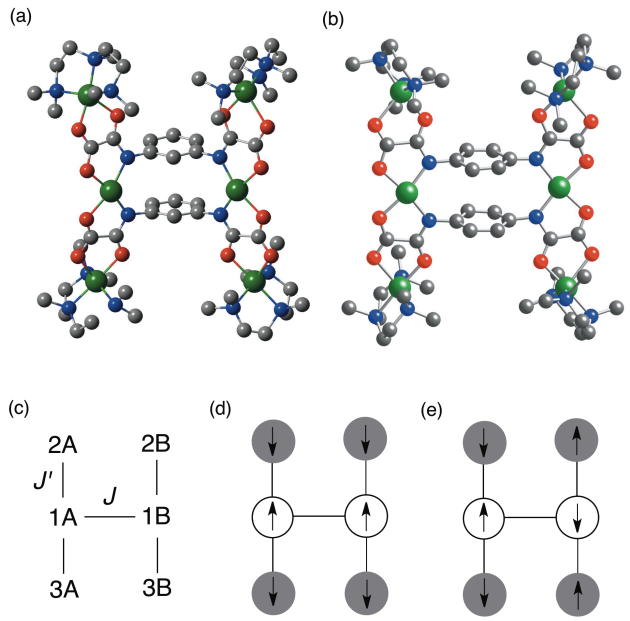

Figure VI.8 (a) and (b) Structures of the oxamato-based hexanuclear copper(II) MOCs with dicopper(II) meta- and paracyclophane cores, respectively. Ligand and metal atoms are represented by sticks and balls, respectively (C, gray; N, blue; O, red; Cu, green). (c) Spin coupling scheme and (d) and (e) spin topologies for the Cu^{II}_6 MOCs with dicopper(II) meta- and paracyclophane cores, respectively.

Metal-Organic Clusters. A definite breakthrough has been accomplished in the field of molecular magnetism upon the syntheses of metal-organic clusters (MOCs).[27] These systems are characterized by highly interesting magnetic properties, and they are attracting much attention as for their inspiring use of the unlimited well of organic molecules combined with inorganic synthesis. Thus, the obtention of discrete high-nuclearity MOCs takes us from high spin molecules to single-molecule magnets.[28] Using this approach, chemists are pushing the limit for new challenges, such as engineering switchable magnetic materials, that is to say, where the magnetic behavior of the MOC can be modified under external stimuli, such as optical and/or electrical.[29]

A series of hexanuclear copper(II) complexes have been rationally prepared starting from oxamato-based dicopper(II) meta- and paracyclophanes as tetrakis-bidentate metalloligands toward coordinatively unsaturate mononuclear copper(II) complexes with acyclic aliphatic polyamines such as *N,N,N',N',N''*-pentamethyldiethylenetriamine (Me_5dien) as blocking ligands (Figure VI.8).[16a,b]

These Cu^{II}_6 MOCs exhibit a ladder-like molecular structure of "dimer-of-trimers" molecular topology (Figure VI.8a and b). Considering this, the nature of the ground state can be rationally interpreted based on the concept of antiferro- (ACU) and ferromagnetic coupling units (FCU) that was earlier used to control the spin in organic polyradicals.[30] Thus, the meta- and paracyclophane Cu^{II}_2 cores act as FCU and ACU respectively, between the two Cu^{II}_3 linear entities ($S_A = S_B = 2S_{Cu} - S_{Cu} = 1/2$) leading to either a ground triplet ($S = S_A + S_B = 1$) or a singlet ($S = S_A - S_B = 0$) spin state for the Cu^{II}_6 molecule (Figures VI.8c–e).[16a,b]

A series of related oxamato-based hexanuclear copper(II) complexes carrying ~~a~~ non-innocent, redox- or photoactive ligands has been synthesized and their electro- and photochemical properties have been investigated (Figures VI.9 and 10).[16c,d]

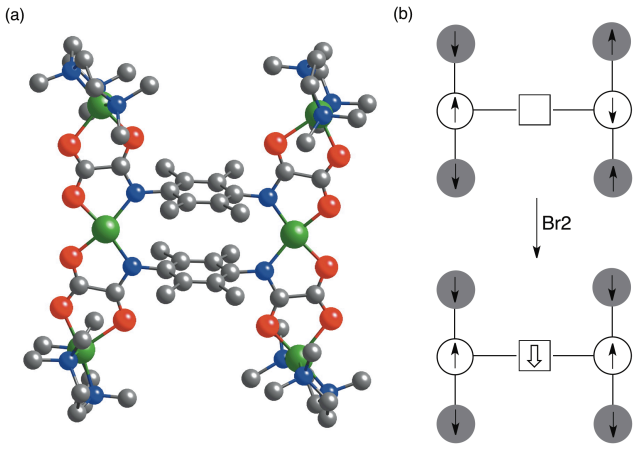

Figure VI.9 (a) Structure of the oxamato-based hexanuclear copper(II) MOC with a permethylated dicopper(II) paracyclophane core. Ligand and metal atoms are represented by sticks and balls, respectively (C, gray; N, blue; O, red; Cu, green). (b) Magnetic electroswitching and spin topologies for the Cu^{II}_6 MOC.

Our preliminary studies on the redox activity of the Cu^{II}_6 MOC with a permethylated dicopper(II) paracyclophane core show a unique magnetic electroswitching behavior (Figure VI.9).[16c] So, a change from a non-magnetic singlet ($S = S_A - S_B = 0$) to a magnetic quartet ($S = S_A + S_B + S_R = 3/2$) ground state occurs due to the π-stacked delocalized monoradical ligand generated upon Br_2 oxidation of the tetramethyl-substituted *p*-phenylene spacers (Figure VI.9b).[16d]

Alternatively, our preliminary studies on the photochemical activity of the Cu^{II}_6 MOC with a dicopper(II) naphthalenophane core show a unique magnetic photoswitching behavior (Figure VI.10). In this case, a change from a non-magnetic singlet ($S = S_A - S_B = 0$) ground state to a pair of magnetically isolated doublet states ($S_A = S_B = 1/2$) occurs due to the [4+4] photocycloaddition of the two facing naphthalene spacers upon UV light irradiation (Figure VI.10b).

Metal-Organic Frameworks. The last decade witnessed an increasing interest in metal-organic frameworks (MOFs) due to their versatility as porous materials for broad applications in gas storage and separation, molecular sensing, and catalysis.[31–34] Among this new class of multifunctional molecular materials, dynamic porous magnets have become a major target for chemists, physicists, and material scientists.[35] Indeed, the coexistence of long-range magnetic ordering and porosity in the same material is a current challenge. With some remarkable exceptions,[36,37] porosity in general requires bridging ligands with long organic spacers that do not facilitate the magnetic exchange interactions between the distant paramagnetic metal centers. So that, the magnetic properties of the resulting MOF would be the same as the ones corresponding to the isolated metallic ions or polynuclear complexes used as precursors. This fact can be happily avoided by using the metalloligand strategy.[38]

The metalloligand design strategy constitutes a clear advantage when comparing to the conventional 'secondary building block' (SBB) strategy for the obtention of MOFs. It consists on bonding metal complexes prepared from organic

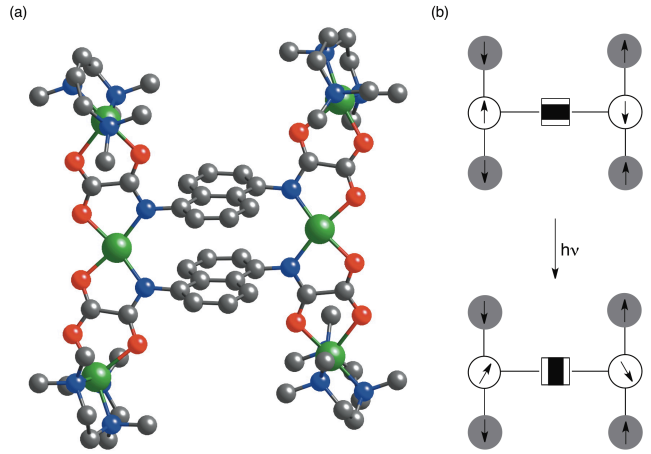

Figure VI.10 (a) Structure of the oxamato-based hexanuclear copper(II) MOC with a dicopper(II) naphthalenophane core. Ligand and metal atoms are represented by sticks and balls, respectively (C, gray; N, blue; O, red; Cu, green). (b) Magnetic photoswitching and spin topologies for the Cu^{II}_6 MOC.

ligands with suitable donor groups, so-called metalloligands, through other metal ions ("metal-mediated self-assembly"). This way, the coordination preferences of ligands, metal ions and metalloligands can be useful to control the final structure and magnetic properties of the resulting mixed-metal-organic framework (M'MOF).

Our strategy in this field has been based on the use of dicopper(II) metallacyclophanes as metalloligands toward first-row transition metal ions, such as manganese(II) and cobalt(II). It allows to synthesize heterobimetallic open-frameworks with controlled topology and dimensionality and with predictable magnetic and adsorption properties that depend on the reactivity of the dinuclear precursors, whose specific nature is a consequence of the substitution pattern and the steric requirements of the aromatic spacer, as well as on the electronic configuration and the magnetic anisotropy of the metal ion.

So, for instance, the simple dicopper(II) metallacyclophanes with polymethyl-substituted 1,3- and 1,4-phenylene spacers can act as metalloligands toward first-row transition metal ions, such as manganese(II) and cobalt(II), to render a variety of oxamato-based heterobimetallic MOFs with brick-wall layer architectures (Figure VI.11).[20a,b] Interestingly, they show overall magnetic and non-magnetic layer ground states resulting from the ferro- and antiferromagnetic interchain interactions between the oxamato-bridged $Mn^{II}Cu^{II}$ ferrimagnetic chains across the permethylated *m*- and *p*-phenylene spacers respectively, constituting thus a unique example of spin control in MOFs.[20b]

Our preliminary studies on the sorption properties of the oxamato-based manganese(II)-copper(II) 2D MOFs with permethylated dicopper(II) paracyclophane cores show a unique magnetic switching behavior after bromine gas adsorption.[20j] So, a change from non-magnetic to magnetic layer ground state occurs upon Br_2 oxidation of the tetramethyl-substituted *p*-phenylene spacers, constituting thus a unique example of electroactive porous magnet.

The use of more sophisticated dicopper(II) metallacyclophane precursors with extended π-conjugated aromatic spacers such as those developed in this thesis, *v.g.* oligophenylenes (OPs),

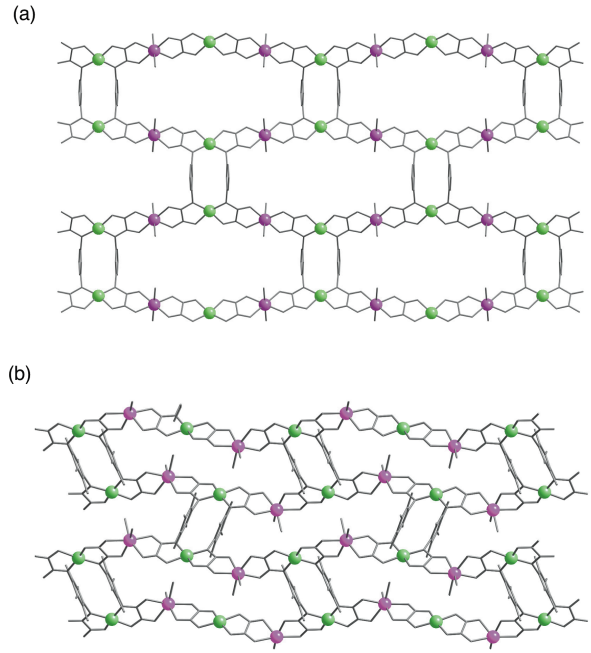

Figure VI.11 (a) and (b) Structures of the oxamato-based brick-wall M'MOFs with dicopper(II) meta- and paracyclophane cores, respectively. Ligand and metal atoms are represented by sticks and balls, respectively (Cu, green; Co and Mn, purple).

oligophenyleneethynylenes (OPEs), oligophenylenevinilenes (OPVs), oligoazaphenylenes (OAPs), oligoacenes (OAs), and oligoacenequinones (OAQs), would open the gate to molecule-based spintronic materials (Figure VI.12). At this respect, several points should be considered in order to obtain a new family of electro- and photoactive porous magnets.

Firstly, a systematic variation of the length of the aromatic spacers of the oxamatocopper(II) precursors can modulate the size of the channels which, in the last term, would afford a selective adsorption (Figure VI.12a and b). For instance, the longer OPEs as 4,4'-diphenylethyne and 1,4-di(4-phenylethynyl)phenylene are suitable candidates to afford large channels available for gas storage or inclusion of interesting organic molecules such as photoresponsive ruthenium(II) complexes or electroactive fullerenes (Figure VI.12a).

Secondly, the utilization of aromatic spacers with electro- or photochemical properties permits the obtention of multifunctional materials possessing host-guest properties of further applications as spintronic devices. In this sense, the shorter OPVs and OAPs like stilbene and azabenzene respectively, are interesting candidates for storage and delivery of gas because of its photochemical reactivity taking advantage of the well known *cis-trans* isomerization to modulate the size of the pores by irradiation ('photo-gated pores') (Figure VI.12b).

In each case, this rational design of porous magnets profits the ability of the aromatic spacers acting as molecular magnetic wires (MMWs) and molecular magnetic switches (MMSs) in the transmission of the magnetic interactions between metal centers separated by relatively long intermetallic distances (Figure VI.12a and b).

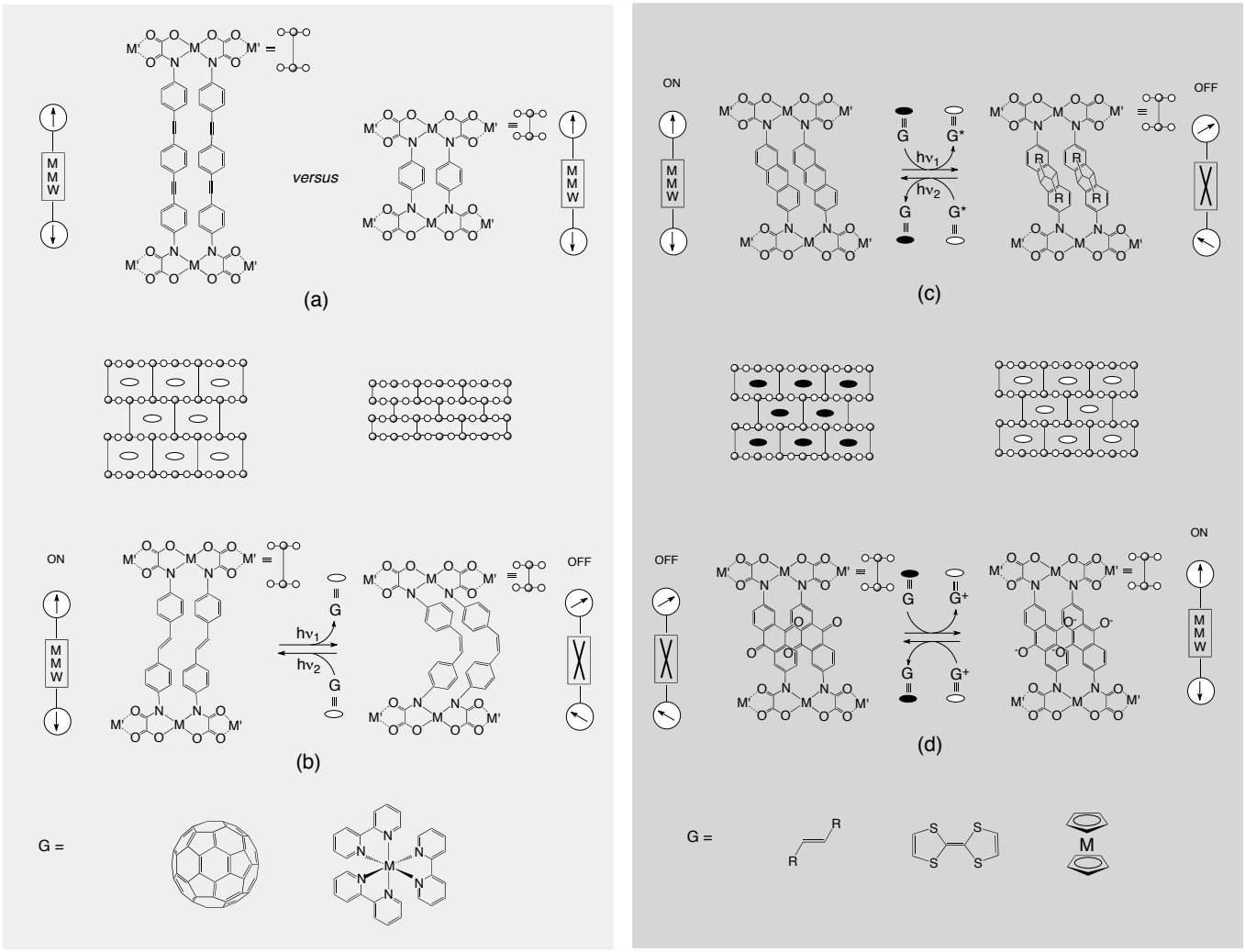

Figure VI.12 Oxamato-bridged 2D M'MOFs from antiferromagnetically coupled dicopper(II) metallacyclophane precursors acting as magnetic sensors of the 'host-guest'-type.

On the other hand, because of their unique Lewis acid (Diels-Alder) and redox properties, OAs and OAQs like anthracene and anthraquinone respectively, can be used for reaction with various organic guest molecules of interest, such as photoresponsive dienophiles or redox-active metallocenes and tetrathiofulvalenes (Figure VI.12c and VI.12d).

So, different dienophiles like styrene can be adsorbed into the host framework by reacting with the anthracene host active sites to give the corresponding [2+4] cycloaddition product in a photochemically reversible reaction (Figure VI.12c). Alternatively, metallocenes and tetrathiofulvalenes can be readily oxidized by the anthraquinone host active sites to give the corresponding magnetic and/or conducting cation radical salts and the dihydroanthraquinonate derivative (Figure VI.12d).

In each case, the spins of the metal centers are antiferromagnetically coupled in one form ('ON' state), whereas they are magnetically isolated in the other one ('OFF' state). So that, collateral magnetic changes are found in the host network, as much as photochemical and redox processes are experimented by the guest molecules (Figure VI.12a and VI.12b). Moreover, the changes in the magnetic properties of the host framework can be used to monitor the binding and transformation of the guest. These dynamic porous magnets are then very appealing candidates as magnetic sensors for applications in nanospintronics.

The impressive potential of the metalloligand approach in designing new molecular spintronic materials constitutes a great scientific challenge for the chemical research community that requires a multidisciplinary formation. New fundamental concepts and future applications in materials science and nanotechnology will emerge from the study of magneto, electro-, and photochemistry as a supramolecular function in metallosupramolecular chemistry. Although it is still in its infancy, this 'bottom-up' approach appears as an advantageous alternative to the classical 'top-down' one to nanoscopic spintronic materials displaying unique magnetic properties as well as redox, optical, conducting, sensor, or catalytic activities. As a matter of fact, the morphosynthesis of novel hybrid materials from the multilevel organization of molecules with interesting chemical and physical properties into suitable ordered host systems is a major current challenge in material science and nanotechnology which requires the collaboration of groups from different disciplines, including organic, inorganic, or theoretical chemists and physicists.

References

[1] a) O. Kahn, Molecular Magnetism, VCH Publishers, New York, **1993**. b) J. Jortner and M. Ratner, *Molecular Electronics*, Blackwell Science, Oxford, **1997**.

[2] Special Issue on "Molecular Spintronics and Quantum Computing" (Guest Editors: E. Coronado, A. J. Epstein): a) Julio Camarero, Eugenio Coronado, *J. Mater. Chem.* **2009**, *19*, 1678. b) M. Mas-Torrent, N. Crivillers, V. Mugnaini, I. Ratera, C. Rovira, J. Veciana, *J. Mater. Chem.* **2009**, *19,* 1691. c) Fujian Wang and Z. Valy Vardeny, *J. Mater. Chem.* **2009**, *19*, 1685. d) Tadashi Sugawara and Michio M. Matsushita, *J. Mater. Chem.* **2009**, *19*, 1738.

[3] a) J. M. Lehn, *Supramolecular Chemistry: Concepts and Perspectives*, VCH, Weinheim, 1995. b) *Transition Metals in Supramolecular Chemistry*, ed. J. P. Sauvage, Wiley, New York, USA, 1999, vol. 5.

[4] Special Issue on "Supramolecular Approaches to Nano and Molecular Electronics" (Guest Editor: J. Weiss): a) J. W. Canary, S. Mortezaei, J. Liang, *Coord. Chem. Rev*. **2010**, *254*, 2249. b) M. Amelia, L. Zou, A. Credi, *Coord. Chem. Rev*. **2010**, *254*, 2267. c) M. C. Dul, E. Pardo, R. Lescouëzec, Y. Journaux, J. Ferrando-Soria, R. Ruiz-García, J. Cano, M. Julve, F. Lloret, D. Cangussu, C. L. M. Pereira, H. O. Stumpf, J. Pasán, C. Ruiz-Pérez, *Coord. Chem. Rev*. **2010**, *254*, 2281. d) S. Mohnani, D. Bonifazi, *Coord. Chem. Rev*. **2010**, *254*, 2342. d) J. K. H. Hui, M. J. MacLachlan, *Coord. Chem. Rev*. **2010**, *254*, 2363. e) G. H. Clever, M. Shionoya, *Coord. Chem. Rev*. **2010**, *254*, 2391. f) H. Yang, K. L. Meter, H. F. Sleiman, *Coord. Chem. Rev*. **2010**, *254*, 2403. g) C. P. Myers, M. E. Williams, *Coord. Chem. Rev*. **2010**, *254*, 2416.

[3] a) E. C. Constable, *Prog. Inorg. Chem*. **1994**, *42*, 67. b) P. J. Stang, B. Olenyuk, *Acc. Chem. Res.* **1997**, *30*, 502. c) M. Albrecht, *Chem. Soc. Rev.* **1998**, *27*, 281. d) G. F. Swiegers, T. J. Malefetse, *Chem. Rev*. **2000**, *100* 3483. e) P. J. Steel, *Acc. Chem. Res*. **2005**, *38*, 243.

[4] a) M. Fujita, *Chem. Soc. Rev.* **1998**, *27*, 417. b) D. L. Caulder, K. N. Raymond, *Acc. Chem. Res.* **1999**, *32*, 975. c) S. Lenninger, B. Olenyuk, J. Stang, *Chem. Rev*. **2000**, *100*, 853. d) S. R. Seidel, P. J. Stang, *Acc. Chem. Res*. **2002**, *35*, 972.

[5] a) S. R. Batten, R. Robson, *Angew. Chem. Int. Ed.* **1998**, *37*, 1461. (b) F. A. Cotton, C. Lin, C. A. Murillo, *Proc. Nat. Acad. Sci.* **2002**, *99*, 4810. c) O. M. Yaghi, M. O'Keeffe, N. W. Ockwig, H. K. Chae, M. Eddaoudi, J. Kim, *Nature* **2003**, *423*, 705. d) G. Férey, C. Mellot-Draznieks, C. Serre, F. Millange, *Acc. Chem. Res.* **2005**, *38*, 217.

[6] a) D. Fiedler, D. H. Leung, R. G. Bergman, K. N. Raymond, *Acc. Chem. Res.* **2005**, *38*, 349. b) M. P. Suh, Y. E. Cheon, E. Y. Lee, Coord. Chem. Rev. **2008**, *252*, 1007. c) D. Farruseng, S. Aguado, C. Pinel, *Angew. Chem. Int. Ed.* **2009**, *48*, 7502. d) R. J. Kuppler, D. J. Timmons, Q. R. Fang, J. R. Li, T. A. Makal, M. D. Young, D. Yuan, D. Zhao, W. Zhuang, H. C. Zhou, *Coord. Chem. Rev.* **2009**, *253*, 3042.

[7] a) J. M. Lehn, *Angew. Chem. Int. Ed.* **2004**, *43*, 3644. b) L. K. Thompson, O. Waldman, *Coord. Chem. Rev*. **2005**, *249*, 2677. c) M. Kurmoo, *Chem. Soc. Rev.* **2008**, *38*, 1353. d) L. R. MacGillivray, G. S. Papaefstathiou, T. Friscic, T. D. Hamilton, D. K. Buar, Q. Chu, D. B. Varshney, I. G. Georgiev, *Acc. Chem. Res.* **2008**, *41*, 280.

[8] a) *Magnetism: A Supramolecular Function* (NATO ASI Series C), O. Kahn, (Ed.), Kluwer, Dordrecht, vol. 484, **1996**. b) Magnetism: Molecular and Supramolecular Perspectives, *Coord. Chem. Rev.* **2005**, *249,* 2677. c) Supramolecular Magnetic Materials, *Aust. J. Chem.* **2009**, *62*, 1079.

[9] a) M. Verdaguer, A. Bleuzen, V. Marvaud, J. Vaissermann, M. Seuleiman, C. Desplanches, A. Scuiller, C. Train, R. Garde, G. Gelly, C. Lomenech, I. Rosenman, P. Veillet, C. Cartier, F. Villain, *Coord. Chem. Rev.* **1999**, *1023*, 190. b) M. Ohba, H. Okawa, *Coord. Chem. Rev.* **2000**, *198*, 313. c) V. Marvaud, J. M. Herrera, T. Barilero, F. Tuyèras, R. Garde, A. Scuiller, C. Decroix, M. Cantuel, C. Desplanches, *Monatsh. Chem.* **2003**, *134*, 149. d) L. M. C. Beltran, J. R. Long, *Acc. Chem. Res*. **2005**, *38*, 325; e) R. Lescouëzec, L. M. Toma, J. Vaissermann, M. Verdaguer, F. S. Delgado, C. Ruiz-Pérez, F. Lloret, M. Julve, *Coord. Chem. Rev*. **2005**, *249*, 2691.

[10] a) S. Decurtins, R. Pellaux, G. Antorrena, F. Palacio, *Coord. Chem. Rev*. **1999**, *841*, 190. b) E. Coronado, M. Clemente-León, J. R. Galán-Mascaros, C. Giménez-Saiz, C. J. Gómez-García, E. Martínez-Ferrero, *J. Chem. Soc., Dalton Trans*. **2000**, *3955*. c) M. Pilkington, M. Gross, P. Franz, M. Biner, S. Decurtins, H. Stoeckli-Evans, A. Neels, *J. Sol. State Chem*. **2001**, *159*, 262. d) E. Coronado, A. Forment-Aliaga, J. R. Galán-Mascaros, C. Giménez-Saiz, C. J. Gómez-García, E. Martínez-Ferrero, A. Nuez, F. M. Romero, *Solid State Sci*. **2003**, *5*, 917. e) M. Gruselle, C. Train, K. Boubekeur, P. Gredin, N. Ovanesyan, *Coord. Chem. Rev*. **2006**, *250*, 2491.

[11] a) E. Pardo, R. Ruiz-García, J. Cano, X. Ottenwaelder, R. Lescouëzec, Y. Journaux, F. Lloret, M. Julve, *Dalton Trans.*, **2008**, *2780*. b) M.-C. Dul, E. Pardo, R. Lescouëzec, Y. Journaux, J. Ferrando-Soria, R. Ruiz-García, J. Cano, M. Julve, F. Lloret, D. Cangussu,; C. L. M. Pereira, H. O. Stumpf, J. Pasán, C. Ruiz-Pérez, *Coord. Chem. Rev*. **2010**, *254*, 2281.

[12] a) G. Blay, I. Fernández, J. R. Pedro, R. Ruiz-García, M. C. Muñoz, J. Cano, R. Carrasco, *Eur. J. Org. Chem.* **2003**, *1627*. b) C. Muñoz, G. Blay, I. Fernández, J. R. Pedro, R. Carrasco, M. Castellano, R. Ruiz-García, J. Cano, *CrystEngComm* **2010**, *12*, 2473.

[13] a) I. Fernández, R. Ruiz, J. Faus, M. Julve, F. Lloret, J. Cano, X. Ottenwaelder, Y. Journaux, M.C. Muñoz, *Angew. Chem., Int. Ed.* **2001**, *40*, 3039. b) E. Pardo, J. Faus, M. Julve, F. Lloret, M.C. Muñoz, J. Cano, X. Ottenwaelder, Y. Journaux, R. Carrasco, G. Blay, I. Fernández, R. Ruiz-García, *J. Am. Chem. Soc.* **2003**, *125*, 10770. c) E. Pardo, R. Carrasco, R. Ruiz-García, M. Julve, F. Lloret, M.C. Muñoz, Y. Journaux, E. Ruiz, J. Cano, *J. Am. Chem. Soc.* **2008**, *130*, 576. d) M. Castellano, J. Ferrando-Soria, E. Pardo, M. Julve, F. Lloret, C. Mathonière, J. Pasán, C. Ruiz-Pérez, L. Cañadillas-Delgado, R. Ruiz-García, J. Cano, *Chem. Commun.* **2011**, *47*, 11035. e) M. Castellano, F. R. Fortea-Pérez, S.-E. Stiriba, M. Julve, F. Lloret, D. Armentano, G. De Munno, R. Ruiz-García, J. Cano, *Inorg. Chem.* **2011**, *50*, 11279. f) J. Ferrando-Soria, M. Castellano, R. Ruiz-García, J. Cano, M. Julve, F. Lloret, J. Pasán, C. Ruiz-Pérez, L. Cañadillas-Delgado, Y. Li, Y. Journaux, E. Pardo, *Chem. Commun.* **2012**, *48*, 8401. (g) M. Castellano, R. Ruiz-García, J. Cano, M. Julve, F. Lloret, Y. Journaux, G. De Munno, D. Armentano, *Chem. Commun*. **2013**, *49*, 3534. h) M. Castellano, R. Ruiz-García, F. Lloret, J. Cano, unpublished work. i) M. Castellano, R. Ruiz-García, F. Lloret, J. Cano, unpublished work. j) M. Castellano, R. Ruiz-García, F. Lloret, J. Cano, unpublished work.

[14] a) E. Pardo, J. Ferrando-Soria, M. C. Dul, R. Lezcouëzec, Y. Journaux, R. Ruiz-García, J. Cano, M. Julve, F. Lloret, L. Cañadillas-Delgado, J. Pasán and C. Ruiz-Pérez, *Chem. Eur. J.* **2010**, *16*, 12838. b) M. C. Dul, E. Pardo, R. Lezcouëzec, L. M. Chamoreau, F. Villain, Y. Journaux, R. Ruiz-García, J. Cano, M. Julve, F. Lloret, J. Pasán, C. Ruiz-Pérez, *J. Am. Chem. Soc.* **2009**, *131*, 14614.

[15] M. C. Dul, X. Ottenwaelder, E. Pardo, R. Lezcouëzec, Y. Journaux, L. M. Chamoreau, R. Ruiz-García, J. Cano, M. Julve, F. Lloret, *Inorg. Chem*. **2009**, *48*, 5244.

[16] a) E. Pardo, K. Bernot, M. Julve, F. Lloret, J. Cano, R. Ruiz-García, F. S. Delgado, C. Ruiz-Pérez, X. Ottenwaelder, Y. Journaux, *Inorg. Chem.* **2004**, *43*, 2768. b) E. Pardo, R. Ruiz-García, F. Lloret, M. Julve, J. Cano, J. Pasán, C. Ruiz-Pérez, Y. Filali, L. M. Chamoreau, Y. Journaux, *Inorg. Chem*. **2007**, *46*, 4504. c) M. Castellano, R. Ruiz-García, F. Lloret, J. Cano, unpublished work. d) M. Castellano, R. Ruiz-García, F. Lloret, J. Cano, unpublished work.

[17] a) E. Pardo, K. Bernot, M. Julve, F. Lloret, J. Cano, R. Ruiz-García, J. Pasán, C. Ruiz-Pérez, X. Ottenwaelder, Y. Journaux, *Chem. Commun.* **2004**, *920*. b) E. Pardo, I. Morales-Osorio, M. Julve, F. Lloret, J. Cano, R. Ruiz-García, J. Pasán, C. Ruiz-Pérez, X. Ottenwaelder, Y. Journaux, *Inorg. Chem.* **2004**, *43*, 7594. c) E. Pardo, M. C. Dul, R. Lescouëzec, L. M. Chamoreau, Y. Journaux, J. Pasán, C. Ruiz-Pérez, M. Julve, F. Lloret, R. Ruiz-García, J. Cano, *Dalton Trans.* **2010**, *39*, 4786. d) E. Pardo, P. Burguete, R. Ruiz-García, M. Julve, D. Beltrán, Y. Journaux, P. Amorós, F. Lloret, *J. Mat. Chem.* **2006**, *16,* 270. e) L. Toma, M. C. Dul, E. Pardo, R. Ruiz-García, M. Julve, Y. Journaux, F. Lloret, *Small 8* **2012**, *2532.*

[18] a) X. Ottenwaelder, J. Cano, Y. Journaux, E. Rivière, C. Brennan, M. Nierlich, R. Ruiz-García, *Angew. Chem. Int. Ed.* **2004**, *43*, 850. b) M. C. Dul, J. Ferrando-Soria, E. Pardo, R. Lezcouëzec, Y. Journaux, R. Ruiz-García, J. Cano, M. Julve, F. Lloret, O. Fabelo, J. Pasán, C. Ruiz-Pérez, *Inorg. Chem.* **2010**, *49*, 11264.

[19] a) E. Pardo, R. Ruiz-García, F. Lloret, J. Faus, M. Julve, Y. Journaux, F. S. Delgado, C. Ruiz-Pérez, *Adv. Mater.* **2004**, *16,* 1597. b) E. Pardo, R. Ruiz-García, F. Lloret, J. Faus, M. Julve, Y. Journaux, M. A. Novak, F. S. Delgado, C. Ruiz-Pérez, *Chem. Eur. J.* **2007**, *13,* 2054. c) J. Ferrando-Soria, E. Pardo, R. Ruiz-García, J. Cano, F. Lloret, M. Julve, Y. Journaux, J. Pasán, C. Ruiz-Pérez, *Chem. Eur. J.* **2011**, *17,* 2176. d) J. Ferrando-Soria, M. T. M. Rood, M. Julve, F. Lloret, Y. Journaux, J. Pasán, C. Ruiz-Pérez, O. Fabelo, E. Pardo, *CrystEngComm.* **2012**, *14*, 761. e) J. Ferrando-Soria, T. Grancha, M. Julve, J. Cano, F. Lloret, Y. Journaux, J. Pasán, C. Ruiz-Pérez, E. Pardo, *Chem. Commun.* **2012**, *48,* 3539.

[20] a) C. L. M. Pereira, E. F. Pedroso, H. O. Stumpf, M. A. Novak, L. Ricard, R. Ruiz-García, E. Rivière, Y. Journaux, *Angew. Chem. Int. Ed.* **2004**, *43,* 956. b) J. Ferrando-Soria, J. Pasán, C. Ruiz-Pérez, Y. Journaux, M. Julve, F. Lloret, J. Cano, E. Pardo, *Inorg. Chem.* **2011**, *50,* 8694. c) J. Ferrando-Soria, T. Grancha, J. Pasán, C. Ruiz-Pérez, L. Cañadillas-Delgado, Y. Journaux, M. Julve, J. Cano, F. Lloret, E. Pardo, *Inorg. Chem.* **2012**, *51,* 7019. d) J.

Ferrando-Soria, R. Ruiz-García, J. Cano, S.-E. Stiriba, J. Vallejo, I. Castro, M. Julve, F. Lloret, P. Amorós, J. Pasán, C. Ruiz-Pérez, Y. Journaux, E. Pardo, *Chem. Eur. J.* **2012**, *18,* 1608. e) J. Ferrando-Soria, P. Serra-Crespo, M. de Lange, J. Gascon, F. Kapteijn, M. Julve, J. Cano, F. Lloret, J. Pasán, C. Ruiz-Pérez, Y. Journaux, E. Pardo, *J. Am. Chem. Soc.* **2012**, *134,* 15301. f) J. Ferrando-Soria, H. Khajavi, P. Serra-Crespo, J. Gascon, F. Kapteijn, M. Julve, F. Lloret, J. Pasán, C. Ruiz-Pérez, Y. Journaux, E. Pardo, *Adv. Mater.* **2012**, *24*, 5625. j) J. Ferrando-Soria, M. Castellano, E. Pardo, F. Lloret, J. Cano, unpublished work.

[21] a) E. Pardo, D. Cangussu, M. C. Dul, R. Lescouëzec, P. Herson, Y. Journaux, E. F. Pedroso, C. L. M. Pereira, M. C. Muñoz, R. Ruiz-García, J. Cano, P. Amorós, M. Julve, F. Lloret, *Angew. Chem. Int. Ed.* **2008**, *47*, 4211. b) D. Cangussu, E. Pardo, M. C. Dul, R. Lescouëzec, P. Herson, Y. Journaux, E. F. Pedroso, C. L. M. Pereira, H. O. Stumpf, M. C. Muñoz, R. Ruiz-García, J. Cano, M. Julve, F. Lloret, *Inorg. Chim. Acta* **2008**, *361*, 3394. c) M. C. Dul, R. Lezcouëzec, L. M. Chamoreau, Y. Journaux, R. Carrasco, M. Castellano, R. Ruiz-García, J. Cano, F. Lloret, M. Julve, C. Ruiz-Pérez, O. Fabelo, E. Pardo, *CrystEngComm* **2012**, *14*, 5639.

[22] *a*) E. Clar, *Polycyclic Hydrocarbons*, Academic Press, London, UK, **1964**, vols. 1 and 2. *b*) Y. Geerts, G. Klärner, K. Müllen, *Electronic Materials: The Oligomer Approach*, eds. K. Müllen and G. Klärner, Wiley-VCH, Weinheim, Germany, **1998**, 48. c) J. J. McCullough, *Chem. Rev*. **1987**, *87*, 811. d) H. D. Becker, *Chem. Rev*. **1993**, *93*, 145. e) H. Bouas-Laurent, A. Castellan, J.P. Desvergne, R. Lapouyade, *Chem. Soc. Rev*. **2000**, *29*, 43.

[23] a) P. F. H. Schwab, M. D. Levin, J. Michl, *Chem. Rev*. **1999**, *99*, 1863. b) S. Szafert, J. A. Gladysz, *Chem. Rev*. **2003**, *103*, 4175. c) P. F. H. Schwab, J. R. Smith, J. Michl, *Chem. Rev*. **2005**, *105*, 1197. d) T. Ren, *Chem. Rev*. **2008**, *108*, 4185.

[24] M. Irie, *Chem. Rev*. **2000**, *100*, 1685.

[25] E. Pardo, K. Bernot, M. Julve, F. Lloret, J. Cano, R. Ruiz-García, F. S. Delgado, C. Ruiz-Pérez, X. Ottenwaelder, Y. Journaux, *Inorg. Chem.* **2004**, *43*, 2768.

[26] E. Pardo, R. Ruiz-García, F. Lloret, M. Julve, J. Cano, J. Pasán, C. Ruiz-Pérez, Y. Filali, L. M. Chamoreau, Y. Journaux, *Inorg. Chem.* **2007**, *46*, 4504.

[27] a) D. Gatteschi, A. Caneschi, R. Sessoli and A. Cornia, *Chem. Soc. Rev*., 1996, **25**, 101. b) D. Gatteschi, R. Sessoli and A. Cornia, *Chem. Commun*., 2000, 725. c) R. E. P. Winpenny, *Adv. Inorg. Chem*., 2001, **52**, 1. d) D. Gatteschi and R. Sessoli, *Angew. Chem. Int. Ed*., 2003, **42**, 268. e) V. Marvaud, J. M. Herrera, T. Barilero, F. Tuyèras, R. Garde, A. Scuiller, C. Decroix, M. Cantuel and C. Desplanches, *Monatsh. Chem*., 2003, **134**, 149. f) L. M. C. Beltran and J. R. Long, *Acc. Chem. Res*., 2005, **38**, 325. g) G. Aromi and E. K. Brechin, *Struct. Bonding,* 2006, **122**, 1. h) K. Thompson and O. Waldman, *Coord. Chem. Rev*., 2005, **249**, 2677. i) E. K. Brechin, *Chem. Commun*., 2005, 5141. j) T. C. Stamatatos and G. Christou, *Inorg. Chem*., 2009, **48**, 3308.

[28] D. Gatteschi, R. Sessoli, J. Villain, *Molecular Nanomagnets*, Oxford University Press, **2006**.

[29] A. Dei, D. Gatteschi, *Angew. Chem. Int. Ed*. **2011**, *50*, 11852.

[30] a) D. A. Dougherty, *Acc. Chem. Res*. **1991**, *24*, 88. b) H. Iwamura, N. Koga, *Acc. Chem. Res*. **1993**, *26*, 346. c) A. Rajca, *Chem. Rev.* **1994**, *94*, 871.

[31] a) O. M. Yaghi, M. O'Keeffe, M. Eddaoudi, H. K. Chae, J. Kim, N. W. Ockwig, *Nature* **2003**, *423*, 705. b) J. R. Long, O. M. Yaghi, *Chem. Soc. Rev.* **2009**, *38*, 1213.

[32] a) S. Kitagawa, R. Kitaura, S.I. Noro, *Angew. Chem. Int. Ed.* **2004**, *43*, 2334. b) S. Kitagawa, K. Uemura, *Chem. Soc. Rev.* **2005**, *34*, 109. c) S. Kitagawa, R. Matsuda, *Coord. Chem. Rev.* **2007**, *251,* 2490.

[33] a) G. Férey, C. Mellot-Draznieks, C. Serre, F. Millange, *Acc. Chem. Res.* **2005**, *38*, 217. b) G. Férey, *Chem. Soc. Rev.* **2008**, *37*, 191. c) G. Férey, C. Serre, *Chem. Soc. Rev.* **2009**, *38*, 130.

[34] a) O. R. Evans, W. Lin, *Acc. Chem. Res.* **2002**, *35*, 511. b) C. Janiak, *Dalton Trans.* **2003**, 2781. c) G. S. Papaefstathiou, L. R. MacGillivary, *Coord. Chem. Rev.* **2003**, *246*, 169. d) C. N. R. Rao, S. Natarajan, R. Vaidhyanaathan, *Angew. Chem. Int. Ed.* **2004**, *43*, 1466. e) D. Bradshaw, J. B. Claridhe, E. J. Cussen, T. J. Prior, M. J. Rosseinsky, *Acc. Chem. Res.* **2005**, *38*, 273. f) R. J. Kuppler, D. J. Timmons, Q.-R. Fang, J.-R. Li, T. A. Makal, M. D. Young, D. Yuan, D. Zhao, W. Zhuang, H.C. Zhou, *Coord. Chem. Rev.* **2009**, *253*, 3042. g) B. Chen, S. Xiang, G. Qian, *Acc. Chem. Res*. **2010**, *43*, 1115.

[35] a) D. Maspoch, D. Ruiz-Molina, J. Veciana, *Chem. Soc. Rev.* **2007**, *36*, 770. b) E. Pardo, R. Ruiz-García, J. Cano, X. Ottenwaelder, R. Lescouëzec, Y. Journaux, F. Lloret, M. Julve, *Dalton Trans.* **2008**, 2780. c) M. Kurmoo, *Chem. Soc. Rev.* **2009**, *38*, 1353. d) M.-C. Dul, E. Pardo, R. Lescouëzec, Y. Journaux, J. Ferrando-Soria, R. Ruiz-García, J. Cano, M. Julve, F. Lloret, D. Cangussu, C. L. M. Pereira, H. O. Stumpf, J. Pasán, C. Ruiz-Pérez, *Coord. Chem. Rev.* **2010**, *254*, 2281. e) P. Dechambenoit, J. R. Long, *Chem. Soc. Rev.* **2011**, *40*, 3249. f) E. Coronado, G. Minguez-Espallargas, *Chem. Soc. Rev.* **2013**, *42*, 1525.

[36] a) A. Rujiwatra, C. J. Kepert, M. J. Rosseinsky, *Chem. Commun.* **1999**, 2307. b) A. Rujiwatra, C. J. Kepert, J. B. Claridge, M. J. Rosseinsky, H. Kumagai, M. Kurmoo, *J. Am. Chem. Soc.* **2001**, *123*, 10584. c) Y.-Q. Tian, C.X. Cai, Y. Ji, X.-Z. You, S.M. Peng, G.-H. Lee, *Angew. Chem. Int. Ed.* **2002**, *41*, 1384. d) Y.-Q. Tian, C.-X. Cai, X.-M. Ren, C.Y. Duan, Y. Xu, S. Gao, X.-Z. You, *Chem. Eur. J.* **2003**, *9*, 5673. e) M. Kurmoo, H. Kumagai, S. M. Hughes, C. J. Kepert, *Inorg. Chem.* **2003**, *42*, 6709. f) M. Kurmoo, H. Kumagai, K. W. Chapman, C. J. Kepert, *Chem. Commun.* **2005**, 3012. g) M.-H. Zeng, X.-L. Feng, W.-X. Zhang, X.-M. Chen, *Dalton Trans.* **2006**, 5294. h) S. Galli, N. Masciocchi, G. Tagliabue, A. Sironi, J. A. R. Navarro, J. M. Salas, J. Mendez-Liñan, M. Domingo, M. Perez-Mendoza, E. Barea, *Chem. Eur. J.* **2008**, *14*, 9890. i) J. A. R. Navarro, E. Barea, A. Rodriguez-Dieguez, J. M. Salas, C. O. Ania, J. B. Parra, N. Masciocchi, S. Galli, A. Sironi, *J. Am. Chem. Soc.* **2008**, *130*, 3978. j) P. Zhu, W. Gu, F.-Y. Cheng, X. Liu, J. Chen, S.-P. Yan, D.-Z. Liao, *CrystEngComm* **2008**, *10*, 963. k) Q.-X. Yao, L. Pan, X.-H. Jin, J. Li, Z.-F. Ju, J. Zhang, *Chem. Eur. J.* **2009**, *15*, 11890. l) X.-N. Cheng, W. Xue, J.-B. Lin, X.-M. Chen, *Chem. Commun.* **2010**, *46*, 246.

[37] a) D. Maspoch, D. Ruiz-Molina, K. Wurst, N. Domingo, M. Cavallini, F. Biscarini, J. Tejada, C. Rovira, J. Veciana, *Nature Mater.* **2003**, *2*, 190. b) N. López, H. Zhao, A. V. Prosvirin, A. Chouai, M. Shatruk, K. R. Dunbar, *Chem. Commun.* **2007**, 4611. c) N. Motokawa, S. Matsunaga, S. Takaishi, H. Miyasaka, M. Yamashita, K. R. Dunbar, *J. Am. Chem. Soc.* **2010**, *132*, 11943.

[38] a) M. Ohba, H. Ohkawa, N. Fukita, Y. Hashimoto, *J. Am. Chem. Soc.* **1997**, *119*, 1011. b) S.-I. Ohkoshi, K.-I. Arai, Y. Sato, K. Hashimoto, *Nature Mater.* **2003**, *2*, 857. c) N. Yanai, W. Kaneko, K. Yoneda, M. Ohba, S. Kitagawa, *J. Am. Chem Soc.* **2007**, *129*, 3496. d) W. Kaneko, M. Ohba, S. Kitagawa, *J. Am. Chem Soc.* **2007**, *129*, 13706. e) J. Milon, M.-C. Daniel, A. Kaiba, P. Guionneau, S. Brandès, J.-P. Sutter, *J. Am. Chem Soc.* **2007**, *129*, 13872. f) S. S. Kaye, H. J. Choi, J. R. Long, *J. Am. Chem. Soc.* **2008**, *130*, 16921. g) D. Pinkowicz, R. Podgajny, M. Balanda, M. Makarewicz, B. Gawel, W. Lasocha, B. Sieklucka, *Inorg. Chem.* **2008**, *47*, 9745. h) B. Sieklucka, R. Podgajny, D. Pinnkowicz, B. Nowicka, T. Korzeniak, M. Balanda, T. Wasiutynski, R. Pelka, M. Makarewicz, M. Czapla, M. Rams, B. Gavel, W. Lasocha, *CrystEngComm* **2009**, *11*, 2032.

EPILOG

The work presented in this thesis is only our **first step** in the area of molecular spintronics and the main reason for us to pursue along this research avenue. This is rightly expressed in the voice of the greek most famous contemporary poet, Constantin P. Cavafy:

The young poet Evmenis
complained one day to Theocritos:
"I have been writing for two years now
and I have composed just one idyll.
It's my only completed work.
I see, sadly, that the ladder of Poetry
is tall, extremely tall;
and from this first step I now stand on
I will never climb any higher."
Theocritos replied: "Words like that
are improper, blasphemous.
Just to be on the first step
should make you happy and proud.
To have come this far is no small
achievement:
what you have done is a glorious thing.
Even this first step
is a long way above the ordinary world.
To stand on this step
you must be in your own right
a member of the city of ideas.
And it is a hard, unusual thing
to be enrolled as a citizen of that city.
Its councils are full of Legislators
no charlatan can fool.
To have come this far is no small
achievement:
what you have done already is a
glorious thing."

(*The First Step,* Collected Poems)

Indeed, this thesis is also meant to be a "**message in a bottle**" for physicists and materials scientists with a large expertice in the manipulation and measurement of single-molecule electron transport properties, as well as in the processing and addressing of molecules into different supports, and those other members of *city of ideas* who may be interested in our work.

EPÍLOGO

El trabajo presentado en esta tesis es sólo un **primer paso** en el área de la espintrónica molecular y nuestra principal razón para continuar a lo largo de esta avenida de investigación. Ello queda muy bien expresado en la voz del más famoso poeta griego contemporáneo, Constantin P. Cavafy:

A Teócrito se quejaba
un día el joven poeta Eumenes:
"Dos años han pasado desde que
escribo y
un idilio he hecho solamente.
Es mi única obra acabada.
Ay de mí, es alta, lo veo,
muy alta la escala de la Poesía;
y del primer escalón aquí donde estoy
nunca he de subir el desdichado".
Dijo Teócrito: "Esas palabras
son impropias y blasfemas.
Y si estás en este primer escalón debes
estar orgulloso y feliz.
Allí donde has llegado, no es poco:
cuanto has hecho, grande gloria.
Y aun este primer escalón
dista mucho de la gente común.
Para que hayas pisado en esta grada
es menester que seas con derecho
ciudadano en la ciudad de las ideas.
Y es difícil y raro que en aquella ciudad
te inscriban como ciudadano.
En su ágora hallas Legisladores
a los que no burla ningún aventurero.
Aquí donde has llegado, no es poco:
cuanto has hecho, grande gloria".

(*El Primer Escalón,* Antología de Poemas)

Así pues, esta tesis es un **"mensaje en una botella"** para físicos y científicos del área de materiales con gran experiencia en la manipulación y la medición de las propiedades de transporte electrónico a través de moléculas, así como en el procesamiento e implementación de las mismas sobre diferentes soportes físicos y, en general, a todos los miembros de esta *"ciudad de las ideas"* que puedan estar interesados en nuestro trabajo.